IMPERIAL COLLEGE LONDON

Investigation of the effects of nano-sized materials at the blood-gas barrier of the lung: implications for cardiovascular reactivity

Elizabeth Smith
PhD Thesis

September 2015

Declaration

This thesis is a presentation of my original research work. Wherever contributions of others are involved, this is indicated clearly, with due reference to the literature and acknowledgement of collaborative research.

The work was carried out under the guidance of Professor Terry Tetley and Dr Andrew Thorley at the National Heart and Lung Institute, Imperial College, London.

Signed:



Elizabeth Smith

Copyright

The copyright of this thesis rests with the author and is made available under a Creative Commons Attribution Non-Commercial No Derivatives licence. Researchers are free to copy, distribute or transmit the thesis on the condition that they attribute it, that they do not use it for commercial purposes and that they do not alter, transform or build upon it. For any reuse or redistribution, researchers must make clear to others the licence terms of this work.

ACKNOWLEDGEMENTS

This work would not have been possible without the help and support of friends, family and colleagues alike. To my supervisors Andrew Thorley and Terry Tetley, thank you for helping me to gain a depth of experience, allowing me the privilege of pursuing my own research interests and ensuring that I am well equipped for the next chapter. I am extremely grateful to Pakatip Ruenraroengsak for your help and guidance throughout my time at Imperial and especially for your help in the production of the confocal images used in this work, Thank you to the Lung Cell Biology team; Agata Nyga, Sinbad Sweeney, Warren Baker, Martina Zambianchi, Maria Miguel Diez, Andee Tay, Maxim Freydin and Dasha Freydina for being a constant sounding board and providing such excellent help and advice. A special thank you to the "R2" group for their guidance, particularly Shu Chen, Hu (Cynthia) Sheng, Pakatip Ruenraroengsak and Milo Shaffer for the provision of the study particles and their material science expertise. Thank you to Simon Maddock, always ready with a cup of tea when experiments didn't quite go to plan and my parents for their constant support, especially during the write-up period. Finally, to my examiners, Dr James Pease and Dr Alison Lansley thank you for taking the time to undertake such a comprehensive review of my work and for making my viva exam such an enjoyable experience.

CONTENTS

Declaration ... 3

Copyright ... 3

Acknowledgements ... 4

Contents ... 5

Figures ... 12

Tables ... 16

Abbreviations ... 18

Abstract ... 21

1. **INTRODUCTION** ... 23

1.1. An overview of airborne particles, pulmonary and cardiovascular health ... 23

Ambient particulate matter ... 23

Engineered nanomaterials ... 24

1.2. Particle deposition within the lungs ... 25

1.3. Local effects of engineered nanoparticles retained within the lungs ... 29

NM intracellular transport ... 29

Oxidative stress ... 30

Inflammation and fibrosis ... 32

Genotoxicity ... 33

1.4. Extra-pulmonary effects of engineered NMs ... 34

Direct cardiovascular toxicity via particle translocation ... 35

Indirect cardiovascular toxicity via pulmonary mediators ... 39

1.5. Carbon nanotubes 40

Carbon nanotubes in medicine 41

Toxicology of carbon nanotubes 43

Systemic distribution of CNTs 44

1.6. Rationale 47

2. **METHODS** 48

2.1 Ethics statement 48

2.2. Cell isolation and culture 48

Culture of immortalised human alveolar type 1-like epithelial cells (TT1s) 48

Isolation and culture of primary human alveolar type-2 epithelial cells (AT2s) 48

Isolation and culture of primary human pulmonary microvascular cells (HPMVECs) 49

Isolation and culture of human lung fibroblasts 50

Culture of the monocytic cell line U937 and its use in HPMVEC-U937 co-cultures 51

2.3. Nanoparticle preparation 52

2.4. Antioxidant treatment of cells 54

2.5. Alkaline phosphatase assay 54

2.6. Angiogenesis/tube formation assay 55

2.7. Immunocytochemistry 55

Primary antibodies 56

Secondary antibodies 57

2.8. Viability assays 57

MTS viability assay 57

LDH (lactate dehydrogenase) cytotoxicity assay 58

BrDU cell proliferation assay 59

2.9. Particle uptake 59

Transmission electron microscopy (TEM) 59

Confocal microscopy 60

2.10. Detecting reactive oxygen species (ROS) 61

2.11. Gene expression analysis 62

RNA extraction 62

cDNA synthesis 63

Real-time PCR 63

2.12. Enzyme-linked immunosorbent assay (ELISA) 65

IL-6/IL-8/VEGF 66

Secretory leukocyte protease inhibitor (SLPI)/Elafin 66

E-selectin 66

Endothelin-1 67

2.13. Western blot analysis 67

2.14. iCELLigence Electrical Cell Impedance System 68

2.15. EB (Evans Blue)-albumin permeability assay 69

2.16. Statistical analysis 70

3. **DIFFERENTIAL RESPONSES OF CELLS OF THE BLOOD GAS BARRIER FOLLOWING EXPOSURE TO FUNCTIONALISED CARBON NANOTUBES: A FOCUS ON CELL DEATH, PARTICLE UPTAKE AND THE INFLAMMATORY RESPONSE** 71

3.1. Introduction 71

The cells of the blood gas barrier 71

The cytotoxic response 72

Particle uptake 73

The inflammatory response 75

Reactive oxygen species 76

3.2. Results 79

Cell characterisation 79

Cell viability 83

Particle uptake 88

Epithelial inflammatory response 93

Endothelial inflammatory response 99

ROS formation following MWNT exposure 104

3.3. Discussion 109

In vitro model characterisation 109

Differential cytotoxic responses observed following functionalised carbon nanotube exposure 110

Particle uptake in alveolar epithelial and microvascular endothelial cells 113

Differential reactivity of carbon nanotubes with TT1 or AT2 epithelial cells: release of inflammatory mediators and reactive oxygen species 115

Contrasting the epithelial and endothelial inflammatory response to functionalised carbon nanotube exposure 116

3.4. Summary 118

4. **ENDOTHELIAL ACTIVATION FOLLOWING MWNT EXPOSURE AND ITS DEPENDENCE ON MWNT SURFACE FUNCTIONALISATION** 119

4.1. Introduction 119

The role of cell adhesion molecules in leukocyte recruitment 120

Cell adhesion molecules and disease progression 123

Endothelium-derived thrombotic mediators 124

Carbon nanotube exposure and increased atherosclerotic plaque formation 125

4.2. Results 129

CAM gene regulation: E-selectin, ICAM-1, VCAM-1 129

E-selectin protein expression: lysates/supernatants 132

U937/HPMVEC co-cultures 135

Thrombotic gene regulation: TF, tPA, PAI-1 140

4.3. Discussion 143

Monocyte recruitment following endothelial f-MWNT exposure 143

The regulation of thrombotic mediators following endothelial exposure to f-MWNT 145

4.4. Summary 148

5. **DISRUPTION OF THE ALVEOLAR-CAPPILLARY BARRIER FOLLOWING EXPOSURE TO F-MWNTS** 149

5.1. Introduction 149

The transcellular pathway 149

The paracellular pathway 150

The VE-cadherin protein in endothelial adherens junction regulation 152

Nanoparticles and barrier permeability 153

5.2. Results 157

Electrical cell-substrate impedance sensing (ECIS) 157

EB-albumin permeability assay 161

VE-cadherin/actin immunostaining 162

VE-cadherin western blots 166

5.3. Discussion 167

The integrity of microvascular endothelial and alveolar epithelial barriers following f-MWNT exposure 167

Contrasting the Electrical Cell Impedance System with traditional permeability assays 169

Endothelial adherens junctions disassembly following MWNT exposure 170

5.4. Summary 173

6. **DEVELOPMENT OF A NOVEL 3D *IN VITRO* MODEL OF THE ALVEOLAR-CAPILLARY UNIT AND ITS RELEVANCE AS A NANOPARTICLE TOXICITY ASSAY** 174

6.1. Introduction 174

An introduction to alveolar-capillary in vitro systems 174

Current co-culture models to study pulmonary nanoparticle toxicity 174

Co-culture versus mono-culture findings 178

6.2. Methods 181

Generation of a TT1 and AT2 cell co-culture model 181

The addition of HPMVECs to form a triple cell co-culture model of the blood gas barrier 183

6.3. Results 186

Co-culture model characterisation 186

Viability 188

Release of inflammatory mediators in the TT1-AT2 co-culture 190

Release of inflammatory and cell-specific mediators from the triple co-culture system 192

6.4. Discussion 197

Establishment of a triple co-culture system 197

The epithelial TT1-AT2 co-culture vs. monoculture toxicity response 198

The response of the epithelial-endothelial triple co-culture system to functionalised nanoparticles 200

6.5. Summary 203

7. **SUMMARY DISCUSSION** 204

8. **FUTURE WORK** 212

9. **REFERENCES** 215

10. **APPENDIX** 244

FIGURES

Figure 1.3.1 The hierarchical oxidative stress model..... 32

Figure 1.4.1 Proposed mechanisms of cardiovascular toxicity following NP and UFP pulmonary exposure..... 35

Figure 1.4.2 Particle translocation across the alveolar epithelium to the circulation..... 37

Figure 2.7.1 Schematic of the catalytic reaction involved in the LDH assay..... 58

Figure 3.2.1 Phase-contrast micrographs displaying the different morphologies of the main cells used in this study..... 79

Figure 3.2.2 Podoplanin and RAGE expression in TT1 cells..... 80

Figure 3.2.3 AT2 Phenotype Characterisation..... 80

Figure 3.2.4 HPMVEC phenotype characterisation: immunocytochemistry..... 82

Figure 3.2.5 HPMVEC Tube formation on BD Matrigel and expression of endothelin-1..... 83

Figure 3.2.6 TT1 viability at 4 hours, 24 hours and 72 hours following exposure to f-MWNTs..... 84

Figure 3.2.7 AT2 viability at 4 hours, 24 hours and 72 hours following exposure to f-MWNTs..... 85

Figure 3.2.8 HPMVEC viability at 4 hours and 24 hours following exposure to f-MWNTs..... 87

Figure 3.2.9 HPMVEC proliferation at 24 hours following exposure to f-MWNTs..... 88

Figure 3.2.10 TEM images showing the cellular distribution and interaction of AR-MWNTs in TT1 cells..... 89

Figure 3.2.11 TEM images showing the cellular distribution and interaction of MWNTs functionalised using the thermochemical grafting from method in TT1 cells..... 90

Figure 3.2.12 TEM images showing the cellular distribution and interaction of AO-MWNTs in TT1 cells..... 91

Figure 3.2.13. f-MWNT uptake by HPMVEC following a 24 hour exposure..... 92

Figure 3.2.14 AO-MWNT uptake in HPMVECs..... 93

Figure 3.2.15 TT1 *IL-6, IL-8* and *MCP-1* gene regulation in response to a 5 or 50μg/ml AR or AO MWNT exposure for 1, 4 or 24 hours..... 95

Figure 3.2.16 AT2 *IL-6*, *IL-8* and *MCP-1* gene regulation in response to a 5 or 50μg/ml AR or AO MWNT exposure for 1, 4 or 24 hours. 96

Figure 3.2.17 Release of the inflammatory mediators IL-6 and IL-8 from TT1 cells exposed to f-MWNTs for 24 or 72 hours. 97

Figure 3.2.18 Release of the inflammatory mediators IL-6 and IL-8 from AT2 cells exposed to f-MWNTs for 24 or 72 hours. 98

Figure 3.2.19 HPMVEC *IL-6*, *IL-8* and *MCP-1* gene regulation in response to a 1 or 10μg/ml AR or AO MWNT exposure for 1, 4 or 24 hours. 101

Figure 3.2.20 HPMVEC IL-6, IL-8 and MCP-1 gene regulation in response to 10μg/ml AR, P(M4-VP), P(MAA), P(PEGMA)or AO MWNTs. 102

Figure 3.2.21 Release of the inflammatory mediators IL-6 and IL-8 from HPMVECs exposed to f-MWNTs for 4 or 24 hours 103

Figure 3.2.22 ROS generation in TT1 cells determined by CM-H2DCFDA. 104

Figure 3.2.23 ROS generation in AT2 cells determined by CM-H2DCFDA 105

Figure 3.2.24 ROS formation in HPMVECs following MWNT exposure. 106

Figure 3.2.25 Effect of antioxidants on ROS formation in HPMVECs following 10μg/ml MWNT exposure. 107

Figure 3.2.26 Effect of antioxidant addition on inflammatory cytokine release from HPMVECs. 108

Figure 4.1.1 Graphic representation of endothelial responses that may be initiated if CNTs induce endothelial activation. 120

Figure 4.1.2 Graphic representation of the role of cell adhesion molecules (CAMs) in leukocyte recruitment, rolling and extravasation 121

Figure 4.1.3 Homeostasis regulation by the vascular endothelium. 124

Figure 4.2.1 MWNT-induced *VCAM-1*, *E-selectin* and *ICAM-1* gene regulation in HPMVEC 130

Figure 4.2.2 f-MWNT-induced *VCAM-1*, *E-selectin* and *ICAM-1* gene regulation in HPMVEC 4 hours post-exposure. 131

Figure 4.2.3 E-selectin levels in HPMVEC lysates following f-MWNT exposure. 133
Figure 4.2.4 Soluble E-selectin levels in HPMVEC supernatants following f-MWNT exposure. . 134
Figure 4.2.5 Monocyte adherence to a non-treated HPMVEC monolayer and HPMVECs stimulated with TNFα. 136
Figure 4.2.6 Monocyte adherence to a HPMVEC monolayer exposed to AR-MWNTs. 137
Figure 4.2.7 Monocyte adherence to a HPMVEC monolayer exposed to f-MWNTs. 138
Figure 4.2.8 Maximum fluorescence intensity (MFI) of FITC-U937 HPMVEC co-culture following exposure to f-MWNTs. 139
Figure 4.2.9 MWNT-induced *TF*, *tPA* and *PAI-1* gene regulation in HPMVEC. 141
Figure 4.2.10 f-MWNT-induced *TF, tPA and PAI-1 gen*e regulation in HPMVEC 4 hours post-exposure. 142
Figure 5.1.1 Diagram depicting the major endothelial cell junction proteins. 151
Figure 5.2.1 TT1 cell iCelligence data. 158
Figure 5.2.2 AT2 cell iCelligence data. 159
Figure 5.2.3 HPMVEC iCelligence data. 160
Figure 5.2.4 Endothelial barrier permeability determined by the EB-albumin permeability assay. 162
Figure 5.2.5 Immunostaining displaying the effect of a 3 hour f-MWNT exposure on HPMVEC junction integrity. 164
Figure 5.2.6 Immunostaining displaying the effect of a 24 hour f-MWNT exposure on HPMVEC junction integrity. 165
Figure 5.2.7 VE-cadherin protein expression following 10μg/ml AR-MWNT exposure determined by immunoblotting. 166
Figure 5.2.8 VE-cadherin protein expression following 10μg/ml AO-MWNT exposure determined by immunoblotting. 167
Figure 5.3.1 Diagram of the ECIS system. 169

Figure 5.3.2 Diagram depicting the likely disassembly of adherens junction proteins, VE-cadherin lysis and actin cytoskeleton rearrangement following MWNT exposure. 171
Figure 6.2.1 Set-up of the triple cell co-culture system. 184
Figure 6.3.1 Alkaline phosphatase staining of TT1 and AT2 cells in mono and co-culture. 186
Figure 6.3.2 Culturing HPMVECs on the underside of a transwell filter membrane. 187
Figure 6.3.3 Micrograph depicting positioning of cells on both sides of a transwell filter membrane 188
Figure 6.3.4 Viability of cells in a TT1-AT2 co-culture following exposure to f-MWNTs. 189
Figure 6.3.5 Release of inflammatory mediators from cells in a TT1-AT2 co-culture following exposure to f-MWNTs. 191
Figure 6.3.6 Release of the inflammatory mediators IL-6 from the co-culture model of the alveolar-capillary barrier following exposure to f-MWNTs for 24 hours. 193
Figure 6.3.7 Release of the inflammatory mediators IL-8 from the co-culture model of the alveolar-capillary barrier following exposure to f-MWNTs for 24 hours. 194
Figure 6.3.8 Release of the cell adhesion molecule E-selectin from the co-culture model of the alveolar-capillary barrier following exposure to f-MWNTs for 24 hours. 195
Figure 6.3.9. Release of the growth factor VEGF from the co-culture model of the alveolar-capillary barrier following exposure to f-MWNTs for 24 hours. 196

TABLES

Table 1.2.1. Anatomy of the respiratory tree. 28

Table 2.3.1 Summary of f-MWNTs used in the study. 53

Table 2.11.1 Primer sequences used in the study. 64

Table 2.13.1 Antibody dilutions used during western blotting 68

Table 3.2.1 Summary of endothelial cell markers observed in HPMVECs isolated for this study. 81

Table 3.2.2 Summary of TT1 cell inflammatory mediator release following a 72 hour exposure to 10µg/ml f-MWNTs. 94

Table 3.2.3 Summary of HPMVEC inflammatory mediator release following exposure to 10µg/ml f-MWNTs. 100

Table 3.4.1. Summary of the variable TT1, AT2 and HPMVEC responses following exposure to functionalised MWNTs 118

Table 4.1.1 Major endothelial cell adhesion molecules involved in leukocyte recruitment. 122

Table 6.1.1 Published co-culture models representing the peripheral airways. 176

Table 6.3.1 Summary of baseline inflammatory mediator release in TT1 and AT2 mono and co-culture systems. 190

APPENDICES

Appendix I. Published works and copyright permissions. 244

Appendix II. Melt curve analysis. 262

Appendix III. TT1 *RAGE, LGAL3* and SAA-*1* gene regulation in response to a 5 or 50µg/ml AR or AO MWNT exposure for 1, 4 or 24 hours 263

Appendix IV. AT2 *RAGE, LGAL3* and SAA-*1* gene regulation in response to a 5 or 50µg/ml AR or AO MWNT exposure for 1, 4 or 24 hours 264

Appendix V. HPMVEC inflammatory, CAM and thombotic gene regulation followng exposure to TNFα. 265

Appendix VI. Immunostaining optimisation for staining of co-culture system. 266

Appendix VII. SLPI adsorption to f-MWNTs and *SLPI* gene regulation in AT2 cells. 267

Appendix VIII. Elafin adsorption to f-MWNTs and *Elafin* gene regulation in AT2 cells. 268

Appendix IX. Depletion of surfactant proteins A and D following MWNT exposure. 269

Appendix X. Total protein recovered from ultracentrifuged fraction of cell supernatant following MWNT exposure. 270

Appendix XI. CNT length as determined by SEM. 270

ABBREVIATIONS

ANOVA	Analysis of Variance
AO	Acid Oxidised
AQP-5	Aquaporin-5
AR	As Received
AT2	Alveolar Type 2 Epithelial Cell
BALF	Bronchoalveolar Lavage Fluid
CM-H_2DCFDA	5-(and-6)-chloromethyl-2',7'-dichlorodihydrofluorescein diacetate, acetyl ester
CNT	Carbon Nanotube
CRP	C-reactive Protein
CVD	Chemical Vapour Deposition
DEP	Diesel Exhaust Particulate
DNA	Deoxyribonucleic Acid
EB	Evans Blue
ECIS	Electrical Cell Impedance Sensing
ELISA	Enzyme Linked Immuno-sorbent Assay
eNOS	Endogenous Nitric Oxide Synthase
E-selectin	Endothelial-selectin
ET-1	Endothelin-1
GAPDH	Glyceraldehyde 3-phosphate dehydrogenase
HBSS	Hanks' Balanced Salt Solution
HPMVEC	Human Pulmonary Microvascular Cells
HUVEC	Human Umbilical Vascular Cells
ICAM-1	Intracellular Adhesion Molecule-1
IL-6	Interleukin-6
IL-8	Interleukin-8

iNOS	Inducible Nitric Oxide Synthase
LAMP-2	Lysosome-Associated Membrane Protein-2
LDH	Lactate Dehydrogenase
LOX-1	Lectin-type Oxidized LDL Receptor 1
MAPK	Mitogen-activated protein kinase
MCP-1	Monocyte chemoattractant protein-1
MTS	[3-(4,5-dimethylthiazol-2-yl)-5-(3-carboxymethoxyphenyl)-2-(4-sulfophenyl)-2H-tetrazolium
MW	Molecular Weight
MWNT	Multi-walled carbon nanotube
NADPH	Nicotinamide Adenine Dinucleotide Phosphate
NCS	Newborn Calf Serum
NM	Nanomaterial
NO	Nitric Oxide
NP	Nanoparticle
NLRP3	NLR pyrin domain containing 3
P(4-VP)	Poly(4-vinylpyridine)
P(M4-VP)	Poly(N-methyl 4-vinylpyridine iodide)
P(MAA)	Poly(methacrylic acid)
P(PEGMA)	Poly((Poly)ethyleneglycol methacrylate)
PAI-1	Plasminogen Activator Inhibitor-1
PARP	Poly [ADP-ribose] Polymerase-1
PBS	Phosphate Buffered Saline
PCR	Polymerase Chain Reaction
PECAM-1	Platelet Endothelial Cell Adhesion Molecule-1
PEG	(Poly)ethyleneglycol
PES	Phenazine Ethosulfate

PFA	Paraformaldehyde
PLNP	Polystyrene Nanoparticles
PM	Particulate Matter
P-selectin	Platelet-selectin
PTX	Paclitaxel
RAGE	Receptor for Advanced Glycation Endproducts
RIPA	Radioimmunoprecipitation assay buffer
QPCR	Real Time Polymerase Chain Reaction
SAA1	Serum Amyloid A-1
SAA2	Serum Amyloid A-2
SLPI	Secretory Leukocyte Protease Inhibitor
SPA	Surfactant Protein A
SPD	Surfactant Protein D
SWCNT	Single Walled Carbon Nanotube
TF	Tissue Factor
TGFβ	Transforming Growth Factor-β
TNFα	Tumour Necrosis Factor-α
tPA	Tissue Plasminogen Activator
TT1	Transformed Type 1-like Alveolar Epithelial Cell
TTC	Thermochemically Treated Control
UFP	Ultrafine Particles
VCAM-1	Vascular Cell Adhesion Molecule-1
VE-cadherin	Vascular Endothelial Cadherin
VEGF	Vascular Endothelial Growth Factor
vWF	Von Willebrand Factor

ABSTRACT

Carbon nanotubes (CNTs) possess a number of unique properties and play a pivotal role in the nanotechnology industry with widespread applications in construction, medicine and electronics. Previous studies have demonstrated an association between CNT inhalation and adverse cardiovascular effects, however, it is currently unclear whether this is due to the release of pulmonary inflammatory mediators or particle translocation across the blood-gas barrier. A better understanding of CNT interactions at this barrier is therefore essential for developing safer nanomedicines and reducing occupational health risks associated with carbon nanotube manufacture.

The working hypothesis of this study was that the physicochemical properties of multi-walled carbon nanotubes (MWNTs) would determine their toxicity and reactivity at the blood-gas barrier.

To test this hypothesis, primary alveolar type-2 epithelial cells (AT2) and microvascular endothelial cells (HPMVEC) were isolated from resected human lung and employed alongside a unique immortalised human type-1 alveolar cell line (TT1). The cells were then exposed to functionalised MWNT to determine the cellular reactivity of the particles.

Using this model, it was shown that MWNT exposure induced endothelial cell activation, characterised by a pro-inflammatory and pro-thrombotic response, and MWNT functionalisation was a key factor in determining the nature of this response. Acid-oxidised MWNTs induced the greatest endothelial activation, however as-received and thermochemically grafted MWNTs induced a lesser pro-inflammatory response that also coincided with an increase in ROS formation. Of the thermochemically grafted MWNTs, P(M4-VP) and P(PEGMA) MWNTs induced the greatest and smallest response respectively.

At the epithelium, MWNTs were far less reactive. All MWNTs were non-toxic to AT2 cells, however a small cytotoxic and inflammatory response was observed in TT1s following chronic

exposures (72h) and MWNTs were present in both vesicles and the cytoplasm of TT1s following 24h exposure. The thermochemically grafted P(M4-VP) MWNTs were shown to induce the greatest pro-inflammatory response during these chronic exposures.

In vivo, disruption of cell-cell junction could have implications for particle translocation, inflammation and atherosclerotic lesion formation. Exposure to MWNTs was shown to increase the permeability of type 1, but not type 2 alveolar epithelial barriers. The greatest disruption was seen at the endothelial cell junctions, which was accompanied by depletion of adherens junction protein and rearrangement of the actin cytoskeleton.

Finally, to assess whether epithelial-endothelial crosstalk could affect particle toxicity a co-culture model of the alveolar blood-gas barrier was constructed using a transwell system where alveolar type 1 and type 2 epithelial cells were separated from pulmonary microvascular cells by a porous membrane. There were disparities between the mono and co-culture findings and acid oxidised MWNTs applied to the epithelial surface of the co-culture induced a significant release of inflammatory mediator into both the apical and basolateral chambers of the co-culture system, indicative of inflammation in both the pulmonary and vascular systems. This highlighted the need to incorporate endothelial cells into NP toxicity assays, especially when considering the cardiovascular reactivity of a particle.

This thesis has demonstrated that MWNT toxicity is both cell and MWNT surface functionalisation dependent, and that endothelial activation could be responsible for the adverse cardiovascular effects observed following CNT inhalation *in vivo*. These findings will aid the generation of safer nanomaterials and further the understanding of CNT induced cardiovascular reactivity.

1. INTRODUCTION

1.1. An overview of airborne particles, pulmonary and cardiovascular health

Ambient particulate matter

For many years is has been recognised that airborne particles can be harmful to human health. Perhaps the most infamous examples of this in the UK is the London smog of December 1952 in which some 4000 excess deaths occurred in one week. These deaths were primarily attributed to exacerbation of lung disease (chronic bronchitis was then a highly prevalent condition in urban Britain), but importantly, it was also apparent that a proportion of deaths were due to an increase in the incidence of heart attacks (Greater London Authority, 2002; Seaton, Tran, Aitken, & Donaldson, 2010).

Epidemiological studies have since attempted to establish the complex relationship between ambient particulate matter (PM) and human health and have revealed some important findings. Exposure to particulate matter (PM) smaller than 10μm (PM10) and 2.5μm (PM2.5) is associated with increased morbidity and mortality (Dockery *et al*., 1993; Maynard & Kuempel, 2005; Schwartz & Morris, 1995; Stone, Johnston, & Clift, 2007; Wichmann & Peters, 2000). Furthermore, evidence suggests that the ultrafine particle (UFP) fraction of this particulate matter may have unique mechanisms of toxicity, not only in the lungs but also the cardiovascular system (Delfino, Sioutas, & Malik, 2005; Ibald-Mulli, Wichmann, Kreyling, & Peters, 2002; Peters, Wichmann, Tuch, Heinrich, & Heyder, 1997; Weichenthal, 2012).

UFP is particulate matter in the nanoscale range (≤ 100nm (Potocnik, 2011) typically generated as a by-product of processes such as combustion (Gwinn & Vallyathan, 2006). These particles are heterogeneous in size and consist of a solid core, either an inorganic material or soot, surrounded by a layer of adsorbed or condensated semi-volatile constituents (Nel, Xia, Mädler, & Li, 2006).

This nano-scale material has an increased life span within the atmosphere when compared to larger counterparts; can be transported over larger distances; has an increased surface area for the transport of other pollutants, and importantly poses significant health risks upon inhalation into the lung (Gwinn & Vallyathan, 2006). Research funded in the wake of the deadly London smog of 1952 found that when considering the median diameter (number) of particles constituting London smog, over half the particles were less than 100nm in diameter (Lawther, Ellison, & Waller, 1968; Seaton et al., 2010).

Engineered nanomaterials

It is the concern surrounding the inhalation of ultrafine particulate matter that led many governments and learned societies to express concern regarding the development of engineered nanomaterials by industries wishing to exploit their novel properties (Oberdörster, Oberdörster, & Oberdörster, 2005; Stone et al., 2007). Nanotechnology is now employed in a wide range of applications including cosmetics, paints, food packaging, sporting goods, electronics and medical applications (Aitken *et al*., 2007; Jachak *et al*., 2011; Yang, Peters, & III, 2008).

As materials enter the nanoscale range, (at least one dimension ≤100nm (Potocnik, 2011)) their properties differ significantly from those at a larger scale (Dowling *et al*., 2004) The increase in surface area can affect reactivity, strength and electrical properties; and towards the lower end of the nanoscale, quantum effects can influence the optical, electrical and magnetic behaviours of materials (Yang *et al*., 2008). These novel attributes, along with the epidemiological studies of inhaled pollution, have led many to call for independent legislations to be established in regards to the safety of nanomaterials (Seaton et al., 2010). Toxicological studies have implied that the surface area, surface chemistry, size, shape and charge may all influence how nanoparticles affect human health (Aitken *et al*., 2007).

Obvious difference exist between non-intentionally produced ambient particulate matter and engineered nanoparticles; the former are polydispersed and chemically complex, however the latter have precise chemically engineered characteristics (Oberdörster et al., 2005). Manufactured NMs exist in many forms including nanoparticles, nanofibres and nanotubes, composite materials and nano-structured surfaces (Yang *et al*., 2008). These are typically formed from either "top down" or "bottom up" processes (Dowling *et al*., 2004). Top down manufacture involves the generation of very small structures from larger counterparts, and conversely bottom up is the assembly of NM from the atomic or molecular level (Dowling *et al*., 2004). The surface of many NMs can be manipulated using adducts to alter the function of the material, for example, to increase solubility or alter reactivity (Donaldson et al., 2006). Depending on the mode of synthesis, metal catalysts may also be present in the matrix of the nanomaterial; cobalt, iron, nickel, and molybdenum contaminants have all been found in carbon nanotubes (CNTs) as a result of the manufacturing process, and all of which have documented toxic effects (Donaldson et al., 2006). Variations in methodology employed to obtain a similar product often lead to differences in yields, purity, and side products (Dahl, Maddux, & Hutchison, 2007). It is due to the rapid expansion of the nanotechnology industry and the wide range of variation introduced during NM synthesis that there is a serious deficit in adequate toxicity evidence.

1.2. Particle deposition within the lungs

Inhaled air enters the lungs via the conducting airways, first encountering the trachea which partitions into two main bronchi that segregate into a series of intra-pulmonary bronchial and bronchiolar airways. The respiratory tree branches in a dichotomous fashion; at each division the diameters and length of each successive airway branch decreases progressively, however no gaseous exchange occurs until air reaches the respiratory zone. This zone constitutes the respiratory bronchioles, a transitional region displaying features that are both bronchiole and alveolar in nature, and the alveoli (Garmann & Stanfield, 2004) (Table 1.2.1).

The physicochemical properties of an inhaled particle are known to strongly influence where within the respiratory tree the particle will deposit, and it has been hypothesised that the toxic effects of different size fractions of PM may be due, in part, to these particle deposition trends (Schmid *et al*., 2009). Particle deposition in healthy individuals has been modelled by the International Commission on Radiological Protection (ICRP) (Bailey, 1994; ICRP, 1994) which has been built upon by Jaques & Kim (2000) and Daigle *et al* (2003) and it is widely accepted that while particles <100nm may diffuse throughout the lung reaching peripheral alveolar units, larger particles >1μm tend to be deposited in the larger airways, primarily at the bifurcation junctions of the respiratory tree (Balashazy, Hofmann, & Heistracher, 2003; Heistracher & Hofmann, 1997; Hofmann, Balásházy, & Heistracher, 2001). This is due to a process known as "impaction" where particles >1.5μm are driven into the airway wall by rapid changes in airflow direction, such as that found in branching airways (Plumlee, Morman, & Ziegler, 2006). In the large airways, clearance of particles is rapid, primarily occurring via the mucociliary escalator with particles moving up the tracheobronchial region, towards the pharynx where they can be subsequently swallowed (Rothen-Rutishauser et al., 2008; Schmid et al., 2009).

Nanomaterials that diffuse to the alveolar region are cleared at a much slower rate; the retention half-time of solid particles in the alveolar region based on clearance via alveolar macrophage phagocytosis is ~70 days in rats and up to 700 days in humans (Oberdörster et al., 2005; Rogueda & Traini, 2007). Nanoparticles that have initially evaded mucociliary clearance may eventually reach the mucocilary escalator via the slower route of engulfment by alveolar macrophages which subsequently travel into the upper airways (Rogueda & Traini, 2007).

Nanoparticles may however, never reach the mucociliary escalator as although alveolar macrophage phagoytosis is the major source of particle clearance in the lung, it has been shown that small nanosized particles may evade macrophage-mediated clearance (Oberdörster et al., 2005; Semmler et al., 2004; Yang et al., 2007). Particles not removed via macrophage mediated clearance mechanisms will be either retained at the epithelium, or may escape the peripheral

alveolar unit via translocation to the underlying circulation, interstitium or lymphatic system (Choi et al., 2010; Kreyling, Hirn, & Schleh, 2010; Oberdörster et al., 2005). Both particles retained within the lung or those that translocate across the epithelial barrier may have consequences for both pulmonary and cardiovascular health.

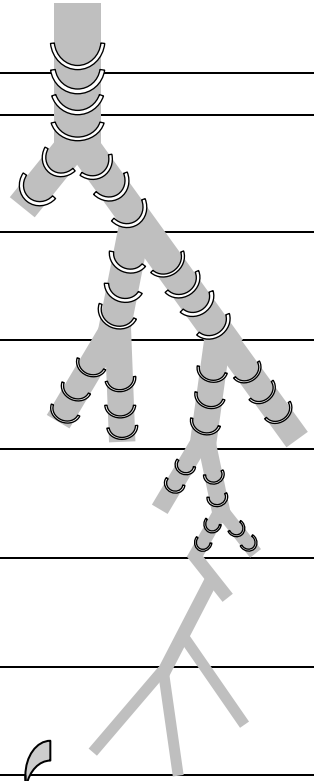
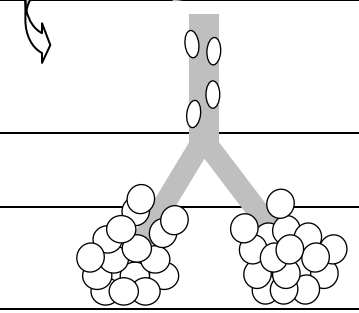
	Anatomy	Structure	Generation	Cytology	Function
Conducting Zone		Larynx	-	• ciliated cells • goblet cells • basal cells	Air conditioning, temperature and humidity, fast particle clearance, air conduction
		Trachea	0	• ciliated cells • goblet cells • basal cells • serous cells • serous gland cells • mucous gland cells	
		Primary bronchi	1		
		Secondary bronchi	2	• ciliated cells • goblet cells • basal cells • serous cells	
		Tertiary bronchi	3		
		Small bronchi	4		
		Bronchioles	5		
		Terminal bronchioles	6-16	• ciliated cells • clara cells • basal cells	
Respiratory Zone		Respiratory bronchioles	17-19	• ciliated cells • clara cells • basal cells • alveolar type 1 cells • alveolar type 2 cells	Air conduction, gas exchange, very slow particle clearance
		Alveolar ducts	20-22	• alveolar type 1 cells • alveolar type 2 cells	Gas exchange, very slow particle clearance
		Alveolar sacs	23		

Table 1.2.1. Anatomy of the respiratory tree. Adapted from (Garmann & Stanfield, 2004).

1.3. Local effects of engineered nanoparticles retained within the lungs

The primary location of nanoparticle mediated toxicity following inhalation is at the pulmonary site of deposition. Rodent studies have observed similar outcomes following NP deposition with inflammation, fibrosis and granuloma formation frequently observed following pulmonary exposure to a range of nanoparticles including metal oxides and siliceous and carbonaceous nanomaterials (Ho *et al*., 2011; Manke, Wang, & Rojanasakul, 2012; Park & Park, 2009). Furthermore, pulmonary inflammation, fibrosis and foreign body granulomas of the pleura were observed in seven workers exposed to polyacrylate nanoparticles over 5-13 months. In these workers the nanoparticles were observed in the cytoplasm and karyoplasm of epithelial and mesothelial cells in addition to the chest fluid (Song, Li, & Du, 2009). The mechanisms underlying the pulmonary toxicity of nanoparticles are both varied and contested due to differences in nanoparticle physicochemistry between studies and the complex intercellular relationships in the respiratory system. There is therefore a need to explore specific NP-cell interactions to discover what is driving NP toxicity.

NM intracellular transport

Smaller particles have a greater tendency to enter subcellular organelles (Boyoglu *et al*., 2013). NM have been visualised using electron microscopy, spectroscopy and fluorescent microscopy in a number of cellular compartments including the cytoplasm, mitochondria, nucleus and lysosome (Pantarotto, Briand, Prato, & Bianco, 2004; Porter et al., 2007; Worle-Knirsch, Pulskamp, Krug, & Wörle-Knirsch, 2006) and are thought to enter the cell either by passive diffusion or energy dependent phagocytosis and endocytosis. Porter *et al* provided evidence for both processes in monocyte derived human macrophages exposed to SWCNT (Porter *et al*., 2007). The absence of a membrane surrounding the CNT indicated that some SWCNTs may be piercing the cellular membrane to gain access to the cell; a plausible mechanism due to the extremely small diameter of SWCNTs (a minimum diameter of around 1nm (Pantarotto *et al*.,

2004)). Mathematical modelling has been used to investigate whether needle-like SWCNTs could theoretically pierce a phospholipid bilayer, which has however, suggested that SWCNTs are more likely to enter a cell via energy-dependent mechanisms such as endocytosis (Pogodin & Baulin, 2010).

Cheng *et al* (2008) demonstrated that the build-up of nucleolar PEGylated SWCNTs was concentration-dependent and that upon removal of the extracellular CNTs they were eventually released from the cell (Cheng *et al*., 2008). This discovery was reinforced by Jin, Heller & Strano (2008) who presented evidence that the rate of DNA-SWCNT endocytosis was equal to that of exocytosis (Jin, Heller, & Strano, 2008). This finding could have profound implications as, depending on whether all CNT are shown to be toxic or whether toxicity is dependent on characteristics of the material, it provides evidence that, if CNT were to be used as drug carriers, as has been proposed by a number of studies (Reviewed by (Liu, Tabakman, Welsher, & Dai, 2009)), a degree of controllable clearance could be achieved (Cheng *et al*., 2008). There is currently insufficient information describing how NP uptake varies between cell types, which should be addressed to fully understand their medicinal and toxic potential.

Oxidative stress

Due to their small size and large surface reactivity NPs are capable of producing higher levels of ROS than their bulk counterparts (Fu, Xia, Hwang, Ray, & Yu, 2014) and a number of studies have implicated reactive oxygen species (ROS) generation in the toxicity of nanoparticles. ROS generation can occur as a result of metal dissolution in the biological environment to produce toxic ions or as a direct result of NP interaction with cellular targets (Ge, Li, *et al*., 2012; Nel *et al*., 2006). Pro-oxidant functional groups on the reactive surface of NPs as well as active redox cycling on the surface of transmission metal NPs may both induce oxidative stress (Manke, Wang, & Rojanasakul, 2013). In addition to being self-oxidant in nature, NPs also react with cells and induce cellular ROS generation through mitochondrial respiration and activation of

NADPH-like enzyme systems (Fu *et al*., 2014). Phagocytic cells induce substantial ROS upon internalisation of NPs via the NADPH oxidase enzyme system (Ye *et al*., 2011). This ROS can be directly injurious to cell DNA, proteins and lipids, however it is also crucial for host defence (Segal, Grimm, Khan, Han, & Blackwell, 2012); the NADPH oxidase enzyme system plays an important part in antimicrobial ROS generation, signalling pathways, chemotaxis, autophagy and antigen cross-presentation (Lam, Huang, & Brumell, 2010).

Overproduction of ROS can result in oxidative stress where cells fail to maintain normal physiological redox-regulated functions. This may generate protein radicals, initiate lipid peroxidation, DNA-strand breaks, modification to nucleic acids, activate redox-sensitive transcription factors and modulate inflammatory responses through signal transduction (Dickinson & Chang, 2011; Fu *et al*., 2014; Meng, Xia, George, & Nel, 2009). The synthesis and release of cytokines involved in inflammation and fibrosis initiated by ROS mediated transcription factors can damage epithelial cells, inducing cell repair mechanisms. In some instances, defects in these cell repair mechanisms can lead to progressive scarring and fibrosis (Nel *et al*., 2006). The effects of increasing oxidative stress are described in Figure 1.3.1.

Although oxidative stress has been implicated in the toxicity of a number of NPs, it is not clear which physicochemical properties are responsible for the increased ROS formation. As a result, it is not known whether processes such as surface functionalisation are able to influence the oxidative potential of the material. Furthermore, the majority of studies into the oxidative potential of NPs have investigated phagocytic cells due to the important role ROS play in these cell types. There is consequently a lack of data describing ROS formation at the blood-gas barrier, and the implications this may have for other cellular processes such as inflammation and barrier permeability.

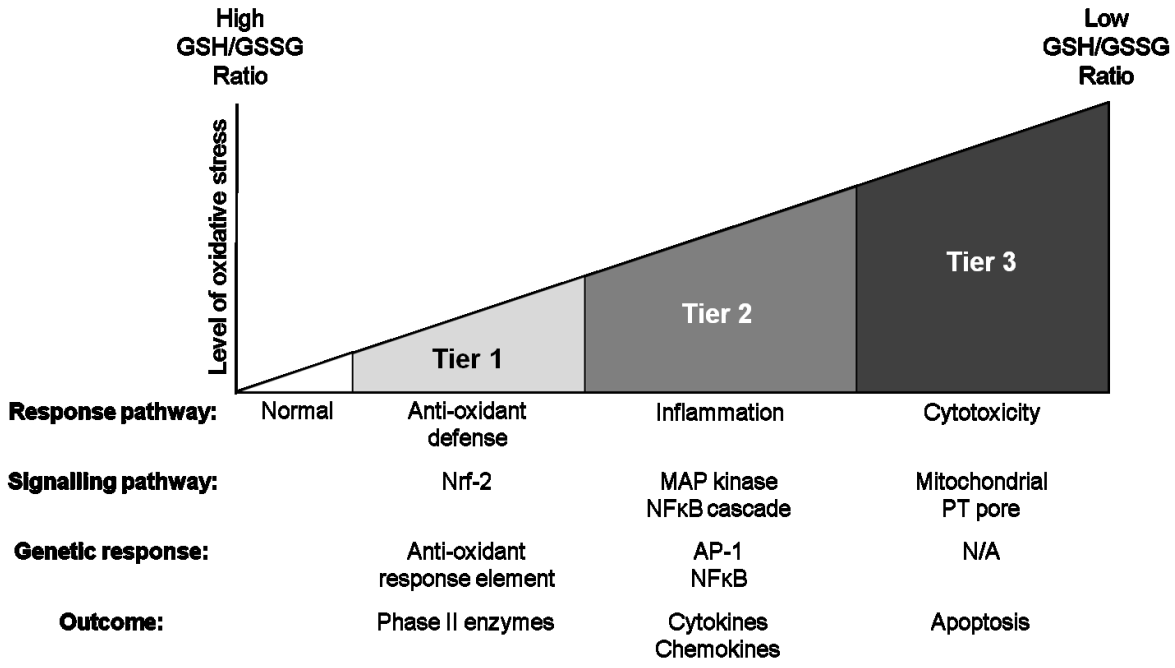


Figure 1.3.1 The hierarchical oxidative stress model. In tier 1, transcriptional activation by Nrf-2 of the anti-oxidant response element triggers phase II antioxidant enzyme release to restore cellular redox homeostasis. In tier 2, activation of the MAPK and NKκB cascades induces a pro-inflammatory response. In tier 3, perturbation of the mitochondrial PT pore and disruption of electron transfer results in cellular apoptosis or necrosis. A further outcome of oxidative stress not depicted in the above figure is genotoxicity via oxidative DNA damage. This is associated with mutagenesis, carcinogenesis and age related disease. Figure adapted from (Nel *et al*., 2006).

Inflammation and fibrosis

Inflammation is a common cellular response following NP exposure and can be both ROS-dependent and -independent (Nyga, Hart, & Tetley, 2015). This is a complex homeostatic response which has evolved to protect biological systems from harmful stimuli but which can also become harmful, as excess or inappropriate inflammation can result in tissue damage (Bhattacharya, Andón, El-Sayed, & Fadeel, 2013). Using murine models, an expansive list of NPs have been shown to induce inflammation in the lung; ZnO and Ag NPs increase pulmonary polymorphonuclear cells in bronchoalveolar lavage fluid (BALF) (Sayes, Reed, & Warheit, 2007; Silva *et al*., 2015), NiO NPs induce inflammatory cytokine release (Morimoto *et al*., 2010) and TiO_2 and SiO_2 activate the NLR pyrin domain containing 3 (NLRP3) inflammasome (Baron *et al*., 2015).

The rapid onset of pulmonary inflammation is an acute response to NP exposure, however long-term, these materials are associated with the development of lung fibrosis and tumours (Dailey *et al*., 2006). Fibrosis or scarring of the lung tissue occurs as a result of a persistent lung-damaging stimulus or the dysregulation of any stage in the tissue repair program (Wynn, 2011). Chronic exposure to NPs including TiO_2 and SWCNTs has been shown to induce fibroproliferative lesions and collagen deposition in the lung (Bermudez et al., 2004; Shvedova et al., 2008). Both inflammation and pulmonary fibrosis have also been associated with an increased risk of lung cancer (Hubbard, Venn, Lewis, & Britton, 2000).

These *in vivo* murine models have provided crucial information about the inflammatory and fibrotic potential of NPs however human models are required to determine whether these findings are likely to be relevant across species. Robust human *in vitro* models are therefore required, in concert with *in vivo* and *in silico* models, for effective NP hazard assessment.

Genotoxicity

Genetic instability triggered either by ROS, inflammation or continuing cycles of tissue damage/repair lead to cell metaplasia and atypia, key features of carcinogenesis (Gonzalez, Lison, & Kirsch-Volders, 2008; Shvedova et al., 2014). Inhaled particles have historically been associated with tumour formation; retention of inhaled crocidolite asbestos fibres at the parietal pleura is known to cause mesothelioma, and ambient particulate matter is a risk factor for lung cancer (Donaldson, Murphy, Duffin, & Poland, 2010; Knaapen, Borm, Albrecht, & Schins, 2004).

In a comparative *in vitro* study by Yang *et al*., (2009) carbon black (CB), carbon nanotubes (CNTs), silicon dioxide (SiO_2) and zinc oxide (ZnO) NPs all induced significant DNA damage as determined by the comet assay. However, the severity of the damage was greatly dependent on the exposure particle, with CNTs inducing the greatest DNA damage. Furthermore, studies have shown that TiO_2 NPs induce DNA-adduct formation in IMR-90 cells (human bronchial

fibroblasts) (Bhattacharya *et al*., 2009) and CNTs and graphite nanofibres are genotoxic in human bronchial epithelial BEAS 2B cells, as measured by the alkaline comet assay and the micronucleus assay (Lindberg *et al*., 2009). A long-term study of carbon nanomaterials administered to mice via pharyngeal aspiration found evidence of increased mutagenesis, but not increased tumour formation, one year post-exposure, supporting the potential genotoxic pulmonary effects of NPs (Shvedova et al., 2014).

1.4. Extra-pulmonary effects of engineered NMs

In addition to the pulmonary toxicity of inhaled nanoparticles, multiple epidemiological studies, *in vivo* and *in vitro* models have suggested that inhaled nanoparticles may have adverse extra-pulmonary effects, particularly when considering the cardiovascular system. Some NM may translocate to the circulation and other organs of the body, and others may have indirect systemic effects through the pulmonary release of mediators into the circulation (Choi *et al*., 2010; Naota, Shimada, Morita, Inoue, & Takano, 2009; Simeonova & Erdely, 2009). A number of *in vivo* studies aiming to discern the mechanism that may link NM and compromised cardiovascular health have been carried out and have demonstrated NM-induced atherosclerosis, thrombosis and altered cardiac function and rhythm (as reviewed by Shannahan, Kodavanti, & Brown, 2012). The potential mechanisms underlying this are summarised in Figure 1.4.1.

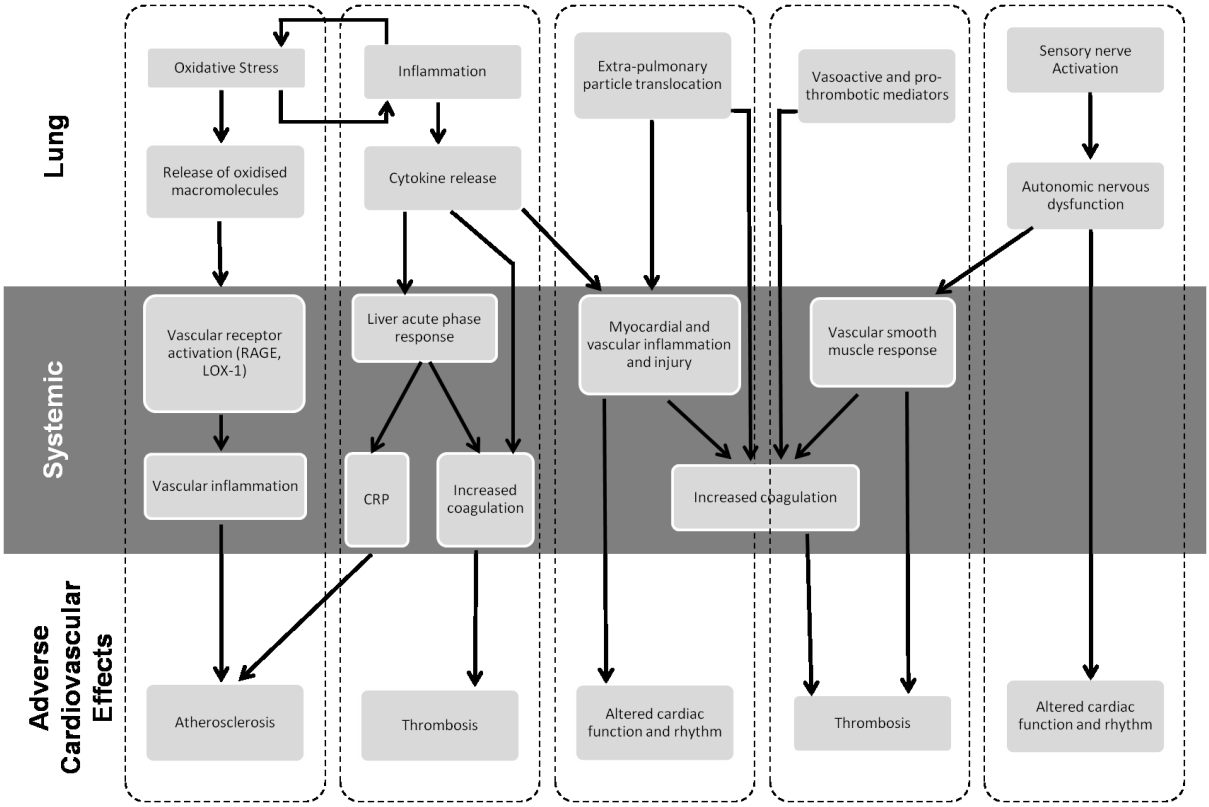


Figure 1.4.1 Proposed mechanisms of cardiovascular toxicity following NP and UFP pulmonary exposure. After inhalation, NP and UFP may trigger pulmonary inflammation and oxidative stress leading to increased systemic levels of oxidized macromolecules, cytokines, and vasoactive and prothrombotic factors. Alternatively NPs in the lung may alter cardiac function via autonomic nervous system dysfunction. NPs that translocate to the circulatory system could interact directly with the cardiovascular system potentially inducing a toxic response. Figure adapted from (Shannahan *et al*., 2012).

Direct cardiovascular toxicity via particle translocation

Upon deposition on the alveolar surface, NM and UFP encounter an extremely thin barrier separating them from the circulation, in places just one cell thick (Figure 1.4.2) (Li, Muralikrishnan, Ng, Yung, & Bay, 2010). It is thought that particles in the nanoscale are able to pass through this barrier following inhalation by paracellular or transcellular transport (Yacobi *et al*., 2010). The alveolar-capillary barrier is semi-permeable to allow the passage of fluid and macromolecules (Mehta, Bhattacharya, Matthay, & Malik, 2004). Material can pass through cells via defects in the plasma membrane, passive or facilitated diffusion across the membrane, or by endocytosis (Yacobi *et al*., 2010). Endocytic uptake via clathrin- and caveolae-mediated processes may not be ubiquitous for all NMs but does allow for intracellular particle movement,

and provide a mechanism by which NM may cross the alveolar-capillary barrier (Rejman, Oberle, Zuhorn, & Hoekstra, 2004). Rejman *et al* demonstrated that 50 and 100nm fluorescent microspheres were taken up by endocytic vesicles to a greater extent than their larger counterparts in the murine melanoma cell line B16-F10 (Rejman *et al*., 2004). Furthermore, Thorley *et al* described passive diffusion of 50nm polystyrene NPs (PLNPs) and clathrin- or caveolin-mediated endocytosis of larger 100nm PLNPs in human alveolar type-1 epithelial cells. (Thorley, Ruenraroengsak, Potter, & Tetley, 2014). SWCNTs and gold NPs have also been shown to be actively transported into the cell via endocytosis (Cheng *et al*., 2008; Jin *et al*., 2008; Porter *et al*., 2007; Rejman *et al*., 2004). Subsequent exocytosis of the NM on the basolateral surface of the alveolus rather than the apical point of entry would hypothetically enable entry into the capillaries surrounding the lung (Sakhtianchi *et al*., 2013).

Paracellular translocation of particles could be exacerbated by pulmonary inflammation triggering changes in membrane permeability allowing for further particle movement (Harder *et al*., 2005). A number of nanoparticles including TiO_2, Fe_2O_3 ZnO have been shown to be cytotoxic or to disrupt the integrity of the tight junctions, potentially enabling the paracellular transport of particles (Al-Qadi, Grenha, Carrion-Recio, Seijo, & Remunan-Lopez, 2011; Apopa *et al*., 2009; Kim *et al*., 2010). Further investigation into the permeability of the alveolar-capillary barrier following NP exposure is required considering the probability of increased paracellular transport influencing particle translocation.

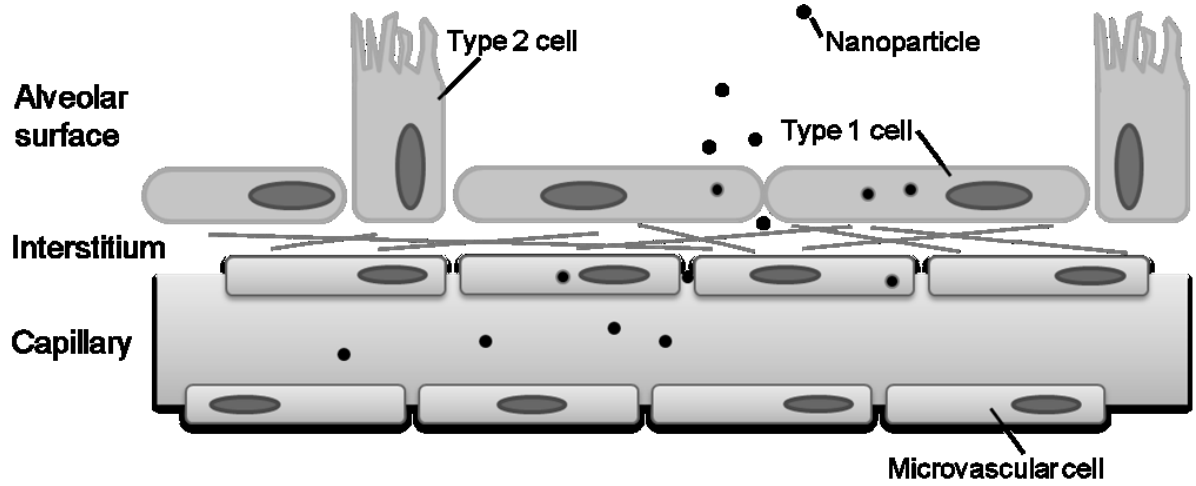


Figure 1.4.2 Particle translocation across the alveolar epithelium to the circulation. It is thought that nanoparticles may pass this barrier via either paracellular or transcellular movement. The rate of nanoparticle uptake or increased barrier permeability is therefore likely to impact on particle translocation.

Translocation of particles into the circulation may have downstream cardiovascular effects via direct NP interaction with circulating cells. In *in vitro* studies of human platelets, it has been shown that SWCNTs can induce partial platelet aggregation. Interestingly, the same study demonstrated that a mix of amorphous carbon and C60 carbon spheres resulted in complete platelet aggregation and granular release (Radomski *et al*., 2005), suggesting size and shape play an important role in the physiological response. It was hypothesised that CNTs stimulate aggregation by mimicking molecular bridges involved in platelet–platelet interactions or alternatively that this is an effect of the electrical charge of the particle or an indirect effect of ROS present on the CNT surface. A further *in vivo* study using Wistar-Kyoto rats confirmed that PM (50μg/ml) instilled into the femoral vein induced thrombosis, indicated by the analysis of blood flow in the carotid artery using an ultrasonic flow probe (Radomski *et al*., 2005). Similar findings have also been observed using polystyrene nanoparticles (PLNPs) (Smyth *et al*., 2014). In this study increased platelet aggregation was observed both in *in vitro* and *in vivo* models however the severity of the reaction was dependent on both NP size and surface chemistry. Of the 50nm PLNPs tested, carboxyl-modified cPLNPs were the most potent, and unmodified

uPLNPs the least, whereas comparison of 100nm PLNPs showed uPLNPs to be the most potent and cPLNPs the least (Smyth *et al*., 2014).

Direct NP interactions with the heart following inhalation are unlikely to initiate toxicity due to factors such as the relatively low number of particles passing the blood-gas barrier, the dilution effect due to distribution through the blood, and the likely uptake of any blood-borne particles by the reticulo-endothelial system (Seaton et al., 2010). Intravenously administered NPs would have access to the heart via the vasculature, however there is still little evidence to suggest that direct cardiac toxicity (eg. via cardiomyocyte dysfunction) is responsible for the adverse cardiovascular effects observed following NP exposure. It is therefore deemed far more likely that toxicity as a result of direct NP interaction with the vascular system is due to responses in circulating cells, as described above, or endothelial cells. Endothelial activation as a result of direct or indirect NP exposure is a serious risk factor for developing a number of cardiovascular diseases including hypertension, coronary artery disease, chronic heart failure, peripheral artery disease, diabetes, and chronic renal failure (Endemann & Schiffrin, 2004). The endothelium is known to release both pro-inflammatory cytokines such as IL-6, IL-8 and TNFα and pro-thrombotic mediators such as tissue factor, thrombin, fibrinogen, von Willebrand factor and plasminogen activator inhibitor-1 (PAI-1) upon activation, all of which may be implicated in thrombosis, and possibly myocardial infarction if the thombus ruptures (Shannahan *et al*., 2012; Shantsila & Lip, 2009; Sun *et al*., 2011; Walker *et al*., 2009). As such, these findings have raised important concerns regarding the use of nanomaterials in medicines which will have ready access to the circulatory system. Robust human models are therefore required to test the safety of these potential nanomedicines, especially considering their potential to interact with the endothelium.

Indirect cardiovascular toxicity via pulmonary mediators

Aside from the potential of nanoparticles to translocate into the circulation following inhalation, there are also less obvious, but equally concerning, indirect effects of NP inhalation. It is hypothesised that some of the adverse cardiovascular events observed following pulmonary exposure may be initiated by local events in the lung. These events are thought to include the release of inflammatory mediators, ROS and oxidised proteins and macromolecules. Oxidised proteins and macromolecules activate the receptor for advanced glycolation endproducts RAGE and leptin-like oxidized low-density lipoprotein receptor-1 LOX-1. Activation of RAGE initiates leukocyte adhesion and contributes to the development of atherosclerosis while LOX-1 activation causes increased vascular inflammation through monocyte and foam cell recruitment eventually leading to atherosclerosis (Shannahan *et al*., 2012).

Cytokines released into the circulation as a consequence of pulmonary toxicity are implicated in endothelial activation, myocardial inflammation and activation of the complement system. Subsequent release of pro-thrombotic and vasoactive mediators induced by increased levels of circulating pro-inflammatory cytokines can also induce events including thrombosis, atherosclerosis and altered cardiac rhythm, (Nemmar, Hoylaerts, Hoet, & Nemery, 2004; Shannahan et al., 2012). Many of the inflammatory mediators observed following NP exposure, such as TNFα and IL-6, are associated with the release of pro-thrombotic factors and the development of cardiovascular disease (Xu, Lupu, & Esmon, 2010).

Mediators released as a consequence of pulmonary toxicity are also implicated in the induction of the acute phase response (Bourdon *et al*., 2012; Saber *et al*., 2014; Sun *et al*., 2011). The acute phase response is a systemic innate immune response initiated when inflammatory cytokines stimulate the liver to produce a number of proteins including C-reactive protein (CRP), Fibrinogen and Factor VII, all of which are known risk factors for myocardial infarction (Shannahan *et al*., 2012). The acute phase response has been shown to be initiated following the inhalation of a number or materials; increased CRP was observed in individuals exposed to

high levels of PM10 (Seaton et al., 1999), and rodents exposed to materials including diesel exhaust particles, amphibole asbestos and SWCNTs showed evidence of an acute-phase response (Donaldson, Stone, Seaton, & MacNee, 2001; Shannahan et al., 2012; Simeonova & Erdely, 2009). The acute phase response is associated with diabetes, myocardial infarction and cardiovascular disease (Shannahan *et al*., 2012).

Changes in the levels of the vasorelaxant nitric oxide (NO) and the vasoconstrictor endothelin have also been linked with NP inhalation exposure. NO is produced in the lung following PM exposure (Becher *et al*., 2007; Yokohira *et al*., 2009); however, it has a short half-life and is therefore unlikely to have a vasorelaxant effect on the systemic vasculature (Shannahan *et al*., 2012). In the vasculature, NO is primarily produced by endogenous nitric oxide synthase (eNOS) within endothelial and smooth muscle cells. Although there is some evidence from rodent studies that DEP exposure inhibits NO-dependent vasorelaxation (Knuckles, Lund, Lucas, & Campen, 2008), the literature is not sufficient to determine the extent of, or mechanisms underlying NP induced vasoconstriction. Particle-induced vasoconstriction and the blood pressure changes this induces could result in impaired cardiac function, and potentially, thrombus rupture (Shannahan *et al*., 2012). It is clear that it is crucial to comprehensively study the local pulmonary response to NP exposure to fully understand what systemic events may be initiated.

1.5. Carbon nanotubes

One of the most promising and economically important of the engineered NPs are carbon nanotubes, first described by the Japanese electron microscopist Iijima in 1991 (Iijima, 1991). These are fullerene related structures which consist of multiple cylindrical sheets of graphene. The arrangement of the carbon atoms within the structure lends these materials astonishing mechanical, electrical and thermal properties (Lau & Hui, 2002). Due to these unique properties they have gained significant commercial interest and are currently being used and

developed for incorporation into diverse areas including construction, electronics and even medicine (De Volder, Tawfick, Baughman, & Hart, 2013). By 2016 the global market for CNTs is projected to increase from $192 million in 2011 to $527 million, of which the market for multi-walled carbon nanotubes (MWCNTs) represents the greatest proportion at 41.56% ($292 million) (data from BCC Research, USA, http://www.bccresearch.com/). The increase in CNT production has however ignited health concerns surrounding both the workplace exposure risk and potential exposure risk to the general public (Donaldson et al., 2006).

Carbon nanotubes in medicine

Of particular relevance to purposeful human exposure is the use of carbon nanotubes in medicine, as this provides a direct route of entry for CNTs into the human body. Carbon nanotubes have attracted global attention as potential therapeutic agents due to their unique properties, including their ability to interact with macromolecules such as protein and DNA through either covalent or adsorptive interactions (Ali-Boucetta & Kostarelos, 2013a; Bianco, Kostarelos, Partidos, & Prato, 2005; Foldvari & Bagonluri, 2008). They have been proposed for use as biosensors (Atashbar, Bejcek, Singamaneni, & Santucci, 2004; Balasubramanian & Burghard, 2006; Wohlstadter *et al*., 2003), ion channel blockers (K. H. Park, Chhowalla, Iqbal, & Sesti, 2003), biological scaffolds (Abarrategi *et al*., 2008; Edwards, Werkmeister, & Ramshaw, 2009; Zanello, Zhao, Hu, & Haddon, 2006) and drug delivery molecules (Foldvari & Bagonluri, 2008; Scheinberg *et al*., 2013; Wong *et al*., 2013).

In oncology research, it has been demonstrated that functionalised carbon nanotubes are able to target tumour tissue; Liu *et al* (2007) used a potent integrin $\alpha_v\beta_3$ antagonist to actively target single walled carbon nanotubes to integrin $\alpha_v\beta_3$–positive U87MG human glioblastoma cells injected into a mouse. Furthermore, CNTs can passively accumulate in tumour tissue as a result of poorly formed, leaky vasculature supplying the rapidly proliferating tumour and diminished lymphatic drainage, a phenomenon known as the enhanced permeability and retention (EPR)

effect (X. Liu *et al*., 2011; Maeda, 2001). CNTs can be functionalised with specific anticancer therapeutics, many of which have shown to have increased efficacy when bound to CNTs, due in part, to the ability of CNTs to traverse biological membranes, retaining their drug load until inside the cell (Ali-Boucetta *et al*., 2008; Feazell, Nakayama-Ratchford, Dai, & Lippard, 2007; Pastorin *et al*., 2006; Wong *et al*., 2013). Liu, *et al*., (2008) demonstrated that paclitaxel (PTX), a widely used chemotherapeutic drug, was more efficacious at suppressing tumour growth in a murine breast cancer model, when conjugated to PEG chains on SWCNTs than the clinical drug formulation Taxol. This was attributed to improved solubility, longer circulation time and increased tumour uptake of PTX conjugated PEG-SWCNTs. It has also been demonstrated that it is possible to destroy tumour tissue using CNTs by exploiting their ability to absorb and convert electromagnetic radiation into heat energy using photothermal therapy (Moon, Lee, & Choi, 2009; Zhou, Wu, Wu, Chen, & Xing, 2011)-

In drug delivery, CNTs have been used to control and target therapeutics to improve the pharmacological activity of bioactive molecules whilst simultaneously diminishing off-target effects (Wong *et al*., 2013). In addition to chemotherapeutic drugs, CNTs have been developed to carry a range of molecules with medicinal value including antimicrobials (Benincasa *et al*., 2011; Wu *et al*., 2005), vaccines (Pantarotto *et al*., 2003), antibodies (McDevitt *et al*., 2007) and siRNA (Podesta *et al*., 2009). Carbon nanotubes are, by nature, very insoluble molecules which can present difficulties when generating drug delivery formulations (Bianco *et al*., 2005). CNTs are therefore not only functionalised with the intention of attaching therapeutic molecules but they are also functionalised to improve their solubility. There are a number of different approaches to improving the solubility of CNTs, however many of these methods severely affect the graphitic framework of the CNT molecule (Shu Chen *et al*., 2014; Menzel *et al*., 2010). Traditional wet-chemical reactions allow the introduction of a wide range of functional surface groups, however these also frequently damage the intrinsic CNT properties of interest. Furthermore these methods are time consuming, inconvenient and generate large volumes of waste consisting of toxic organic solvent or corrosive mineral acids which can significantly limit

the economical viability of these approaches (Menzel *et al*., 2010). Thus, there is a drive to discover alternative methods of generating functionalised CNTs with improved solubility, for biomedical applications, and discovering the bioreactivity of these molecules (Shu Chen *et al*., 2014).

Toxicology of carbon nanotubes

Due to the increasing utilisation of carbon nanotubes in a number of industries there has been an increased research effort to understand the toxic potential of these materials. Initial safety concerns were raised due to the fibrous nature of the material, with many drawing comparisons between CNTs and the known carcinogenic fibre, asbestos (Donaldson et al., 2013). Initial results were indeed concerning as granuloma formation was observed following CNT exposure in murine inhalation studies (Lam, James, McCluskey, & Hunter, 2004; Ma-Hock *et al*., 2009). Furthermore, early murine studies showed that CNTs were persistent in the lung for up to 60 days post-exposure and induced pulmonary inflammation, oxidative stress and early onset of lung fibrosis (Muller et al., 2005; Shvedova et al., 2005). It has since been shown however that CNT toxicity is a complex process with a number of factors influencing the bioreactivity of the material, including CNT length, presence of metal impurities, surface modifications and structure (Liu, Zhao, Sun, & Chen, 2013).

Increasing research has demonstrated that one of the most important factors underlying CNT toxicity is the degree of impurities, especially catalyst metal contaminants such as the transition metals iron, yttrium, nickel, molybdenum and cobalt (Liu *et al*., 2013). CNTs with fewer metal impurities have been shown to be less toxic than their impure counterparts, an effect which has been hypothesised to be due to the oxidative nature of the impurities (Fenoglio *et al*., 2008; Ge, Li, *et al*., 2012). Similarly, long carbon nanotubes are thought to be more toxic, due in part to the inability of macrophages to successfully engulf and remove these particles (Sato *et al*., 2005; Sweeney *et al*., 2014). Short multi-walled CNTs or single-walled CNTs have been shown by

Yamashita *et al* (2010) to induce less DNA damage and inflammation than long multi-walled CNTs in an *in vitro* lung carcinoma cell line. CNTs with higher stiffness and rigidity also tend towards agglomeration, another feature which has been associated with increase CNT toxicity (Wick *et al*., 2007). CNTs for medical application have therefore been developed that not only contain functional groups and are easily dispersed, but also contain low levels of impurities, are of a shorter length and exist as individual fibres rather than large agglomerates (Battigelli, Ménard-Moyon, Da Ros, Prato, & Bianco, 2013; Kostarelos, 2008).

Outside of the pulmonary system, *in vivo* studies have demonstrated that inhaled CNTs can induce vascular thrombosis, altered baroreflex, atherosclerosis and aortic mtDNA damage (Legramante *et al*., 2009; Z. Li *et al*., 2007; Radomski *et al*., 2005). Li *et al* (2007) observed that intratracheally administered CNTs elicited an oxidative response in the vasculature of mice, and furthermore, in an ApoE-/- mouse model, SWCNTs administered over an 8 week period significantly increased atheroma formation. Similarly, *in vivo* murine studies demonstrated that intra-tracheally instilled MWCNTs induced pulmonary inflammation, resulting in platelet activation and P-selectin mediated thrombosis (Nemmar et al., 2007). The adverse cardiovascular health observed following inhalation exposures may be due to the interconnectivity of the pulmonary and cardiovascular systems where inflammatory signals are readily relayed, however it has also been hypothesised that this effect may be due to direct CNT interactions with the cardiovascular system following CNT traversal of the blood-gas barrier (Shannahan *et al*., 2012), however this is yet to be fully elucidated.

Systemic distribution of CNTs

Due to their small diameter, carbon nanotubes penetrate deeper into the lungs, while very long fibres (>20μm) predominantly remain in the upper airways (Hoet, Brüske-Hohlfeld, & Salata, 2004; Lippmann, 1990; Oberdörster, 2000, 2002). Mercer *et al* (2013) discovered that CNTs administered to mice via inhalation were evident 12 days after exposure, not only in lung

associated tissues (lymph nodes, diaphragm and chest wall) but also in extra-pulmonary organs. Individual MWCNT fibres were observed to be persistent in the brain, liver, kidney and heart of mice at 336 days following the initial exposure. A number of other studies have also observed CNTs in distant organs following pulmonary exposure using a variety of approaches including radiolabelled CNTs (Czarny *et al*., 2014) and raman spectroscopy (Ingle *et al*., 2012).

Conversely, intravenous administered CNTs are frequently observed in large quantities in the pulmonary region (Chen *et al*., 2015). CNTs are thought to become initially trapped in the lung due to the large reservoir of blood in the area, and subsequent entrapment in the fine pulmonary microvasculature (Yang *et al*., 2007). CNT length typically exceeds the renal excretion threshold; only small CNTs (<50 nm in length, diameter 1–2 nm) are thought to be excreted via the urine (Liu, Davis, *et al*., 2008).

Functionalisation of CNTs may also influence their biodistribution as well as their reactivity; pristine or non-covalently functionalised CNTs were shown to accumulate predominately in the mouse liver, spleen and lungs following intravenous instillation whereas covalent functionalisation of CNTs promoted urinary excretion (Ali-Boucetta & Kostarelos, 2013b; Jain *et al*., 2011). A second study showed that intravenously injected MWNTs showed less accumulation in tissues following a higher degree of MWNT-NH_3^+ functionalisation. Pristine MWNTs coated with serum proteins prior to injection accumulated almost entirely in the lung and liver in large dark clusters (Lacerda *et al*., 2008). Al-Jamal *et al* (2012) also described how the degree of CNT functionalisation can affect the biodistribution of intravenously administered material in mice. The organ distribution and excretion profile was dependent on the degree of chemical functionalisation, which was hypothesised to impact on the number of CNTs present as individual fibres. Only individualised CNTs with a diameter of 20-30nm could be excreted via the kidney, while liver accumulation was attributed to *in vivo* CNT bundling. All functionalised MWNTs were observed within the lung however some MWNTs translocated from the lung to

the spleen whilst those present as large clusters remained in the lung up to 30 days post-exposure (Al-Jamal *et al*., 2012).

These *in vivo* studies provide clear evidence that both intratracheally and intravenously administered CNTs may have a significant degree of interaction with the pulmonary microvasculature. Current knowledge surrounding the interaction of CNTs with the human microvasculature is however extremely sparse and there is a lack of understanding on the importance of CNT functionalisation in is this reaction. Due to the importance of cardiovascular events in CNT-mediated toxicity and the significance of endothelial activation it is therefore important to understand both the epithelial and the endothelial toxicity of these materials.

1.6. Rationale

CNTs have been shown to induce adverse cardiovascular events following both pulmonary and intravenous exposure in animals; however, how this relates to human exposure, and the mechanisms underlying the adverse events, are currently unclear. Inhaled CNTs are hypothesised to induce indirect effects as a result of pulmonary toxicity but have also been shown to translocate to systemic organs providing the opportunity for direct CNT interaction with the cardiovascular system.

Due to the increased interest in the potential use of CNTs for biomedical applications, and evidence that CNTs introduced intravenously can become entrapped in the microvasculature surrounding the lungs, it is crucial to understand the nature of CNT interactions at the blood-gas barrier to appreciate the safety risks of these materials. Thus this study will investigate the interaction of a suite of CNTs at both the alveolar and vascular interface using *in vitro* human cell models.

As CNTs are inherently non-soluble it is necessary for these materials to be modified to improve their solubility for use as medicinal products. This work will describe the bioreactivity of CNTs made water-stable using the following methods:

- a conventional acid-oxidation method (generating CNT structural changes),
- a novel grafting-from thermochemical reaction to improve water-stability through covalent functionalisation of the CNT surface without damaging the structural integrity of the CNT
- a non-modified CNT control.

2. METHODS

2.1 Ethics statement

All primary tissue used in this study was obtained following resection for lung carcinoma. Written informed consent was obtained from patients for all samples and the study was carried out with the approval of the Royal Brompton and Harefield Ethical Committee (Ref: 08/H0708/73). Transfer of primary tissue was through the BRU Biobank which is supported by the National Institute for Health Research (NIHR).

2.2. Cell isolation and culture

Culture of immortalised human alveolar type 1-like epithelial cells (TT1s)

Immortalised human alveolar type 1-like epithelial cells (TT1) (Kemp *et al*., 2008) were cultured on tissue culture plates in Defined Cell Culture Medium-1 (DCCM-1) media (Biological Industries, Beit-Haemek, Isreal) containing 10% newborn calf serum (NCS), 100 U/ml penicillin, 100 mg/ml streptomycin and 2 mM glutamine (Sigma-Aldrich, Poole, UK). For experiments TT1 cells were seeded at 24,000 cells per cm^2 and grown to confluence prior to carbon nanotube (CNT) exposures.

Isolation and culture of primary human alveolar type-2 epithelial cells (AT2s)

Alveolar type 2 epithelial cells (AT2) were isolated from healthy regions of lung tissue following surgical resection for lung carcinoma using the protocol described by Witherden and Tetley (Witherden & Tetley, 2001). Briefly, to remove excess blood and macrophages, lung sections were perfused by injection of Hank's Balanced Salt Solution (HBSS) (Sigma-Aldrich, Poole, UK) until the draining lavage ran clear. The tissue was then digested with trypsin (Sigma-Aldrich, Poole, UK) and DNase (Sigma-Aldrich, Poole, UK), followed by mechanical disruption. This

tissue was then passed through a series of filters of decreasing size to remove large cell/tissue debris. The cell suspension was then centrifuged and resuspended in DCCM-1 media, and AT2 cells were purified by differential adherence to remove any remaining macrophages.

Cells were seeded at a concentration of 210,000 cells per cm^2 on tissue culture plates that had been previously treated with 1% PureCol collagen solution (Advanced BioMatrix, San Diego, USA) and allowed to air dry. Cells were cultured in DCCM-1 containing 10% newborn calf serum (NCS), 100 U/ml penicillin, 100 mg/ml streptomycin and 2 mM glutamine (Sigma-Aldrich, Poole, UK).

AT2s typically formed a monolayer 2-3 days after seeding; once a monolayer had formed the cells were then cultured in serum-free media for 24 hours prior to nanoparticle exposure. Experimental procedures were not performed on cells older than 7 days as typically there is a significant change from the AT2 to the AT1 phenotype beyond this time. Purity of AT2 monolayers was confirmed by positive staining for AT2 markers including alkaline phosphatase and surfactant proteins A and D (Section 3.2).

Isolation and culture of primary human pulmonary microvascular endothelial cells (HPMVECs)

HPMVECs were isolated from healthy regions of lung tissue following surgical resection. A mixed, mostly single cell population was achieved using the method described above. The cell suspension was transferred to a T-75 culture flask for 30 minutes to allow contaminating macrophages to adhere and the cell suspension was then transferred to a new T-75 for a further 90 minutes to allow HPMVECs to adhere. At this point non-adherent cells were removed and the media was replaced with Microvascular Endothelial Growth Media-2 (EGM-2 MV) (Lonza, Slough, UK). The flasks were cultured for 3-7 days until 70% confluent and endothelial cells were isolated using αCD31-conjugated Dynabeads.

Generation of αCD31-conjugated Dynabeads was achieved by incubating Dynabeads protein G (Invitrogen, Paisely, UK) with CD31 antibody (AbD Serotec, Kidlington, UK) using a modified

version of the manufacturers protocol (Invitrogen, Paisely, UK). Briefly, 50µl Dynabeads were suspended in 1ml 0.1% BSA in Dulbecco's PBS (buffer 1) and separated by magnetism. The supernatant was discarded and the resulting pellet was resuspended in 1ml buffer 1. Following a second magentic separation, the supernatant was discarded and Dynabeads were incubated with 2µg CD31 in buffer 1 with rotation for 10 minutes. CD31 conjugated Dynabeads were washed three times with 1ml buffer 1 prior to incubation with cells using the magnetic seperation method described above.

Cells were removed from culture flasks using TrypLE Select (Invitrogen, Paisely, UK) and centrifuged for 10 minutes at 490 x g. Pelleted cells were resuspended in 1ml buffer 1 and incubated with CD31-conjugated Dynabeads for 20 minutes at 4°C with gentle rotation. CD31 positive cells were then isolated using magnetism and washed 3 times in buffer 1. CD31 positive cells were then resuspended in EGM-2 MV, and cultured in tissue culture flasks.

Fresh EGM-2 MV was added every two days and HPMVECs were sub-cultured at a ratio of 1:6 with TrypLE select (Invitrogen, Paisely, UK) treatment of the confluent monolayer. After a second isolation with CD31-conjugated Dynabeads, cells were shown to be positive for endothelial markers including CD31, vascular endothelial (VE)-cadherin and endothelin-1(ET-1) (Section 3.2). For experiments, HPMVECs were seeded at 30,000 cells per cm^2 and grown to confluency prior to nanoparticle exposures.

Isolation and culture of human lung fibroblasts

Human lung fibroblasts (HLFs) were used as a control cell for the Endothelin-1 ELISA. These cells were isolated from healthy regions of lung tissue following surgical resection. A mixed, cell population was achieved by enzyme digestion and mechanical disruption as described in section 2.2 "Isolation and culture of primary human alveolar type-2 epithelial cells (AT2s)". The cell suspension was transferred to a T-75 culture flask for 30 minutes to allow contaminating macrophages to adhere and the cell suspension, plus 10% newborn calf serum, was transferred

to a new T-75 for a further 90 minutes to allow HLFs to adhere. At this point non-adherent cells were removed and the medium was replaced with Dulbecco's Modified Eagle's Medium (DMEM) containing 10% newborn calf serum (NCS), 100 U/ml penicillin, 100 mg/ml streptomycin and 2 mM glutamine.

HLFs were typically cultured for 7-14 days following isolation and medium was changed every three days. Cells were seeded at 30,000/cm^2 and used at passage 3-8.

The morphology of cultured cells was typical of HLFs and furthermore these cells did not express the endothelial cell marker endothelin-1 (ET-1), as determined using the Endothelin-1 ELISA (see page 67).

Culture of the monocytic cell line U937 and its use in HPMVEC-U937 co-cultures

The monocytic cell line U937 was used in the HPMVEC-U937 co-cultures, to assay monocyte adhesion to the endothelial surface following MWNT exposure. Passage 24 to 30 of U937 were cultured in suspension in RPMI media containing 10% foetal calf serum (FCS), 100 U/ml penicillin, 100 mg/ml streptomycin and 2 mM glutamine. Cells were a kind gift from Miss Agata Nyga.

For the HPMVEC-U937 co-cultures, HPMVECs were cultured as described in section 2.2 "Isolation and culture of primary human pulmonary microvascular cells (HPMVECs)" in a 24 well plate. At confluency, HPMVECs were exposed to MWNTs as described in section 2.3 for 4 hours, followed by a wash with pre-warmed PBS. At this stage HPMVEC were incubated with fluorescently-labelled U937 cells.

U937 cells were fluorescently labelled by incubating the U937 cell suspensions (500,000 cells/ml) with Alexa Fluor 488-wheat germ agglutinin (WGA) (Invitrogen, Paisely, UK) at 10μg/ml for 15 mins. The cells were then washed by centrifugation for 10 minutes at 490 x g followed by pellet resuspension in 10ml PBS. This wash step was then repeated and following a

third centrifugation for 10 minutes at 490 x g the pellet was resuspended in RPMI media containing 10% foetal calf serum (FCS), 100 U/ml penicillin, 100 mg/ml streptomycin and 2 mM glutamine. 500,000 U937 cells were applied to each well of the MWNT-exposed HPMVEC cultures and the cells were co-cultured for 3 hours at 37ºC. The supernatant was then removed and cells were washed with pre-warmed PBS to removed non-adherent cells. Cells were fixed with 4% paraformaldehyde (PFA) (Sigma-Aldrich, Poole, UK) for ten minutes before three further PBS washes. Adherent fluorescent cells were visualised using the Zeiss Axiovert 200 fluorescent microscope.

2.3. Nanoparticle preparation

In order to attach functional groups to the surface of MWNT, a novel method was employed that involved a series of chemical reactions. This was carried out by Dr Shu Chen and Hu Sheng under the supervision of Prof Milo Shaffer at Imperial College London (Shu Chen *et al*., 2014)

MWNTs (diameter 12.1 nm, s.d. 3.7) synthesised via chemical vapour deposition (CVD) were purchased from Arkema SA (Lacq-Mourenx, France). MWNT functionalisation was performed using a novel thermochemical grafting method. Briefly, this involved heating the MWNTs to 1000°C under vacuum to create "activated" MWNTs. The heat activation of MWNTs exploits existing defective groups on the MWNT surface, which decompose at high temperatures and generate free radicals (Menzel *et al*., 2010). After heat activation MWNTs are cooled under vacuum and incubated with the reactant overnight to allow for functionalisation of the MWNT through covalent grafting of monomers. Any reactant that has not grafted to the MWNT surface is removed through a series of filtrations and washes. Details of the functionalised MWNTs and nomenclature used in this study can be found in Appendix I (Shu Chen *et al*., 2014).

An acid oxidised (AO)-MWNT sample was also included in the study as AO-MWNT are the most commonly used MWNT used in biological studies. AO-MWNTs remain dispersed in an aqueous

medium and have a large number of highly reactive –COOH groups on the nanotube surface providing sites for surface functionalisation.

To generate AO-MWNTs, a mix of sulphuric acid and nitric acid (3:1) was heated to 120°C in the presence of MWNTs for 30 minutes. Carbonaceous debris was removed using a base wash, and the AO-MWNTs were purified using a series of washes (Shu Chen *et al*., 2014).

Sample	Sample Code	Zeta-potential (mV) in pH7 HPLC water	Grafting ratio (wt%)	IEP	D/G ratio
As Received	AR	-10.0±1.6		4.9	1.09±0.03
Thermochemically treated control	TTC				
Poly(4-vinylpyridine)	P(4-VP)	-0.1±6.4	4.1	7.0	1.13±0.02
Poly(N-methyl 4-vinylpyridine iodide)	P(M4-VP)	8.7±2.4	8.7	9.8	1.16±0.03
Poly((Poly)ethyleneglycol methacrylate)	P(PEGMA)	-7.8±5.3	18.3	4.6	1.14±0.09
Poly(methacrylic acid)	P(MAA)	-17.2±1.3	3.4	4.3	1.04±0.07
Acid Oxidised	AO				1.51±0.09

Table 2.3.1 Summary of f-MWNTs used in the study. Zeta potential is a key indicator of the stability of colloidal dispersions, grafting ratio is an indicator of the ratio of the weight of functional groups to the weight of the MWNT, isoelectric point (IEP) is the pH at which the f-MWNT carries no net electrical charge and the D/G ratio is achieved using Raman spectroscopy and provides information on the degree of damage to the MWNT structure.

MWNTs were diluted to a stock concentration of 1mg/ml in DCCM-1 cell culture medium, vortexed for 1 minute and sonicated in a water bath (42 kHz, 135 W, VWR International, USA) for 10 minutes. MWNTs were then diluted to the required concentration 0-50μg/ml in DCCM-1 medium, and sonicated briefly immediately prior to application to the cells.

Where a single concentration was used to compare the effects of f-MWNTs, a concentration of 10μg/ml was chosen as this reflects a concentration that is being used in rodent studies investigating the safety of MWNTs for imaging, biodistribution studies and direct tumour

injection (Pacurari *et al*., 2012). To study the hepatotoxicity of MWNT, Ji *et al* (2009) intravenously administered MWNT to Kunming mice at a dose of 250μg - 1.5mg MWNT/ml blood (10-60mg/kg b.w., ~25g b.w., 1ml blood/animal). In addition, Deng *et al* (2007) studied the translocation and fate of MWNT also using Kunming mice and doses from 10μg to 2mg MWNT/ml blood with no observed mortality. Lacerda *et al* (2008) studied MWNT distribution in nude rats following a 20μg MWNT/ml blood exposure (300μg MWNT/rat, ~200g b.w., 15ml blood/animal). Xu *et al* 2012 used a lower dose range of 0.67-2.67μg MWNT/ml blood (50-200μg/kg b.w., ~200g b.w., 15ml blood/animal), however the higher concentration induced a significant exacerbation of atheromatous lesions and lipid deposition in the aortic intima ($p<0.01$). The concentration of 10μg/ml was therefore deemed to be a reasonable exposure dose which is comparable to many *in vivo* studies.

2.4. Antioxidant treatment of cells

To test the effect of antioxidants on cell reactivity, cells were treated with either 5mM N-acetylcysteine (NAC), 1mM glutathione (GSH) or 100μM ascorbic acid for 30 mins prior to MWNT exposure. MWNT were resuspended in medium containing the aforementioned concentrations of antioxidants for the duration of the experiment.

2.5. Alkaline phosphatase assay

In order to confirm the phenotype of AT2 cells, alkaline phosphatase (AP) staining was performed. Alkaline phosphatase staining is widely accepted as a positive marker for the alveolar type 2 epithelial cell (AT2) phenotype (Witherden & Tetley, 2001; Witherden et al., 2004). In the presence of fast red violet LB salt, alkaline phosphatase will hydrolyse napthol-AS-bisphophate to produce a red precipitate. The alkaline phosphatase assay was carried out as previously described (Witherden & Tetley, 2001); briefly, 10mg napthol-AS-bisphophate (Sigma-Aldrich, Poole, UK) was dissolved in 40μl dimethyl sulphoxide (Sigma-Aldrich, Poole,

UK) and diluted to a final volume of 10ml with alkaline phosphatase buffer (0.625M MgCl (Sigma-Aldrich, Poole, UK), 0.125M amino methyl propanol (Sigma-Aldrich, Poole, UK) in distilled water, pH 8.9). 10mg fast red violet LB salt (Sigma-Aldrich, Poole, UK) was added, the solution was vortexed and incubated at room temperature for five minutes, before being passed through a 0.22μm syringe filter. This solution was then immediately applied to the cells and incubated at 37°C for 20 minutes and the presence or absence of the stain was qualitatively assessed by light microscopy.

2.6. Angiogenesis/tube formation assay

Endothelial cells grown on BD Matrigel will spontaneously form tube like structures, therefore tube formation on BD matrigel can be used a marker of a positive endothelial cell phenotype.

BD Matrigel Basement Membrane Matrix (BD Biosciences, Oxford, UK) is extracted from the Engelbreth-Holm-Swarm (EHS) mouse sarcoma, and is a solubilised basement membrane rich in extracellular matrix proteins; its major component is laminin, followed by collagen IV and heparan. BD Matrigel Basement Membrane Matrix also contains a number of other cellular proteins which occur naturally in the EHS sarcoma, including TGF-beta, epidermal growth factor, insulin-like growth factor and fibroblast growth factor.

For the angiogenesis tube formation assay Matrigel was defrosted on ice and 10μl/well was transferred onto a μ-slide angiogenesis (Ibidi, Munich, Germany) using pre-chilled pipette tips. The gel was allowed to set at 37°C for 1 hour before 10,000 HPMVECs were added to each well in 50μl EGM-2 MV cell culture medium, in the presence or absence of carbon nanotubes. Images were taken every 30mins for 6 hours.

2.7. Immunocytochemistry

Immunocytochemistry was used to characterise cell phenotypes, as well as to study changes in cell morphology in response to MWNT treatment.

For immunocytochemical staining, TT1 cells and HPMVECs were grown to confluence on an 8 well Nunc® Lab-Tek® II Chamber Slide™ system (Thermo Fisher Scientific, East Grinstead, UK), AT2 cells were cultured on an 8 well µ-slide. All chamber slides were treated with 1% PureCol collagen solution (Advanced BioMatrix, San Diego, USA) and allowed to air dry prior to cell seeding. Further investigations were carried out in mono- and co-culture on permeable membrane supports (polyester, 1.12cm^2 growth surface area, 0.4µm pore size) (Appleton Woods, Brimingham, UK). Cells were washed in PBS and fixed with 4% paraformaldehyde (PFA) for ten minutes before three more PBS washes. HPMVEC cells were permeabilised with 0.2% TritonX in PBS for 15mins, AT2 and TT1 cells were permeabilised with 0.2% TritonX in PBS for 50mins. A blocking stage of one hour in 1% BSA in PBS was included before primary antibody incubation. Primary antibodies were diluted in PBS containing 1% BSA (1:200) and incubated with the cells overnight at 4°C. Cells were then washed three times with PBS and incubated with a flurochrome coupled secondary antibody in PBS containing 1% BSA (1:400) for one hour. Unbound secondary antibody was removed with three PBS washes and cells were mounted and nuclei counterstained with DAPI containing Prolong Diamond Antifade Mountant (Invitrogen, Paisely, UK). Permeable filters were nuclear stained with 1µg/ml Hoescht (Sigma-Aldrich, Poole, UK) followed by three PBS washes and mounting was achieved by cutting out the permeable filter, placing it onto a slide containing one drop of mounting media, covering the permeable filter with a second drop of mounting media and finally sealing with a cover slip.

Confocal images were obtained using the Leica SP5 inverted confocal microscope at the Facility for Imaging by Light Microscopy (FILM) at Imperial College London.

Primary antibodies

Mouse polyclonal anti-human surfactant protein A (SPA), mouse monoclonal anti-human surfactant protein D (SPD) and podoplanin (T1α) and rabbit monoclonal aquaporin-5 (AQP-5) were purchased from Abcam (Cambridge, UK). Mouse monoclonal anti-human CD44v6 and

CD31 (PECAM-1) were obtained from AbD Serotec (Kidlington, UK). Mouse monoclonal anti-human VE-cadherin and lysosome-associated membrane protein-2 (LAMP-2) were purchased from Santa Cruz (Heidelberg, Germany). Mouse monoclonal anti-human receptor for advanced glycation endproducts (RAGE) was purchased from Merck Millipore (Darmstadt, Germany) and rabbit polyclonal anti-human caveolin-1 from BD biosciences (Oxford,UK).

Secondary antibodies

The fluorochrome coupled secondary antibodies AlexaFluor 488 goat anti-rabbit, AlexaFluor 594 goat anti-rabbit, AlexaFluor 568 goat anti-mouse, AlexaFluor 555 goat anti-rabbit and AlexaFluor 350 goat anti-mouse were obtained from Invitrogen (Paisley, UK). FITC goat anti-mouse was purchased from BD Biosciences (Oxford,UK).

2.8. Viability assays

MTS viability assay

The MTS compound is reduced by dehydrogenase enzymes within living cells and can therefore be used as an indicator of metabolic activity and cell viability. In the presence of an electron coupling reagent the reduction of this salt yields a soluble formazan product, the absorbance of which can be measured using a spectrophotometer. In this study, cell viability was determined using the CellTiter 96® AQueous One Solution (MTS) reagent which contains the tetrazolium compound, 3-(4,5-dimethylthiazol-2-yl)-5-(3-carboxymethoxyphenyl)-2-(4-sulfophenyl)-2H-tetrazolium and the electron coupling reagent, phenazine ethosulfate (PES).

One hour prior to the end of the exposure period 1% Triton X was added as a control for 100% cell death. All exposures were performed in triplicate, and the assay was carried out according to the manufacturer's protocol. Briefly, conditioned media was removed and replaced with a 1:10 dilution of the MTS reagent in cell culture media. Following a 1 hour incubation at 37°C,

5% CO_2, media was transferred to a new 96 well plate and the absorbance was measured at 492nm using a spectrophotometer (Tecan Infinite F50 plate reader).

LDH (lactate dehydrogenase) cytotoxicity assay

LDH is present in the cytoplasm of all cells and is released into the cell culture supernatant following damage to the plasma membrane. As a result, the amount of LDH present in the cell culture supernatant is directly proportional to cell death. The LDH assay (Roche Applied Science, Mannheim, Germany) measures levels of the cytoplasmic enzyme lactate dehydrogenase (LDH).

LDH activity is determined using an enzymatic test; initially NAD^+ is converted to $NADH/ H^+$ by the LDH catalysed conversion of lactate to pyruvate. This is followed by the catalyst (diaphorase) depedent transfer of H/H^+ from $NADH/H^+$ to the tetrozolium salt INT which is then reduced to a formazan product (Figure 2.8.1). The absorbance of the formazan product can be determined using a spectrophotometer.

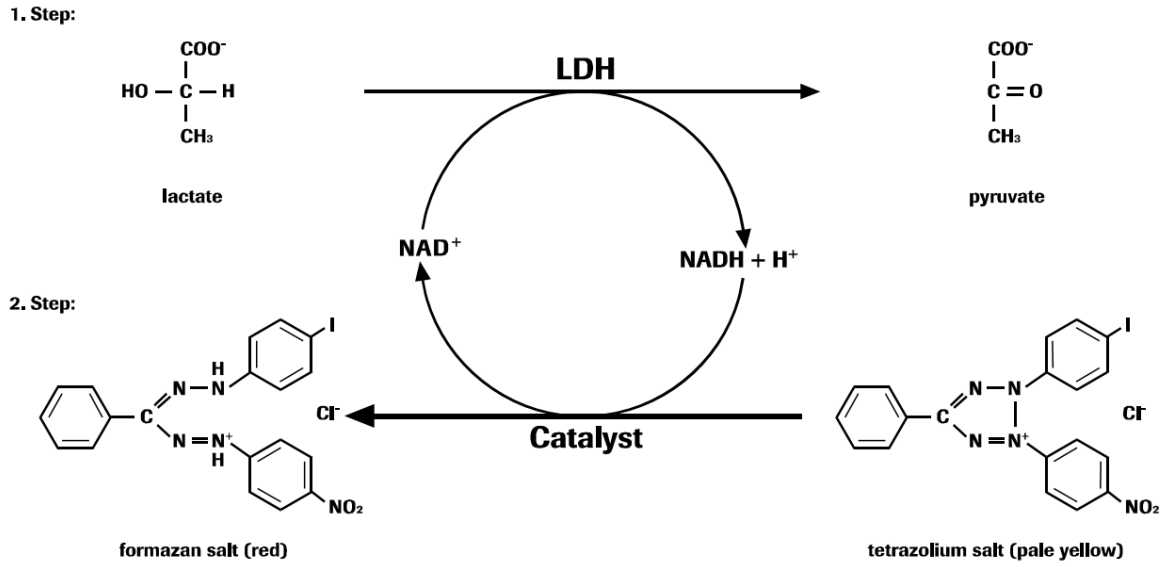


Figure 2.8.1 Schematic of the catalytic reaction involved in the LDH assay. Lactate is catalytically converted to pyruvate by the enzyme lactate dehydrogenase (LDH). This is followed by the catalyst (diaphorase) depedent transfer of H/H^+ from $NADH/H^+$ to the tetrozolium salt INT which is then reduced to a formazan product. The absorbance of the formazan product can be determined using a spectrophotometer. Image is taken from the LDH assay protocol (Roche Diagnostics Ltd., 2011).

The conditioned cell culture media removed prior to initiating the MTS assay were centrifuged at 1690 x g for 10mins in v-bottom plates to removed MWNT aggregates. The absorbance of the supernatant alone at 490nm was then obtained using a Tecan Infinite F50 plate reader. The LDH assay was then performed on the cell supernatants as per the manufacturers protocol, the background absorbance of the conditioned media alone was subtracted from the final absorbance value during analysis.

BrDU cell proliferation assay

The BrDU assay measures cell proliferation by quantifying incorporation of 5-bromo-2'-deoxyuridine (BrdU) in place of thymidine in the genomic DNA of replicating cells. Following cell fixation, DNA is denatured and an anti-BrDU-peroxidase enzyme is added. This binds to the newly synthesised cellular DNA and the immune complexes are detected by TMB substrate reaction. This produces a colorimetric result which correlates to the rate of DNA synthesis and can be read using a spectrophotometric plate reader.

Following MWNT treatment, cells were washed with PBS and incubated with BrDu labelling reagent for 2 hours. For this study the Cell Proliferation ELISA, BrdU (colorimetric) (Roche Applied Science, Mannheim, Germany) was used and the assay was carried out as per the manufacturer's protocol. Absorbance at 450nm was measured using a spectrophotometer (Tecan Infinite F50 plate reader).

2.9. Particle uptake

Transmission electron microscopy (TEM)

TEM analysis was used to study nanoparticle uptake and was carried out by Dr Shu Chen (Imperial College London) and detailed in (Shu Chen *et al*., 2014).

Functionalised MWNTs were first sonicated in a water bath (45 kHz, 80W, VWR International, USA) in high performance liquid chromatography (HPLC) grade water for 15 min with an initial concentration of 1mg/ml MWNT. The aggregates were removed by centrifugation (15 min at 10,000 x g), and the supernatants, containing dispersed MWNTs were used for cell exposure studies. MWNTs were diluted to 5µg/ml in DCCM-1 media and sonicated immediately prior to application to TT1 cells.

TT1 cells were seeded at 24,000 cells/cm^2 on 24 well plates and grown to 100% confluency. Cells were then serum starved for 24h before exposure to MWNT suspensions. After the 24h exposure period, the cells were rinsed with HEPES buffer and fixed with 2.5% glutaraldehyde for 1h. The samples were then post-fixed in 1% osmium tetroxide for 30 min. Each sample was then dehydrated in a graded ethanol series of 50%, 70%, 90% and 100% (volume ratio of ethanol to distilled H_2O) ethanol for 15 min (3x) each, at room temperature. After dehydration, samples were progressively infiltrated with 25% and 50% araldite resin/ethanol solution (Agar Scientific, UK) and each well was incubated for 15 min (2x), at room temperature. The specimens were then embedded into resin. The embedded cell monolayers were cut using an ultramicrotome with a 35° diamond knife to a thickness of 50-100nm. The obtained sections were observed in a JEOL 2000 transmission electron microscope operated at an accelerating voltage of 80kV. Multiple cells (>100 per sample) from three cell exposures were surveyed by TEM.

Confocal microscopy

Particle uptake in HPMVECs was assessed by confocal microscopy. HPMVECs were seeded at 30,000 cells/cm^2 on an 8 well Nunc® Lab-Tek® II Chamber Slide™ system (Thermo Fisher Scientific, East Grinstead, UK) and grown to confluency. Prior to seeding, chamber slides were treated with 1% PureCol collagen solution (Advanced BioMatrix, San Diego, USA) and allowed to air dry. HPMVECs were exposed to 10µg/ml AR, P(MAA), P(M4-VP), P(PEGMA) and AO-MWNTs

for 24 hours as detailed in section 2.3. Following exposure, cells were washed in PBS and fixed with 4% paraformaldehyde (PFA) for ten minutes before three more PBS washes. HPMVEC cells were permeabilised and immunostained using the lysosome-associated membrane protein-2 (LAMP-2) as detailed in section 2.7. Nuclei were counterstained with DAPI containing Prolong Diamond Antifade Mountant (Invitrogen, Paisely, UK).

Confocal images were obtained using the Zeiss LSM-510 inverted confocal microscope at the Facility for Imaging by Light Microscopy (FILM) at Imperial College London. Co-localisation of MWNT aggregates visualised by dark field microscopy and immunofluroescent LAMP-2 was assessed using the FIJI image analysis software (Schindelin *et al*., 2012).

2.10. Detecting reactive oxygen species (ROS)

The fluorescent dye CM-H_2DCFDA (Invitrogen, Paisely, UK) is a chloromethyl derivative of H_2DCFDA, a commonly used indicator for reactive oxygen species (ROS) in cells. The chloromethyl derivative of H_2DCFDA exhibits better retention in live cells, as once the dye has passively diffused into the cell, acetate groups are cleaved by intracellular esterases and thiol-reactive chloromethyl groups react with intracellular glutathione and other thiols. Once the dye is inside the cell, oxidation yields a fluorescent adduct that can be measured as an indicator of ROS in the cell.

The CM-H_2DCFDA dye was diluted to a concentration of 1mM in anhydrous DMSO, before being diluted to a working concentration of 1μM in HBSS. For this assay, cells were cultured in black 96 well plates as described in section 2.2. Following MWNT exposures, cells were washed three times in HBSS and incubated with the CM-H_2DCFDA dye for 45 minutes. Fluorescence was measured at excitation 485/20nm with emission 528/20nm, using the Synergy HT Multimode Microplate Reader.

2.11. Gene expression analysis

In order to quantify the expression of genes of interest, RNA was extracted from treated and untreated cells. Messenger RNA (mRNA) is an intermediary product that carries genetic information from DNA to the ribosome where it encodes the amino acid sequence of a protein product. mRNA is therefore a useful indicator of gene expression levels as, unlike protein, it is not subject to post-translational modifications.

RNA was converted by reverse transcription to the more stable complementary DNA (cDNA), a product which can be readily used in a real time quantitative polymerase chain reaction (qPCR). qPCR uses the signal from fluorescently labelled nucleotides; as nucleotides are incorporated into a DNA strand during the PCR reaction, the fluorescent signal will increase. The level of fluorescence in each PCR cycle is compared to internal controls to determine the relative expression levels of each gene. This study utilises SYBR green technology which employs a dye that fluoresces when bound to double stranded DNA; the more starting material, the earlier a fluorescent signal will be detected.

RNA extraction

Total RNA was isolated from HPMVEC, TT1 and AT2 cells using the E.Z.N.A Total RNA Kit 1 (Omega Biotek, Norcross, USA). For RNA isolation, HPMVECs were grown on 6 well plates and TT1 and AT2 cells on 24 well plates. One well per condition was used for each RNA extraction. To each well 350µl TRK lysis buffer was added, which achieves near instant lysis of the cell and release of RNA. Lysates were mixed with an equal volume of 70% ethanol and applied to a HiBand RNA column. The column was centrifuged at 10,000 x g for one minute, before undergoing a series of washes as detailed in the manufacturers protocol. Briefly, 500µl RNA wash buffer I was applied directly to the HiBand RNA column and centrifuged at 10,000 x g for 60 seconds, followed by 2 washes with RNA wash buffer II where 500µl was applied directly to the HiBand RNA column and centrifuged at 10,000 x g for 60 seconds. Finally the columns

containing bound and washed RNA were dried with a final centrifuge step and 50µl DEPC H_2O was applied directly to the centre of the column matrix and incubated for five minutes at room temperature. The column was transferred to a clean microcentrifuge tube and RNA was eluted with a final centrifuge step of 17,000 x g for one minute, and then immediately placed on ice.

RNA quantity and quality were measured using the Nanodrop Lite Spectrophotometer (Termo Scientific), before being transferred to -80°C for storage until analysis.

cDNA synthesis

During cDNA synthesis 1µg of RNA was used per 20µl reaction. cDNA synthesis was performed using the High capacity cDNA RT kit (Life technologies) according to manufacturer's instructions. Briefly, the 2X Reverse Transcription (RT) Master Mix is prepared on ice using the following reagents: 10X RT buffer, dNTP mix (100 mM), 10X RT random primers, MultiScribe™ reverse transcriptase and nuclease-free H_2O. 10 µL of 2X RT master mix is then added to each individual tube and mixed with 10 µL of RNA. The cDNA synthesis reaction then was carried out using a thermal cycler (Multigene, Labnet, Edison, USA), using the following program: 25°C for 10 minutes, 37°C for 120 minutes, 85°C for 5 minutes, followed by a 4°C hold. After synthesis, cDNA was diluted 1:5 with DEPC water and stored at -20°C until use.

Real-time PCR

For real-time quantitative PCR 4µl cDNA was used in a total volume of 20µl that contained 10µl 2X Power SYBR Green PCR Master Mix (Sigma-Aldrich, Poole, UK) and 1µM predesigned KiCqStart™ Primers (Table 2.11.1, Sigma-Aldrich, Poole, UK).

PCR reactions, consisting of 95°C for 10 min (1 cycle), 95°C for 15 s and 60°C for 1 min (40 cycles) were performed on an ABI 7500 Fast Real-Time PCR Instrument (Applied Biosystems). Melt curve analysis was used to confirm primer specificity (Appendix II). Data was analysed with ABI Prism 7500 V2.0.6 software and quantified using the comparative threshold cycle (CT)

method with *GAPDH* as a housekeeping gene reference. The results are expressed as fold change relative to the non-treated control and log(2) of the fold change relative to the non-treated control.

Gene product	Gene symbol	Primer sequence	
		Forward	**Reverse**
CRP	*CRP*	5'-AACTTTCAGCCGAATACATC-3'	5'-TGCTTTGAGGGATACATAGG-3'
E-selectin	*SELE*	5'-GAGAATTCACCTACAAGTCC-3'	5'-AGGCTTGAACATTTTACCAC-3'
ET-1	*EDN1*	5'-CAAGCAGGAAAAGAACTCAG-3'	5'-CTGGTTTGTCTTAGGTGTTC-3'
GAPDH	*GAPDH*	5'-ACAGTTGCCATGTAGACC-3'	5'-TTTTTGGTTGAGCACAGG-3'
ICAM-1	*ICAM1*	5'-ACCATCTACAGCTTTCCG-3'	5'-TCACACTTCACTGTCACC-3'
IL-6	*IL-6*	5'-GCAGAAAAAGGCAAAGAATC-3'	5'-CTACATTTGCCGAAGAGC-3'
IL-8	*IL-8*	5'-GTTTTTGAAGAGGGCTGAG-3'	5'-TTTGCTTGAAGTTTCACTGG-3'
iNOS	*NOS2*	5'-AGCTCAACAACAAATTCAGG-3'	5'-ATCAATGTCATGAGCAAAGG-3'
LOX-1	*OLR1*	5'-AATGATAGAAACCCTTGCTC-3'	5'-AGTCCTGAACAATTTGCTAC-3'
MCP-1	*CCL2*	5'-AGACTAACCCAGAAACATCC-3'	5'-ATTGATTGCATCTGGCTG-3'
PAI-1	*SERPINE1*	5'-ATCCACAGCTGTCATAGTC-3'	5'-CACTTGGCCCATGAAAAG-3'
tPA	*PLAT*	5'-GGAATTCCATGATCCTGATAG-3'	5'-TCCGGCAGTAATTATGTTTG-3'
P-selectin	*SELP*	5'-CAAAGGCATAGCATCACTTC-3'	5'-ATGATGCCTACAGTACATGG-3'
RAGE	*AGER*	5'-ACTGGATGAAGGATAACCAG-3'	5'-TCCATTCCTTTCTTGTTGAC-3'
SAA1	*SAA1*	5'-GAGAGAAGCCAATTACATCG-3'	5'-CTCTGGATATTCTCTCTGGC-3'
SAA2	*SAA2*	5'-GCAGAAGTGATCAGTTTATTTTC-3'	5'-CACTGAATCTTCATTGCCTG-3'
TF	*F3*	5'-GGAGAAAACTACTGTTTCAGTG-3'	5'-TCTCTGAATTCCCCTTTCTC-3'
TGFβ	*TGFB1*	5'-AACCCACAACGAAATCTATG-3'	5'-CTTTTAACTTGAGCCTCAGC-3'
VCAM-1	*VCAM1*	5'-ACTTGATGTTCAAGGAAGAG-3'	5'-TCCAGTTGAACATATCAAGC-3'
VEGF	*VEGFA*	5'-AATGTGAATGCAGACCAAAG-3'	5'-GACTTATACCGGGATTTCTTG-3'
vWF	*VWF*	5'-TGTATCTAGAAACTGAGGCTG-3'	5'-CCTTCTTGGGTCATAAAGTC-3'

Table 2.11.1 Primer sequences used in the study. Primers are predesigned KiCqStart™ primers purchased from Sigma-Aldrich (Poole, UK).

2.12. Enzyme-linked immunosorbent assay (ELISA)

ELISAs were performed in order to detect protein levels in either the cell culture supernatant or cell lysates. ELISA is a commonly employed assay which uses antibodies conjugated to an enzyme, which when presented with their substrate induce a colour change which can be read using a spectrophotometric plate reader.

Briefly, Nunc-Immuno 96 MicroWell plates (Sigma-Aldrich, Poole, UK) were prepared with the appropriate mouse anti-human capture antibody (supplier recommended concentration in PBS with 0.1-1% BSA), sealed and incubated at room temperature overnight. The plates were washed by aspiration of the wells followed by three washes using 0.05% Tween-20 in PBS. Plates were then incubated with 1% BSA in PBS for 1 hour to block non-specific binding sites and washed as before. They were then loaded with duplicate volumes of conditioned media (appropriately diluted to appear within the linear range of the standard curve) and a seven point purified recombinant protein standard curve of the relevant protein. After a 2 hour incubation, plates were washed as before and subsequently incubated with appropriate biotinylated goat anti-human antibody (supplier recommended concentration in PBS with 0.1-1% BSA) for another 2 hours. Plates were washed again before the addition of streptavadin-horseradish peroxidase (supplier recommended concentration in PBS with 0.1-1% BSA) and incubation for 20 minutes. After a final wash, as previously described, peroxidase activity was determined using the chromogenic substrate tetramethylbenzidine (TMB). After 20 minutes, colour development was stopped using 2N H_2SO_4 yielding a yellow colour which was measurable at 450nm using a spectrophotometer (Tecan Infinite F50 plate reader). Protein concentrations were calculated using a linear regression equation derived from the standard curve plot of known values.

IL-6/IL-8/VEGF

Cell supernatants were collected from experiments performed in an identical manner to those described for the LDH assay. Concentrations of the inflammatory mediators interleukin-6 (IL-6) and interleukin-8 (IL-8) and the growth factor vascular endothelial growth factor (VEGF) were determined using a DuoSet® sandwich ELISA according to the manufacturer's protocol (R&D Systems, Abingdon, UK).

Secretory leukocyte protease inhibitor (SLPI)/Elafin

Available levels of the secretory leukocyte protease inhibitor (SLPI) and Elafin proteins were measured both following incubation of the recombinant protein with MWNTs and in cell supernatants.

Binding of recombinant SLPI and Elafin proteins was determined by incubating 1ml of the appropriate recombinant protein at a known concentration of 1000pg/ml with 1-50µg/ml of f-MWNTs for 2 hours at 37°C. Particles were then separated by centrifugation at 17,000 x g for 20 minutes and the supernatant containing the free, un-bound protein underwent ELISA analysis.

Cell supernatants were collected from experiments performed in an identical manner to those described for the LDH assay. Concentration of the mediators SLPI and Elafin was determined using a sandwich ELISA according to the manufacturer's protocol (R&D Systems, Abingdon, UK).

E-selectin

E-selectin was measured both in cell supernatants and cell lysates. Collection of cell supernatants was performed as described previously for the LDH assay. Cells were lysed using radioimmunoprecipitation assay buffer (RIPA) buffer, supplemented with the protease inhibitor phenylmethanesulfonyl fluoride solution (1:1000). Lysates were diluted 1:2 in reagent diluent

and the E-selectin DuoSet ELISA was carried out according to the manufacturer's protocol (R&D Systems, Abingdon, UK).

Endothelin-1

Cell supernatants were collected from HPMVECs and HLF cultured in 24 well plates for 24 hours. Concentration of the potent vasoconstrictor endothelin-1 (ET-1) was determined using the Endothelin-1 Quantikine ELISA Kit (R&D Systems, Abingdon, UK) according to the manufacturer's protocol.

2.13. Western blot analysis

Western Blot analysis was employed as an alternative to ELISA in order to quantify protein expression. Western Blot analysis involves the resolution of proteins by gel electrophoresis followed by protein transfer to a membrane which is probed with an antibody raised against the protein of interest. This can then be visualised in a number of ways, here we have employed chemiluminescence.

Whole cell extracts were prepared from HPMVECs exposed to 10μg/ml f-MWNTs for 1, 2, 4, 6, 8, and 24 hours and AT2 cells exposed to 1-50μg/ml AR-MWNTs for 24 hours. Cells were cultured in six-well culture plates using seeding densities described in section 2.2. At the end of the exposure conditions, cells were lysed with 200μl/well CellLytic reagent (Sigma-Aldrich, Poole, UK), and proteases were inhibited with an inhibitor cocktail P8340 (Sigma-Aldrich, Poole, UK) before agitatation on ice for 30 minutes. Cell debris was removed by centrifugation at 17,000 x g at 4°C for 20 minutes. Protein concentration in the supernatant were determined using Bradford reagent (Sigma-Aldrich, Poole, UK), with samples compared to a standard curve generated using bovine serum albumin (BSA). Loading protein concentrations were adjusted to 20μg per sample using lithium dodecyl sulfate (LDS) sample buffer (Invitrogen, Paisely, UK), and denatured at 95°C for 5 minutes.

The samples containing 20µg of cellular protein were subjected to Western Blot analysis. Total protein was resolved for 45 minutes, 180V, 200mA on a 4-12% NuPAGE Bis-Tris gel (Invitrogen, Paisely, UK) and transferred to nitrocellulose membrane using the iBlot® 7-Minute Blotting System (Invitrogen, Paisely, UK). Membranes were blocked for 1 hour with 5% milk in TBS-0.1% Tween, probed with primary antibody (Table 2.13.1) at 4°C overnight followed by incubation with polyclonal goat anti-mouse or polyclonal goat anti-rabbit immunoglobulins conjugated with horse radish peroxidase (1:5000, Dako, Ely, UK). Membranes were developed using enhanced chemiluminesence reagent (ECL) Prime (GE Healthcare, Little Chalfont, UK) and analysis was carried out using the GelDoc-It Imaging System (UVP, Cambridge, UK) using VisionWorks®LS analysis software.

Antibody	**Manufacturer**	**Dilution Factor**
Mouse polyclonal anti-human surfactant protein A (SPA),	Abcam (Cambridge, UK)	1:10,000
Mouse monoclonal anti-human surfactant protein D (SPD)	Abcam (Cambridge, UK)	1:5,000
Mouse monoclonal anti-human VE-cadherin	Santa Cruz (Heidelberg, Germany).	1:3,000
Rabbit polyclonal anti-human caveolin-1	BD biosciences (Oxford,UK).	1:1,000
HRP conjugated goat polyclonal anti-mouse immunoglobulins	Dako, Ely, UK	1:5000
HRP conjugated goat polyclonal anti-rabbit immunoglobulins	Dako, Ely, UK	1:5000

Table 2.13.1 Antibody dilutions used during western blotting

2.14. iCELLigence Electrical Cell Impedance System

The iCELLigence System is a cell based microelectronic biosensor system, which provides real-time, label-free cellular analysis. In this system cells are grown on E-plates, a micro-electrode configuration that covers 80% of each well bottom's surface area. The presence of cells, strength of cell adhesions and cell-cell interactions will increase the electrode impedance;

described as Cell Index (CI) values. The CI values can therefore be used to monitor cell viability, number, morphology and cell-cell interactions in a non-invasive, real-time assay.

200µl cell culture medium was added to each well of an E-plate L8 prior to cell addition to obtain the background impedance measurements. 20,000 TT1 or HPMVEC cells, or 200,000 AT2 cells were seeded in each well. TT1 and AT2 cells were cultured in DCCM-1 containing 10% newborn calf serum (NCS), 100 U/ml penicillin, 100 mg/ml streptomycin and 2 mM glutamine for 24 hours prior to a 24 hour culture period in serum-free media. HPMVECs were cultured for 24 hours in EGM-2 MV. All cells were then exposed to 10µg/ml of AR, P(M4-VP), P(MAA), P(PEGMA) or AO MWNTs for 72 hours and the impedance signal expressed as the cell index at each time point per concentration was recorded.

To assess whether the presence of MWNTs is able to influence the impedance value, each MWNT was applied to the E-plate in both DCCM-1 and EGM-2 MV media in a cell free system.

2.15. EB (Evans Blue)-albumin permeability assay

The Evans Blue (EB)-albumin permeability assay was used as an indicator of endothelial barrier integrity. The assay tracks the movement of protein across a transwell system using albumin conjugated to the coloured "Evans Blue" azo dye.

The permeability assay was adapted from previous studies (Patterson, Rhoades, & Garcia, 1992). HPMVECs were seeded at 30,000 cells/cm^2 in 12 well transwell inserts (0.4µm pore, Corning) and cultured at 37°C in 5% CO^2 for 3 days. Culture medium was then replaced with 0.5ml EGM-2 MV containing MWNTs (1-50µg/ml), or EGM-2 MV alone and cells incubated for 24 hours. Media was removed and 0.5ml EB-albumin (0.67µg/ml EB in EGM-2 MV containing 4% BSA) was applied to the upper chamber and 1.5ml EGM-2 MV containing 4% BSA was added to the lower chamber for one hour. The absorbance of the solution in the lower chamber was read at 595nm and values were compared to that of the well containing HPMVECs treated with EGM-2 MV alone.

2.16. Statistical analysis

Data from each experiment is presented as the mean ± standard error (SEM) unless otherwise indicated. Each experiment was performed at least in duplicate and at least three independent experiments were performed of cells of three different passage generations (immortalised human alveolar type 1-like epithelial cells (TT1s)) or at least three different donors (primary human alveolar type-2 epithelial cells (AT2s) and primary human pulmonary microvascular cells (HPMVECs)). Treated groups were compared to an untreated control.

Statistical tests included:

- One-way ANOVA, non-parametric Friedman test with Dunnett's Multiple Comparison Test to compare various particle concentrations (eg. ELISAs, viability assays)
- One-way sample t-test to compare treated value to a normalised control value. To achieve a more Gaussian distribution these values were expressed in log2 and compared to a non-treated control value of 0 (eg. gene expression analysis).
- Mann Whitney t-test to compare changes between two treatments (untreated and exposure to a single concentration of f-MWNT) on mediator release (eg. Triple co-culture mediator release)

In all analyses, a P value <0.05 was considered significant.

3. DIFFERENTIAL RESPONSES OF CELLS OF THE BLOOD GAS BARRIER FOLLOWING EXPOSURE TO FUNCTIONALISED CARBON NANOTUBES: A FOCUS ON CELL DEATH, PARTICLE UPTAKE AND THE INFLAMMATORY RESPONSE

3.1. Introduction

The cells of the blood gas barrier

At the alveolar-capillary barrier, alveolar epithelial cells are separated from the underlying microvascular endothelial cells by a shared, fused basement membrane. The alveolar-capillary barrier is extremely thin (<0.2μm) to allow for efficient pulmonary gas exchange (Maniatis, Kotanidou, Catravas, & Orfanos, 2008). Normal physiology of this barrier is essential for pulmonary processes such as gas exchange, fluid homeostasis and defence mechanisms, and as a consequence, damage to this barrier is the major contributing factor in pathological processes such as acute lung injury (Hermanns et al., 2009). To investigate the implications of MWNTs interacting with cells at this barrier, type 1 and type 2 alveolar epithelial cells and pulmonary microvascular cells were used in this study. Each cell type has a distinct function at the alveolar-capillary barrier and a distinct morphology.

Alveolar type 1 (AT1) cells cover 93% of the alveolar surface and are thin, squamous cells with a large surface to allow for gas exchange, and a protruding nucleus (Crapo, Barry, Gehr, Bachofen, & Weibel, 1982; van den Bogaard, Dailey, Thorley, Tetley, & Forbes, 2009). Alveolar type 2 (AT2) cells are cuboidal and cover just 7% of the alveolar surface, despite accounting for approximately 66% of the alveolar epithelial cells by number (Crapo *et al*., 1982). AT2 cells are responsible for the production of lung surfactant, the primary function of which is to reduce surface tension and prevent alveolar collapse during ventilation (Swain, Kemp, Goldstraw, Tetley, & Stevens, 2010). Lung surfactant is stored within lamellar bodies in AT2 cells which, in

addition to phospholipids, contains approximately 10% protein which includes the surfactant proteins A, B, C and D (Fehrenbach, 2001).

In close association with the honeycomb structure of the alveolus is the capillary network which allows for efficient gas exchange with the circulatory system. As a result, the capillary network is vast; endothelial cells constitute a large proportion of the total cell population in the lung, accounting for approximately 37% of all cells present (Crapo *et al*., 1982).

Although immune cells such as the alveolar macrophage are a key defence mechanism in the lung, the cells of the blood-gas barrier should also be recognised as a dynamic system capable of initiating and regulating an inflammatory response and whose health is key to normal pulmonary and cardiovascular function (Mehta & Malik, 2006; Papritz *et al*., 2010; Snyder-Talkington et al, 2013).

The cytotoxic response

When testing the safety and efficacy of drugs and other compounds, it is important to initially determine the cytotoxic potential of the compound. Increased alveolar epithelial cell death is associated with a number of disease pathologies including pulmonary emphysema, acute lung injury and pulmonary fibrosis (Budinger *et al*., 2011; Fernandez & Eickelberg, 2012; Yokohori, Aoshiba, & Nagai, 2004). Loss of cells at the alveolar surface can also impact on the underlying capillary network; vascular endothelial growth factor (VEGF) expressed by epithelial cells, is a trophic factor required for the survival of endothelial cells (Kasahara *et al*., 2001). It has been hypothesised that decreased levels of VEGF following either epithelial cell death or injury may induce endothelial apoptosis, exacerbating the progression of diseases such as emphysema (Kasahara *et al*., 2001). Furthermore, pulmonary microvascular cell death exposes sub-endothelial Tissue Factor to circulating thrombotic factors, thus inducing clot formation (Steffel, Lüscher, & Tanner, 2006).

A cytotoxic response has been observed *in vitro* following carbon nanotube exposure in a number of cell types including bronchial and alveolar epithelial cell lines and primary aortic endothelial cells, however the influence of the novel thermo-chemical "grafting from" functionalisation method is unknown (Ursini *et al*., 2014; Walker *et al*., 2009). During the course of previous MWNT cytotoxicity studies, it has been noted that a number of cell viability assays are unsuitable for use with carbon nanotubes. For example, carbon nanotubes have been shown to stabilise formazan crystals formed during the MTT assay. Dissolution of these crystals is essential to provide an accurate spectrophotometric reading and use of this assay has in the past lead to an overestimation of the cytotoxic potential of carbon nanotubes (Worle-Knirsch *et al*., 2006). For this study we therefore selected an assay that produces a water-soluble tetrazolium salt, MTS, that like other water-soluble tetrazolium salts such as WST-1, XTT, or INT does not interact with the carbon nanotube (Worle-Knirsch *et al*., 2006). We have used both the MTS viability assay and the LDH cytotoxicity assay in concert to safeguard against potential CNT interference with spectrophotometric assays.

Particle uptake

A wide range of inhaled nanoparticles, including MWNTs, have been observed in cells of the peripheral airways during *in vivo* studies, indicating that these small particles are not only able to reach the alveolus, but also once there, they are uptaken by the resident cells (Mercer et al., 2013; Mitchell et al., 2007). In rodent studies, MWNTs have primarily been observed in alveolar macrophages; however there is also evidence of rapid uptake of MWNTs by alveolar epithelial cells following both inhalation and pharyngeal aspiration allowing MWNTs access to the interstitium and lymphatic system (Porter *et al*., 2010, 2013).

In rodent lungs, inhaled microparticles have limited access to the interstitial spaces, while nanoparticles have been shown to readily translocate to the epithelium and underlying interstitium (Kreyling et al, 2013). During these rodent studies it is primarily nanoparticles and

not microparticles that are also able to reach the circulatory system. Significant fractions of 20nm TiO_2 NPs have been found in rat endothelial cells following inhalation, however, there is currently no direct proof of NP accumulation in the endothelial cells of large animal species, including man. Evidence from canine and monkey inhalation studies does however indicate that nanoparticle relocation in these species is similar to that of rodents. However, in contrast, canine studies indicate that, in addition to nanoparticles, microparticles may also be able to traverse the epithelium to the underlying interstitium and circulatory system (Kreyling *et al*., 2013).

Further evidence for cellular uptake of nanoparticles comes from *in vitro* studies, where nanoparticles such as SWCNTS, biodegradable 6-coumarin PLGA NPs and fluorescent latex NPs have been identified within a wide range of cells, including immune cells, epithelial cells and vascular cells (Davda & Labhasetwar, 2002; Kemp *et al*., 2008; Porter *et al*., 2007). It has been suggested that the uptake of CNTs could be independent of both cell type and functional groups present on the CNT surface, despite the well-established variations in uptake mechanisms between cell types (Kostarelos et al., 2007). Phagocytosis occurs in specialised cells including monocytes, macrophages and neutrophils whereas pinocytosis in endothelial or epithelial cells can occur via a number of mechanisms including clathrin- or caveolin-mediated endocytosis or marcopinocytosis (Conner & Schmid, 2003).

It has previously been observed that nanoparticles are readily internalised by both type 1-like alveolar epithelial cells and endothelial cells (Davda & Labhasetwar, 2002; Kemp *et al*., 2008). In contrast, only a relatively small amount of particle uptake is seen in cultured AT2 cells (Kemp et al., 2008; Thorley et al., 2014). This information originates from the study of spherical nanoparticles; it is thought that the mechanism of uptake of needle-like CNTs which can become tangled may be distinct from that of spherical particles, however this is not fully understood (Liu *et al*., 2013; Raffa et al, 2010), Evidence from several groups has indicated that functionalisation of MWNTs can affect their the rate of cellular uptake (Ali-Boucetta *et al*., 2011;

Ursini *et al*., 2014). It is therefore important to establish the degree of uptake of our study particles - functionalised carbon nanotubes, as nanoparticle uptake is unlikely to be a "one size fits all" phenomenon.

The inflammatory response

It has been observed that nanoparticles may initiate diverse inflammatory responses in the lung (Li *et al*., 2010). During a murine *in vivo* oropharyngeal aspiration study, high nickel MWNTs induced pathological changes including increased cellularity (inflammation) in the lung. These *in vivo* results were associated with inflammasome activation and cytokine release in murine alveolar macrophages exposed *in vitro* to MWNTs (Hamilton et al, 2012). Further murine studies have observed an increase in polymorphonuclear leukocytes and the neutrophil chemoattractant KC following MWNT inhalation exposure (D. W. Porter *et al*., 2010) and the release of the inflammatory mediators IL-33, CCL3, CCL18 and MMP3 accompanied by increased inflammatory cell infiltration and impaired pulmonary function following oropharyngeal MWNT exposure (Wang *et al*., 2011). The importance of inflammatory regulators such as mast cells in MWNT induced pulmonary and cardiovascular toxicity has also been highlighted (Katwa *et al*., 2012).

Although the relationship between CNT inhalation and adverse cardiovascular health is not fully understood (see section 1.5), pulmonary inflammation is associated with adverse cardiovascular outcomes (Van Eeden et al, 2012). Systemic inflammation is therefore one possible hypothesis linking CNT inhalation and adverse cardiovascular health; however, it is possible that CNTs could initiate a vascular inflammatory response autonomously if they are able to interact with the vasculature directly, either via particle translocation or intravenous administration (Walker *et al*., 2009).

Interestingly some studies have recorded no increase in pulmonary inflammation following MWNT exposure in mice (Mitchell et al., 2007), and at least one study has noted a decrease in

innate immunity following MWNT exposure (Mitchell et al, 2009). This suggests that MWNT toxicity is likely to be highly dependent on the physicochemical characteristics of the material including metal content, length and surface chemistry, as well as the experimental design.

Reactive oxygen species

Nanoparticle induced toxicity and more specifically, CNT induced toxicity is often attributed to generation of reactive oxygen species (ROS) following exposure (Manke *et al*., 2013). ROS generation is an important mechanism when considering nanotoxicity as sustained elevated levels of ROS can result in oxidative stress (Fu *et al*., 2014; Gonzalez *et al*., 2008). Furthermore, ROS is often associated with nanoparticle-induced inflammation and has been identified as both a common initiating factor and end product of this process (Møller *et al*., 2014; Yang *et al*., 2009).

Using human lung fibroblasts cultured *in vitro*, both short and long SWCNTs induced ROS formation; however, SWCNTs elicited a more robust oxidative response than short SWCNTs, indicating a length-dependent effect (Manke *et al*., 2014). In addition, increased ROS was observed in primary mouse embryo fibroblasts exposed to CNTs. This coincided with reduced intracellular levels of the antioxidant enzymes superoxide dismutase and glutathione, and increased lipid peroxidation, indicative of oxidative stress (Yang *et al*., 2009). In contrast to these fibroblast studies, MWNT have been shown to scavenge free radicals, including ROS, in a cell free environment (Nymark *et al*., 2014). Following a 30 minute bronchial epithelial cell exposure to MWNTs, there was a net decrease in ROS, indicating scavenging activity (Nymark *et al*., 2014), and no oxidative DNA damage was observed in bronchial (BEAS-2B) or epithelial lung cancer cells (A549) following a 24 hour exposure to pristine or –COOH MWNTs (Ursini *et al*., 2014). Increased ROS and malondialdehyde formation and decreased catalase and glutathione activity have however been reported in human lung cancer cells (A549) following 6-24 hour exposures to MWCNTs (Srivastava *et al*., 2011). These conflicting results indicate that the role

of ROS in pulmonary toxicity is complex and highly dependent on not only the cell type studied but also the physicochemical properties of the CNT. Due to the important role of ROS in inflammation, fibrosis and genotoxicity, more studies are required to elucidate which NP properties affect ROS formation and cellular reactivity in the lung.

In endothelial cells, there is some evidence that MWNT exposure elicits an oxidative response. Un-modified MWNTs induced ROS formation in immortalised human microvascular cells at 8 hours, and anti-oxidant treatment reduced MWNT induced endothelial barrier permeability (Pacurari *et al*., 2012). Evidence is, however, sparse; the effect of MWNT physicochemical properties on endothelial ROS formation in not known. Oxidative stress is implicated in the disruption of endothelial cell-cell junctions and vascular endothelial dysfunction, and therefore plays an important role in the pathophysiology of various vascular diseases and disorders (Lum & Roebuck, 2001; van Wetering *et al*., 2002). Understanding the effect of MWNT properties on endothelial ROS formation will therefore be crucial in developing safe CNT-based nanomedicines.

Overview:

This chapter describes the alveolar epithelial and microvascular endothelial cells used in this study and investigates the response of these cells when exposed to functionalised carbon nanotubes. Here we investigate common responses comparable between cell types, including cell viability, particle uptake, the inflammatory response and production of reactive oxygen species. We use these parameters to compare and contrast the differential responses of the cells and discuss the potential importance of these results in light of occupational or therapeutic exposure.

Hypothesis:

We hypothesised that MWNT exposure would induce cell death, release of inflammatory mediators and generation of ROS in the cells of the blood-gas barrier. Furthermore we hypothesised that MWNT uptake would differ between these cell types and that functionalisation of MWNT would affect their bioreactivity *in vitro*. Our specific aims were to establish:

I. Does MWNT exposure induced a change in TT1, AT2 or HPMVEC viability?
II. Are functionalised MWNTs internalised by the cells of the blood-gas barrier, and if so, by what processes is this likely to occur?
III. Could MWNT exposure trigger an inflammatory response in alveolar epithelial cells and microvascular endothelial cells?
IV. Does MWNT exposure influence ROS levels in the cells of the blood gas barrier and is ROS induction a key initiator of inflammation?
V. Crucially, are the aforementioned processes modulated by MWNT surface modifications?

3.2. Results

Cell characterisation

When visualised using light microscopy, cultured HPMVEC, AT2 and TT1s have a distinct morphology; HPMVECs are large, flat cells with a distinct cobblestone appearance, and large dark nuclei. TT1 cells are large, flat cells with a large nucleus and AT2 cells have a cuboidal morphology and appear the smallest of the three cells types when visualised using a microscope (Figure 3.2.1).

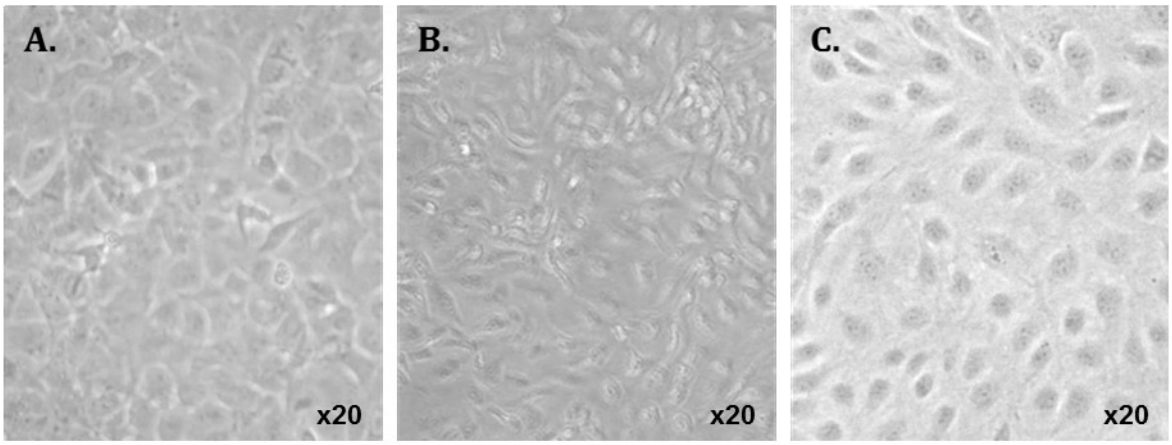


Figure 3.2.1 Phase-contrast micrographs displaying the different morphologies of the main cells used in this study. The image shows the following cell types: (A.) immortalised human alveolar epithelial type 1-like cells (TT1), (B.) primary human alveolar epithelial type 2 cells (AT2) and (C.) primary human pulmonary microvascular endothelial cells (HPMVEC).

Immunocytochemistry demonstrated that immortalised TT1 cells were postive for the type-1 epithelial cell markers podoplanin and RAGE (Figure 3.2.2). Alveolar type II cells isolated using the method described by Witherden & Tetley (2001) were shown to have a purity of greater than 95% as demonstrated by positive expression of alkaline phosphatase, surfactant protein D, epithelial cell adhesion molecule and intermitantly expressed surfactant protein A (Figure 3.2.3).

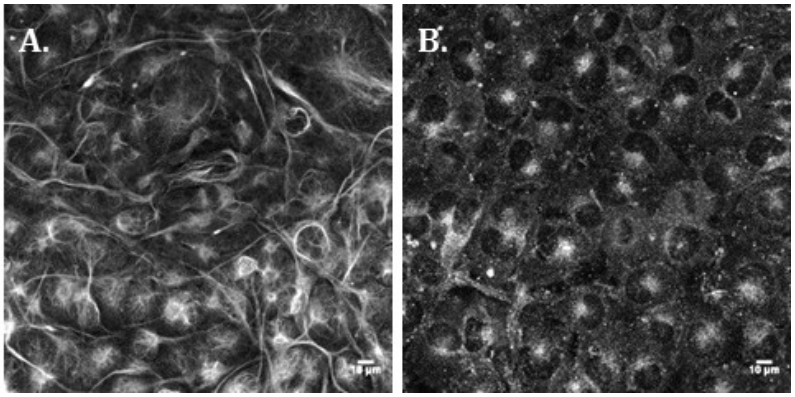


Figure 3.2.2 Podoplanin and RAGE expression in TT1 cells. TT1 cells expressed the markers podoplanin (A.) and RAGE (B.). Images were obtained by confocal microscopy. No immunofluescence was detectable in the mouse IgG isotype control. Scale bars indicate a distance of 10μm.

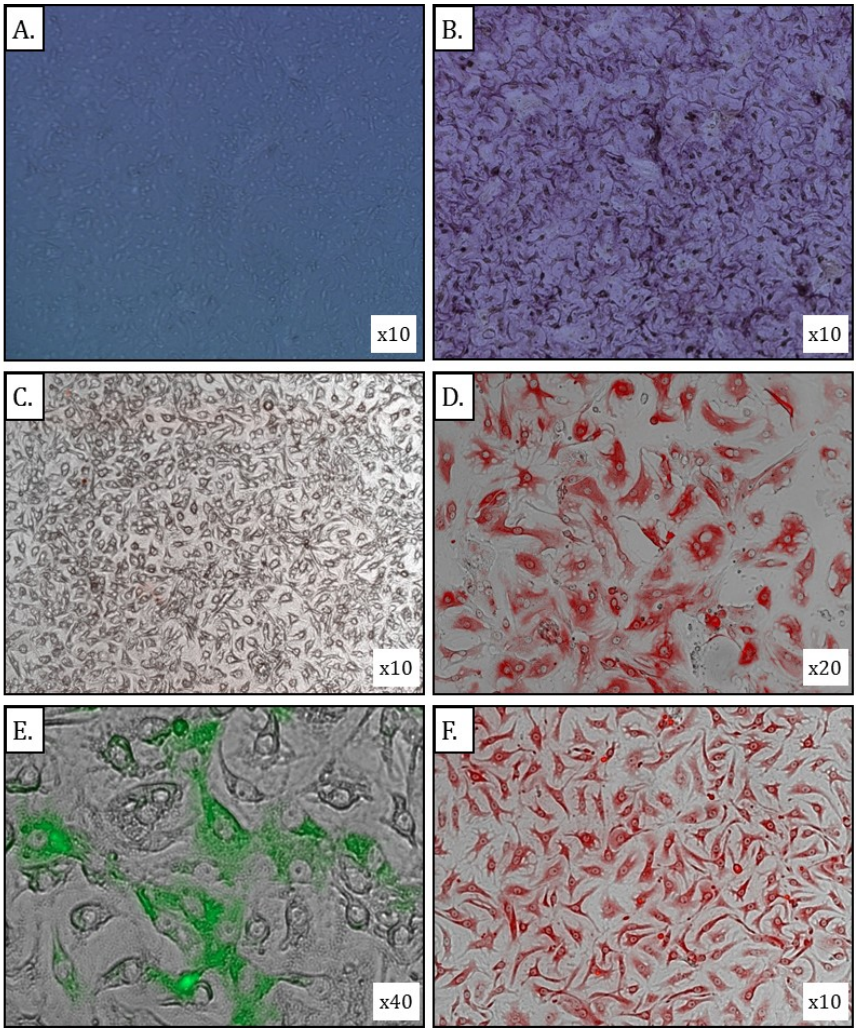


Figure 3.2.3 AT2 Phenotype Characterisation. (A. – B.) Alkaline Phosphatase Staining: AT2 cells 72 hours after seeding. A.) non-treated cells, B.) alkaline phosphatase positive cells. (C. – F.) Immunostaining: AT2 cells 72 hours after seeding following methanol fixation. Cells are stained with the following antibodies C.) non-exposed mouse epitope D.) surfactant protein D. E.) surfactant protein A. F.) epithelial cell adhesion molecule (intracellular domain).

Cultures of HPMVECs were positive for characteristics typical of an endothelial cell, these included a cortical arrangement of f-actin fibres and expression of VE-cadherin, CD31, caveolin-1 and RAGE (Figure 3.2.4). These cells also formed tubes on BD matrigel and expressed endothelin-1 (Figure 3.2.5). A full summary of the endothelial makers studied and the assays used to detect the marker can be found in Table 3.2.1.

Marker	HPMVEC
CD31 (PECAM-1)	++[a] and ++[c]
CD54 (ICAM-1)	++[b]
CD106 (VCAM-1)	++[b]
CD144 (VE-cadherin)	++[a] and ++[c]
CD62P (P-selectin)	++[b]
CD62E (E-selectin)	++[b] and ++[e]
CD142 (Tissue Factor) [inducible]	++[b]
von Willebrand factor	++[b]
Tube formation	++[d]
Endothelin-1	++[b] and ++[e]
RAGE (Receptor for advanced glycation endproducts)	++[a], ++[b] and ++[c]
Caveolin-1	++[a] and ++[c]

[a] *immunofluorescence*
[b] *reverse transcription with polymerase chain reaction*
[c] *western blot*
[d] *angiogenesis assay on BD Matrigel*
[e] *enzyme-linked immunosorbent assay*

Table 3.2.1 Summary of endothelial cell markers observed in HPMVECs isolated for this study.

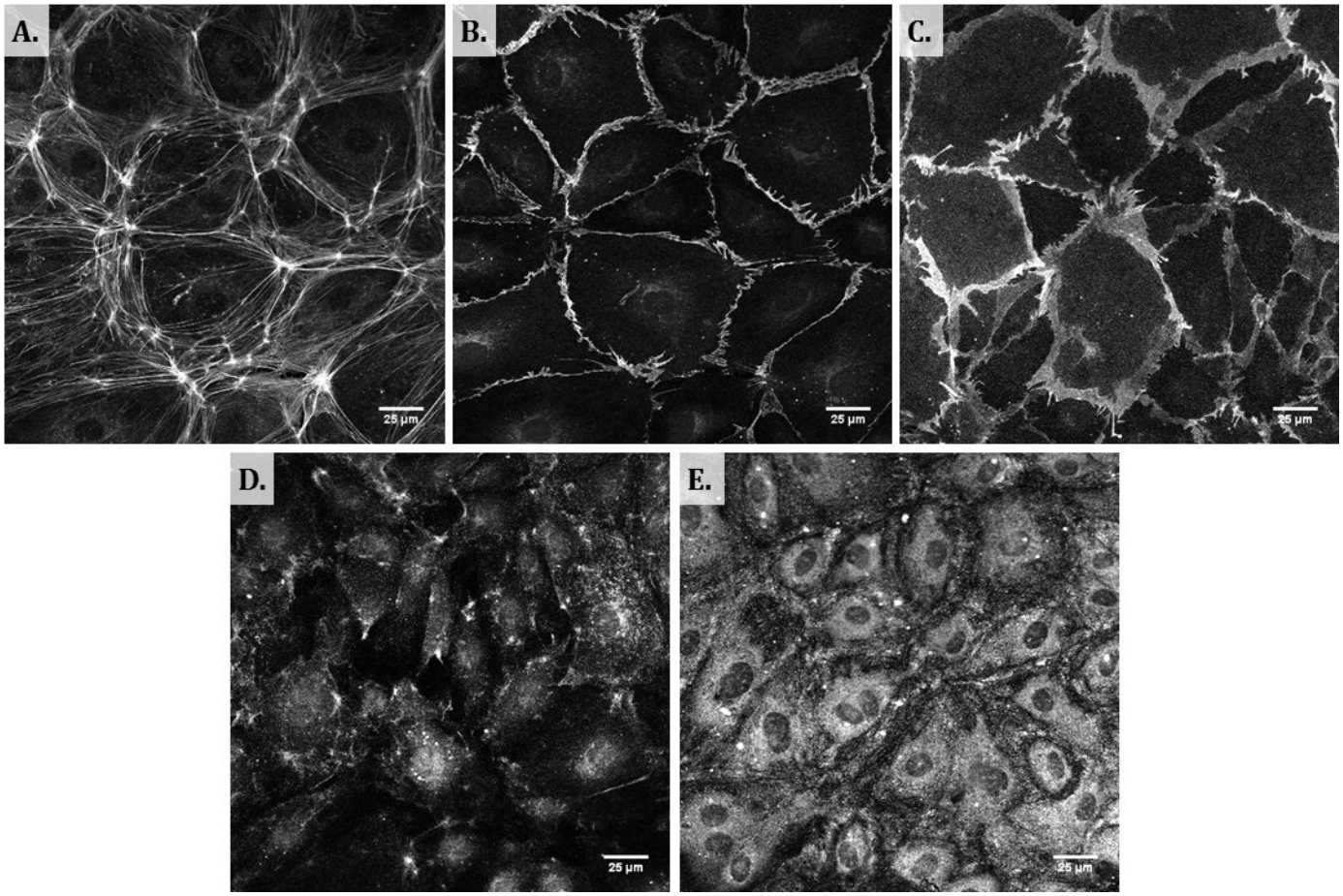


Figure 3.2.4 HPMVEC phenotype characterisation: Cells were immunofluorescently stained for markers of an endothelial phenotype. Cells displayed cortical arrangement of f-actin fibres (A.), and were positive for VE-cadherin (B.), CD31 (C.) caveolin-1 (D.) and receptor for advanced glycation endproducts (RAGE) (E.). No immunofluescence was detectable in the mouse and rabbit IgG isotype controls. Scale bars indicate a distance of 25µm.

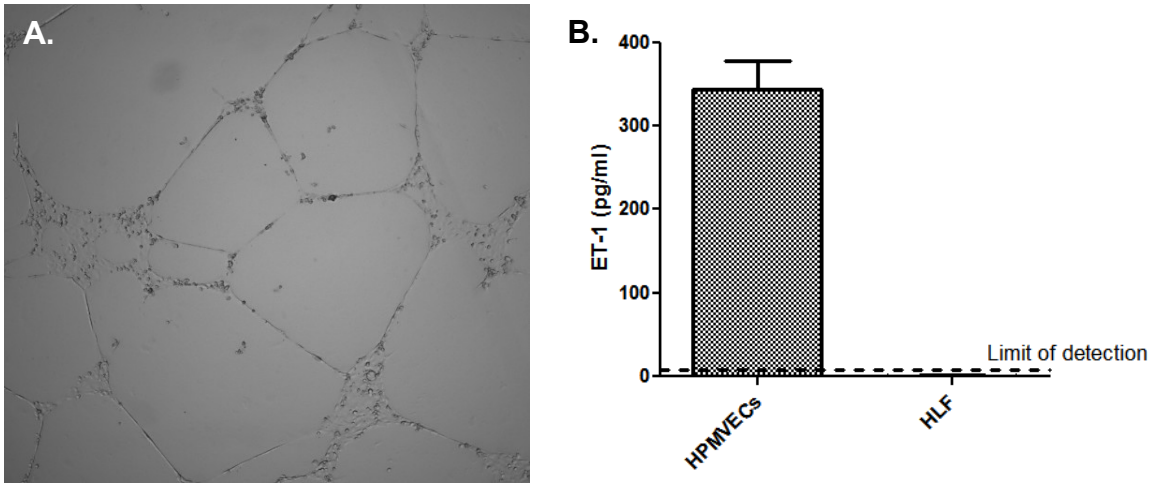


Figure 3.2.5 HPMVEC tube formation on BD Matrigel and expression of endothelin-1. HPMVECs formed tube like structures 4 hours after cells were seeded on BD matrigel, (A.). Additionally, following 24 hours in culture, high levels of endothelin-1 (ET-1) were detected in the supernatants of HPMVEC cultures; no ET-1 was detected in cultured human lung fibroblasts (HLF) used as a control (B.). These results support the evidence for an endothelial monoculture, in the absence of contaminating cells.

Cell viability

MWNTs were not acutely cytotoxic to alveolar epithelial cells. A small, significant decrease (<11%, $p<0.05$) in TT1 cell viability was indicated by the MTS assay following 50µg/ml exposure to TTC and P(4-VP)-MWNTs at 4 hours and AR and P(4-VP)-MWNTs at 24 hours. The LDH assay indicated that high concentrations of P(MAA) and AO-MWNTs have damaged the membrane integrity at 24 hours (<18% LDH release, $p<0.05$). The LDH assay indicated that at 72 hours all particles had induced some cell membrane damage, however LDH release never exceeded 14% of the total and only P(4-VP), P(M4-VP) and P(MAA)-MWNT induced a small but significant ($p<0.05$) reduction in cell viability, as measured by the MTS assay (Figure 3.2.6).

In AT2 cells, an increase in mitochondrial activity was observed following a 4 hour exposure to MWNTs, however this was only significant for 10 and 25µg/ml TTC-MWNT treated cells (16.1%, $p<0.01$ and 14.3%, $p<0.05$ respectively). No increase in extracellular LDH was observed at 72 hours and only 5µg/ml P(MAA)-MWNTs induced a small but significant ($p<0.01$) reduction in cell viability of 2.24% (Figure 3.2.7). At 4 hours LDH levels were below the limit of detection for both TT1 and AT2 cells (results not shown).

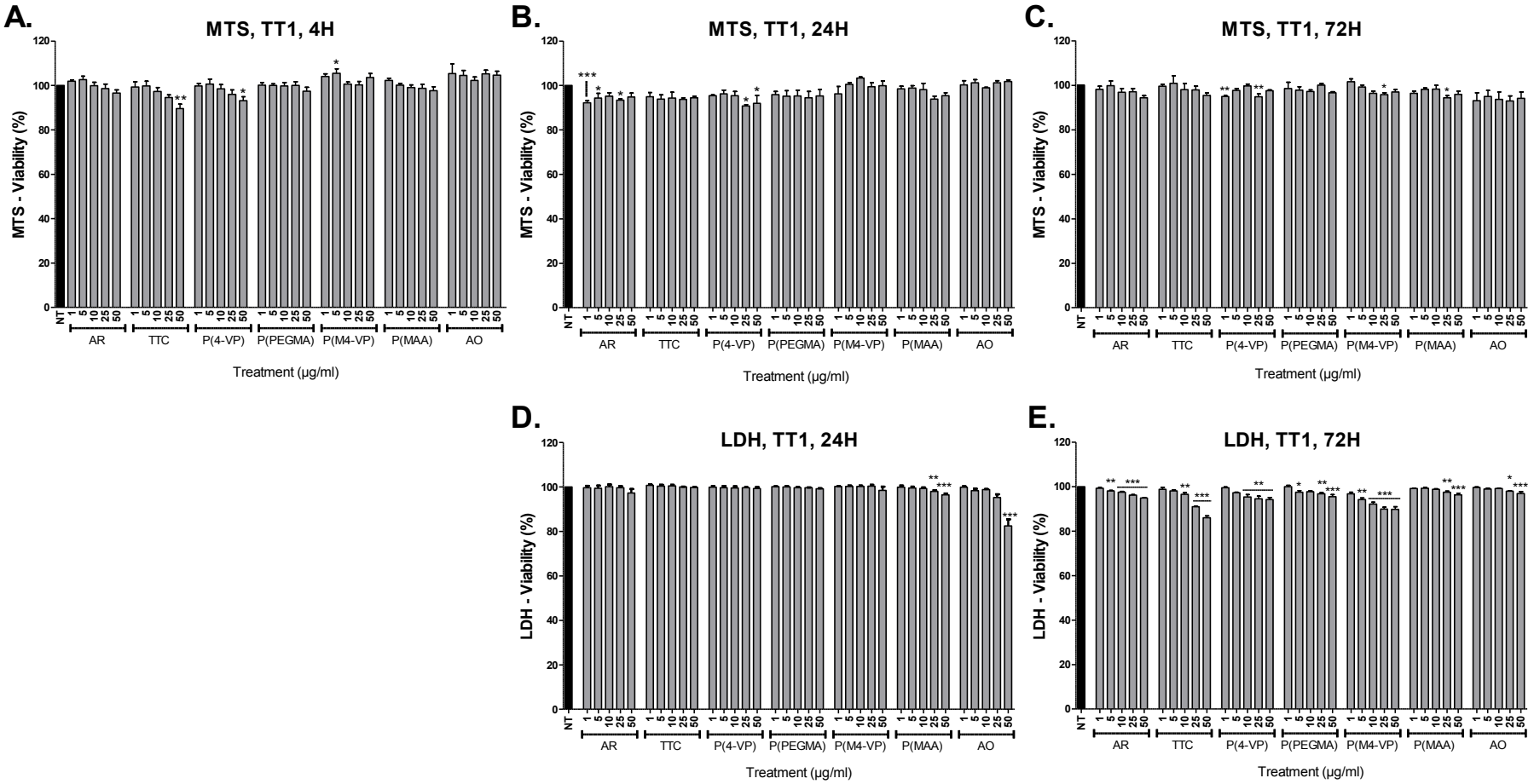


Figure 3.2.6 TT1 viability at 4 hours, 24 hours and 72 hours following exposure to f-MWNTs. TT1 cells were exposed to 1-50µg/ml AR, TTC, P(4-VP), P(PEGMA), P(M4-VP), P(MAA) or AO MWNTs for 4 (A.), 24 (B. & D.) or 72 hours (C. & E.) and viability was determined by the MTS (A., B. & C.) and LDH (D. & E.) assays. Values represent % of untreated control, data is expressed as mean ± SEM, n=4. One-way ANOVA followed by Dunnett's post-test; *p<0.05, **p<0.01, ***p<0.001.

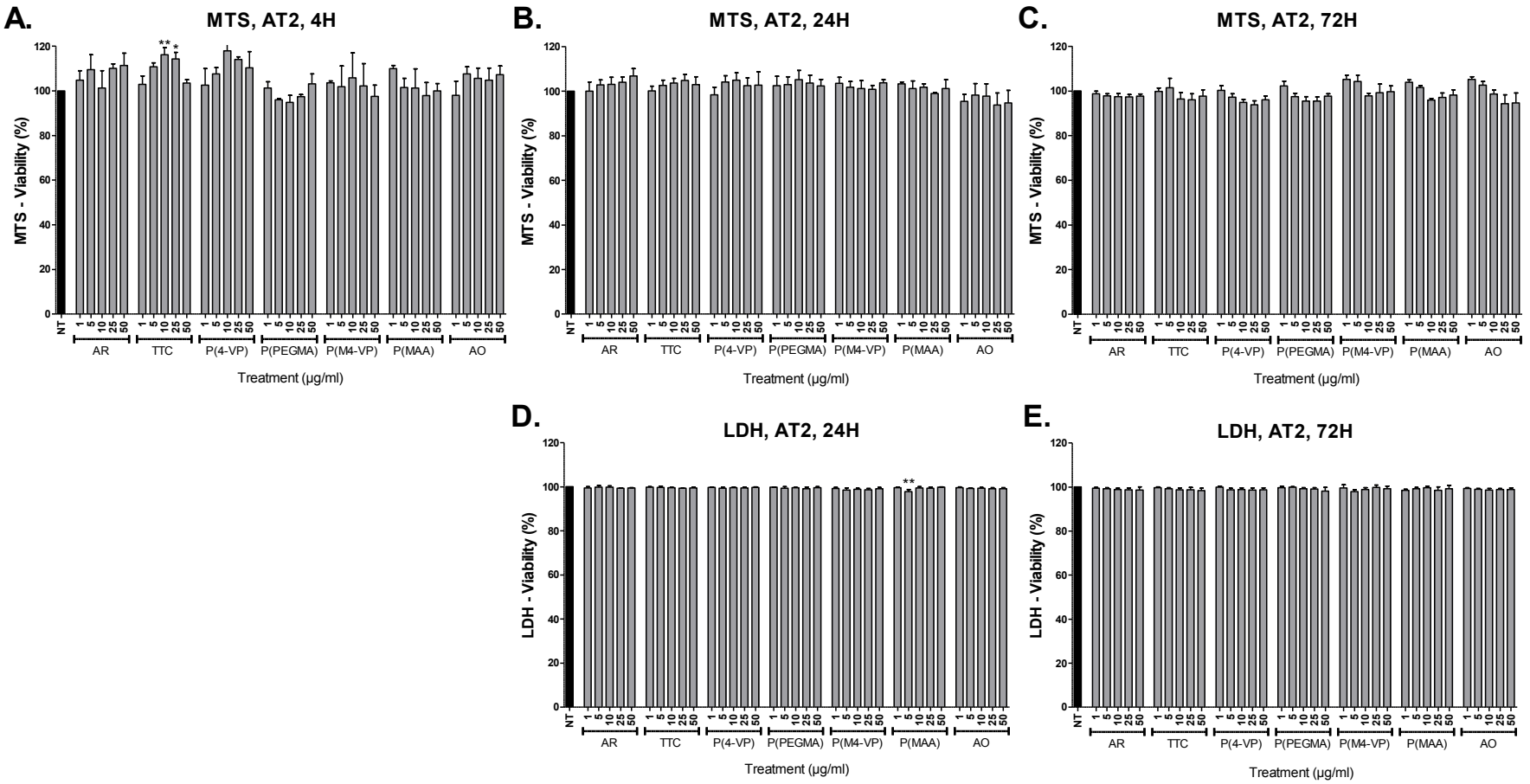


Figure 3.2.7 AT2 viability at 4 hours, 24 hours and 72 hours following exposure to f-MWNTs. AT2 cells were exposed to 1-50µg/ml AR, TTC, P(4-VP), P(PEGMA), P(M4-VP), P(MAA) or AO MWNTs for 4 (A.), 24 (B. & D.) or 72 hours (C. & E.) and viability was determined by the MTS (A., B. & C.) and LDH (D. & E.) assays. Values represent % of untreated control, data is expressed as mean ± SEM, n=4. One-way ANOVA followed by Dunnett's post-test; *p<0.05, **p<0.01, ***p<0.001.

A significant concentration-dependent decrease in mitochondrial activity was observed in HPMVECs following a 4 hour exposure to AR, TTC P(PEGMA) and P(M4-VP)-MWNTs (<25.38, <19.84, <19.58 and <19.65% respectively, $p<0.05$), indicating a loss of cell viability. By 24 hours, a decrease in viability was no longer observed following exposure to any of the MWNTs, in fact a significant increase in mitochondrial activity as high as 19.8% was detected following exposure to ≥25μg/ml P(PEGMA) and P(M4-VP)-MWNTs ($p<0.05$) and 50μg/ml AR and P(MAA)-MWNTs ($p<0.001$) (Figure 3.2.8).

Investigation into the disparity in cell viability at 4 and 24 hours using the BrdU assay indicated that the observed recovery and subsequent increase could be due to an increase in HPMVEC proliferation. AR, P(PEGMA) and P(PM4-VP)-MWNTs exposure resulted in a significant decrease in cell viability at 4 hours, but induced a significant level ($p<0.001$) of cell proliferation at 24 hours (Figure 3.2.8, Figure 3.2.9); 50μg/ml of these particles induced a >100% increase in the baseline level of cell proliferation. AO-MWNTs induced a much lower increase in cell proliferation which is consistent with the absence of a decrease in cell viability. Only 50μg/ml AO-MWNT induced a significant increase in cell proliferation, which was lower than that observed for other particles, at 25% ($p<0.05$) (Figure 3.2.9).

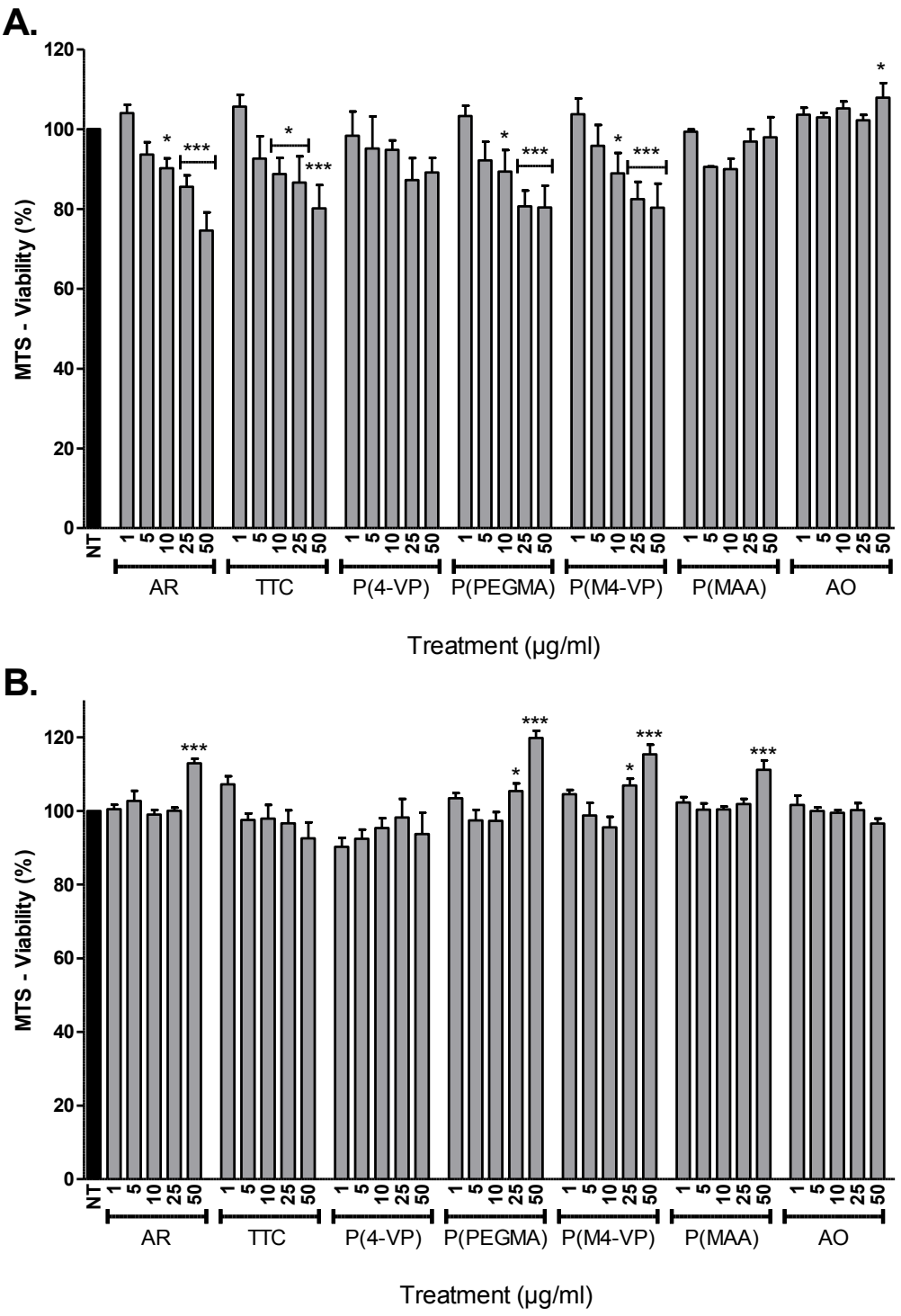


Figure 3.2.8 HPMVEC viability at 4 hours and 24 hours following exposure to f-MWNTs. HPMVECs were exposed to 1-50µg/ml AR, TTC, P(4-VP), P(PEGMA), P(M4-VP), P(MAA) or AO MWNTs for 4 (A.) or 24 hours (B.) and viability was determined by the MTS assay. Values represent % of untreated control, data is expressed as mean ± SEM, n=4. One-way ANOVA followed by Dunnett's post-test; *p<0.05, ***p<0.001.

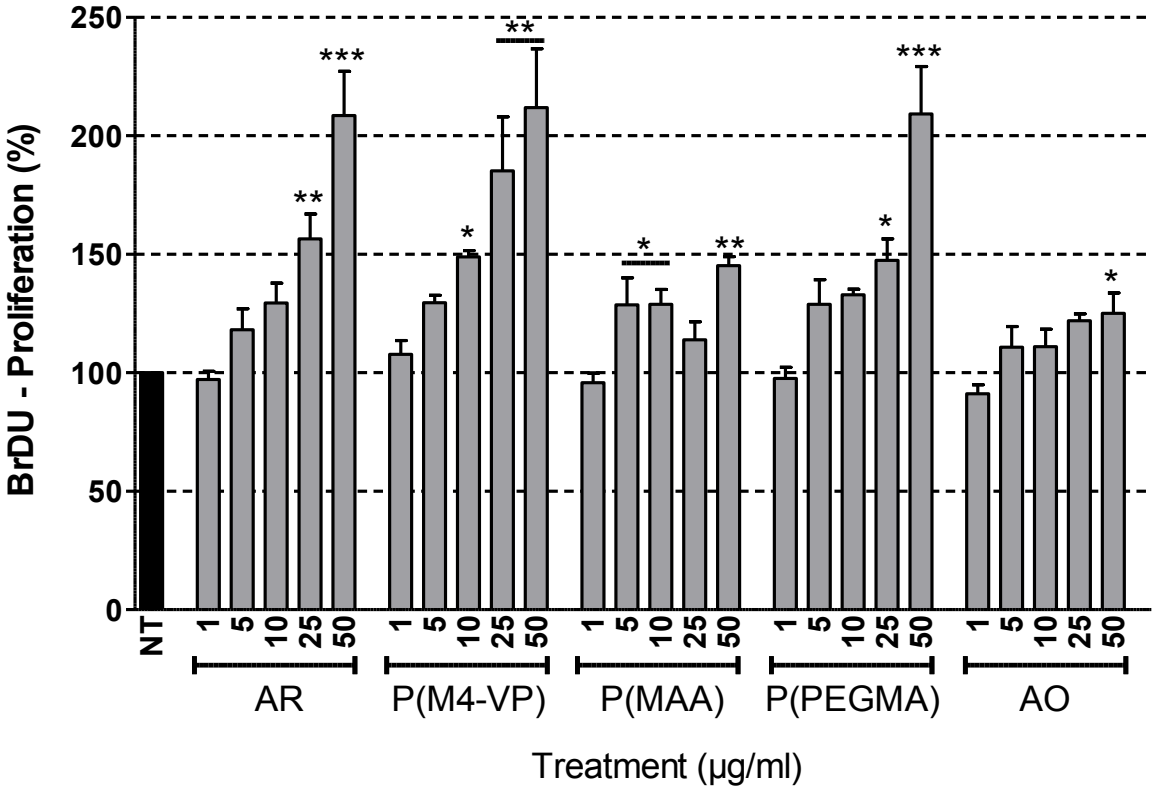


Figure 3.2.9 HPMVEC proliferation at 24 hours following exposure to f-MWNTs. HPMVECs were exposed to 1-50µg/ml AR, P(PEGMA), P(M4-VP), P(MAA) or AO MWNTs for 24 hours and cell proliferation was determined by the BrdU assay. Values represent % of untreated control, data is expressed as mean ± SEM, n=4. One-way ANOVA followed by Dunnett's post-test; *p<0.05, **p<0.01, ***p<0.001.

Particle uptake

TEM studies demonstrated that the majority of AR-MWNTs present within TT1 cells were visible as large agglomerates inside endosome-like structures, suggesting uptake via endocytic pathways (Figure 3.2.10). AR-MWNTs were present as both very large agglomerates surrounded by very large membrane protrusions, suggesting micropinocytosis (b), and smaller clusters engulfed by other endocytic pathways (a, c). A small population of individual AR-MWNTs were also found inside the cytoplasm and the plasma membrane (indicated by arrows).

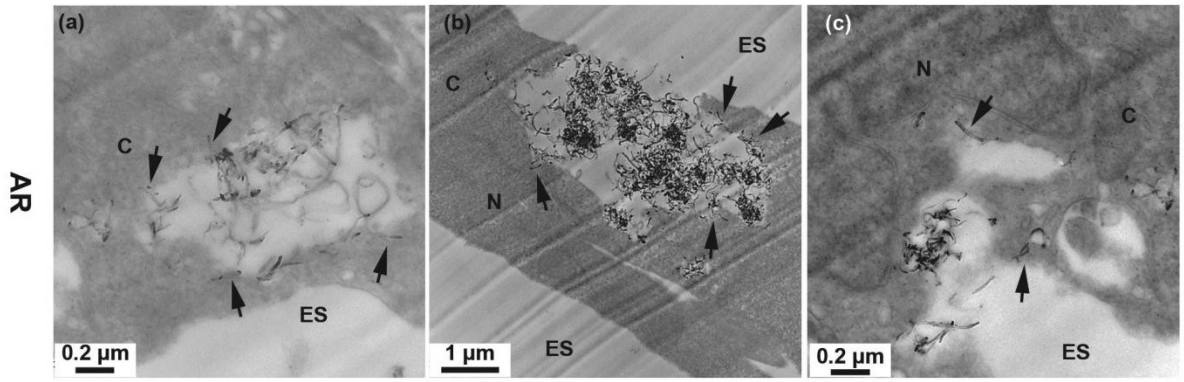


Figure 3.2.10 TEM images showing the cellular distribution and interaction of AR-MWNTs in TT1 cells. TT1 cells were exposed to 5µg/ml AR-MWNTs for 24 hours. The majority of AR-MWNTs are seen inside cellular vesicles; AR-MWNT are observed within a smaller vesicles (a), and are also present within large vesicles indicative of macropinoctosis (b). (c) shows an example of early vesicle formation following AR-MWNT exposure. Arrows indicate where single AR-MWNT fibres can be seen embedded in the plasma membrane. ES = extracellular space; C = cytoplasm; N = nucleus. Image adapted from (Shu Chen *et al*., 2014) with appropriate copyright permissions (Appendix I).

Thermochemically functionalised MWNTs, (P(PEGMA), P(MAA) and P(M4-VP), were also present in both vesicles and the cell cytoplasm, however there was evidence that the presence of functional groups affected MWNT interactions with the cell (Figure 3.2.11). There is evidence of endocytosis of all particles, including both macropinocytosis and other endocytic mechanisms. Negatively charged P(MAA)-MWNTs were however frequently aligned parallel to the plasma membrane (Figure 3.2.11 e-f) and positively charged P(M4-VP)-MWNTs exhibited more frequent contact with the plasma membrane than the other MWNTs (Figure 3.2.11 h-i).

AO-MWNTs were also present within the TT1 cells, however there was no evidence of macropinocytosis following exposure to these particles (Figure 3.2.12). The majority of AO-MWNTs were present in smaller vesicles ~0.1µm in diameter (Figure 3.2.12 a), however these particles were also observed at the plasma membrane (Figure 3.2.12 b) and within the cell cytoplasm (Figure 3.2.12 c).

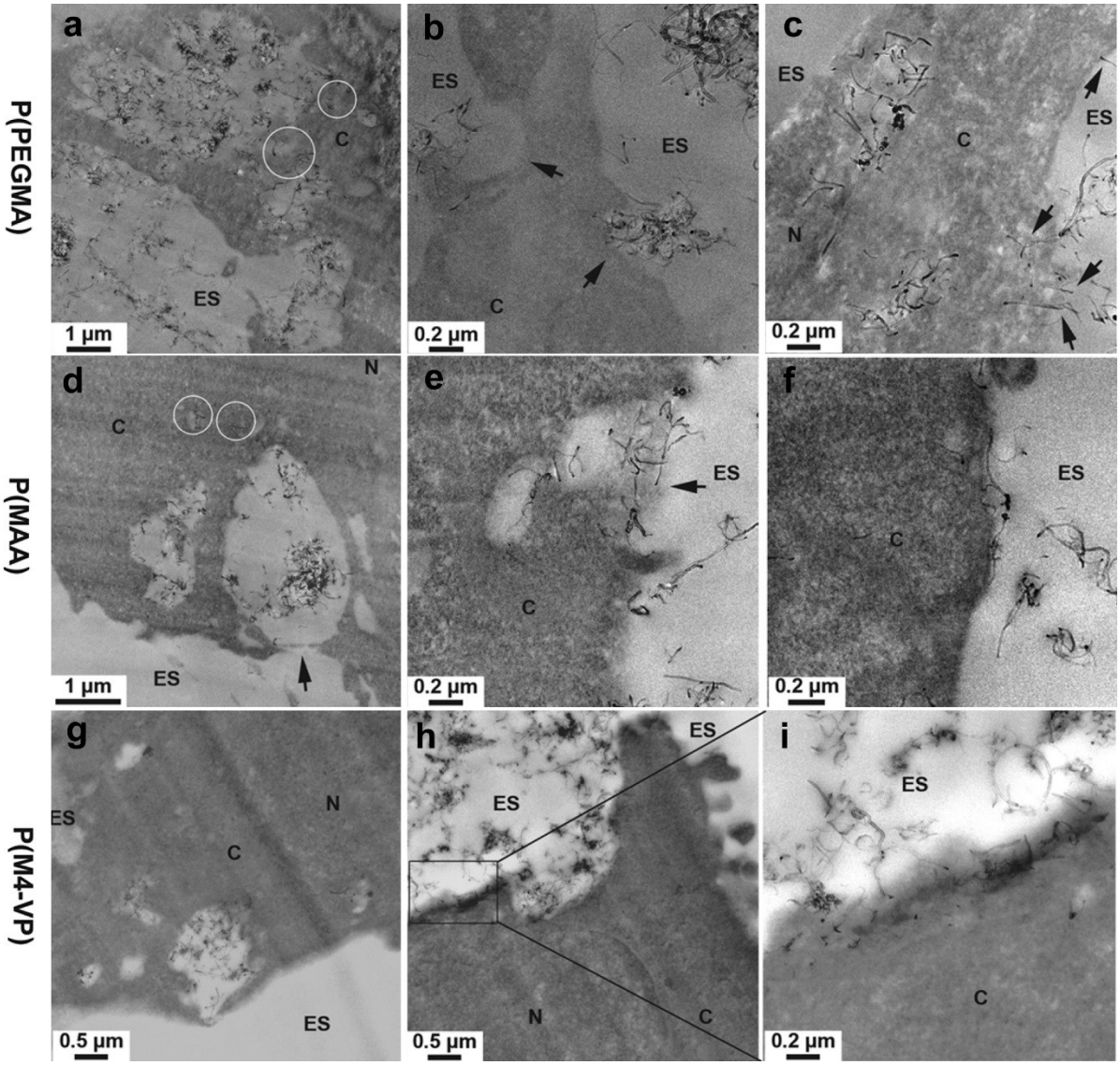


Figure 3.2.11 TEM images showing the cellular distribution and interaction of MWNTs functionalised using the thermochemical "grafting from" method in TT1 cells. The cellular location of the following particles is shown following a 24 hour exposure to 5µg/ml (a-c) P(PEGMA)-MWNTs, (d-f) P(PMAA)-MWNTs and (g-i) P(M4-VP)-MWNTs. Individual MWNTs are indicated by circles. P(PEGMA)-MWNTs were present within large protrusions of the plasma membrane (>1 mm) (a) and smaller vesicles (b). Individual P(PEGMA)-MWNTs are also visible inside the cytoplasm (a (circled) and c). P(MAA)-MWNTs were observed inside vesicular structures (d and e), uptaken by macropinocytosis (d (arrow)) and other endocytic mechanisms (e (arrow)) and within the cytoplasm (d (circled)).). P(MAA)-MWNTs, were frequently aligned parallel to the plasma membrane (e-f). P(M4-VP)-MWNT were also distributed within the cytoplasm and endocytic vesicular structures (g-i). These particles exhibited more frequent contact with the plasma membrane than the other MWNTs (h-i); (i) is a higher resolution TEM image of boxed area in (h). ES = extracellular space; C = cytoplasm; N = nucleus. Image adapted from (Shu Chen *et al*., 2014) with appropriate copyright permissions (Appendix I).

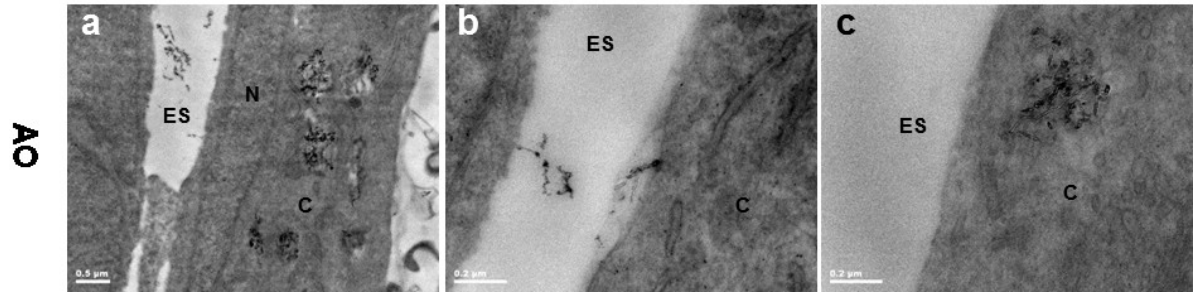


Figure 3.2.12 TEM images showing the cellular distribution and interaction of AO-MWNTs in TT1 cells. TT1 cells were exposed to 5μg/ml A0-MWNTs for 24 hours. The majority of AO-MWNTs are seen inside smaller cellular vesicles (a) however these particles are also found at the plasma membrane (b) and within the cell cytoplasm (c). ES = extracellular space; C = cytoplasm; N = nucleus. Image adapted from (Shu Chen *et al*., 2014) with appropriate copyright permissions (Appendix I).

Confocal microscopy demonstrated distinct clustering of P(M4-VP)-MWNTs around the HPMVEC nucleus (Figure 3.2.13 C. & F.). Large agglomerates of AR and thermochemically functionalised MWNTs were visualised throughout the cell monolayer using brightfield microscopy (Figure 3.2.13 Bii, Cii, Dii & Eii). In contrast, AO-MWNTs were only visible around the HPMVEC nucleus (Figure 3.2.13 F.). The location of MWNTs indicated by the red darkfield image showed good association with the MWNTs visualised using brightfield imaging in Figure 3.2.13 ii.); the darkfield image was advantageous in that it could distinguish at which plane the particle was present at. No co-localisation of MWNTs and lysosomes was observed (absence of yellow, Figure 3.2.13 i.).

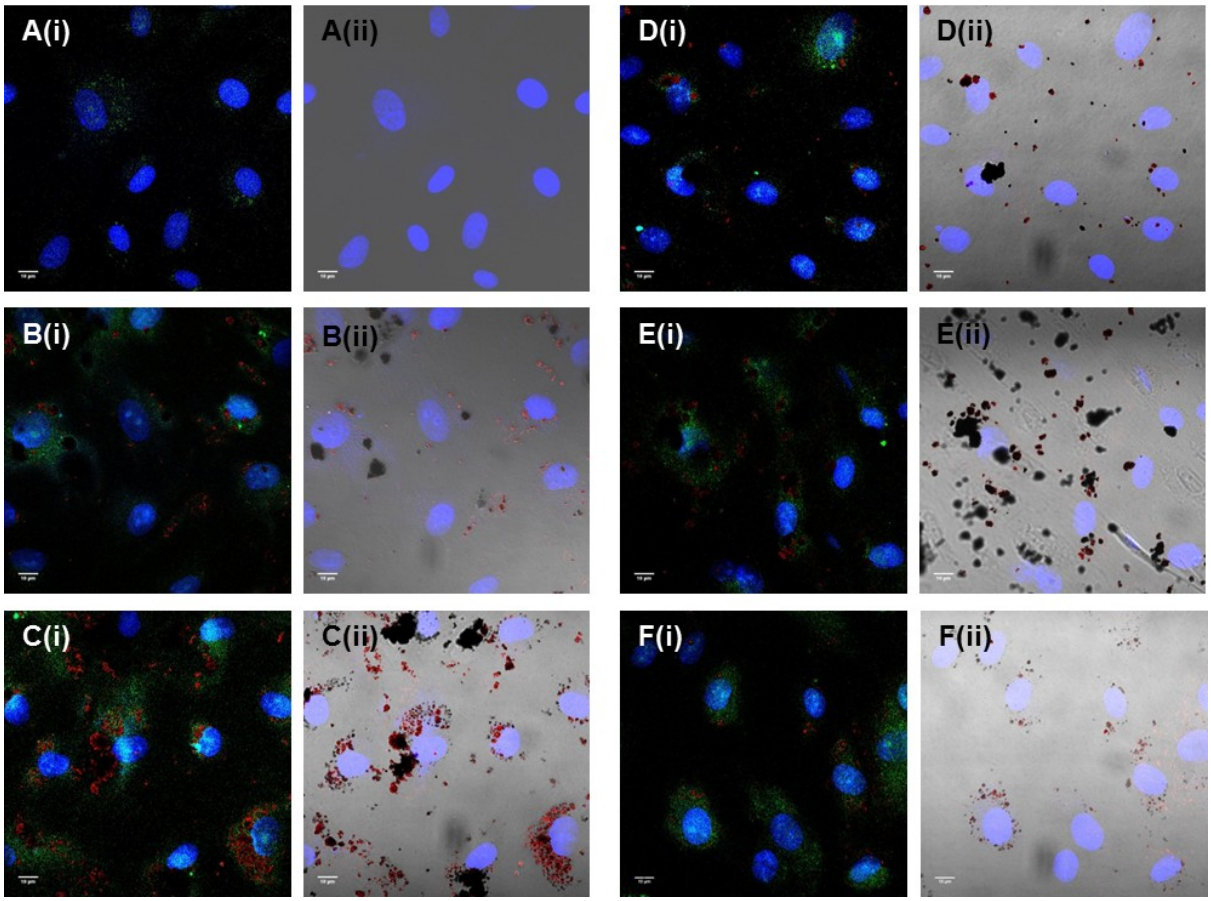


Figure 3.2.13. f-MWNT uptake by HPMVEC following a 24 hour exposure. The nucleus is shown in blue, f-MWNTs are shown by darkfield microscopy in red, i.) Lysosomes are shown in green and ii.) f-MWNTs are also shown by brightfield microscopy. Images are taken following a 24 hour exposure to 10μg/ml of the following particles, B.) AR-MWNTs, C.) P(M4-VP)-MWNTs, D.), P(MAA)-MWNTs, E.) P(PEGMA)-MWNTs and F.) AO-MWNTs. Panel A.) is the non-treated control. f-MWNTs are observed in all but the non-treated control. C.) P(M4-VP) and E.) AO-MWNT show distinct clustering of the MWNTs around the cell nucleus. Scale bars indicate a distance of 10μm.

High resolution imaging of HPMVECs following exposure to AO-MWNTs, showed AO-MWNTs present as both small and large circular structures localised to the area around the cell nucleus; a pattern indicative of particle uptake via endocytic mechanisms (Figure 3.2.14). Figure 3.2.14 Aii.) clearly shows an absence of AO-MWNT (red) and lysosome (green) co-localisation (yellow), however AO-MWNTs were localised to the general cell region where lysosomes are present. Figure 3.2.14 Bii.) demonstrates the ability of darkfield microscopy to detect AO-MWNT particles.

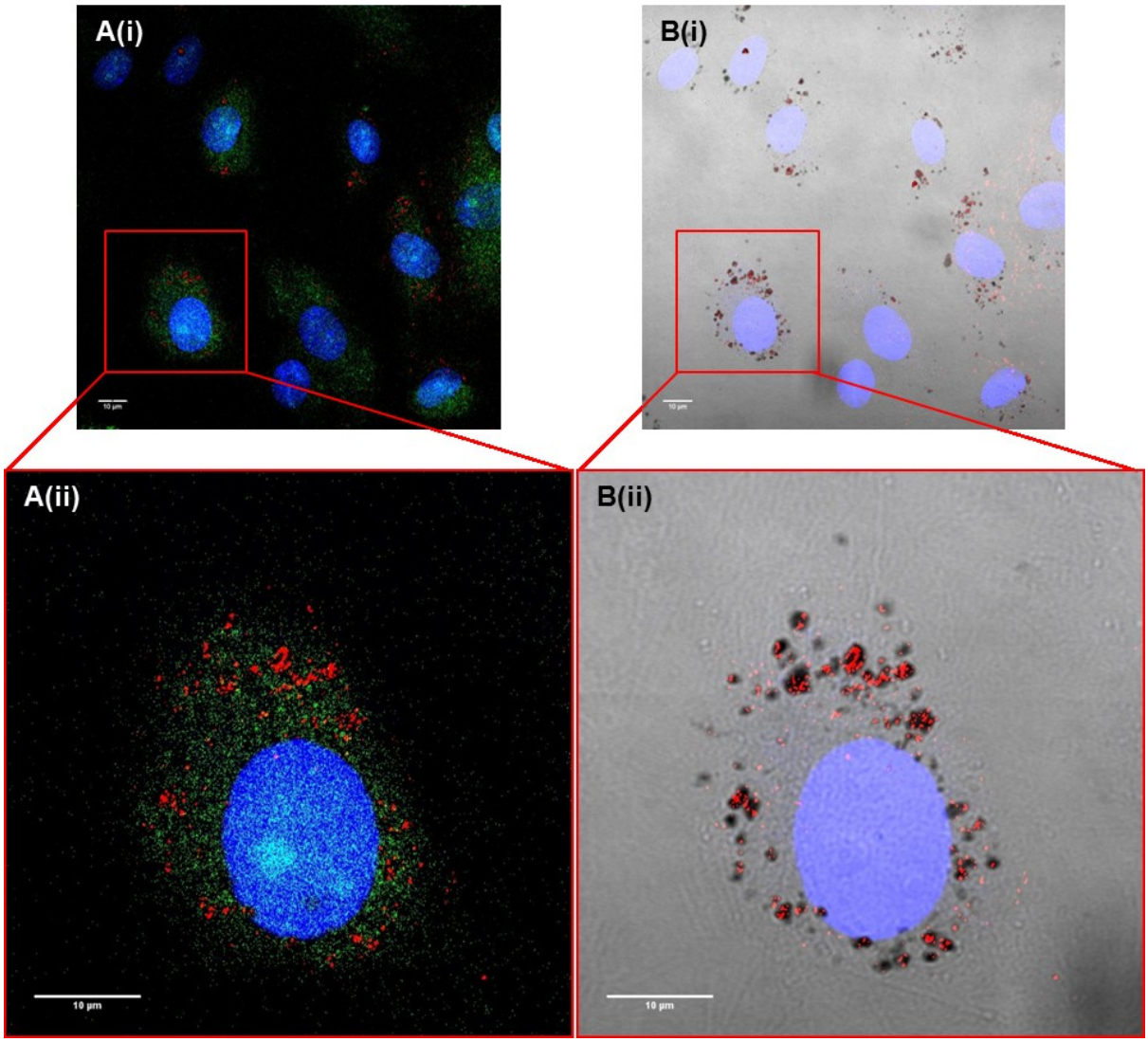


Figure 3.2.14 AO-MWNT uptake in HPMVECs. Following exposure to 10µg/ml AO-MWNTs for 24 hours, MWNTs were localised around the HPMVEC nucleus. ii.) is a magnified image of the cell shown in the red box in i.). The nucleus is depicted in blue, AO-MWNTs were visualised by darkfield microscopy in red, A). Lysosomes are shown in green and B) f-MWNTs are shown by brightfield microscopy. Aii.) AO-MWNT are localised in the cell region containing the lysosomes. Bii.) The red darkfield image is associated with the f-MWNT observed using brightfield microscopy. Scale bars indicate a distance of 10µm.

Epithelial inflammatory response

In order to study the inflammatory potential of MWNTs at the blood-gas barrier, and furthermore, the effect of surface modifications on the severity of this reaction, we investigated the gene and protein expression of the inflammatory mediators IL-6 and IL-8 as a biomarkers of an inflammatory response.

MWNT exposure induced no increase in either the gene expression or protein expression of the inflammatory mediators IL-6 and IL-8 in TT1 or AT2 cells at time points up to 24 hours (Figure 3.2.15-18). Interestingly, in epithelial cells, MWNT exposure appeared to have some anti-inflammatory effects. At 4 hours, a non-significant ($p=0.768$) down-regulation in the expression of the *IL-6* gene is observed in TT1 cells (Figure 3.2.15-A), however this is accompanied by a significant ($p<0.05$) reduction of IL-6 protein expression at 24 hours (Figure 3.2.17-A). No significant reduction in IL-8 protein is observed in TT1 cells at 24 hours ($p>0.05$) (Figure 3.2.17-B).

By 72 hours an increase in inflammatory mediators was, however, observed following MWNT exposure and the differential inflammatory effects of the functional groups could be observed (Figure 3.2.17-C&D). P(M4-VP)-MWNTs had the most pronounced pro-inflammatory effect on TT1 cells and the increase in levels of the inflammatory mediator IL-8 was greater than the increase in IL-6; P(M4-VP)-MWNTs resulted in an IL-8 release that is as high as 7x that of the than the non-treated control value. As previously discussed, the differential effects of the functional groups could be observed in TT1 cells at 72 hours. Exposure to 10μg/ml MWNTs resulted in an increase from the baseline values for AR, P(M4-VP), P(MAA), P(PEGMA and AO-MWNT treated cells, however this increase was variable as summarised in Table 3.2.2.

Mediator	**Non-treated control**	**MWNT sample**				
		AR	P(M4-VP)	P(MAA)	P(PEGMA)	AO
Interleukin-6	256±14	470±29***	786±7***	401±41(ns)	396±14***	305±10(ns)
Interleukin-8	185±6	835±18***	1312±39***	634±7***	614±79***	413±13***

Table 3.2.2 Summary of TT1 cell inflammatory mediator release following a 72 hour exposure to 10μg/ml f-MWNTs. Data is expressed as pg/ml, mean ± SEM, n=4. One-way ANOVA followed by Dunnett's post-test; ns=non-significant, ***$p< 0.001$.

A concentration of 10μg/ml MWNT induced the greatest increase in both IL-6 and IL-8 mediator release in TT1 cells which was highly significant ($p<0.001$). P(MAA) and P(PEGMA)-MWNT

induced a smaller inflammatory response in these cells than AR-MWNTs and AO-MWNTs induced the smallest change in inflammatory mediator levels in these cells (Table 3.2.2).

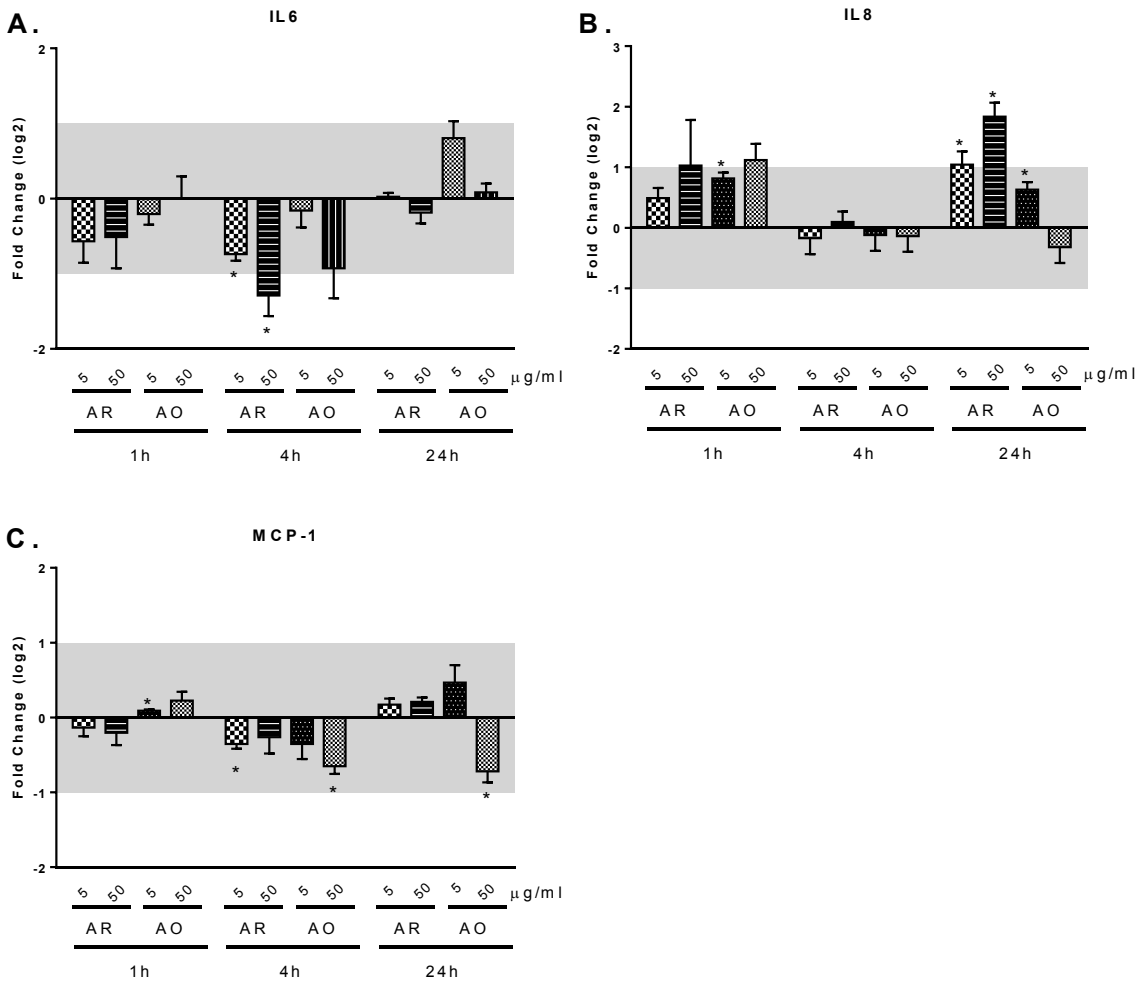


Figure 3.2.15 TT1 *IL-6, IL-8* and *MCP-1* gene regulation in response to a 5 or 50µg/ml AR or AO MWNT exposure for 1, 4 or 24 hours. Values were normalised to a GAPDH loading control and compared to an untreated control using the ΔΔCt method. Data is expressed as mean ±SEM, n=4. For statistical analysis a one sample t-test was performed with values compared to a non-treated control value of 0, *p<0.05

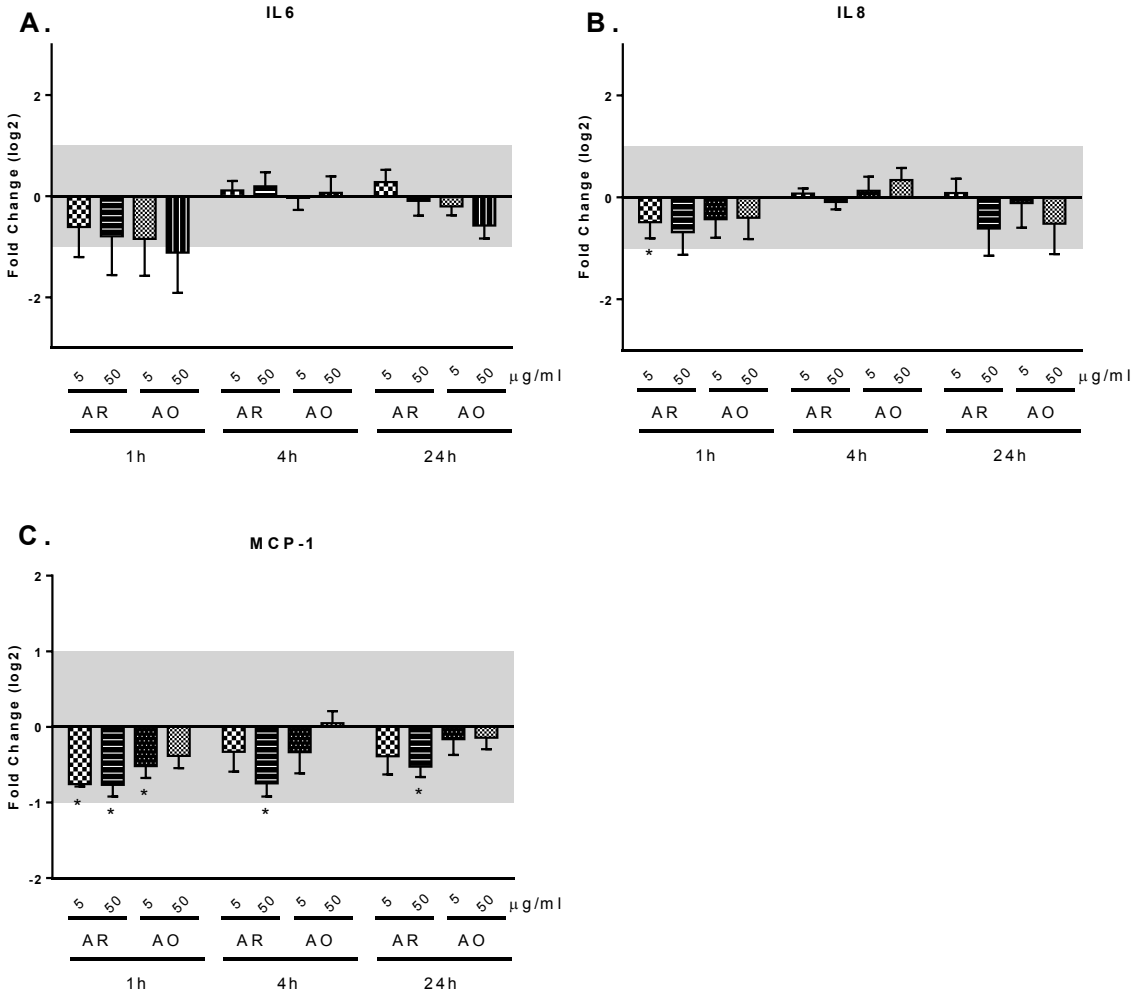


Figure 3.2.16 AT2 *IL-6*, *IL-8* and *MCP-1* gene regulation in response to a 5 or 50µg/ml AR or AO MWNT exposure for 1, 4 or 24 hours. Values were normalised to a GAPDH loading control and compared to a untreated control using the ΔΔCt method. Data is expressed as mean ±SEM, n=4. For statistical analysis a one sample t-test was performed with values compared to a non-treated control value of 0, *p<0.05

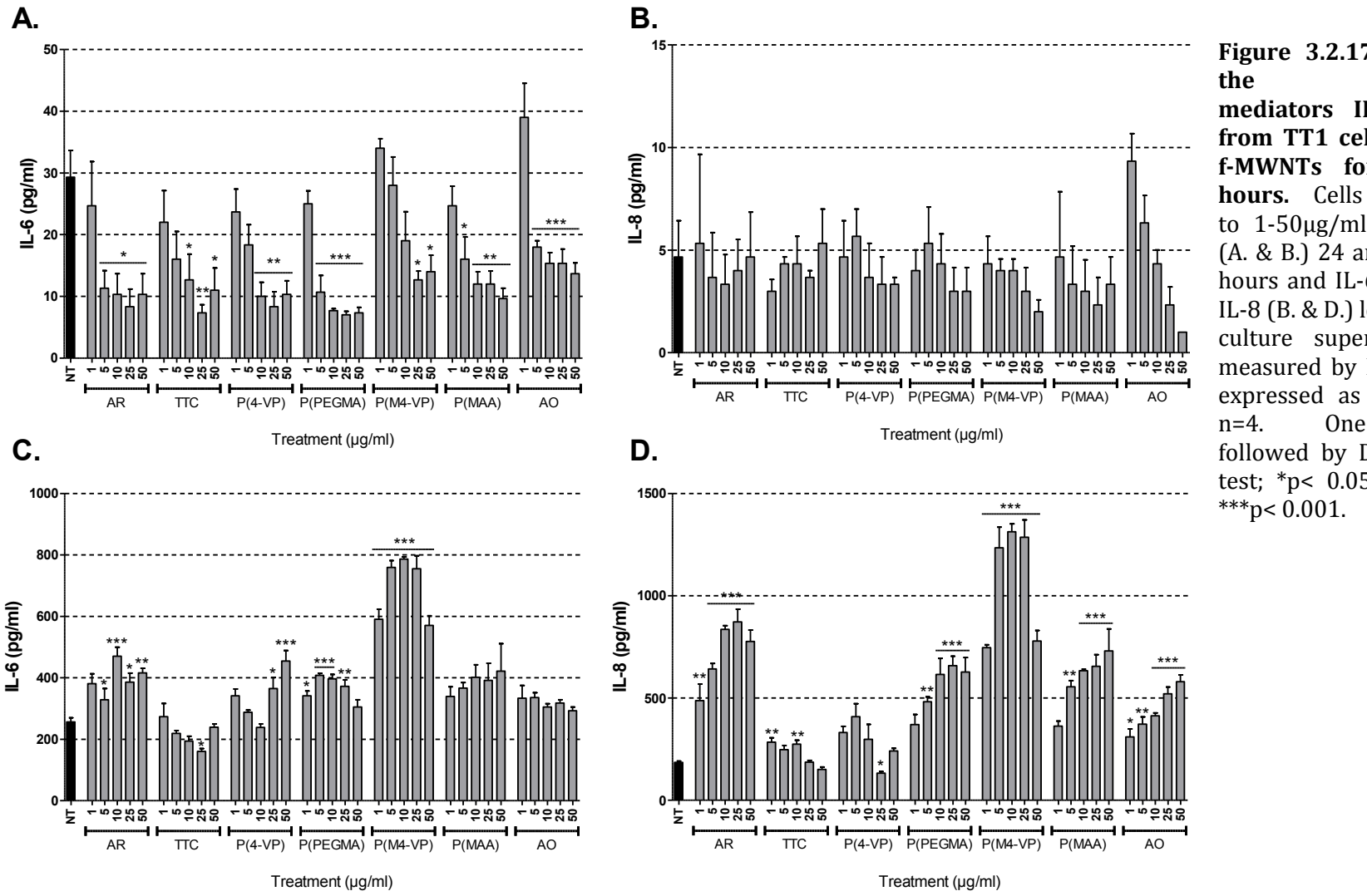


Figure 3.2.17 Release of the inflammatory mediators IL-6 and IL-8 from TT1 cells exposed to f-MWNTs for 24 or 72 hours. Cells were exposed to 1-50µg/ml f-MWNTs for (A. & B.) 24 and (C. & D.) 72 hours and IL-6 (A. & C.) and IL-8 (B. & D.) levels in the cell culture supernatants were measured by ELISA. Data is expressed as mean ± SEM, n=4. One-way ANOVA followed by Dunnett's post-test; *p< 0.05, **p< 0.01 & ***p< 0.001.

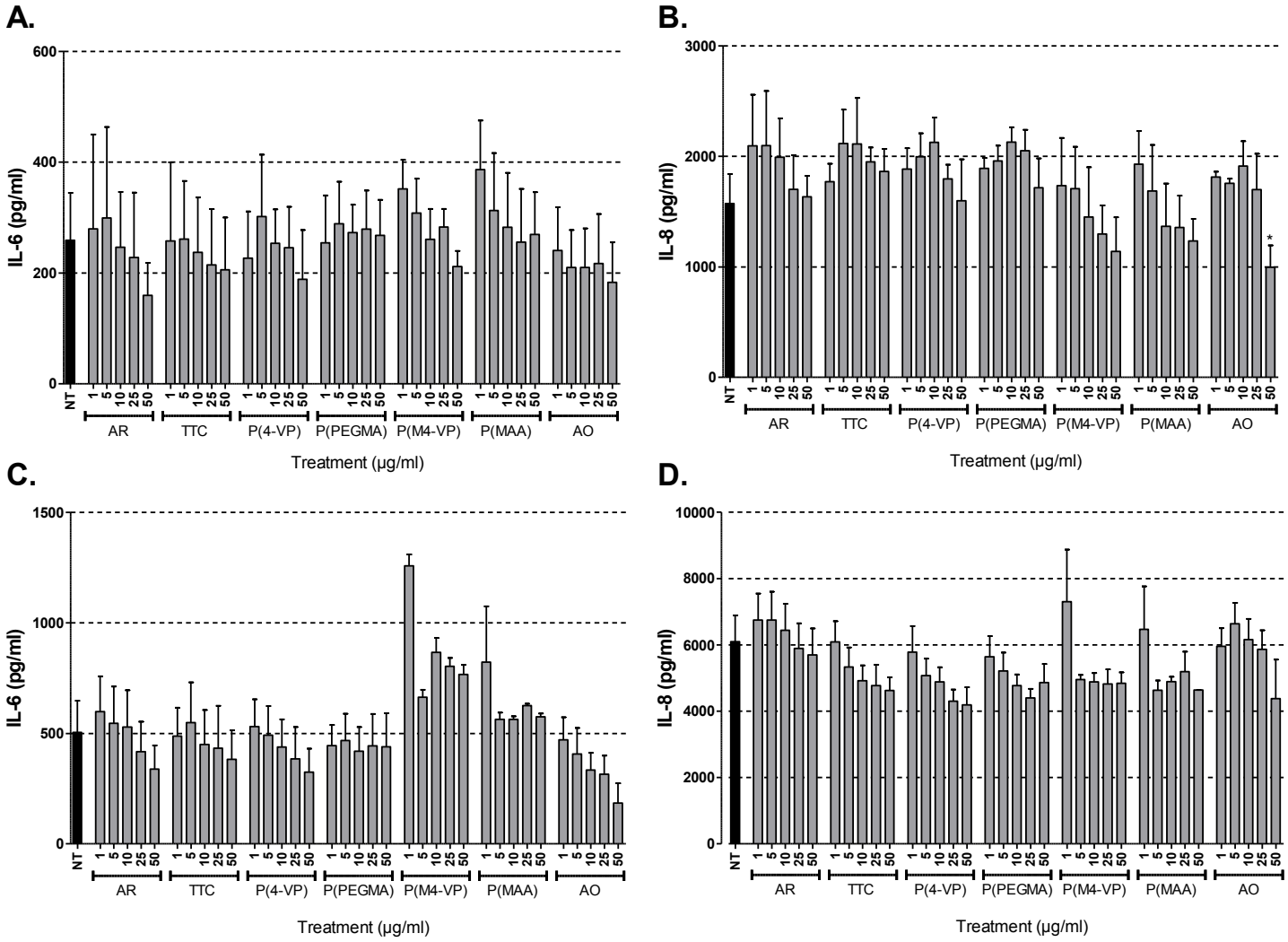


Figure 3.2.18 Release of the inflammatory mediators IL-6 and IL-8 from AT2 cells exposed to f-MWNTs for 24 or 72 hours. Cells were exposed to 1-50µg/ml f-MWNTs for (A. & B.) 24 and (C. & D.) 72 hours and IL-6 (A. & C.) and IL-8 (B. & D.) levels in the cell culture supernatants were measured by ELISA. Data is expressed as mean ± SEM, n=4. One-way ANOVA followed by Dunnett's post-test.

Endothelial inflammatory response

In contrast to the responses observed in epithelial cells, all MWNTs induced an inflammatory response in HPMVECs as early as 4 hours post-exposure. Furthermore, functional groups present on the MWNT surface determined the severity of the inflammatory response. Gene expression analysis indicated that of the time points studied (1, 4 and 24 hours), the greatest change in gene expression was observed at 4 hours. At 4 hours, regulation of the gene expression of inflammatory mediators was observed following exposure to just 1μg/ml AO-MWNTs, however the observed change was not statistically significant. 10μg/ml of both AR-MWNTs and AO-MWNT induced changes in *IL-6, IL-8* and *MCP-1*, however the magnitude of the reaction was dependent on surface functionalisation (Figure 3.2.19). AO-MWNTs induced a more sustained inflammatory response than AR-MWNTs and following the higher concentration of 10μg/ml, upregulation of inflammatory genes was still apparent at 24 hours (Figure 3.2.19).

The effects of AR, P(M4-VP), P(MAA), P(PEGMA) and AO-MWNTs on *IL-6, IL-8* and *MCP-1* gene regulation was therefore investigated further at 4 hours post-exposure, using concentrations of 10μg/ml (Figure 3.2.20). The gene expression profile closely resembled the expression pattern of the corresponding protein; P(M4-VP) and AO-MWNTs induced the greatest increase in IL-6 and IL-8 mRNA (Figure 3.2.20) and protein levels (Figure 3.2.21). The inflammatory response following exposure to P(PEGMA)-MWNTs was not as great as that induced by the other MWNTs studied at both the gene (Figure 3.2.20) and protein expression level (Figure 3.2.21) which inferred that P(PEGMA) functionalisation of MWNTs may provide a slight protective effect against an inflammatory response induced by MWNT exposure.

HPMVECs produced very low basal levels of IL-6, however a concentration-dependent increase in IL-6 was observed at both 4 and 24 hours following MWNT exposure. At 4 hours, this increase was only significant for the highest concentration of 50μg/ml P(M4-VP) and P(MAA)-MWNTs ($p<0.05$) and AO-MWNTs ($p<0.01$) (Figure 3.2.21-A). By 24 hours a concentration-

dependent increase was observed following exposure to all f-MWNTs however the effect was most striking for AO-MWNTs; 1μg/ml resulted in an increase from 3pg/ml to 28pg/ml IL-6 which increased to statistically significant values ($p<0.01$) of 414pg/ml and 422pg/ml at 25μg/ml and 50μg/ml respectively (Figure 3.2.21-C).

All f-MWNTs also induced a concentration-dependent increase in IL-8 at 24 hours. Baseline levels of IL-8 were 28±8 pg/ml and 225±62 pg/ml at 4 and 24 hours respectively (Figure 3.2.21). At 24 hours, 5μg/ml of P(M4-VP) and AO-MWNTs induced a significant ($p<0.05$) increase in IL-8 to 857 and 1208 pg/ml respectively. The greatest IL-8 response (x11 fold greater than baseline) was induced by 25μg/ml AO-MWNT (Figure 3.2.21-D).

The differential inflammatory effects of the functional groups was most striking at 24 hours post-exposure and a concentration of 10μg/ml resulted in an increase in IL-6 and IL-8 for AR, P(M4-VP), P(MAA), P(PEGMA and AO-MWNT treated cells, which is summarised below (Table 3.2.3). AO-MWNTs induced the greatest release of both IL-6 and IL-8. P(M4VP)-MWNTs induced the next greatest increase in IL-8 and P(MAA) and P(PEGMA) functionalised MWNTs induced less IL-8 release than the AR, un-modified MWNTs (Table 3.2.3.).

Mediator	**Non-treated control**	**MWNT sample**				
		AR	P(M4-VP)	P(MAA)	P(PEGMA)	AO
Interleukin-6	3±1	8±3(ns)	12±4(ns)	11±5(ns)	9±3(ns)	200±149(ns)
Interleukin-8	225±62	910±382*	1080±317**	748±281*	712±196*	1747±343***

Table 3.2.3 Summary of HPMVEC inflammatory mediator release following a 24 hour exposure to 10μg/ml f-MWNTs. Data is expressed as pg/ml, mean ± SEM, n=4. One-way ANOVA followed by Dunnett's post-test; ns=non-significant, *p< 0.05, **p< 0.01 & ***p< 0.001.

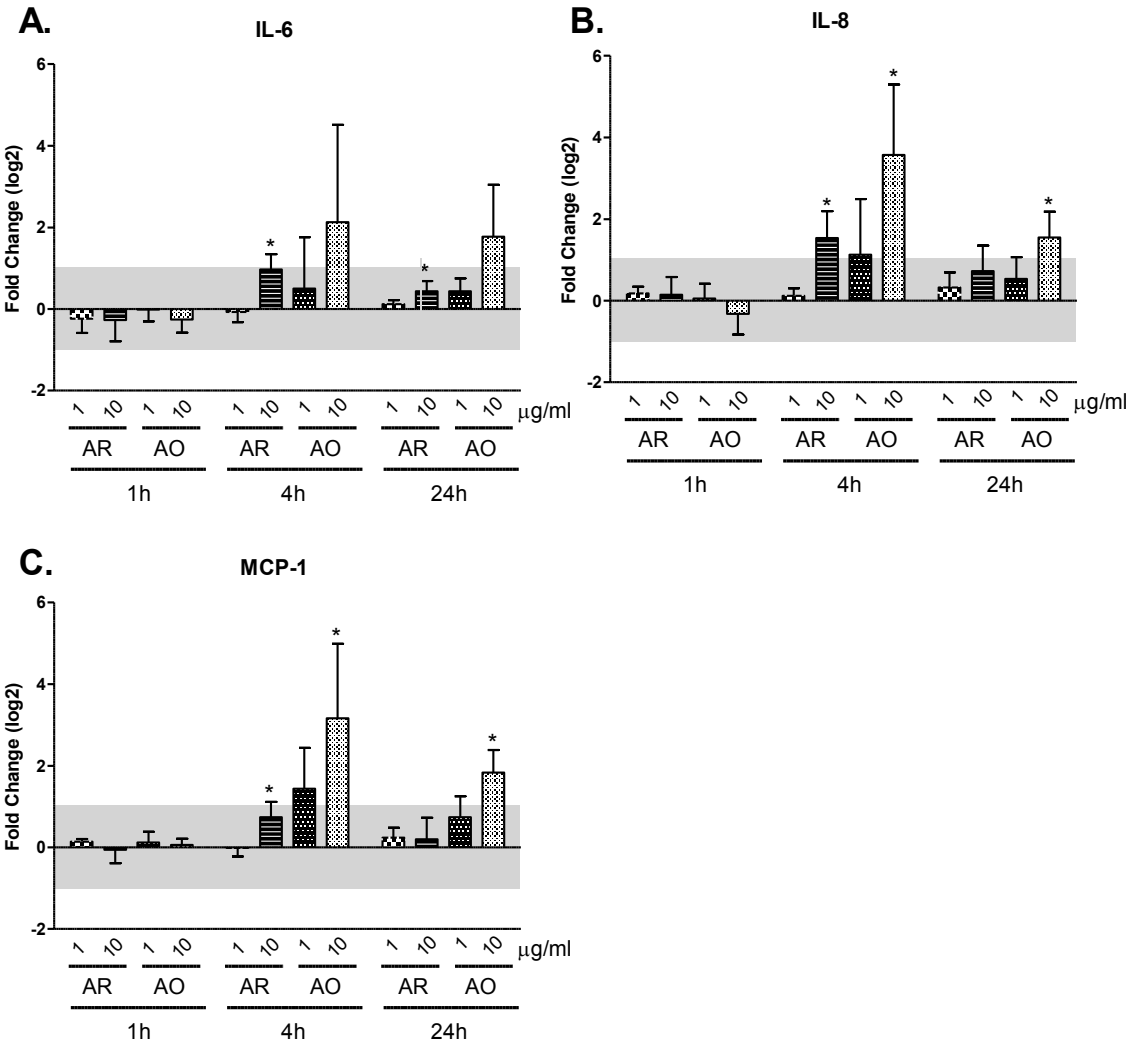


Figure 3.2.19 HPMVEC *IL-6*, *IL-8* and *MCP-1* gene regulation in response to a 1 or 10µg/ml AR or AO MWNT exposure for 1, 4 or 24 hours. Values were normalised to a GAPDH loading control and compared to an untreated control using the ΔΔCt method. Data is expressed as mean ±SEM, n=4. For statistical analysis a one sample t-test was performed with values compared to a non-treated control value of 0, *p<0.05

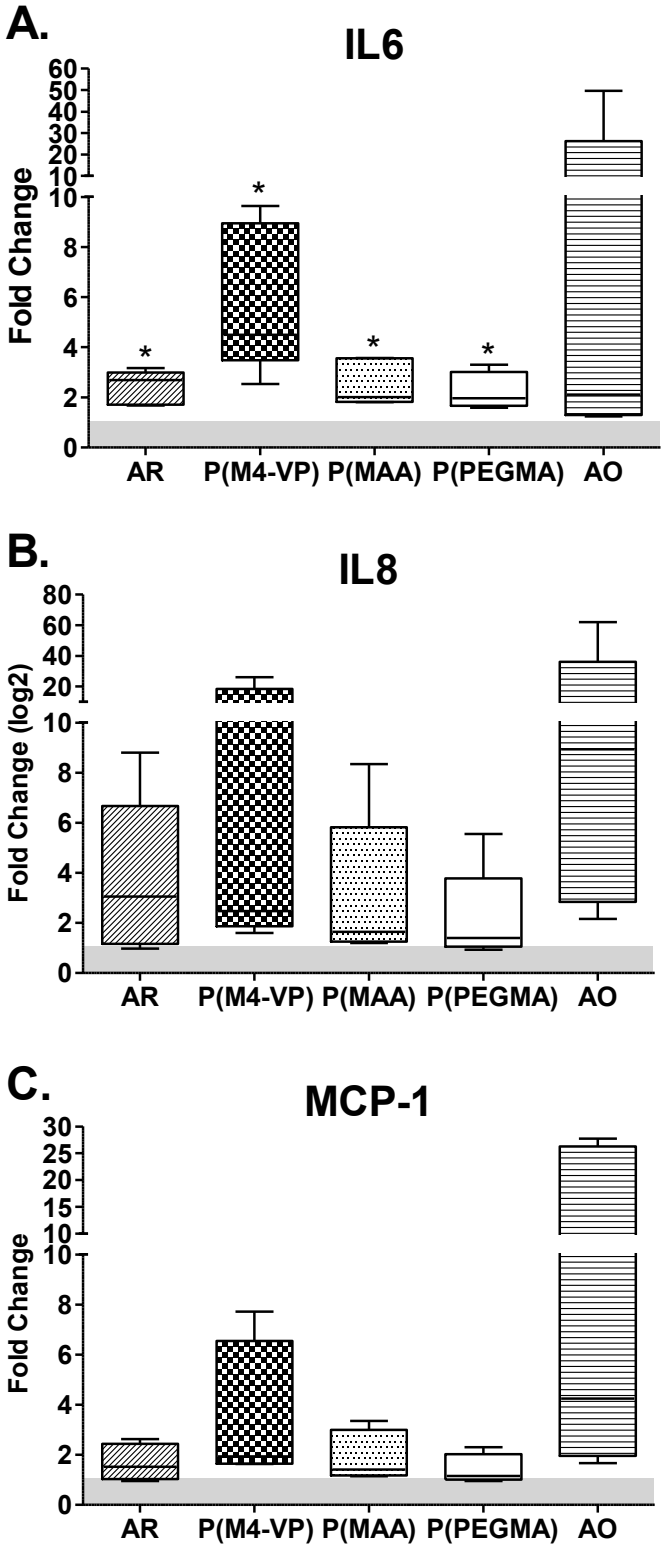


Figure 3.2.20 HPMVEC IL-6, IL-8 and MCP-1 gene regulation in response to 10µg/ml AR, P(M4-VP), P(MAA), P(PEGMA)or AO MWNTs. Values were normalised to a GAPDH loading control and compared to an untreated control using the ΔΔCt method. Data is expressed as median ±SEM, n=5. For statistical analysis values were transformed to their logarithms to make the distribution more Gaussian, a one-sample t-test was then performed with values compared to a non-treated control value of 0, *p<0.05

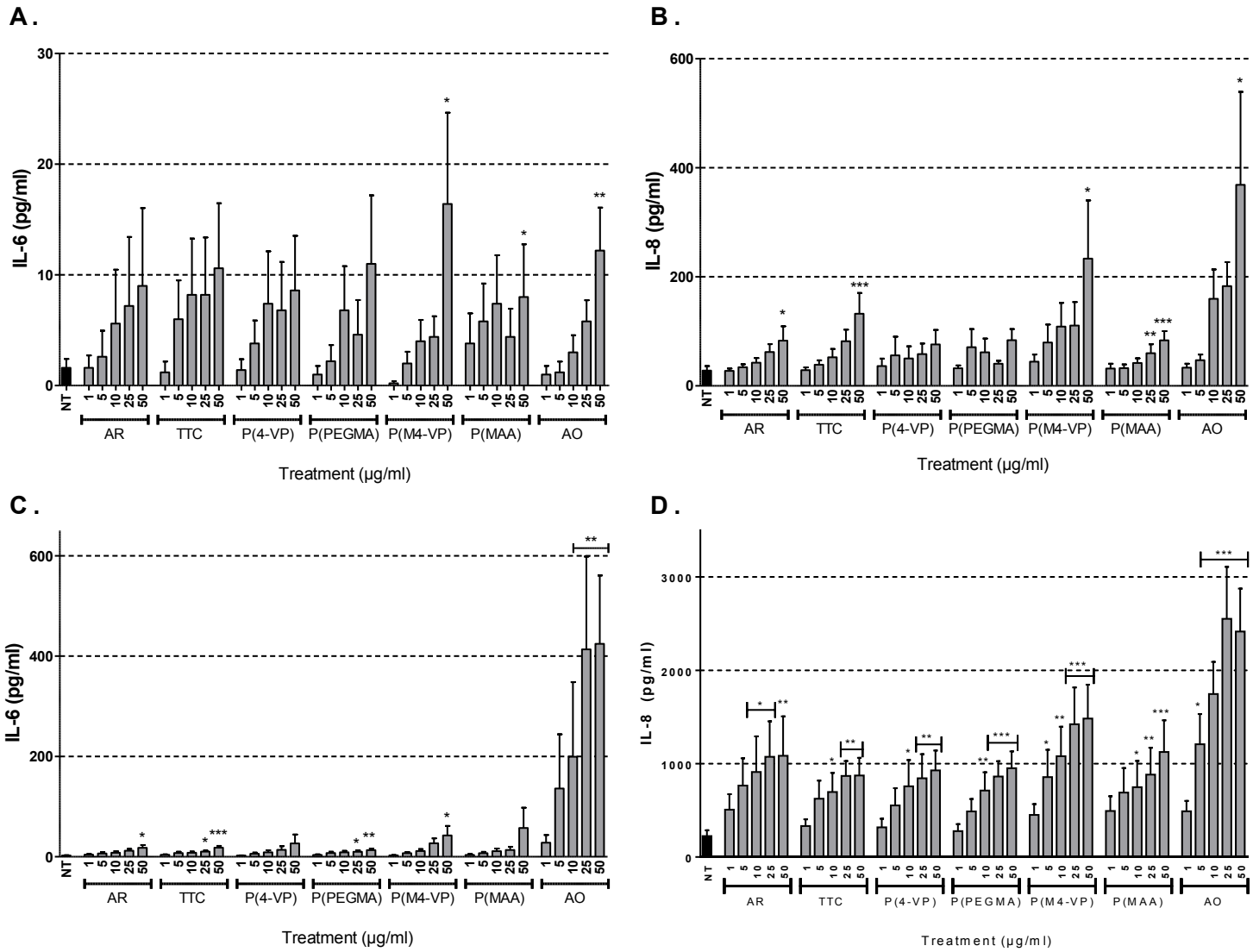


Figure 3.2.21 Release of the inflammatory mediators IL-6 and IL-8 from HPMVECs exposed to f-MWNTs for 4 or 24 hours.

Cells were exposed to 1-50µg/ml f-MWNTs for (A. & B.) 4 and (C. & D.) 24 hours and IL-6 (A. & C.) and IL-8 (B. & D.) levels in the cell culture supernatants were measured by ELISA. Data is expressed as mean ± SEM, n=4. One-way ANOVA followed by Dunnett's post-test; *p< 0.05, **p< 0.01 & ***p< 0.001.

ROS formation following MWNT exposure

Following a 24 hour exposure to MWNTs, a significant reduction in ROS was observed in TT1 cells ($p<0.001$), this was further reduced at 72 hours post exposure (Figure 3.2.22). This result was concentration-dependent and at the highest concentration of 50µg/ml values were up to 31% and 33% lower than the control values at 24 and 72 hours respectively. At both 24 and 72 hours AO-MWNT exposure resulted in the least variation in ROS levels. The observed decrease in ROS was significant at MWNT concentrations as low as 1µg/ml for P(M4-VP) and AO-MWNT treated cells at 24 hours and all particles except P(PEGMA)-MWNTs at 72 hours.

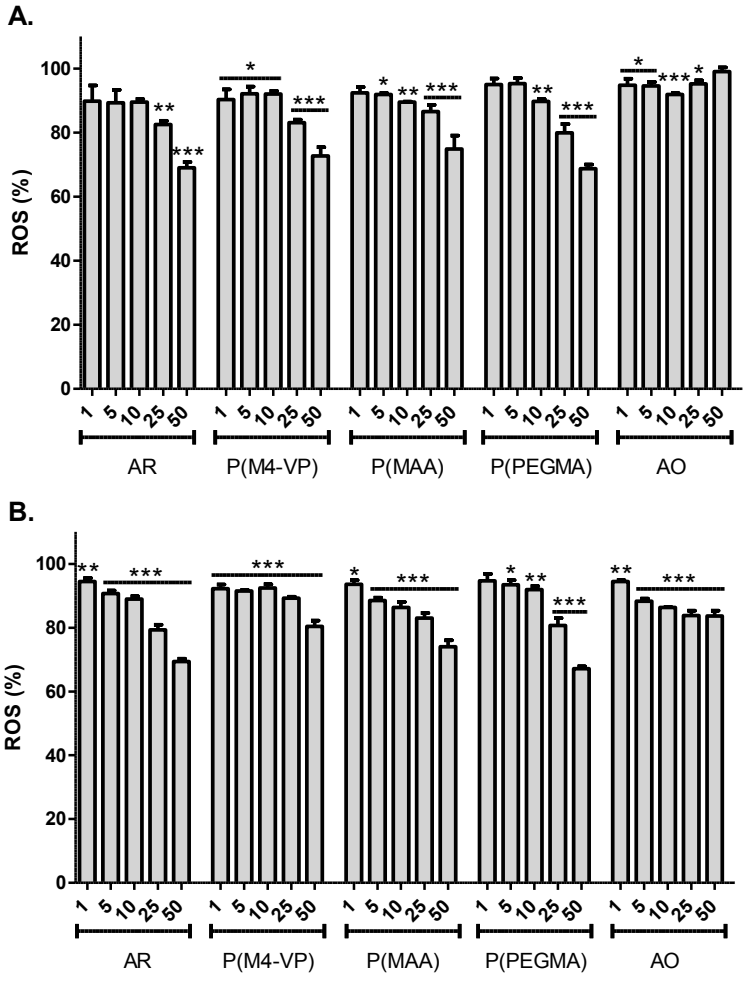


Figure 3.2.22 ROS generation in TT1 cells determined by CM-H2DCFDA. TT1 cells were exposed to 1, 5, 10, 25 and 50µg/ml of the indicated CNTs. Levels of ROS were determined using the CM-H2DCFDA dye at 24 (A.) and 72 (B.) hours post exposure. Values represent % of untreated control, data is expressed as mean ± SEM. One-way ANOVA followed by Dunnett's post-test; *$p<0.05$, **$p<0.01$, ***$p<0.001$, n=4.

No obvious change in AT2 ROS was detected using the CM-H2DCFDA dye (n=1) (Figure 3.2.23). Due to the absence of cytotoxic or inflammatory response and the availability of primary human lung tissue this was not investigated further.

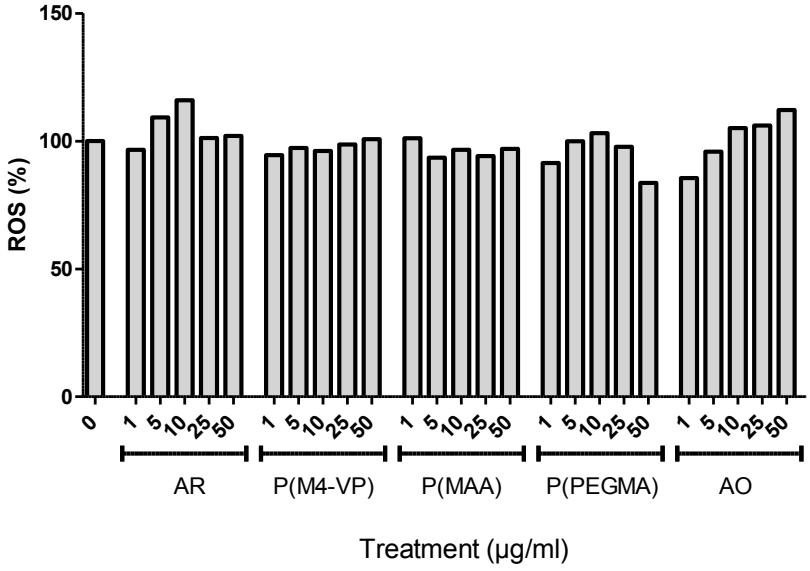


Figure 3.2.23 ROS generation in AT2 cells determined by CM-H2DCFDA. AT2 cells were exposed to 1, 5, 10, 25 and 50µg/ml of the indicated CNTs. Levels of ROS were determined using the CM-H2DCFDA dye at 24 hours post exposure. Values represent % of untreated control, n=1.

Following exposure to MWNT for 1 hour, concentrations ≥25µg/ml of P(M4-VP) and 25µg/ml P(PEGMA)-MWNTs resulted in a significant increase in HPMVEC ROS ($p<0.05$). By 3 hours, a significant effect was also observed in AR-MWNT treated cells (≥10µg/ml, $p<0.05$) and at 6 hours all particles except AO-MWNT resulted in a concentration dependent increase in ROS in HPMVECs (>5µg/ml, $p<0.05$); an effect which was sustained at 24 hours. The greatest increase in ROS was observed following exposure to P(M4-VP)-MWNTs; at 6 hours and 24 hours 25µg/ml P(M4-VP)-MWNTs increased ROS by 107% ($p<0.01$) and 166% ($p<0.001$) respectively (Figure 3.2.24).

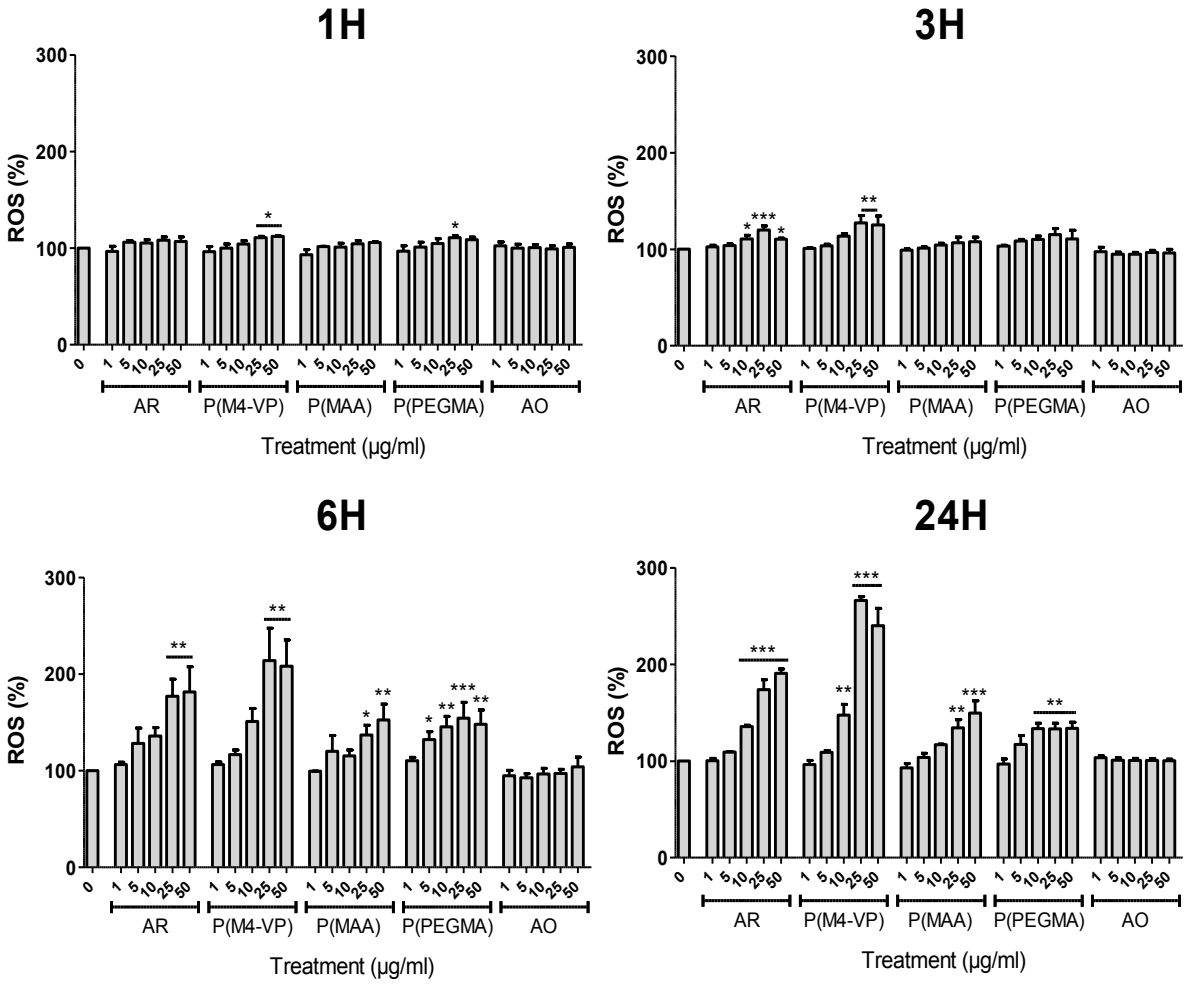


Figure 3.2.24 ROS formation in HPMVECs following MWNT exposure. HPMVECs were exposed to 1-50µg/ml f-MWNTs for 1, 3, 6 or 24 hours and ROS formation was determined using the CM-H2DCFDA dye. Data is expressed as mean ± SEM, n=4. One-way ANOVA followed by Dunnett's post-test; *p< 0.05, **p< 0.01.

ROS generated in HPMVECs following exposure to 10µg/ml AR, P(M4-VP), (PMAA), and P(PEGMA)-MWNTs could be significantly reduced (p<0.01 – p<0.05) with the use of 5mM N-acetylcysteine (NAC), 1mM glutathione or 100µM ascorbic acid anti-oxidants (Figure 3.2.25). Antioxidants had no effect on AO-MWNT which is expected as AO-MWNTs induced no significant ROS in these cells (Figure 3.2.25).

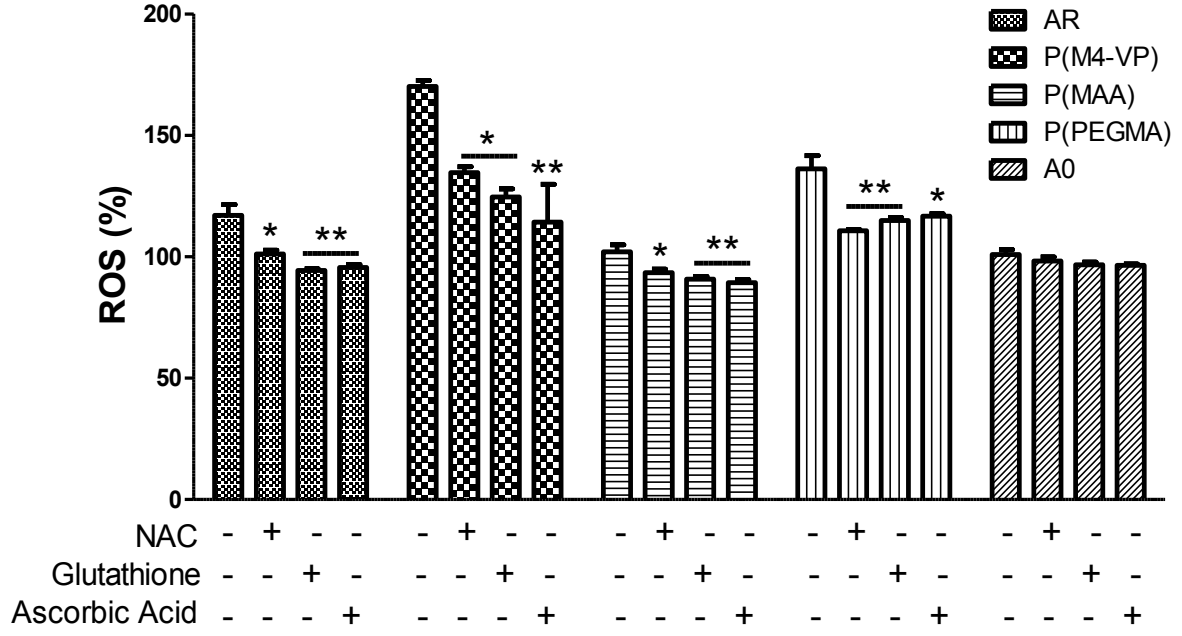


Figure 3.2.25 Effect of antioxidants on ROS formation in HPMVECs following 10µg/ml MWNT exposure. HPMVECs were pre-treated with 5mM N-acetylcysteine (NAC), 1mM glutathione or 100µM ascorbic acid, before exposure to 10µg/ml f-MWNTs in the presence of the aforementioned antioxidants for 24 hours. ROS formation was determined using the CM-H2DCFDA dye. All antioxidants significantly reduced ROS induced by MWNT exposure. Data is expressed as mean ± SEM, n=4. Mann-Whitney t-test; *p< 0.05, **p< 0.01.

Baseline release of IL-6 was unaffected by glutathione treatment, however, glutathione inhibited AO-MWNTs induced IL-6 release; the addition of glutathione reduced 25µg/ml AO-MWNT induced IL-6 release from 521pg/ml to 303pg/ml (Figure 3.2.26 A+B).

Following treatment with 1mM glutathione, baseline release of IL-8 was reduced from 1074 to 402 pg/ml (Figure 3.2.26 C+D). Similarly, IL-8 release following MWNT exposure was also partially inhibited, for example 5µg/ml AO-MWNT induced IL-8 release decreased from 2007pg/ml to 1241pg/ml (Figure 3.2.26 C+D).

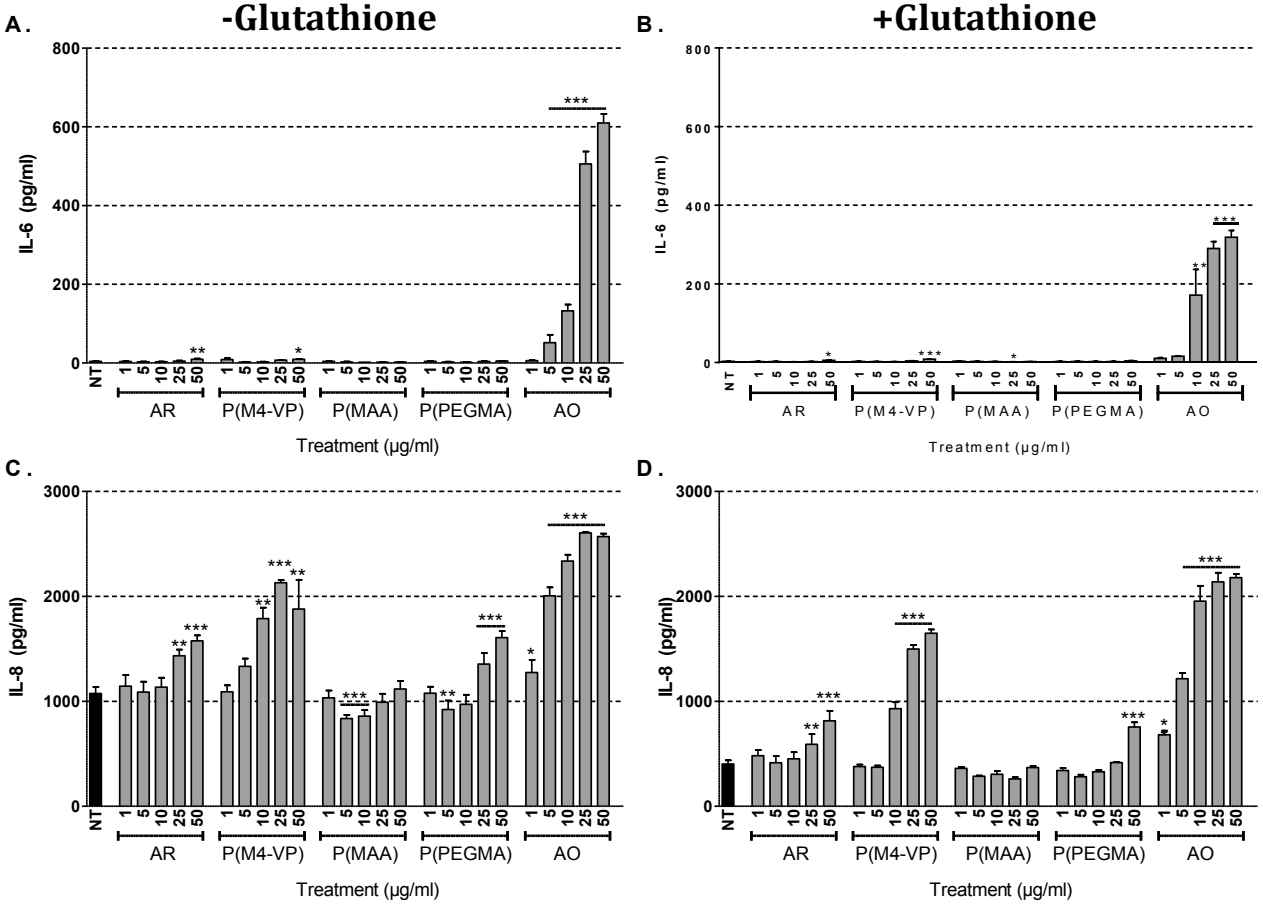


Figure 3.2.26 Effect of antioxidant addition on inflammatory cytokine release from HPMVECs.

HPMVECs were either pre-treated with 1mM glutathione prior to exposure to 1-50µg/ml f-MWNTs in the presence of 1mM glutathione (B. & D.) or exposed to 1-50µg/ml f-MWNTs in the absence of glutathione (A. & C.) for 24 hours. Release of the inflammatory cytokines IL-6 (A. & B.) and IL-8 (C. & D.) Data is expressed as mean ± SEM, n=3. One-way ANOVA followed by Dunnett's post-test; *p< 0.05, **p< 0.01.

3.3. Discussion

In vitro model characterisation

The isolated primary human pulmonary endothelial cells (HPMVECs) used in this study were profiled for a range of endothelial markers as we developed a modified protocol for their isolation that had not been previously used. It is well established that it is not only macro and microvascular endothelial cells that differ, but that there is also heterogeneity between microvascular endothelial cells from different organ sites (Hewett & Murray, 1993; Kim & Kim, 1991; Magee, Stone, Oldham, & Guice, 1994; Stevens, 2011). It was therefore deemed important that we use pulmonary microvascular endothelial cells in this study, over other common alternatives such as human umbilical vein endothelial cells (HUVECs).

Following the first isolation with anti-CD31-conjugated dynabeads, some cell cultures contained fibroblast-like cells that if left, would continue to grow over the cell monolayer, thus a second isolation step was required. Following the second isolation with anti-CD31 dynabeads, the cells were extensively characterised. At passages 2-8, cells displayed a number of characteristics indicative of an endothelial phenotype. Cells formed tubular structures on BD-matrigel, produced endothelin-1 and E-selectin and were VE-cadherin, CD31, RAGE and caveolin-1 positive. A number of genes that are differentially expressed in endothelial cells in response to inflammatory stimuli were also induced in these cells following TNFα treatment, including *ICAM-1, VCAM-1, E-selectin* and *Tissue Factor*. After the cell isolation protocol had been successfully established, cells from each donor were determined to be of an endothelial phenotype using VE-cadherin staining alone.

Using this cell isolation method, it was possible to generate HPMVECs and AT2 cells from a single donor tissue without compromising either *in vitro* model, thus allowing for patient matched comparisons between cell types.

Differential cytotoxic responses observed following functionalised carbon nanotube exposure

The MWNTs used is this study were not acutely cytotoxic to alveolar epithelial cells *in vitro* at concentrations as high at 50μg/ml. Epithelial cells play a crucial role in lung defence and are essential components of the barrier between air and the underlying tissue (Fehrenbach, 2001; Thorley & Tetley, 2013; Thorley *et al*., 2011). The lung is continuously exposed to inhaled particulate matter and thus it is unsurprising that these cells are able to tolerate some degree of particle load. The LDH assay performed on TT1 cell supernatants, indicated that longer exposures of 24 and 72 hours resulted in cell membrane damage, a feature often associated with a cytotoxic response. At 24 hours this was only apparent in cells treated with high concentration (≥25μg/ml) of P(MAA) or AO-MWNTs. Interestingly, -COOH groups introduced to the MWNT surface by acid oxidation and P(MAA) functional groups both carry a negative charge, indicating that at 24 hours the negatively charged particles may result in greater membrane damage. By 72 hours all particles resulted in a concentration dependent release of LDH ($p<0.001$). The MTS assay did not however indicate that there was a consistent, concentration dependent reduction in cell viability at 24 or 72 hours. That the MTS and LDH assay do not correlate could be because the LDH assay is more sensitive than the MTS assay, that the LDH assay is detecting membrane damage induced by MWNTs that is not resulting in cell death, or alternatively that the cells are proliferating to counteract cell death.

Neither the LDH nor MTS assays detected any change in AT2 viability following MWNT exposure. The finding that CNTs were more reactive with TT1 than AT2 cells is important as AT2 cells are able to proliferate and differentiate into AT1 cells (Fehrenbach, 2001). It is possible that damage as a result of AT1 toxicity could therefore be more transient than that as a result of AT2 toxicity due the ability of AT2 cells to divide, differentiate and repair barrier integrity. The differential response of type-1 and type-2 alveolar epithelial cells could be due to the presence of the surfactant layer in AT2 cultures. It is important to note that, *in vivo*, surfactant secreted by AT2 cells would also cover type-1 alveolar epithelial cells, and so the

presence of surfactant in TT1 cultures is more representative of the *in vivo* situation. The presence of surfactant may reduce the amount of MWNTs that reach the cell surface, or provide a surfactant coating to the MWNT making them more inert. Previous studies have indeed shown that the composition of the protein corona of nanoparticles can affect their bioreactivity (Saptarshi, Duschl, & Lopata, 2013).

No study has previously addressed the question of the potential cytotoxic response to functionalised MWNT in primary human alveolar type-2 epithelial cells, however studies using the epithelial carcinoma cell line A549 (Pulskamp, Diabaté, & Krug, 2007), demonstrated that CNTs induced no cytotoxicity in these cells at concentration as high as 100µg/ml, but that some CNTs did induce ROS formation. The four CNTs used in this study had a number of variables including their diameter, metal content and being both single and multi-walled. In addition not all CNTs were well characterised and so although the authors suggested that metal-contaminants were the underlying cause of ROS generation following exposure, it is unclear what the effect each variable had on toxicity. In contrast, a second study investigating the differential effects of alveolar epithelial and bronchial epithelial cells using the cells lines A549 and BEAS-2B found MWNT to induce a small reduction in alveolar epithelial cell viability at similar concentrations to those used in this study, however MWNTs were much more toxic to the bronchial epithelial cells (Ursini *et al*., 2014). The effect of functionalised MWNTs exposure on type-1 alveolar cell viability was addressed in the TT1 cell line in work completed by myself and published in an article published by our group in 2014 (Shu Chen *et al*., 2014).

Not only could alveolar epithelial death disrupt the efficacy of gas exchange within the lungs but disruption of the alveolar-capillary barrier could allow increased access of particles to the underlying endothelium. Functionalised MWNTs showed signs of acute toxicity in microvascular endothelial cells. Using the MTS assay HPMVEC viability appeared to decrease at 4 hours, however the MTS assay indicated that populations had largely recovered by 24 hours. This could have been due to either an increase in mitochondrial activity or an increase in cell

proliferation that counteracted the reduction in cell activity due to cell death. The BrdU assay was therefore carried out to investigate whether cell proliferation was occurring following MWNT exposure. Results from the BrdU assay indicated that a likely cause of apparent recovery of the cell population could be increased cell proliferation; AR, P(M4-VP) and P(PEGMA)-MWNT which resulted in a significant, concentration-dependent reduction in mitochondrial activity at 4 hours, also displayed a significant concentration-dependent increase in cell proliferation at 24 hours. Furthermore, P(MAA) and AO-MWNT exposure did not result in a significant decrease in HPMVEC viability at 4 hours and these same particle induced the smallest increase in cell proliferation at 24 hours (Figure 3.2.8 & Figure 3.2.9).

Endothelial proliferation typically follows inflammation as part of the wound repair process; during proliferation additional extra-cellular matrix proteins are deposited to restore integrity to the wound and angiogenesis occurs to sustain the new tissue (Li, Zhang, & Kirsner, 2003). This is regulated by a number of growth factors including vascular endothelial growth factor (VEGF), angiopoietin-1 (Ang-1) fibroblast growth factor (FGF) and transforming growth factor beta (TGF-β) (Dimmeler & Zeiher, 2000; J. Li *et al*., 2003).

Angiogenesis has previously been observed following *in vivo* instillation of fibres; following the intraperitoneal injection of crocidolite asbestos fibres into mice, vasculature was formed around clusters of asbestos fibres (Branchaud, MacDonald, & Kane, 1989). Furthermore, angiogenesis has been observed in *in vitro* models following CNT exposure (Azad *et al*., 2013; Snyder-Talkington *et al*., 2013). In both CNT studies, angiogenesis was attributed to an increase in the pro-angiogenic factor VEGF. HPMVECs do not however express detectable levels of the VEGF protein in monoculture (Snyder-Talkington *et al*., 2013). Any angiogenic effect seen in HPMVEC monocultures would therefore be due to an increase in non-VEGF pro-angiogenic factors such as Ang-1 or nitric oxide or down-regulation of angiogenesis inhibitors such as thrombospondin (Dimmeler & Zeiher, 2000). Whether f-MWNT exposure has an effect on HPMVEC angiogenesis should be analysed using assays such as the tube formation assay seen in Figure 3.2.5.

As previously mentioned, endothelial cell death could have implication for disease progression as this exposes circulating thrombotic factors to underlying Tissue Factor, thus inducing clot formation and the potential for plaque formation (Steffel *et al*., 2006). Furthermore, endothelial cell death interrupts the integrity of the endothelial barrier which is essential for normal pulmonary function and tissue integrity (Mehta *et al*., 2004). The increase in cell proliferation following the reduction in cell viability may be a reflection of the importance that the endothelial barrier remain functional.

Particle uptake in alveolar epithelial and microvascular endothelial cells

Levels of MWNT particle uptake varied greatly between both AT2 and TT1 epithelial cells and also between these epithelial cells and endothelial cells. TEM analysis showed that TT1 cells internalised MWNT in very large macropinocytotic vesicles, resulting in an extremely high particle load in some cells. This could account for the reduced cell viability over the longer periods of exposure and additionally contribute to the inflammatory response seen at 72 hours in TT1 cells. Conversely, very few MWNTs were observed in AT2 cells, which coincided with the lack of a cytotoxic or inflammatory response, and the absence of any detectable ROS.

Ursini *et al* (2014) studied the cytotoxic and inflammatory effects and the uptake of MWNT and COOH-MWNTs using the alveolar epithelial cell line, A549 and the bronchial epithelial cell line, BEAS-2B. This study found higher uptake of MWNTs that had been -COOH modified, which corresponded to a higher cytotoxic response in BEAS-2B cells and a greater inflammatory response in A549 cells. Although commonly used in *in vitro* studies due to their availability and the ease with which they can be cultured, A549 cells do not provide a perfect model for either type 1 or type 2 alveolar epithelial cells. Using Raman spectroscopy it has been shown that A549 are more similar to differentiated AT1 cells than undifferentiated AT2 cells (Swain *et al*., 2010). There are however key differences in the phenotypes of AT1 cells and A549 cells which have meant that typically A549 cells are used as a type 2 alveolar epithelial cell model. These

characteristics include the presence of lamellar bodies and microvilli and the production of the proteinase inhibitors SLPI and elafin (Davoren *et al*., 2007; Foster *et al*., 1998; van den Bogaard *et al*., 2009).

Kostarelos *et al* indicated that their findings regarding CNT toxicity may be due to an uptake mechanism that is at least partially endocytosis-independent. Despite investigating nanoparticle uptake in a number of cell types including carcinoma cells, fibroblasts and keratinocytes this study does not address the question of f-MWNT uptake in primary human lung cells (Kostarelos et al., 2007). Work by our group indicates that uptake of NPs varies significantly between these cells, notably the rate of particle uptake by type 1-like and type 2 alveolar epithelial cells is markedly different (Kemp *et al*., 2008).

Both TT1 cells and HPMVECs endocytosed large quantities of MWNTs following exposure. In TT1 cells there was evidence of macropinocytosis following exposure to all particles except AO-MWNTs, which is likely due to the highly dispersed and water stable nature of AO-MWNTs, resulting in the absence of large agglomerates. P(M4-VP)-MWNTs were frequently associated with the plasma membrane, a phenomenon which has been hypothesised to be due to electrostatic attraction between the cationic, positively charged particle and the plasma membrane (Chen *et al*., 2014). Similarly, P(MAA)-MWNTs were often observed aligned parallel to, rather than inserted into the plasma membrane as was seen with other MWNTs. It has been hypothesised that this may be due to electrostatic repulsion of the anionic, negatively charged P(MAA)-MWNTs (Chen *et al*., 2014). Individual MWNT observed within the cell cytoplasm may have entered by piercing the plasma membrane (Al-Jamal *et al*., 2011; Chen *et al*., 2014; Shi et al, 2011); this provides a potential explanation for the increased TT1 LDH release observed following MWNT exposure.

HPMVECs have a great potential for the uptake of particles due to the large number of caveolae in these cells, (Mehta *et al*., 2004). The greatest particle uptake in HPMVECs was observed following exposure to P(M4-VP) and AO-MWNTs. Cells exposed to these particles had

distinctive localisation of CNTs to the area surrounding the cell nucleus where an abundance of lysosomes was also present. Co-localisation of particles and lysosomes was not evident, however this may be due to MWNTs interfering with the fluorescent signal as has been observed in previous studies (Breznan *et al*., 2015). As P(M4-VP) and AO-MWNTs were internalised to a greater extent than other MWNTs, and also induced the greatest inflammatory response, MWNT toxicity in HPMVEC may be uptake-dependent. This should be further investigated using endocytosis inhibitors such as RNA interference technology targeting caveolin or clathrin formation. It was not possible to determine whether MWNTs were present inside the cytoplasm or plasma membrane of HPMVEC due to the lower resolution of confocal microscopy.

Differential reactivity of carbon nanotubes with TT1 or AT2 epithelial cells: release of inflammatory mediators and reactive oxygen species

No inflammatory response was observed following exposure of AT2 cells to MWNT for 72 hours. In contrast, in TT1 cells there was a slight down-regulation of *IL-6* gene expression accompanied by a decrease in IL-6 cytokine levels at 24 hours. By 72 hours a pro-inflammatory response was evident in TT1 which was greatest for P(M4-VP)-modified MWNTs .

As our MWNT induced no discernible toxic responses in AT2 cells, and only a moderate response in TT1 cells with prolonged exposure, it may be that these particles are tolerated at the alveolar epithelium in the short term. Repeated exposure or inefficient particle clearance by resident macrophages could however lead to type 1 alveolar cell toxicity. As AT2 cells are pluripotent and differentiate into type-1 epithelial cells (Fehrenbach, 2001), it may be that type-1 cells lost as a result of MWNT exposure could be replaced by the largely unaffected AT2 cell population.

That MWNT exposure is unlikely to be acutely toxic to AT2 cells is supported by a number of other *in vitro* and *in vivo* studies. A study using the pulmonary carcinoma cell line A549

demonstrated that MWNTs were not acutely cytotoxic to these cells however the presence of transmission metals did result in an increase in ROS production (Pulskamp *et al*., 2007). During this study we observed no increase in either type-1 or type-2 epithelial cell ROS production, in fact MWNT appeared to induce a decrease in TT1 ROS. Several studies have previously identified that purified MWNTs can efficiently quench ROS, and it is thought that this might be due to grafting of the radical to the surface of the carbon nanotube (Fenoglio *et al*., 2006; Nymark *et al*., 2014). As the reduction in TT1 cell ROS was least in AO-MWNTs treated cells, this may be due to the fact that these particles may already be saturated with surface oxygen groups. Interestingly, ROS levels are still low even when an inflammatory response is observed 72 hours following exposure.

Contrasting the epithelial and endothelial inflammatory response to functionalised carbon nanotube exposure

The response of endothelial cells to MWNT exposure was strikingly different from that of epithelial cells. Whereas an inflammatory response was absent in AT2 cells and only observed after 72 hour exposure in TT1 cells, endothelial cells showed an inflammatory response at just 4 hours at both the gene expression and protein level. The CM-H2DCFDA dye showed that, unlike the response seen in epithelial cells, where ROS actually decreased following MWNT exposure, ROS levels in endothelial cells increased from as early as 1 hour and became highly significant by 6 hours for all particles except AO-MWNT. It appears that the ROS quenching observed in TT1 cells is either overcome by the dramatic increase in HPMVEC ROS production or does not occur in this cell system.

It was in endothelial cells that the functionalisation of MWNT had the greatest effect on their reactivity. P(M4-VP) and AO-MWNT consistently induced the greatest up-regulation of pro-inflammatory cytokines at both the gene expression and protein levels, however interestingly AO-MWNTs were the only MWNT not to induce any discernible ROS formation, even at 24

hours. In contrast, exposure to P(M4-VP)-MWNTs increased ROS by up to 166% (Figure 3.2.24). In both TT1 and HPMVECs, P(M4-VP) modified carbon nanotubes were more pro-inflammatory than AR-MWNTs and P(PEGMA) and P(MAA) groups on the CNT surface reduced the pro-inflammatory effects of the AR material. Interestingly, acid oxidised MWNT caused the largest pro-inflammatory response in HPMVECs, however this was one of the least pro-inflammatory materials in TT1 cells. This would indicate that the mechanism of toxicity varies between TT1 and HPMVEC cells for this particle. In HPMVECs, toxicity may be at least partially dependent on MWNT uptake as P(M4-VP) and AO-MWNTs showed both the greatest uptake and the greatest pro-inflammatory response, which in AO-MWNT treated cells was independent of ROS formation.

Antioxidants were used to investigate whether ROS formation could be driving the pro-inflammatory response observed in endothelial cells, and the application of anti-oxidants was effective in diminishing the levels of ROS detectable by the CM-H2DCFDA dye (Figure 3.2.25). It was discovered however, that although antioxidants did reduce the baseline level of the inflammatory chemokine IL-8, the inflammatory response was still apparent. Due to the fact that antioxidant addition reduced baseline IL-8 levels it could not be conclusively determined whether the reduction in IL-6 and IL-8 levels was a result of a general reduction of these mediators in HPMVECs, or whether antioxidants were abrogating the effect of the MWNTs. The pro-inflammatory effects of MWNTs have been attributed to ROS induction (Møller *et al*., 2014); however, ROS is not necessarily the cause of inflammation (Fenoglio *et al*., 2006). Indeed, during this study an inflammatory response was observed in TT1 cells accompanied by a decrease in ROS. ROS can instead arise as a result of cellular damage, whereby the correct functioning of the mitochondria has been disturbed, or ROS can also act as a messenger molecule. It should also be noted that the CM-H2DCFDA dye will also detect reactive nitrogen species, such as nitric oxide (NO) which is a potent vasodilator released by endothelial cells. We attempted to measure NO alone using both the Greiss assay which measures nitrite and a NO

probe, however the cells did not yield enough NO to be detected by either system suggesting that NO was not a significant contributor to the increased fluorescence observed .

3.4. Summary

Whilst functionalised MWNT were not toxic to primary alveolar type 2 cells, they did induce a pro-inflammatory response and LDH release in type 1-like alveolar cells following a 72 hour exposure. MWNT were more toxic to microvascular endothelial cells, inducing early cell death, a pro-inflammatory response and increase in reactive oxygen species (ROS). In both TT1 cells and HPMVECs, P(M4-VP) modified carbon nanotubes were more pro-inflammatory than as-received (AR) carbon nanotubes, and P(PEGMA) and P(MAA) groups on the CNT surface reduced the pro-inflammatory effects of the AR material. A striking finding was the highly pro-inflammatory nature of the acid oxidised (AO) CNTs in the endothelial and not the epithelial cells that was independent of ROS formation, indicating a cell specific toxicity mechanism.

Cell type	Viability	Particle Uptake?	Pro-inflammatory?	ROS?
TT1	↓	↑↑	↑	↓
AT2	-	↑	-	-
HPMVEC	↓↓	↑↑	↑↑	↑↑

↓↓ large decrease
↓ moderate decrease
↑ moderate increase
↑↑ large increase

Table 3.4.1. Summary of the variable TT1, AT2 and HPMVEC responses following exposure to functionalised MWNTs

4. ENDOTHELIAL ACTIVATION FOLLOWING MWNT EXPOSURE AND ITS DEPENDENCE ON MWNT SURFACE FUNCTIONALISATION

4.1. Introduction

In the 1960s, it was thought that endothelial cells were simply an inert lining to blood vessels which provided an anti-thrombotic surface to allow the free passage of blood. However, it is now recognised that these cells play complex metabolically active roles in policing the interface between blood and underlying tissues (Hunt & Jurd, 1998). The endothelium is able to do this by playing an active role in recruiting circulating leukocytes, maintaining vascular tone, allowing the passage of water, solutes and macromolecules via adjusting the endothelial barrier integrity, and inducing or inhibiting coagulation (Hunt & Jurd, 1998; Stevens, 2011).

The quiescent endothelium supports vasodilatation, suppresses coagulation and platelet activity, promotes fibrinolysis, and censors inflammatory processes, including those that rely on activation and adhesion of leukocytes (van Hinsbergh, 2012). If however the endothelium is perturbed it can enter into a pro-inflammatory and pro-thrombotic state (Becker, Heindl, Kupatt, & Zahler, 2000); this process is necessary for repair but can also have implications in the progression of diseases such as atherosclerotic lesion formation (Johnson-Tidey, McGregor, Taylor, & Poston, 1994; K Ley & Huo, 2001).

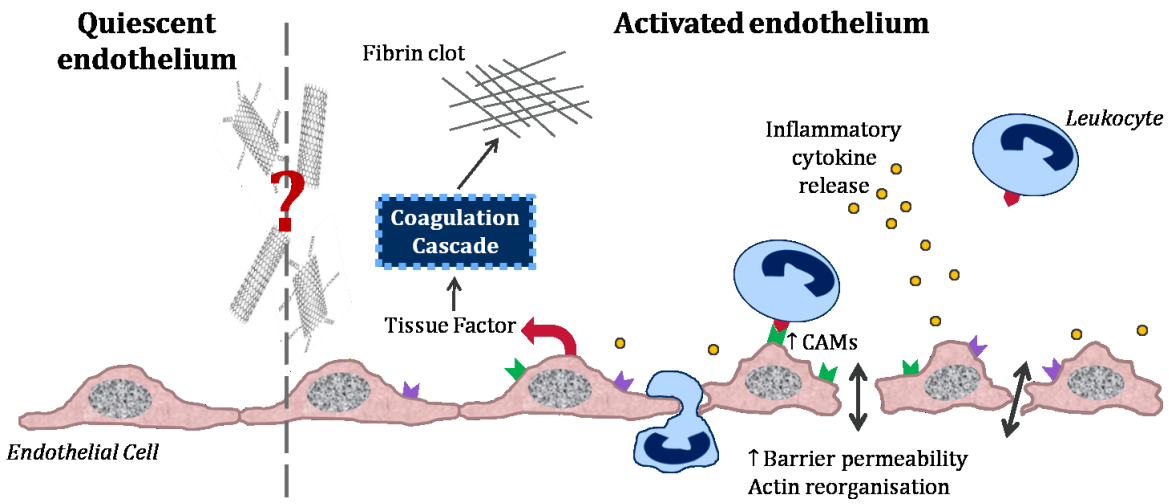


Figure 4.1.1 Graphic representation of endothelial responses that may be initiated if CNTs induce endothelial activation. Perturbed endothelium enters a pro-thrombotic, pro-inflammatory state. Inflammatory cytokines and chemokines are released in response to stimuli which can signal to neighbouring cells and enter the systemic circulation. In addition, cell adhesion molecules (CAMs) on the endothelial surface are upregulated which induce leukocyte recruitment, rolling and extravasation to underlying tissue. Tissue factor is expressed by activated endothelium which is a key initiator of the coagulation cascade, the process which regulates thrombin formation, coagulation and fibrin deposition at the vascular wall. Activated endothelium also induces platelet aggregation and signals to smooth muscle cells to induce vasoconstriction (not shown).

The role of cell adhesion molecules in leukocyte recruitment

Leukocyte adhesion to endothelial cells is a key process in the development and progression of inflammation and is the result of selectin and immunoglobulin-like adhesion molecules on the endothelial cell surface interacting with their complimentary ligands on leukocyte membranes (Alon & Feigelson, 2002; Granger & Senchenkova, 2010; Kjaergaard, Dige, Krog, Tønnesen, & Wogensen, 2013). Cell adhesion molecules activated on the endothelial cell surface include E-selectin (CD62E), ICAM-1 (CD54), VCAM-1 (CD106) and PECAM-1 (CD31); these molecules play different roles in leukocyte adhesion, rolling and extravasation and have distinct ligands on the leukocyte surface (Table 4.1.1) (Kjaergaard *et al*., 2013).

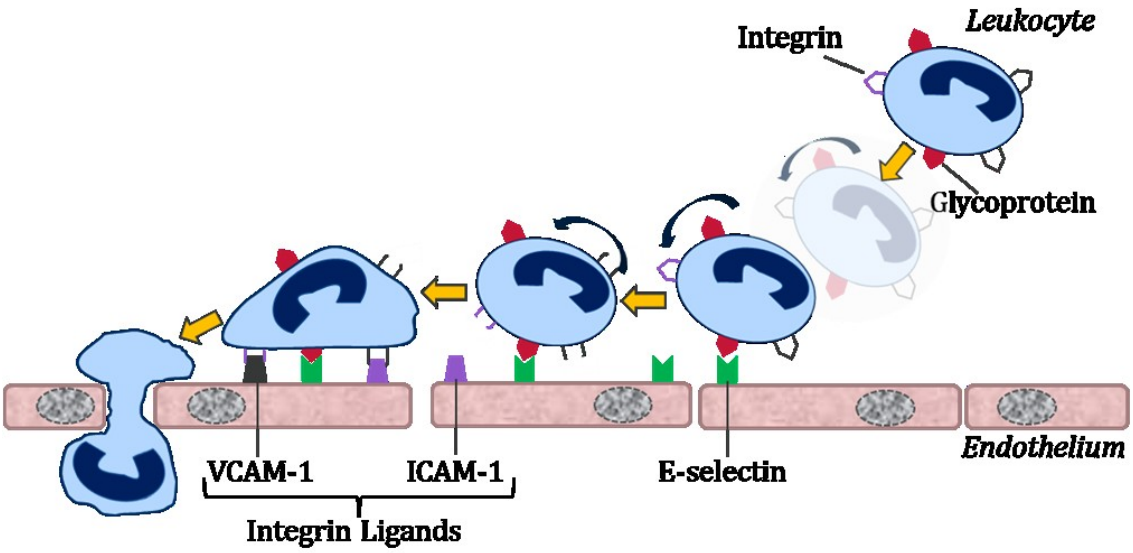


Figure 4.1.2 Graphic representation of the role of cell adhesion molecules (CAMs) in leukocyte recruitment, rolling and extravasation. Leukocytes initially tether to the endothelium via selectin mediated mechanisms; shown here is the interaction of glycoprotein on the leukocyte surface with endothelial E-selectin. Firm attachment is aided by the interaction of immunoglobulin-like adhesion molecules including ICAM-1 and VCAM-1 which interact with integrins on the leukocyte surface. VCAM-1, ICAM-1 and leukocyte integrin interactions remain weak until the integrins become activated by arrest chemokines or leukocyte engagement of selectins. Figure adapted from (Springer, 1990).

Once immune cells have become tethered to the endothelial wall by cell adhesion molecules these cells are in close proximity to endothelial chemokines, integrin ligands, and potential ligands for costimulatory receptors (Alon & Feigelson, 2002; Granger & Senchenkova, 2010). Chemokines, such as monocyte chemoattractant protein (MCP)-1 (CCL2), MCP-2 (CCL8), MIP-1α (CCL3), MIP-1β (CCL4) and RANTES (CCL5) have been implicated in leukocyte recruitment in animal models of atherosclerosis (Rao, Yang, Garcia-Cardena, & Luscinskas, 2007). These chemokines bind to chemokine receptors on the leukocyte surface and this binding triggers a signalling cascade culminating in activation of the leukocyte β1 and β2 integrins (Hogg, Patzak, & Willenbrock, 2011). These integrins then bind to their counter-receptors on the endothelium which include the immunoglobulin-like adhesion molecules ICAM-1 and VCAM-1.

Molecule	Cell expression	Ligand	Role in cascade	Reference
E-selectin	EC	L-selectin, Sialyl Lewis^x, carbohydrates	Rolling	(Granger & Senchenkova, 2010; Rao *et al*., 2007)
P-selectin	Pla, EC	PSGL-1, L-selectin, CD43	Capture, Rolling	(Granger & Senchenkova, 2010; Rao *et al*., 2007)
ICAM-1	EC, SMC, Leu	β2 integrins: $\alpha_L\beta_2$ (LFA-1), $\alpha_M\beta_2$ (Mac-1), $\alpha_D\beta_2$, $\alpha_X\beta_2$	Firm adhesion, extravasation	(Alon & Feigelson, 2002; Granger & Senchenkova, 2010; Rao *et al*., 2007)
VCAM-1	EC, SMC	α_4 integrins: $\alpha_4\beta_1$ (VLA-4), $\alpha_4\beta_7$	Rolling, firm adhesion	(Alon & Feigelson, 2002; Granger & Senchenkova, 2010; Rao *et al*., 2007)
PECAM-1	EC, Pla, Leu	PECAM-1	Signalling, extravasation	(Granger & Senchenkova, 2010; Rao *et al*., 2007)

Cell types: EC, endothelial cells; Pla, platelets; Leu, Leukocytes; SMC, smooth muscle cells

Table 4.1.1 Major endothelial cell adhesion molecules involved in leukocyte recruitment.

This study focused on the effect of MWNTs on the mRNA levels of the CAMs E-selectin, ICAM-1 and VCAM-1. Although all CAMs in Table 4.1.1 have been associated with atherosclerotic plaques in humans, not all CAMs increase mRNA expression in response to environmental stressors.

The CAM P-selectin plays an important role in leukocyte trafficking in both mice and humans, however despite the observation of a sustained increased in expression of *P-selectin* on the surfaces of endothelial cells in human tissues with chronic or allergic inflammation, NF-κB– and ATF-2–dependent activators do not up-regulate expression of the human *Selp* gene; the gene encoding the P-selectin protein (Liu *et al*., 2010). A study by Liu *et al* found that, following LPS and TNFα treatment, mice expressing the murine *Selp* gene displayed a significant increase in murine *P-selectin* mRNA. Mice expressing the human *Selp* gene however, downregulated human *P-selectin* mRNA following the same LPS or TNFα treatment (Liu *et al*., 2010). This study implies that upregulation of the *P-selectin* gene in mouse models may not be an accurate depiction of the potential atherogenic effects of a substance in humans as there is clearly a disparity in the mode of expression between these species. As upregulation of the *Selp* gene is

not observed in human cells in response to pro-thrombotic or pro-inflammatory stimuli this CAM was excluded from our gene expression studies.

Despite a clear role for PECAM-1 in leukocyte extravasation and evidence for PECAM association with atherosclerotic plaques the *PECAM-1* gene is constitutively expressed and is not up-regulated by a pro-inflammatory stimulus (Hajra *et al*., 2000; Jefferson *et al*., 2011; Li *et al*., 2006).

Cell adhesion molecules and disease progression

Up-regulation of cell adhesion molecules, inflammation and induction of the coagulation cascade are part of the host-defence response that is central to wound repair and haemostasis. Over-expression of cell adhesion molecules is, however, implicated in the pathogenesis of a number of diseases including atherosclerosis (Galkina & Ley, 2007).

Atherosclerosis is the underlying cause of the majority of cardiovascular events and is central to the pathogenesis of a number of diseases including coronary heart disease (CHD), peripheral arterial disease and ischaemic stroke (Lloyd-Jones *et al*., 2010; Napoli *et al*., 2006). In 2012, ischaemic heart disease and stroke were the first and third leading causes of premature loss of life, respectively (World Health Organisation (WHO), 2014).

Up-regulation of P- and E-selectins and ICAM-1, PECAM-1 and VCAM-1 has been observed on endothelial surfaces overlying atherosclerotic lesions in humans (Johnson-Tidey *et al*., 1994; Li *et al*., 2006; O'Brien *et al*., 1993; van der Wal, Das, Tigges, & Becker, 1992). A number of studies have further elucidated the role of these proteins in atherosclerotic plaque formation using mouse models. Collins and co-workers studied lesion formation in double knockout *Apoe*$^{-/-}$ mice and *ICAM*$^{-/-}$ mice that had received a low-fat, low-cholesterol diet. *ICAM*$^{-/-}$ mice demonstrated a 30% reduction in lesion formation and a 45% and 24% reduction in lesion formation was seen in *P-selectin*$^{-/-}$ and *E-selectin*$^{-/-}$ mice respectively (Collins *et al*., 2000). A dramatic reduction of 50-70% in the area of the aorta containing atherosclerotic fatty streaks was also observed in

C57BL/6 mice that had homozygous mutations in the β2 integrin gene and the endothelial CAMs, *ICAM-1* and *P-selectin* and were fed a high-fat diet (Nageh *et al*., 1997). Polymorphisms in the *E-selectin* gene have also been associated with an increased adhesive capacity under flow conditions and an increased risk of myocardial infarction (Wenzel et al, 1996; Yoshida et al, 2003).

Endothelium-derived thrombotic mediators

In addition to the pro-inflammatory response previously mentioned, endothelial cells that enter into an activated state may also assume a pro-thrombotic state. Thrombin formation, coagulation and fibrin deposition at the vascular wall is regulated by the coagulation cascade (Becker *et al*., 2000). The initial haemostatic response of the endothelium is triggered by circulating trace amounts of fVIIa and locally exposed tissue factor (Tanaka, Key, & Levy, 2009).

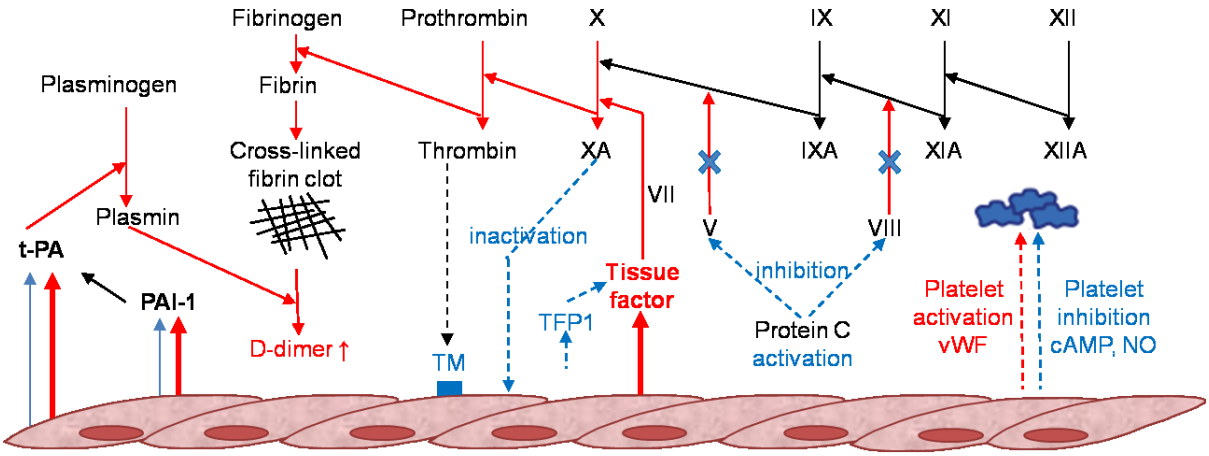


Figure 4.1.3 Homeostatic regulation by the vascular endothelium. Blue lines reflect normal endothelium activity and red lines show changes associated with dysfunctional endothelium. cAMP, cyclic adenosine monophosphate; NO, nitric oxide; PAI-1, plasminogen activator inhibitor type 1; TFPI, tissue factor pathway inhibitor; TM, thrombomodulin; t-PA, tissue-type plasminogen activator; vWF, von Willebrand factor. Figure adapted from (Shantsila & Lip, 2009).

Tissue factor (TF), formerly known as thromboplastin is a 47kDA protein expressed in vascular and non-vascular cells, and is the main stimulus for thrombin generation (Mann, 2002; Sabatier, 2002; Steffel *et al*., 2006). TF is constitutively expressed in sub-endothelial cells and can trigger

rapid initiation of the coagulation cascade if the vessel wall is damaged. To prevent inappropriate coagulation, endothelial and monocytic cells do not produce TF under normal physiological conditions (Libby & Simon, 2001; Steffel *et al*., 2006). Endothelial TF is induced in response to a number of stimuli, including cytokines such as TNF-α, interleukin-1β or CD40 ligand, by biogenic amines such as serotonin or histamine, and by mediators such as thrombin, oxidized LDL, or vascular endothelial growth factor (Steffel *et al*., 2006). TF can interact with either the active or inactive form of circulating factor VII, the inactive form undergoes activation once conjugated to the TF protein. The TF-VIIa complex can then either directly convert factor X to factor Xa or act via an intermediary protein, factor IX. Factor Xa catalyses the conversion of prothrombin to thrombin, leading to fibrin formation, platelet activation and ultimately clot formation (Figure 4.1.3) (Shantsila & Lip, 2009; Steffel *et al*., 2006).

Fibrin clot formation is regulated by the plasminogen activator system; a crucial role of this system is the conversion of plasminogen to plasmin by plasminogen activators. Plasmin is a serine protease which plays an essential role in the degradation of fibrin and extracellular matrix protein complexes. The activation of plasminogen into plasmin is mediated by two types of activators, urokinase-type plasminogen activator (u-PA) and tissue-type plasminogen activator (t-PA). The activity of u-PA and t-PA is regulated by plasminogen activator inhibitors (PAI), of which the rapidly acting molecule PAI-1 is the principal inhibitor of both u-PA and t-PA (Figure 4.1.3) (Cesari, Pahor, & Incalzi, 2010).

Carbon nanotube exposure and increased atherosclerotic plaque formation

As discussed in section 1.1 the ultrafine fine (UF) fraction of ambient air pollution has been associated with adverse cardiovascular outcomes. This discovery sparked concerns surrounding the safety of NP and specifically CNT-induced cardiovascular reactivity and it has been hypothesised that CNTs may have similar adverse effects on cardiovascular health to those observed following UFP exposure (Legramante *et al*., 2009; Simeonova & Erdely, 2009).

In vivo mouse studies investigating this hypothesis found an association between respiratory exposure to CNTs and adverse cardiovascular outcomes, including accelerated atheroma formation (Cao et al., 2014; Erdely et al., 2009; Li et al., 2007; Nemmar et al., 2007; Xu et al., 2012). A study of $Apoe^{-/-}$ mice fed an atherogenic diet discovered that these animals displayed an accelerated rate of atherosclerotic plaque formation following a single intrapharyngeal instillation of SWCNTs (Li *et al*., 2007). Furthermore, 24 hours post-exposure, mice intratracheally exposed to MWNTs had elevated plasma procoagulant microvesicular TF activity (Nemmar et al., 2007). This was accompanied by transient activation of circulating platelets and enhanced peripheral thrombogenicity. Neutralisation of *P-selectin* abolished CNT-induced thrombogenicity. indicating that this process was mediated by *P-selectin* activation (Nemmar et al., 2007). SWCNTs intratracheally instilled in spontaneously hypertensive rats induced thickened arterial vessels, oedema, mild disordered arrangement of blood vessel cells in arterioles and histological lesions in the left ventricle 24 hours after the final exposure dose was administered (0.6mg SWCNT/rat was administered once a day for two continuous days). In the same study, increased levels of the thrombotic mediators endothelin-1 (ET-1) and angiotensin converting enzyme (ACE) in plasma were also found in SWCNT-treated groups at both 24 and 72 hours after exposure (Ge, Meng, *et al*., 2012). Whether these responses are a result of direct particle interaction with vessels, or an indirect response to mediators released by cells of the pulmonary or immune systems, is currently unclear. There is however some evidence that direct interaction between MWNTs and the vasculature could result in adverse cardiovascular health. A low dose of 200μg MWNTs per kg body weight intravenously administered to Sprague-Dawley rats induced a significant exacerbation of atheromatous lesions and lipid deposition in the aortic intima. Furthermore, the same *in vivo* dose also increased vWF levels in endothelial cells and serum concentrations of 20 and 50μg/ml MWNT significantly increased vWF levels at 24 hours post-exposure in a HUVEC *in vitro* model (Xu *et al*., 2012).

Much of the current literature only investigates the effects of unmodified CNTs, despite the fact that CNTs are likely to be used in commercial products in a modified, rather than pristine form

so these findings may not be directly relevant to real life exposure. Furthermore, these studies do not address whether functionalisation of CNTs could have implications for cardiovascular health *in vivo* or whether this effect is a direct result of CNT-induced endothelial activation. It is therefore important to determine whether the adverse cardiovascular events observed following CNT exposure *in vivo* could be due to direct CNT interaction with the endothelium. CNTs entering the body via the pulmonary system have been observed in systemic organs providing evidence that these particles are able to translocate and interact directly with systemic targets including the vasculature (Chen *et al*., 2015; Mercer *et al*., 2013; Reddy, Krishna, Reddy, & Himabindu, 2010). Furthermore, due to the increasing research into CNTs for biomedical applications, and the subsequent potential for a direct route of entry into the body, it is important to fully understand the importance CNT modification may have on CNT vascular reactivity (Lanone, Andujar, Kermanizadeh, & Boczkowski, 2013).

Overview:

Here we investigate, using a primary *in vitro* model of the pulmonary microvasculature, whether direct interaction of f-MWNTs with the endothelium could have implications for cardiovascular health. This is achieved by investigating the regulation of endothelial cell adhesion molecules and the subsequent effect this has on the adhesion of a monocytic cell line to the endothelial surface. Furthermore, activators and inhibitors of the coagulation cascade are studied at the pre-transcriptional level as an indication of the presence or absence of a pro-thrombotic response.

Hypothesis:

We hypothesised that MWNT exposure would increase HPMVEC cell adhesion molecule expression, leukocyte recruitment to the endothelium and regulation of thrombotic mediators. Furthermore we hypothesised that the endothelial response to MWNTs would be modulated by surface functionalisation of the MWNT. Our specific aims were to determine:

I. Whether MWNT exposure upregulates mRNA levels of the CAMs *ICAM-1*, *VCAM-1* and *E-selectin*, and if CAM expression was affected by MWNT surface modification.
II. If upregulation of CAM mRNA translated to an increase in protein expression, and whether this response was transient or sustained.
III. Whether MWNT exposure could trigger increased leukocyte adhesion to the endothelium.
IV. If MWNT exposure could affect thrombotic gene regulation.

4.2. Results

CAM gene regulation: E-selectin, ICAM-1, VCAM-1

Assessment of CAM expression levels in HPMVECs following a 1 and 10μg/ml exposure to AR and AO-MWNTs revealed that both particles were able to induce CAM gene upregulation *in vitro*. No effect was seen at the 1 hour time point for either AR or AO-MWNT exposed cells. At 4 hours, 10μg/ml of both AR and AO-MWNTs induced an increase in the expression of *VCAM-1*, *ICAM-1* and *E-selectin* mRNA, however the acid oxidised MWNTs were far more reactive than their as received counter parts (Figure 4.2.1). 10μg/ml AO-MWNT increased median *E-selectin* mRNA 9.8 fold at 4 hours whereas AR-MWNT increased *E-selectin* mRNA 1.4 fold ($p<0.05$) (Figure 4.2.1 & Figure 4.2.2). For all genes studied, the response was greatest at 4 hours, however AO-MWNTs induced a sustained increase in *ICAM-1* and *E-selectin* expression that was still evident at 24 hours post-exposure. At 24 hours *ICAM-1* and *E-selectin* mRNA was significantly increased, median values were 3.3 and 5.7 times higher than control values respectively ($p<0.05$). A large degree of variation was observed between cells from different donors, however all data followed the same trend; the maximal increase in gene expression at 4 hours with AO-MWNTs inducing a greater reaction than AR-MWNTs (Figure 4.2.1).

Following the above optimisation study, the expression of CAMs following exposure to 10μg/ml AR, P(M4-VP), P(MAA), P(PEGMA) and AO-MWNTs was determined at 4 hours, the time point shown at which the greatest increase in the expression of CAMs following MWNT exposure was observed. All MWNTs induced an increase in CAM expression; P(M4-VP) and AO-MWNTs induced a greater increase in *ICAM-1*, *VCAM-1* and *E-selectin* mRNA expression than AR-MWNTs, whereas P(PEGMA) induced a smaller increase in CAM mRNA than AR-MWNTs (Figure 4.2.2). AO-MWNT exposure induced the greatest increase in *ICAM-1*, *VCAM-1* and *E-selectin* mRNA expression (median values 3.4, 13.7 and 9.8 fold greater than control values, respectively, $p<0.05$).

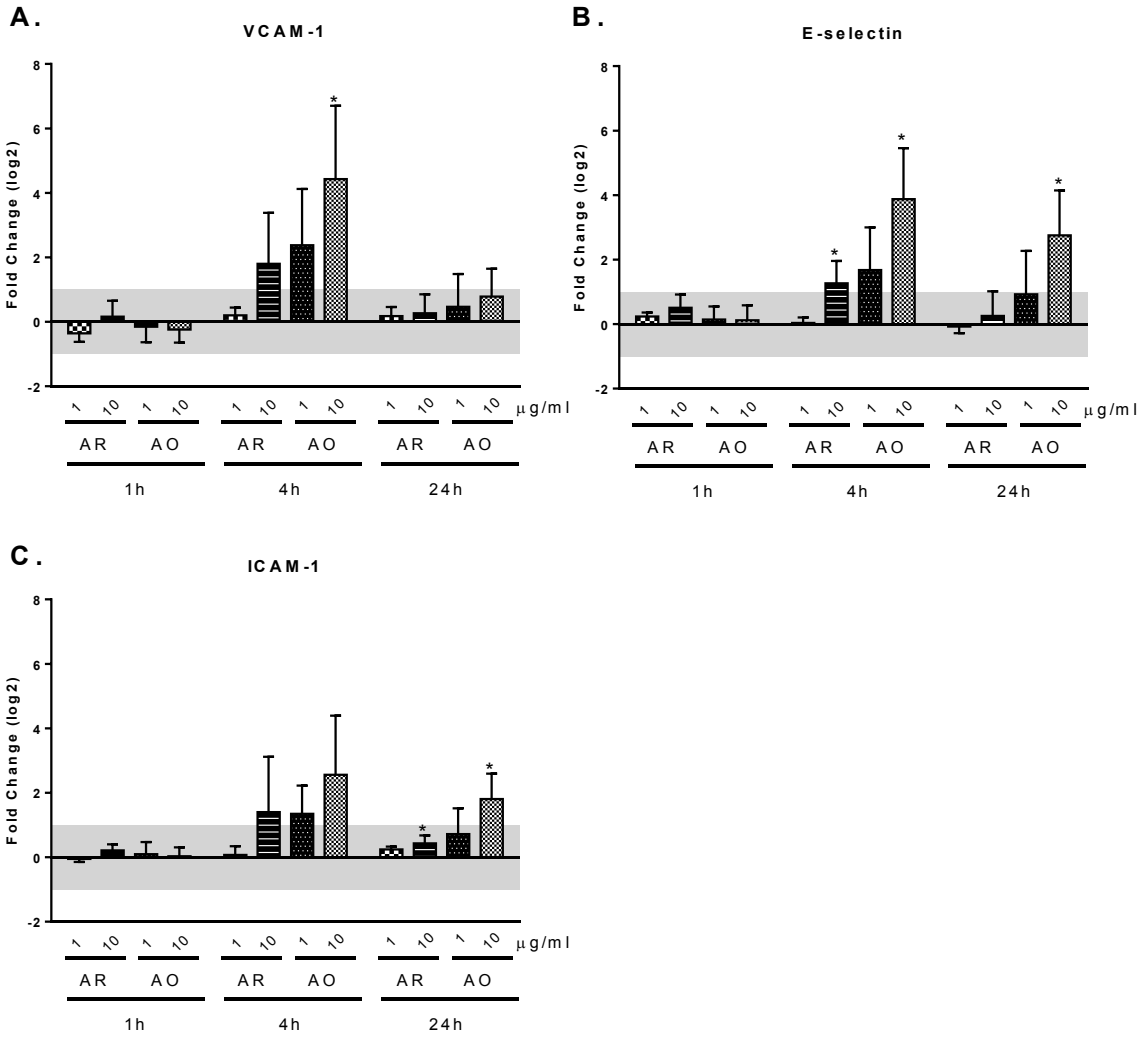


Figure 4.2.1 MWNT-induced *VCAM-1*, *E-selectin* and *ICAM-1* gene regulation in HPMVEC. HPMVEC were exposed to 1 or 10µg/ml AR or AO MWNTs for 1, 4 or 24 hours. A). *E-selectin* B.) *VCAM-1* and C.) *ICAM-1* gene expression was assayed by RT-PCR. Values were normalised to a GAPDH control and compared to an untreated control using the ΔΔCt method. Data is expressed as mean ±SEM, n=4. For statistical analysis a one-way sample t-test was performed with values compared to a non-treated control value of 0, *p<0.05.

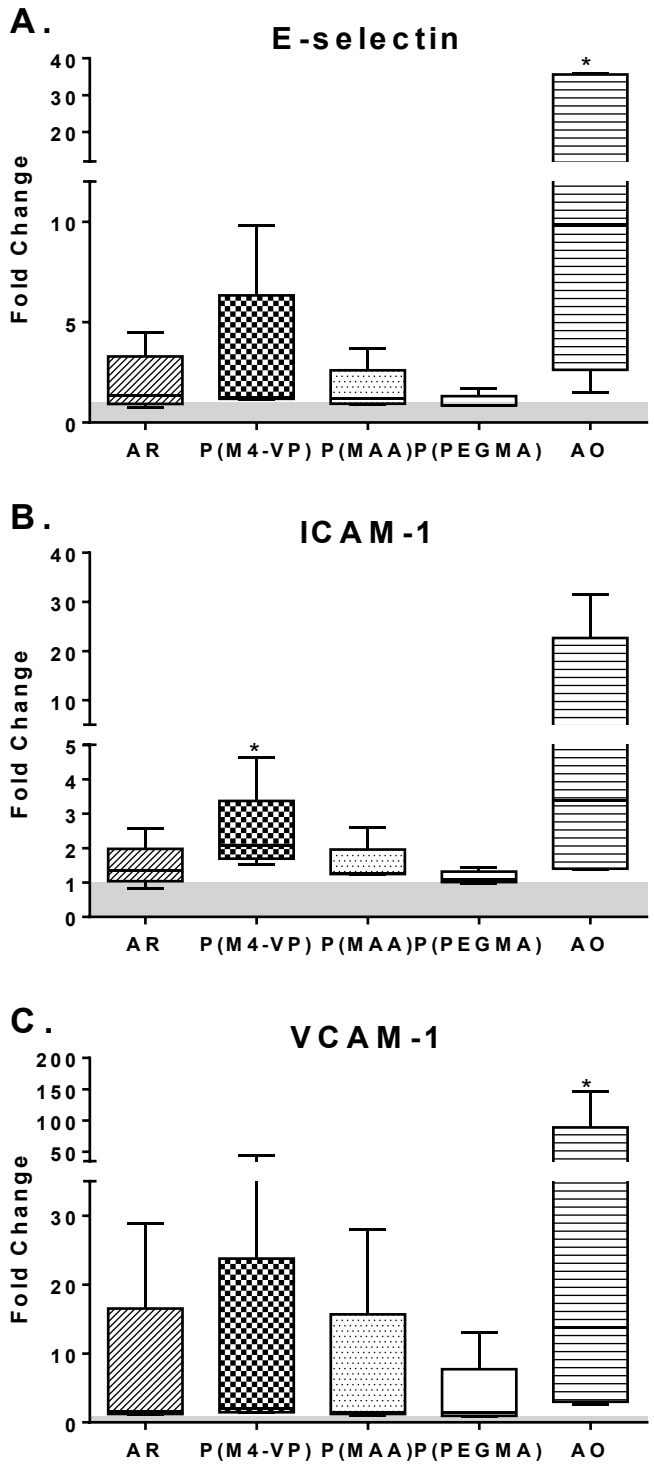


Figure 4.2.2 f-MWNT-induced *VCAM-1*, *E-selectin* and *ICAM-1* gene regulation in HPMVEC 4 hours post-exposure. HPMVEC were exposed to 10µg/ml AR, P(M4-VP), P(MAA), P(PEGMA) or AO MWNT for 4 hours. The expression of A). *E-selectin,* B.) *ICAM-1* and C.) *VCAM-1* genes was assayed by RT-PCR. Values were normalised to a GAPDH control and compared to an untreated control using the ΔΔCt method. Data is expressed as median ±SEM, n=5. For statistical analysis values were log transformed, a one-sample t-test vs non-treated control value of 0 was used, *$p<0.05$.

E-selectin protein expression: lysates/supernatants

Under resting conditions, bound E-selectin (derived from cell lysates) was approx. 1000pg/ml at 4, 24 and 72 hours in HPMVECs. HPMVECs are contact inhibited cells and will not proliferate beyond confluency, thus 1000pg/ml E-selectin is the baseline level of the confluent HPMVEC monolayer (Figure 4.2.3). E-selectin levels in HPMVECs exposed to P(M4-VP)-MWNTs and AO-MWNT increased over 4 to 24 hours (2476 to 3244 and 3544 to 6346pg/ml respectively), whereas the expression of E-selectin following exposure to AR, P(PEGMA) and P(MAA)-MWNT was similar at 4 and 24 hours (Figure 4.2.3 A & B). By 72 hours E-selectin levels have largely returned to baseline with only a small significant increase (<24%, $p<0.05$) observed in cells exposed to ≥25μg/ml P(M4-VP) and P(MAA)-MWNTs. Cells exposed to ≥25μg/ml AO-MWNTs however, still expressed very high levels of E-selectin; E-selectin levels increased to 3561 and 5729pg/ml for 25 and 50μg/ml exposures respectively ($p<0.05$) (Figure 4.2.3-C). At 4, 24 and 72 hours, doses as high as 50μg/ml P(PEGMA)-MWNTs induced no significant increase in bound E-selectin (Figure 4.2.3).

In addition to bound E-selectin, soluble E-selectin (sE-selectin) was also measured in cell supernatants. AR, P(M4-VP), P(MAA) and AO-MWNT exposure increased protein levels of the CAM E-selectin in a dose dependent manner. Low levels of the soluble form of E-selectin (sE-selectin) were detected in cell culture supernatants at all time points at both baseline and following MWNT exposure; at 4 hours all levels were below the limit of detection (data not shown). At 24 hours sE-selectin levels increased following exposure to all MWNTs except those that had been functionalised with the PEGMA group (Figure 4.2.4-A). The maximal increase in sE-selectin was observed following exposure to 50μg/ml AO-MWNTs, which was 7.5 fold greater than control values ($p<0.001$). This increase in sE-selectin was greater at 72 hours; the same particle, AO-MWNT induced a 34 fold increase at this time point ($p<0.001$). At 72 hours 25 and 50μg/ml P(PEGMA)-MWNTs induced a small but significant increase in sE-selectin levels of 10 and 13pg/ml (1.8 and 2.1 fold increase) respectively ($p<0.05$) (Figure 4.2.4-B).

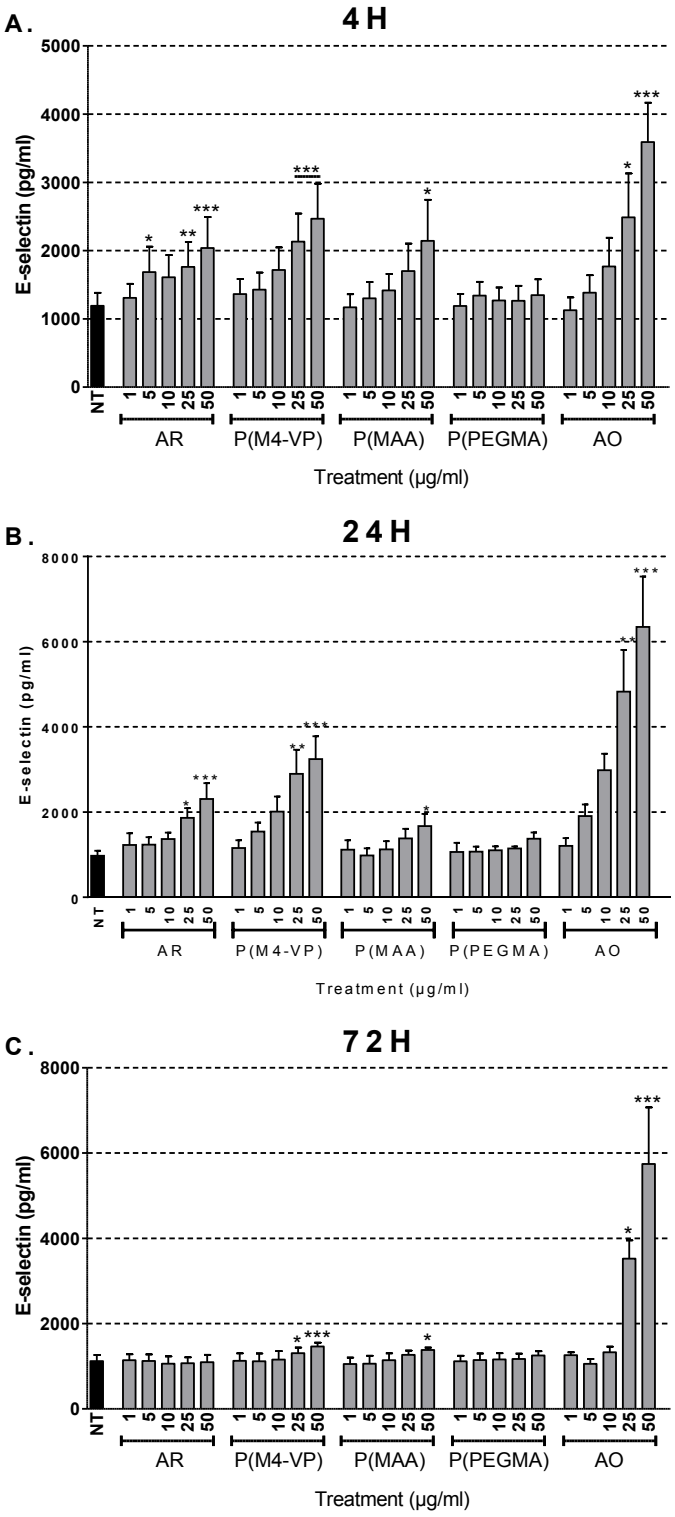


Figure 4.2.3 E-selectin levels in HPMVEC lysates following f-MWNT exposure. Cells were exposed to 1-50µg/ml f-MWNTs for (A.) 4, (B.) 24 and (C.) 72 hours and E-selectin levels in the cell lysates were measured by ELISA. Assay limit of detection = 93.8pg/ml. Data is expressed as mean ± SEM, n=4. One-way ANOVA followed by Dunnett's post-test; *p< 0.05, **p< 0.01 & ***p< 0.001.

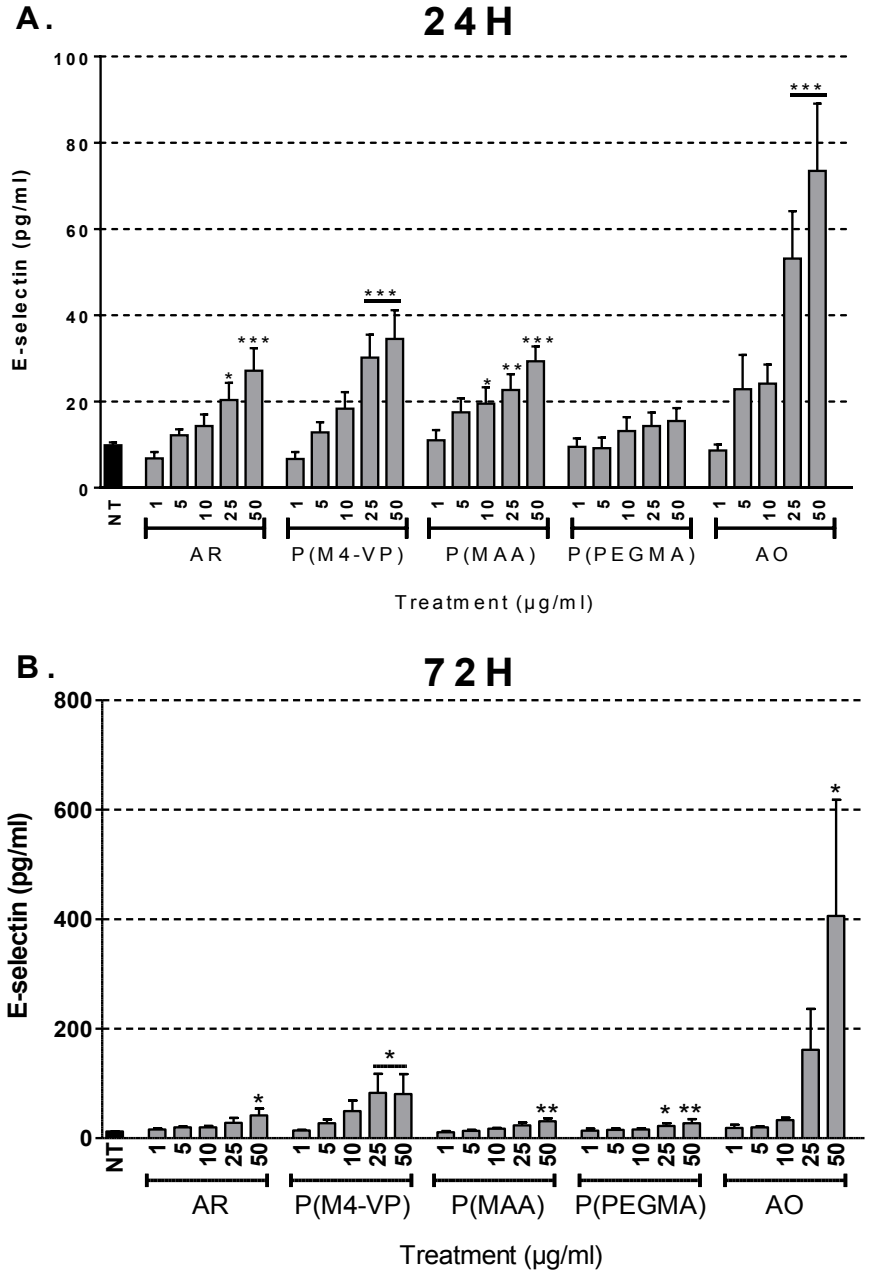


Figure 4.2.4 Soluble E-selectin levels in HPMVEC supernatants following f-MWNT exposure. Cells were exposed to 1-50µg/ml f-MWNTs for (A.) 24 and (B.) 72 hours and sE-selectin levels in the cell culture supernatants were measured by ELISA. Assay limit of detection = 93.8pg/ml. Data is expressed as mean ± SEM, n=4. One-way ANOVA followed by Dunnett's post-test; *p< 0.05, **p< 0.01 & ***p< 0.001.

U937/HPMVEC co-cultures

Upregulation of CAM expression coincided with an increase in monocyte adhesion to the endothelial monolayer. HPMVECs exposed to a positive control of 10ng/ml TNFα expressed high levels of the CAMs *ICAM-1*, *VCAM-1* and *E-selectin* (Appendix V) which was associated with an increased number of adherent fluorescently labelled U937 monocytic cells following a 3 hour co-culture (Figure 4.2.5).

Similarly, MWNTs also increased monocyte adhesion; when exposed to concentrations of 1, 5, 10 and 25μg/ml AR-MWNTs, there was a dose-dependent increase in the number of fluorescently labelled monocytes visible (Figure 4.2.6). The increase was not however significant at 10μg/ml following exposure to this particle. Following exposure to 10μg/ml AR, P(M4-VP), P(MAA), P(PEGMA) and AO-MWNTs only P(M4-VP) and AO-MWNTs induced a significant increase in fluorescently labelled monocytes adhered to the endothelial monolayer (Figure 4.2.7 & Figure 4.2.8). P(M4-VP)-MWNTs significantly increased the maximum fluorescent intensity of the image shown in Figure 4.2.7 by 164%, and AO-MWNTs increased this value by 125% ($p<0.05$) (Figure 4.2.8).

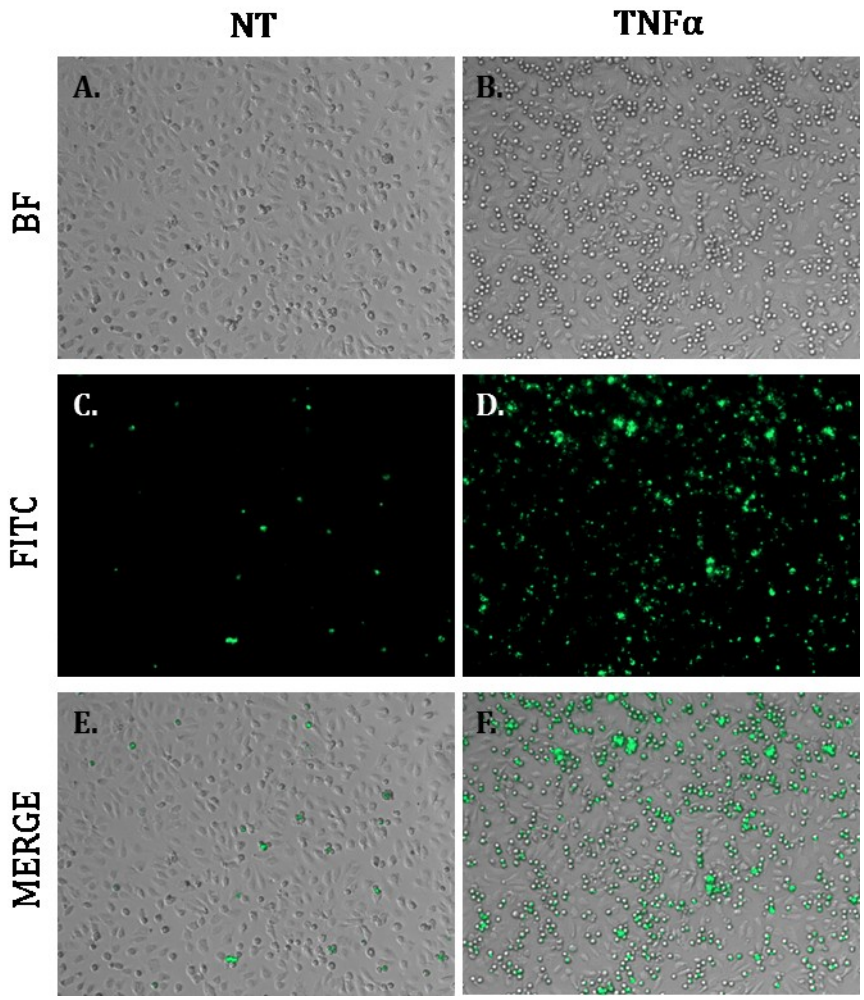


Figure 4.2.5 Monocyte adherence to a non-treated HPMVEC monolayer and HPMVECs stimulated with TNFα. Fluorescently labelled U937 monocytes were co-cultured with non-treated (A., C. & E.) and 10ng/ml TNFα stimulated (B., D., & F.) HPMVECs. Following a 3 hour co-culture non-adherent cells were removed by PBS washes and adherent cells were visualised by fluorescent microscopy. Data shown is from a single experiment, representative of n=1.

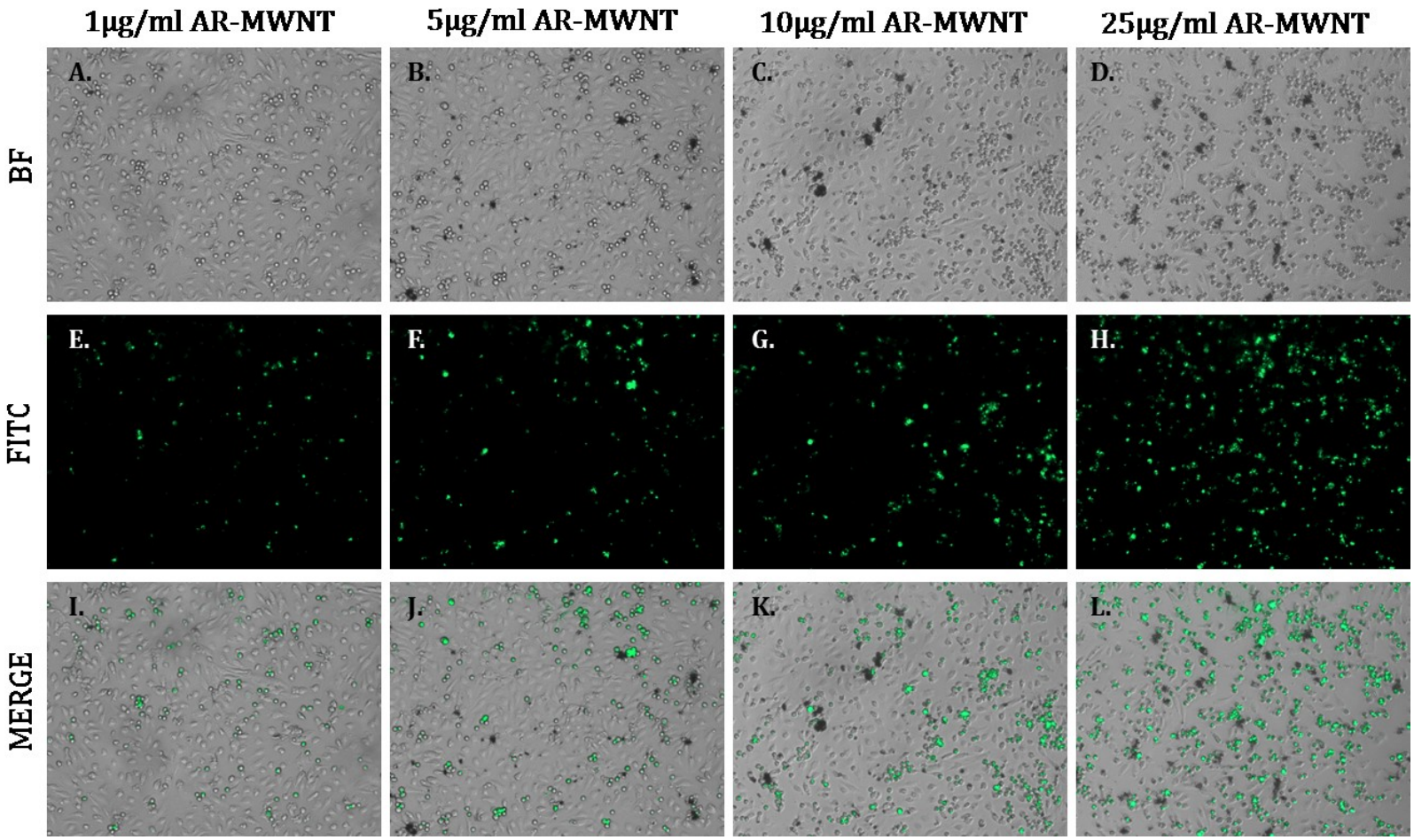


Figure 4.2.6 Monocyte adherence to a HPMVEC monolayer exposed to AR-MWNTs. Fluorescently labelled U937 monocytes were co-cultured with HPMVECs exposed to 1µg/ml (A., E. & I.), 5µg/ml (B., F. & J.), 10 µg/ml (C., G. & K.) and 25 µg/ml (D., H. & L.) AR-MWNTs. Following a 3 hour co-culture non-adherent cells were removed by PBS washes and adherent cells were visualised by fluorescent microscopy. Data shown is from a single experiment, representative of n=1.

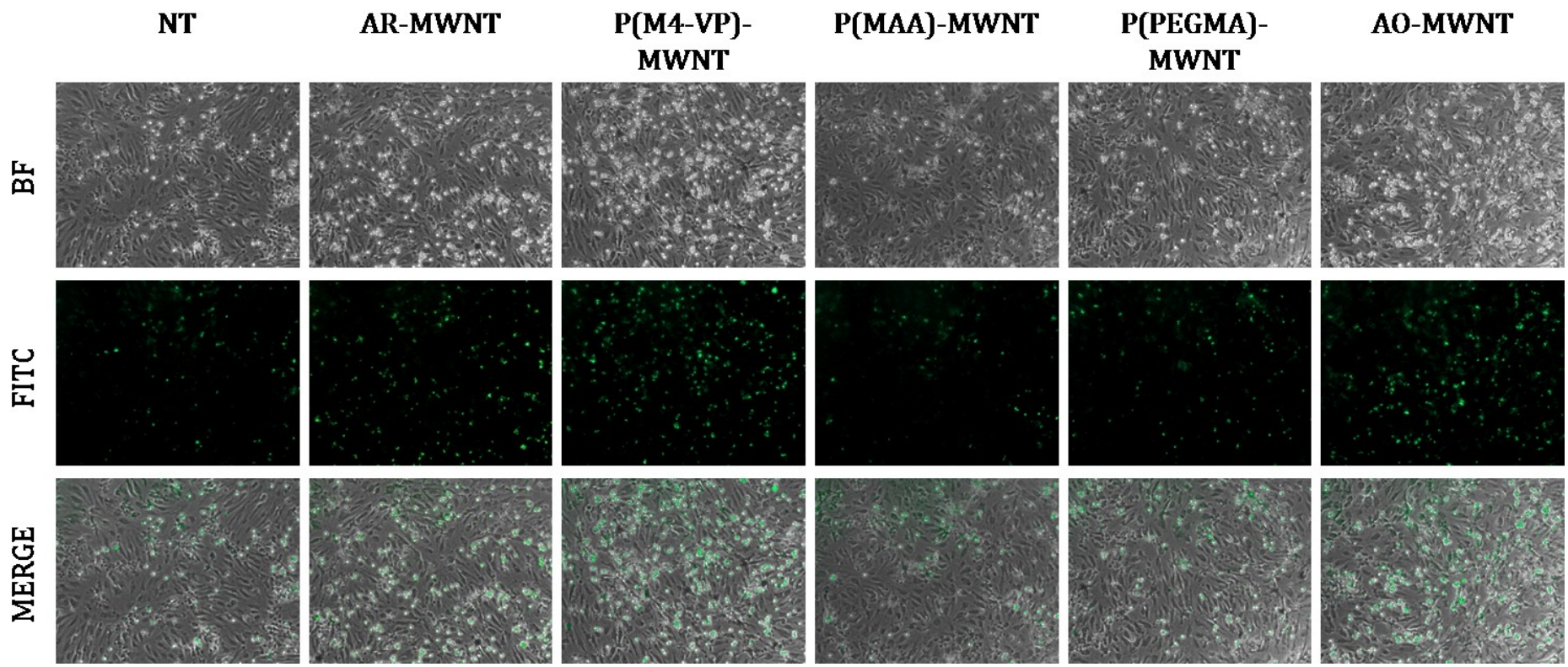


Figure 4.2.7 Monocyte adherence to a HPMVEC monolayer exposed to f-MWNTs. Fluorescently labelled U937 monocytes were co-cultured with HPMVECs exposed to 10μg/ml AR, P(M4-VP), P(MAA), P(PEGMA) and AO MWNTs. Following a 3 hour co-culture non-adherent cells were removed by PBS washes and adherent cells were visualised by fluorescent microscopy. Data shown is from a single experiment, representative of n=1.

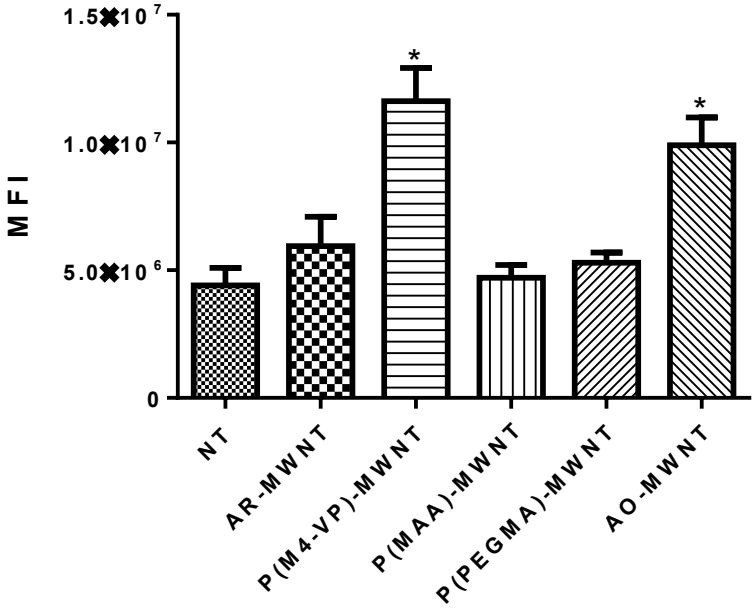


Figure 4.2.8 Maximum fluorescence intensity (MFI) of FITC-U937 HPMVEC co-culture following exposure to f-MWNTs. Fluorescently labelled U937 monocytes were co-cultured with HPMVECs exposed to 10µg/ml AR, P(M4-VP), P(MAA), P(PEGMA) and AO MWNTs. 5 images were obtained from 5 replicates taken from a single plate using a FITC fluorescent lamp. All images were acquired from the centre of a well of a 24 well cell culture plate. Mann-Whitney t-test; *p< 0.05.

Thrombotic gene regulation: TF, tPA, PAI-1

TF gene expression levels increased at 4 hours in HPMVECs following exposure to 10μg/ml AR and AO-MWNTs. The maximum increase in *TF* from endothelial cells derived from any donor was 4.9 fold when exposed to 10μg/ml AR-MWNT ($p<0.05$) compared to 14.7 fold when exposed to the same concentration of AO-MWNTs (Figure 4.2.9A). The median *TF* mRNA fold change was however less in AO-MWNT exposed cells than AR-MWNT exposed cells, median *TF* mRNA fold change was 2.7 and 1.5 respectively. This increase was transient and had resolved 24 hours following exposure. AR and AO-MWNTs exposure resulted in up-regulation of *PAI-1* and down-regulation of *tPA*. At 4 hours, 1μg/ml and 10μg/ml AO-MWNT induced a significant upregulation in *PAI-1* gene expression compared to control (1.3 and 1.7 fold respectively; $p<0.05$). 10μg/ml but not 1μg/ml AR-MWNT also induced a significant increase in *PAI-1* mRNA of 1.4 fold ($p<0.05$) (Figure 4.2.9B). Both 1μg/ml and 10μg/ml AO-MWNT induced a significant decrease in *tPA* mRNA, median values were 34% and 57% lower than control values respectively ($p<0.05$) (Figure 4.2.9C).

The expression of thrombotic mediators following exposure to 10μg/ml AR, P(M4-VP), P(MAA), P(PEGMA) and AO-MWNTs was determined at 4 hours, the time point shown in Figure 4.2.9 at which the greatest change in thrombotic mediator expression following MWNT exposure was observed. At 4 hours, all MWNTs increased *TF* expression and this increase was significant for all particles ($p<0.05$) except P(PEGMA) and AO-MWNTs. P(M4-VP)-MWNT exposure induced the greatest increase in *TF* mRNA, median values were 4.9 fold greater than control values ($p<0.05$) and P(PEGMA)-MWNT induced the smallest increase in *TF* mRNA of 1.7 fold (Figure 4.2.10).

P(M-4VP) and AO-MWNT exposure resulted in the greatest change in *PAI-1* expression, median values increased by 1.9 and 1.7 fold respectively following exposure to these particles ($p<0.05$)

(Figure 4.2.10C). Only AO-MWNT exposure resulted in a significant down-regulation of *tPA,* a decrease of 57% ($p<0.05$) (Figure 4.2.10B).

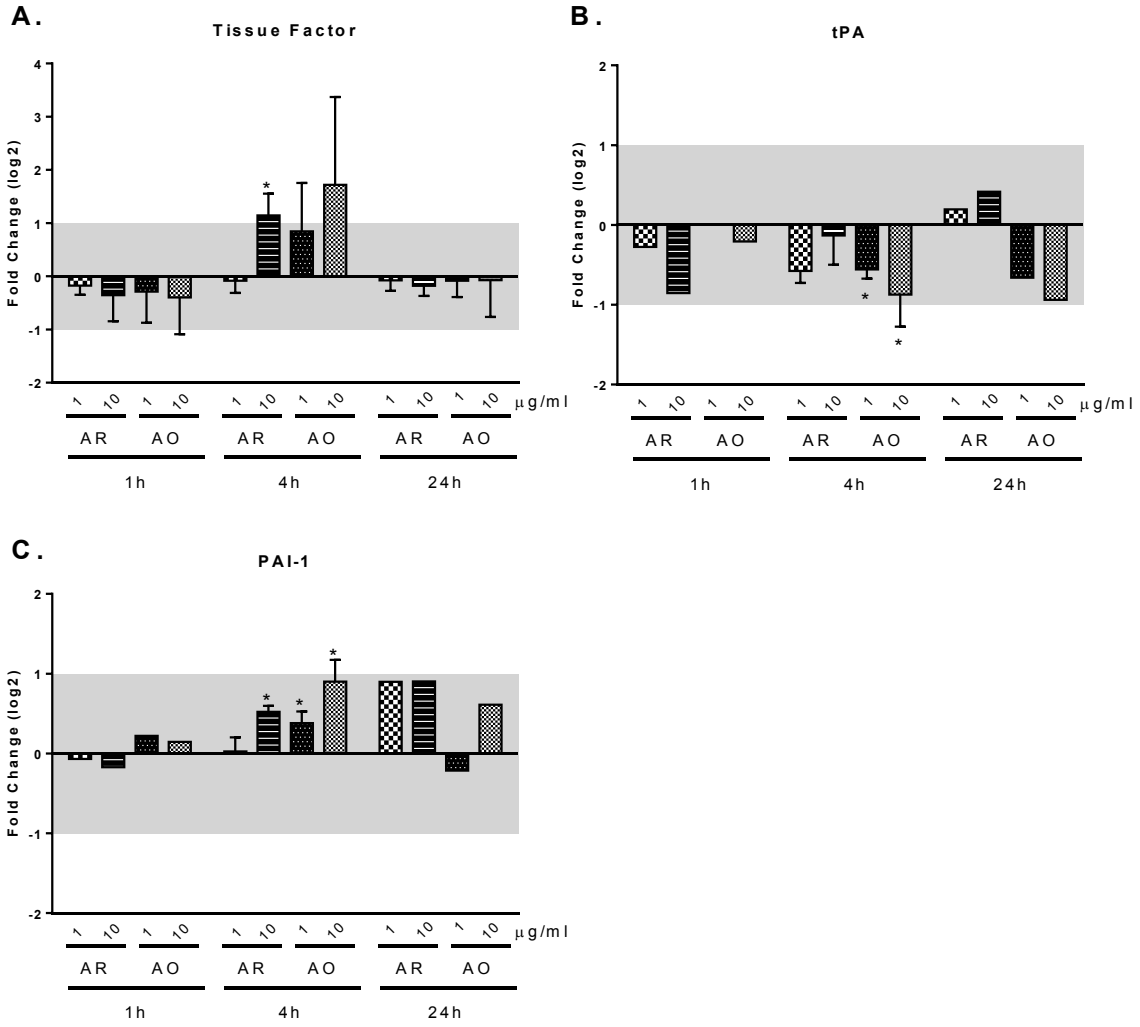


Figure 4.2.9 MWNT-induced *TF*, *tPA* and *PAI-1* gene regulation in HPMVEC. HPMVEC were exposed to 1 or 10µg/ml AR or AO MWNTs for 1, 4 or 24 hours. A). *tissue factor (TF)* B.) *tissue plasminogen activator (tPA)* and C.) *plasminogen activator inhibitor-1 (PAI-1*) gene expression was assayed by RT-PCR. Values were normalised to a GAPDH control and compared to an untreated control using the ΔΔCt method. Data is expressed as mean ±SEM, n=4. For statistical analysis a one-way sample t-test was performed with values compared to a non-treated control value of 0, *$p<0.05$.

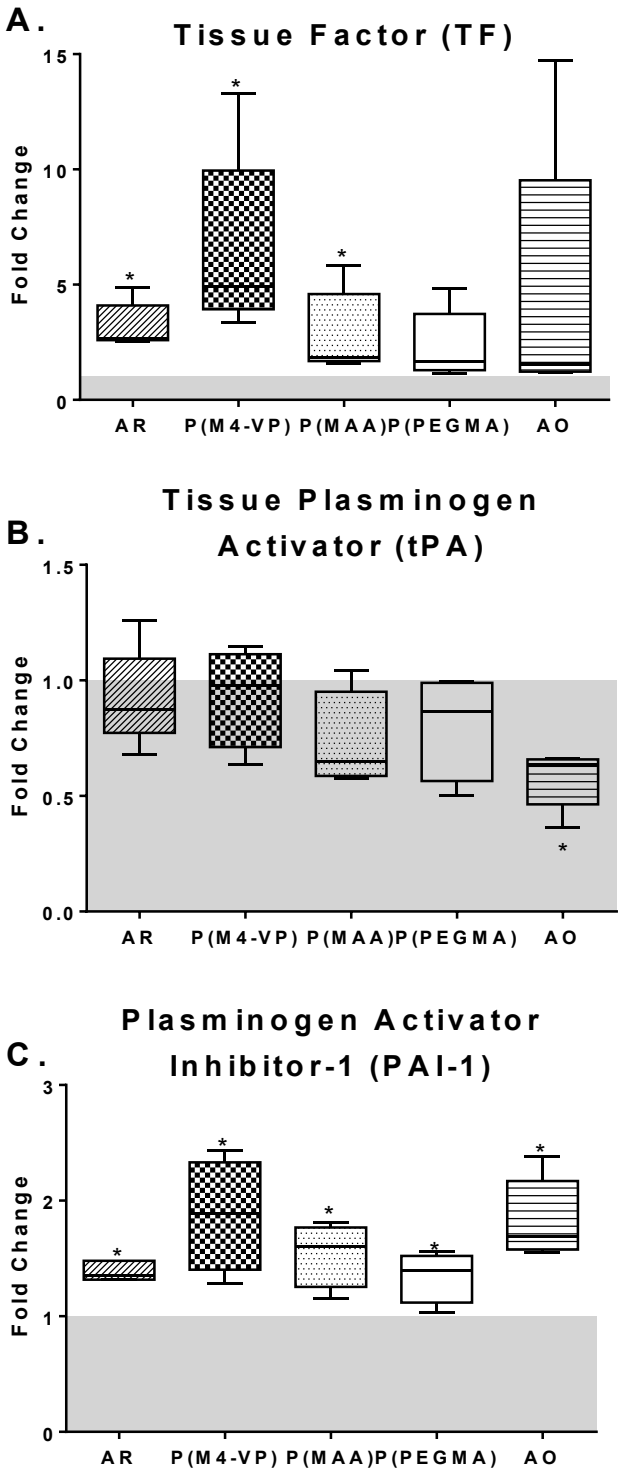


Figure 4.2.10 f-MWNT-induced *TF, tPA and PAI-1 gene* regulation in HPMVEC 4 hours post-exposure. HPMVEC were exposed to 10µg/ml AR, P(M4-VP), P(MAA), P(PEGMA) or AO MWNT for 4 hours. The expression of A). *tissue factor (TF)* B.) *tissue plasminogen activator (tPA*) and C.) *plasminogen activator inhibitor-1 (PAI-1)* genes was assayed by RT-PCR. Values were normalised to a GAPDH control and compared to an untreated control using the ΔΔCt method. Data is expressed as median ±SEM, n=5. For statistical analysis values were log transformed, a one-sample t-test was then performed with values compared to an untreated control value of 0, *$p<0.05$.

4.3. Discussion

Monocyte recruitment following endothelial f-MWNT exposure

This study has clearly demonstrated for the first time that MWNTs induce upregulation of endothelial CAM expression in primary human pulmonary microvascular endothelial cells and that the degree of CAM upregulation is dependent on surface functionalisation. MWNTs in their as-received state initiated a mild up-regulation of the cell adhesion molecules *ICAM-1*, *VCAM-1* and *E-selectin* at the transcriptome level, which was accompanied by an observed dose-dependent increase in both cellular and extracellular E-selectin protein. P(M4-VP) and AO-MWNTs increased CAM expression at both the pre- and post-translational level to a greater extent than AR-MWNTs. This could have implications for cardiovascular health as increased CAM expression and pulmonary inflammation in humans is associated with atherosclerosis and acute ischemic events (Galkina & Ley, 2007; Van Eeden *et al*., 2012).

At 24 hours the trend in sE-selectin levels closely resembles levels of cell bound E-selectin which concurs with a previous study that demonstrated that soluble CAMs can be used as reliable biomarkers of endothelial activation, characterised by increased CAM expression at the cell surface (Kjaergaard *et al*., 2013). Assaying soluble levels of E-selectin would be a useful biomarker for endothelial activation following f-MWNT exposure *in vivo,* as circulating levels could be assayed via a simple blood test. The role of soluble cell-adhesion molecules is unclear however circulating CAMs migrate throughout the systemic vasculature and are associated with a number of diseases such as coronary heart disease and diabetes (Blankenberg *et al*., 2001; Meigs, Hu, Rifai, & Manson, 2004; Ridker, Buring, & Rifai, 2001). It is thought that these molecules are generated either by the shedding of ectodomains of the membrane-bound forms of these molecules, or produced from transcript variants lacking the transmembrane domain (Kiechl *et al*., 2011).

A small but significant increase was observed in sE-selectin levels in cells exposed to AR and P(PEGMA)-MWNTs that was not reflected in E-selectin derived from cell lysates (Figure 4.2.3 & Figure 4.2.4). This may be due to shedding of E-selectin molecules into the cell supernatant which are not replaced by increased E-selectin production, this would indicate that the E-selectin levels in the supernatants may reflect an acute change in E-selectin expression.

Increased expression of cell adhesion molecules was accompanied by an increase in monocyte adhesion to the endothelial monolayer following MWNT exposure. That there are monocytes adhered to unstimulated endothelial cells is unsurprising as, *in vivo*, leukocytes are continually trafficked along the endothelial wall. The function of over-expression of cell adhesion molecules is to increase recruitment and adhesion of leukocytes to the endothelial cell wall and promote extravasation; this enables increased trafficking of leukocytes to points of injury so that these immune cells can aid in the repair process (Muller, 2009). As observed in Figure 4.2.3 baseline *E-selectin*, (involved in initial leukocyte recruitment) is relatively high. Baseline levels of CAMs involved in firm leukocyte adhesion and extravasion such as *VCAM-1*, is reportedly much lower (Ley & Huo, 2001). Although increased monocyte adhesion was observed following exposure to all MWNTs, this was only significant for those which had been either modified with the P(M4-VP) molecule or those which had been acid oxidised (AO-MWNTs). Both particles also increased the expression of endothelial CAMs at the pre- and post-transcriptional level indicating that the increase in CAM expression would be sufficient to induce increased adhesion of monocyte to the endothelium – a process which is associated with the formation and progression of atherosclerotic lesions (Mestas & Ley, 2008). To elucidate the role of specific CAMs in monocyte-endothelial interaction following f-MWNT exposure, siRNA could be employed to silence each of the CAMs or their corresponding monocyte ligand, and the subsequent effect this has on monocyte adhesion studied.

A number of studies have observed pulmonary inflammation following intratracheal CNT exposure in murine models (Ma-Hock *et al*., 2009; Muller *et al*., 2005; Porter *et al*., 2010). In

addition to playing a role in local vascular toxicity, increased CAM expression could contribute to this pulmonary inflammation. CAMs play a crucial role in leukocyte extravasation to underlying tissue (Muller, 2009) and thus, these results indicate that if MWNT were able to reach the underlying endothelium following inhalation, they have the potential to upregulate molecules involved in leukocyte transendothelial migration. The extravasation of circulating leukocytes to the pulmonary system could exacerbate inflammation generated by resident cells.

Although CAM and monocyte adhesion to the endothelium are involved in the development of atherosclerosis, it is important to note that this is also an important aspect of the immune response, required to protect against injury or infection (Cronstein & Weissmann, 1993). The initiation of defence mechanisms, coupled with proliferation following an early reduction in cell viability (section 3.2) is an indication that the endothelium may adapt to, and survive, stresses inflicted by acute MWNT exposure. Other NPs including ZnO and CuO induce a largely cytotoxic response with an equivalent dose of 10μg/ml resulting in a 40 and 60% reduction in cell viability at 24 hours respectively (Sun *et al*., 2011).

The regulation of thrombotic mediators following endothelial exposure to f-MWNT

MWNT exposure induced a prothrombotic response; it increased mRNA expression of the key pro-thrombotic mediators tissue factor (*TF*) and plasminogen activator inhibitor type-1 (*PAI-1*). The severity of this reaction was highly dependent on MWNT functionalisation with P(M4-VP) and AO-MWNT inducing a greater pro-thrombotic response. Exposure to AO-MWNTs also significantly decreased expression of the thrombosis inhibitor tissue-type plasminogen activator (*tPA*) indicating that following exposure to this particle, not only would there be an increase in fibrin clot formation but also a decrease in clot breakdown.

Despite the higher water stability of the particles, P(M4-VP) and AO-MWNTs may not be ideal candidates for use in medicine due to the pro-thombotic nature of these particles and the subsequent potential for adverse cardiovascular side effects. P(MAA) or P(PEGMA)-MWNTs

were less thrombogenic and may therefore induce less off-target effects. P(PEGMA)-MWNTs induced a slightly smaller increase in *TF* expression than AR-MWNTs, indicating that P(PEGMA) functionalisation might provide a modest protection against the pro-thrombotic effect of as-received MWNTs. P(MAA) functionalisation did not appear to affect the regulation of pro-thromobotic genes when compared to AR-MWNTs.

Thrombosis can be a secondary effect of inflammation; pro-inflammatory stimuli are able to disturb the haemostatic balance on the surface of endothelial cells by changing the expression of several thrombotic factors, including *TF*, *PAI-1* and *tPA*, in a concerted way that facilitates blood clot formation and thrombosis (Nan, Lin, Lumsden, Yao, & Chen, 2005). The pro-thrombotic response observed following MWNT exposure may therefore be a secondary effect of the observed inflammation. Indeed, it was P(M4-VP) and AO-MWNTs that induced not only the greatest pro-inflammatory response but also induced the greatest pro-thrombotic response. It is important to note that both the pro-inflammatory and pro-thrombotic responses observed following AO-MWNT exposure occurred in the absence of ROS formation (chapter 3.2) suggestive of a ROS-independent mechanism of toxicity for this particle.

Tissue factor (*TF*) is the key initiator of the coagulation cascade and is not expressed by the resting endothelium. Furthermore, induction of tissue factor following endothelial activation primarily occurs at the transcriptional level (Steffel *et al*., 2006). Due to the low baseline expression of *TF*, an increase in expression results in a large fold change, as was evident in this study. Unlike *TF*, *PAI-1* and *tPA,* which regulate fibrin clot retention and breakdown respectively, are detectable in the quiescent endothelium. Furthermore, *tPA* is stored in the Weibel-Palade bodies of endothelial cells and transiently released to promote fibrinolysis. (Tanaka *et al*., 2009). All particles studied induced a significant increase in *PAI-1* expression, however the greatest increase was following exposure to P(M4-VP)-MWNTs, however this was less than compared to the fold change in *TF*. The differential expression of these thrombotic mediators in the resting endothelium is a likely cause of the less pronounced relative change in

PAI-1 and *tPA* than *TF* gene expression following MWNT exposure. As a key propagator of the coagulation cascade, the initiation of TF expression is central to disease progression (Steffel *et al*., 2006).

Following exposure to all MWNTs except P(PEGMA) and AO-MWNTs, *TF* expression was significantly increased at 4 hours. There was a large degree of variability in the data for the AO-MWNT particles. It is possible that the onset of *TF* mRNA transcription was earlier or later than the 4 hour time point studied, or that AO-MWNTs induced a greater induction in *TF* in HPMVECs derived from different individuals.

It is well recognised that a number of genetic loci are associated with a susceptibility to atheroma formation and cardiovascular disease (Lippi, Franchini, & Targher, 2011) and indeed, HPMVECs derived from different donors displayed variation in the magnitude of the response to 10ng/ml TNFα exposure (Appendix V). This suggests that the variability may be due to a general heightened or lessened response between donors to pro-inflammatory and pro-thrombotic stimuli. To study this phenomenon, HPMVECs derived from a larger donor pool should be employed to determine whether any correlations are observed between the presence of disease and MWNT toxicity. This could determine whether MWNT exposure is especially harmful to individuals with pre-existing conditions. A study of normotensive control Wistar-Kyoto (WKY) and spontaneously hypertensive (SH) rats found a greater adverse cardiovascular reaction in SH rats following MWNT intratracheal instillation. This was evidenced by a persistent decrease in heart rate, increased plasma fibrinogen and obvious morphological lesions in abdominal arteries of SH rats 30 days after exposure. The authors of this study highlighted that more attention should be paid to the long-term toxic effects of MWCNTs, especially in those individuals with pre-existing cardiovascular diseases (Chen *et al*., 2015).

MWNT interaction with the endothelium is a potential mechanism for the cardiovascular toxicity observed *in vivo* following MWNT exposure. The potential for MWNT induced endothelial toxicity exists following both pulmonary exposure and intravenous injection due to

the ability of MWNTs to cross the pulmonary barrier to reach systemic organs (reported by Chen *et al*., 2015; Mercer *et al*., 2013; Reddy *et al*., 2010). Here we have shown that, in a microvascular *in vitro* model, MWNTs induce monocyte adhesion to the endothelial cell surface and the release of thrombotic mediators, events associated with atherosclerotic plaque formation and thrombus formation *in vivo*.

4.4. Summary

MWNT exposure increased both pre- and post-translation levels of cell adhesion molecules in HPMVECs. The intensity of this response was affected by MWNT surface functionalisation; P(M4-VP) and AO-MWNTs resulted in the greatest increase in CAM expression, corresponding to a significant increase in monocyte adherence at the endothelial surface. MWNT exposure also resulted in a pro-thrombotic gene expression profile, with upregulation of the thrombotic genes *tissue factor* and *tissue plasminogen activator inhibitor-1* and down regulation of the thrombosis-inhibitor *tissue plasminogen activator.* Upregulation of endothelial CAM and pro-thrombotic mediators is a plausible mechanism underlying the adverse cardiovascular effects observed following CNT exposure *in vivo*.

5. DISRUPTION OF THE ALVEOLAR-CAPPILLARY BARRIER FOLLOWING EXPOSURE TO F-MWNTS

5.1. Introduction

For efficient gas exchange to occur there must be a highly specialised barrier separating air in the lung from fluid filled tissues (Overgaard, Mitchell, & Koval, 2012). Maintenance of the air-liquid interface integrity, through regulation of fluid transport and cell-cell interactions (Overgaard *et al*., 2012), is essential as alveoli are extremely sensitive to disrupted fluid balance (Mehta *et al*., 2004). Loss of this function results in tissue inflammation which is a hallmark of a number of inflammatory diseases including pulmonary oedema and acute respiratory distress syndrome (ARDS) (Lum & Malik, 1994; Mehta *et al*., 2004; Mehta & Malik, 2006).

Barrier permeability is defined by the movement of fluid and macromolecules via both transcellular and paracellular pathways. Transcellular transport of fluid and proteins occurs through vesicular carriers, whereas paracellular transport of fluid and proteins occurs via gaps between adjacent cells (Lum & Malik, 1994; Prasain & Stevens, 2009).

The transcellular pathway

Transport of proteins across the healthy alveolar epithelium occurs primarily via the transcellular route, which may be either protein specific receptor mediated transcytosis or non-specific fluid-phase endocytosis (Kim & Malik, 2003). Similarly, the transport of protein and liquid in the undisturbed endothelium generally occurs via the transcellular pathway; however, in response to intrinsic and extrinsic stimuli, the endothelium also activates signalling pathways that allow transport of solutes through the paracellular pathway (Mehta & Malik, 2006).

Proteins such as albumin, are typically transported via the transcellular pathway via vesicular carriers, such as caveolae. Albumin and other transported proteins are critical for maintaining the protein flux between the vascular and extravascular space and furthermore, can act as

circulating chaperones for hydrophobic substances, fatty acids, and hormones (Mehta & Malik, 2006).

The paracellular pathway

The degree of movement of molecules and cells via the paracellular pathway is dependent on cell-cell adhesion molecules. In both alveolar epithelial cells and microvascular endothelial cells these adhesion molecules can be classed as forming either tight junctions, adherens junctions or gap junctions (Dejana & Orsenigo, 2013; Turowski *et al*., 2008). Both cell types have a number of adhesion molecules that are cell specific, however others are conserved between cell types, for example, desmosomes are present at epithelial, but not endothelial junctions (Dejana & Orsenigo, 2013). The major tight junction classes are the claudins, occludins and junctional adhesion molecules (JAMs), which are present in both epithelial and endothelial cells. Adherens junctions are located either immediately below tight junctions as part of the tripartite junctional complex, a structure which borders the apico-basolateral membrane and is implicated in barrier function (desmosomes form the third structure of this complex), or adherens junctions are also found separate from the tripartite complex (Niessen, 2007) (Figure 5.1.1).

In a healthy endothelium only molecules with a molecular radius of less than 3nm can cross the endothelium via the paracellular or interendothelial junction pathway. There are however a number of factors that can influence the permeability of the paracellular pathway including nutrients, cytokines and immune cells (Nusrat, Turner, & Madara, 2000). Although circulating immune cells are able to cross the endothelial barrier to underlying tissue by transcellular migration, the primary site of diapedesis occurs at endothelial borders via paracellular migration (Ley, Laudanna, Cybulsky, & Nourshargh, 2007; Muller, 2011). As leukocytes primarily transcend tissue barriers by paracellular migration, it is important that the endothelial and epithelial cell barriers are able to adapt to the changing needs of the

environment. Significant loosening of the intercellular junctions is thought to be essential for effective paraceullar movement of leukocytes (Muller, 2011).

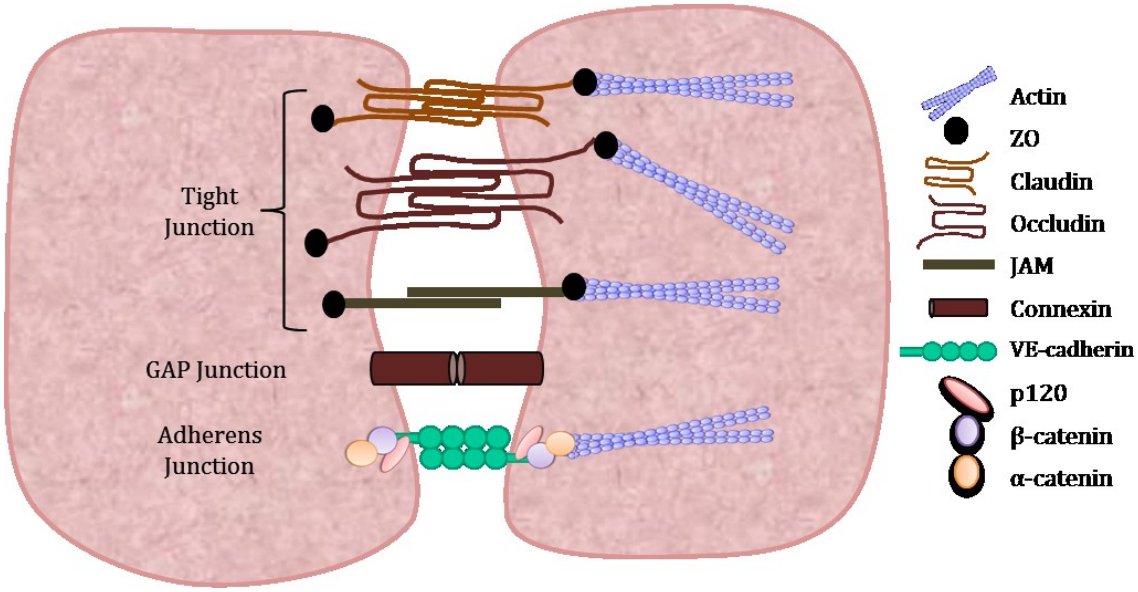


Figure 5.1.1 Diagram depicting the major endothelial cell junction proteins. Tight junctions are characterised by occludin, claudins, and junctional adhesion molecules (JAMs); gap junctions are formed by connexins and adherens junctions, primarily by VE-cadherin. While the extracellular domains of these proteins maintain cell-cell contact, intracellular domains provide junctional stability through their linkages with the actin cytoskeleton via catenins (β-catenin, α-catenin, p120-catenin) or zona occluden-1 protein (ZO-1). Gap junctions allow the rapid exchange of information between adjacent cells in the form of low-molecular-mass second messengers. Adapted from (Mehta & Malik, 2006)

The intracellular domains of tight junction and adherens junction proteins are connected to the actin cytoskeleton via zona occludin-1 (ZO-1) and catenins (α, β, γ, and p120), respectively (Mehta & Malik, 2006) (Figure 5.1.1). These cell–cell interactions, in concert with cell–matrix adhesion structures, counteract actomyosin contractile tension maintaining barrier function. Pathophysiological conditions, such as inflammation, trigger a series of signalling events which promote cell contraction and induce phosphorylation and disorganization of junction molecules resulting in intercellular gap formation and paracellular hyperpermeability (Qiang, Wu, & Yuan, 2009). Under pathological conditions passive diffusion of molecules via the paracellular route, may become the primary route of protein leakage (Kim & Malik, 2003). Protein accumulation in alveoli may reduce the surface activity of surfactant, contributing to collapse of alveoli and

alveolar flooding, promote fibrosis, and generate reactive oxygen and nitrogen species leading to the precipitation and modification of proteins (Kim & Malik, 2003). High levels of serum protein are found in the BAL of patients with pulmonary oedema, furthermore, large quantities of precipitated protein are observed in patients with acute respiratory distress syndrome (ARDS), and non-survivors have three times more protein in their air spaces than survivors (Kim & Malik, 2003). The resolution of pulmonary edema requires a functional and intact alveolar epithelial barrier (Kim & Malik, 2003).

In epithelial cells, it is thought that tight junctions are the critical determinant of epithelial barrier function (Overgaard *et al*., 2012). Of the protein complexes that form tight junctions, claudins are the primary component that regulate the tight junction barrier and a decrease in claudin expression is associated with a number of diseases including pulmonary fibrosis, alcoholic lung syndrome and sepsis-induced ARDS (Förster, 2008; Kimata *et al*., 2003; Overgaard *et al*., 2012).

The VE-cadherin protein in endothelial adherens junction regulation

Whereas epithelial barrier integrity is primarily regulated by tight junctions, vascular permeability is increased by modifications in the expression of adherens junction components (Dejana & Orsenigo, 2013). The vascular endothelial (VE)-cadherin adherens junction complex is the major component of the endothelial adherens junctions and is specific to endothelial cells (Dejana & Orsenigo, 2013; Vincent, Xiao, Buckley, & Kowalczyk, 2004). Adjacent VE-cadherin molecules form homophilic interactions in trans formation, and lateral interactions in cis, and are closely linked to the cell cytoskeleton through their association with actin microfilaments (Dejana & Orsenigo, 2013).

The VE-cadherin adherens junction complex is known to rearrange to accommodate the need for trans-endothelial migration (TEM) of leukocytes and in response to other pro-inflammatory stimuli (Dejana & Orsenigo, 2013; Luscinskas et al, 2002; Turowski *et al*., 2008). Disassembly of

VE-cadherin is initiated by phosphorylation of sites such as the p120 and β-catenin binding sites of VE-cadherin protein (Allingham, van Buul, & Burridge, 2007; Turowski *et al*., 2008). Phosphorylation of the site associated with β-catenin binding leads to uncoupling of VE-cadherin from the actin cytoskeleton, thereby weakening intercellular junctions (Allingham *et al*., 2007). p120-catenin stabilises VE-cadherin at junctions by preventing clathrin-mediated endocytosis, (Xiao *et al*., 2005); phosphylation of VE-cadherin at the site associated with p120 binding therefore promotes VE-cadherin endocytosis (Potter, Barbero, & Cheresh, 2005).

Nanoparticles and barrier permeability

Under normal physiological conditions, the aforementioned transport mechanisms are tightly regulated, however, it has been observed that NPs can interfere with cell-cell junctions, thereby increasing barrier permeability.

There is some evidence that NPs may have such an effect at the epithelium; an *in vitro* study of rat alveolar epithelial cells showed that exposure to UFP suspensions, quantum dots and SWCNTs (but not polystyrene nanoparticles) significantly decreased transepithelial electrical resistance (TEER), a technique routinely used to determine the integrity and permeability of cell monolayers (Yacobi *et al*., 2007). A decrease in TEER was also observed in Calu-3 human airway epithelial cells exposed to MWNTs, which was accompanied by an increase in mannitol transport across the epithelial cell monolayer. In the same study SWCNTs induced lesser changes in TEER and carbon black nanoparticles had no effect (Rotoli et al., 2008). The effect of fibre length on Calu-3 TEER was also investigated using long and short MWNTs and SWCNTs and it was found that only the longer CNTs (0.5-100μm and 5-9μm for SWCNTs and MWNTs, respectively) induced a significant reduction in TEER at a concentration of 73μg/cm^2 for an exposure period of 8 days (Rotoli et al., 2009). Although there is some evidence to support NP induced epithelial barrier disruption, the influence of NP physicochemistry is poorly understood, as are the mechanisms underlying the increased permeability. There is also a

dearth of data surrounding the effects of NPs at the microvascular endothelium. *In vitro* models using human microvascular cells have shown that iron oxide nanoparticles and multi walled carbon nanotubes increase cell monolayer permeability through oxidative stress mediated microtubule and actin remodelling, caused by an excess of ROS (Apopa *et al*., 2009; Pacurari *et al*., 2012). Furthermore, TiO_2 NP exposure is thought to disrupt endothelial VE-cadherin homophilic complexes via direct TiO_2 interaction with VE-cadherin molecules (Setyawati *et al*., 2013). The information regarding NP induced microvascular permeability is however extremely scarce and the effect of NP functionalisation is unknown.

In vivo, total BAL protein, as an indicator for maintenance of alveolar-capillary permeability, has been studied in rats following intratracheal exposure to MWNTs.; total protein markedly increased with MWNT exposure on day 1 and although this trend attenuated toward control levels thereafter, it was persistently higher than control values until day 91 (Aiso *et al*., 2010). Furthermore, subcutaneously injected TiO_2 NPs increased leakiness of subcutaneous blood vessels in mice; leakiness was determined using Evan's blue dye administered to the circulation. Intravenously administered TiO_2 NP also increased tumour metastases, a marker of increased vessel leakiness (Setyawati *et al*., 2013). Taken together, the *in vitro* and *in vivo* findings indicate that, although there is some evidence supporting the implication of NPs in increased alveolar-capillary permeability, the role of NP physiochemical properties is poorly understood. In particular there is a lack of data surrounding the effects of NP functionalisation on cell-cell interactions at this barrier, which is an area of particular concern given the increasing interest in NPs for biomedical applications.

Due to the ability of NPs to cross biological barriers via the paracellular route, the ability of nanoparticles to disrupt barrier integrity could have significant implications for their biodistribution following inhalation or injection. Whilst this could have potentially deleterious health effects in certain circumstances, there is increasing research attempting to exploit the ability of nanoparticles to cross barriers for use in drug delivery. Researchers have for many

years been investigating how to manipulate the paracellular pathway for the delivery of drugs; biological barriers such as the blood brain barrier are difficult for therapeutics to transcend due to the lack of paracellular openings, pinocytosis and significant protein mediated efflux (Lockman, Koziara, Mumper, & Allen, 2004). It is hoped that nanoparticle therapies will be an innovative way of allowing therapeutics to traverse these tightly regulated biological barriers (Biddlestone-Thorpe *et al*., 2012). In doing so, it is hoped that increased therapeutic availability at the disease site could allow the use of lower doses with increased efficacy and fewer off target effects (Rogueda & Traini, 2007).

Overview:

This chapter will explore whether MWNT exposure can affect barrier function using an electrical cell-substrate impedance system alongside a protein transport assay. In addition, the integrity of cell-cell junctions following exposure to MWNTs will be investigated by visualising the endothelial VE-cadherin complex using immunoblotting and immunostaining techniques. We use these parameters to compare and contrast the differential responses of the cells to the suite of functionalised CNTs and discuss the potential importance of these results in light of occupational or therapeutic exposure.

Aims and Hypotheses:

We hypothesised that MWNT exposure would disrupt epithelial and endothelial cell-cell interactions and increase the permeability of an *in vitro* model of barrier integrity, and that the degree of disruption would be dependent on MWNT surface functionalisation. Furthermore, we hypothesised that the disruption in endothelial cell-cell interactions would be apparent in the adherens junction complexes. Our specific aims were to determine:

I. Whether MWNT exposure affected epithelial and endothelial barrier integrity using an electrical cell-substrate impedance system.
II. If the results of the electrical cell-substrate impedance system were comparable to a traditional barrier permeability assay.
III. Whether any loss in endothelial barrier integrity would be accompanied by changes in cell morphology and adherens junction protein expression.
IV. If MWNT functionalisation was a critical determinant in the nature and severity of the aforementioned reactions.

5.2. Results

Electrical cell-substrate impedance sensing (ECIS)

Cell proliferation and barrier integrity were measured using a technique called electrical cell-substrate impedance sensing (ECIS), which can measure changes in cell behaviour in real time. Figure 5.2.1-A illustrates a typical plot of TT1 cell proliferation using the ECIS system, prior to MWNT exposure. Cells were serum starved 24 hours after seeding (indicated by the arrow) and incubated for a further 24 hours in culture prior to MWNT exposure; during this time the cell index continued to rise, indicating that these cells continued to proliferate. Furthermore, the cell index did not plateau when a confluent monolayer was observed but instead, would continue to rise indicating that these cells may not possess contact inhibition of growth.

Exposure to MWNTs resulted in a decrease in the normalised cell index (CI) compared to non-treated controls (Figure 5.2.1-B). Normalised values are compared to the non-treated control at the time of exposure. AO-MWNTs had the smallest effect on the TT1 cell CI at 24 hours, whereas P(PEGMA)-MWNTs had the greatest effect; AO-MWNTs induced a 4% decrease in CI, whereas P(PEGMA)-MWNTs induced 29% decrease (Figure 5.2.1-C). Despite P(PEGMA)-MWNT exposure resulting in the greatest decrease in CI, the only significant decrease in TT1 CI at 24 hours was observed following P(MAA)-MWNT exposure (19%, $p<0.05$) due to the variablity in results (Figure 5.2.1-C). Beyond 58 hours following particle exposure we see a small decrease in the non-treated control value indicating a reduction in the integrity of the cell layer (Figure 5.2.1-B).

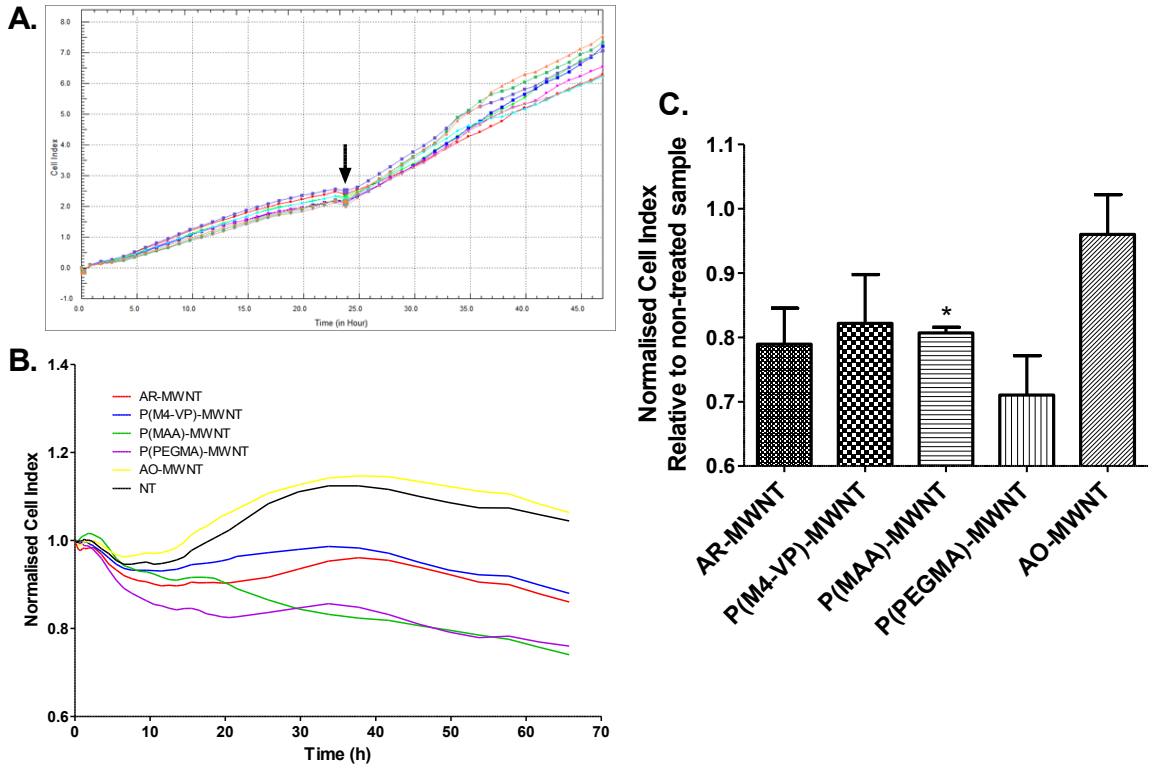


Figure 5.2.1 TT1 cell iCelligence data. (A.) A typical curve depicting increases in Cell Index corresponding with TT1 cell growth on iCelligence E-plates. The arrow indicates the addition of serum-free medium at 24 hours. (B.) An example plot of TT1 normalised cell index values following exposure to functionalised carbon nanotubes. Normalised values are compared to the non-treated control at the time of exposure (t=0h). (C.) A snapshot of cell index values compared to the untreated value at 24 hours following exposure to f-MWNTs. C.) Data is expressed as mean ±SEM, n=3. For statistical analysis values were transformed to their logarithms to make the distribution more Gaussian, a one-sample t-test was then performed with values compared to a non-treated control value of 0, *$p<0.05$.

When the above experiments were repeated with primary human AT2 cells it took approximately 10 hours for the AT2 cells to begin to firmly attach to the E-plate; after this period, the AT2 cell index rapidly increased. The AT2 cell index reached a maximal value of approximately 12.7 before falling to approximately 11.5 where the value then plateaued. A small spike can be seen where the serum-free media was applied (arrow) however following this period the cell index returned to its previous value. Unlike TT1 cells, the AT2 cell index did not increase following serum starvation indicating a lack of continued cell proliferation (Figure 5.2.2-A).

Following the addition of MWNTs the AT2 cell index value did not vary significantly from that of the non-treated control; at approximately 50 hours post exposure (Figure 5.2.2-B) the cell index values began to drop for all conditions, including the untreated control. These values then continue to decrease until the experiment is terminated.

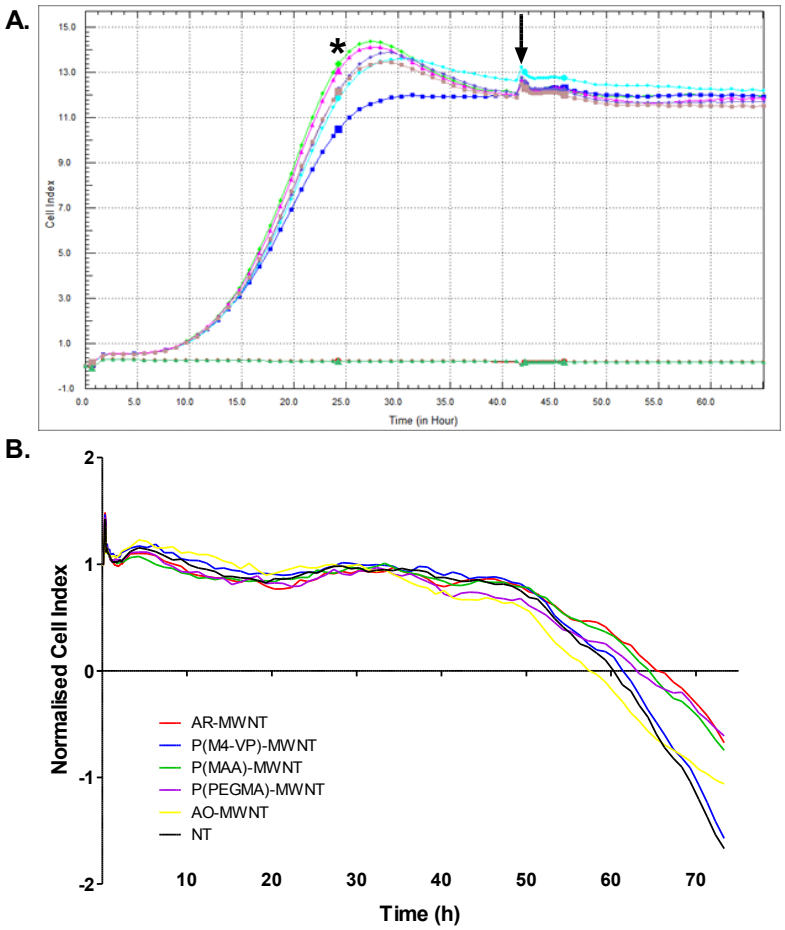


Figure 5.2.2 AT2 cell iCelligence data. (A.) A typical curve depicting increases in Cell Index corresponding with AT2 cell growth on iCelligence E-plates. The asterisk indicates where the cell medium is replaced at 24 hours to remove non-adherent cells, the arrow indicates the addition of serum-free medium following a further 24 hours in culture. (B.) An example plot of AT2 normalised cell index values following exposure to functionalised carbon nanotubes. Normalised values are compared to the untreated control at the time of exposure (t=0h).

Following a settling period of approximately 2.5 hours, the cell index of HPMVECs increased gradually. Unlike TT1 cells, this value plateaued at 48 hours, indicating that these cells possess contact inhibition of growth and that at this point the cells have reached confluence and formed stable cell-cell adhesions (Figure 5.2.3-A). A disturbance in the growth curve can be seen following the addition of the 10X concentrate MWNT exposure solution (100µg/ml f-MWNTs

were applied as a 10X concentrate to achieve a final concentration of 10µg/ml). This was evident in both cells which had received media alone or the f-MWNT treatment (Figure 5.2.3-B).

The AO-MWNT-exposed and non-treated normalised CI values were similar, however all other MWNTs induced a significant decrease in CI ($p<0.05$). This decrease was greatest in P(M4VP)-MWNT exposed cells with CI values decreasing by 40%, P(MAA) and P(PEGMA)-MWNT induced a lesser decrease in normalised CI values, 30 and 35% respectively ($p<0.05$) (Figure 5.2.3-C). Despite this decrease compared to non-treated cells at 24 hours, the cell index value of all cells continued to rise slightly overall, indicating an increase in cell monolayer integrity (Figure 5.2.3-B).

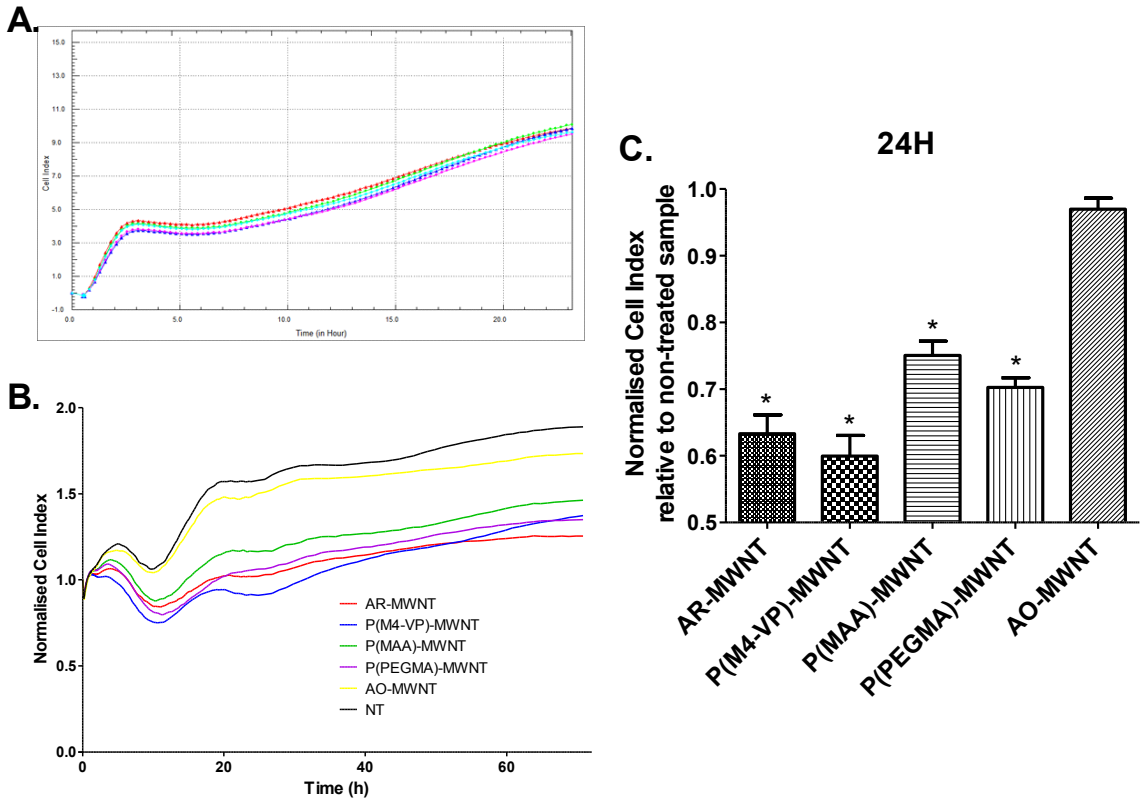


Figure 5.2.3 HPMVEC iCelligence data. (A.) A typical curve depicting increases in Cell Index corresponding with HPMVEC growth on iCelligence E-plates. (B.) An example plot of HPMVEC normalised cell index values following exposure to functionalised carbon nanotubes. Normalised values are compared to the untreated control at the time of exposure (t=0h). (C.) A snapshot of cell index values compared to the non-treated value at 24 hours following exposure to f-MWNTs. C.) Data is expressed as mean ±SEM, n=3. For statistical analysis values were transformed to their logarithms to make the distribution more Gaussian, a one-sample t-test was then performed with values compared to a non-treated control value of 0, *$p<0.05$.

EB-albumin permeability assay

In order to confirm observations using the new ECIS method, the effect of MWNTs on barrier permeability was also assessed using the traditional Evans Blue permeability assay. For this study, the MWNTs that caused the least and greatest barrier disruption using ECIS were compared (Figure 5.2.4-A). HPMVECs treated with AR-MWNTs displayed a dose dependent increase in barrier permeability which was significant at concentrations greater than 5μg/ml ($p<0.05$) and resulted in an 8.4-fold increase in permeability at the highest concentration ($p<0.001$) compared to untreated cells. In stark contrast, AO-MWNTs did not induce any significant increase in HPMVEC barrier permeability, as observed with ECIS.

To compare the differential barrier disrupting properties of functionalised MWNT, a dose of 10μg/ml was used (Figure 5.2.4-B). At 24 hours, only as received and P(M4-VP)-MWNTs induced a significant increase in barrier permeability using this assay, resulting in a 5.7x ($p<0.001$) and 4.8x ($p<0.01$) increase respectively. Although not statistically significant, both P(MAA) and P(PEGMA)-MWNTs increased HPMVEC barrier permeability by 3.4 fold. AO-MWNTs did not induce any detectable change in barrier permeability using this assay.

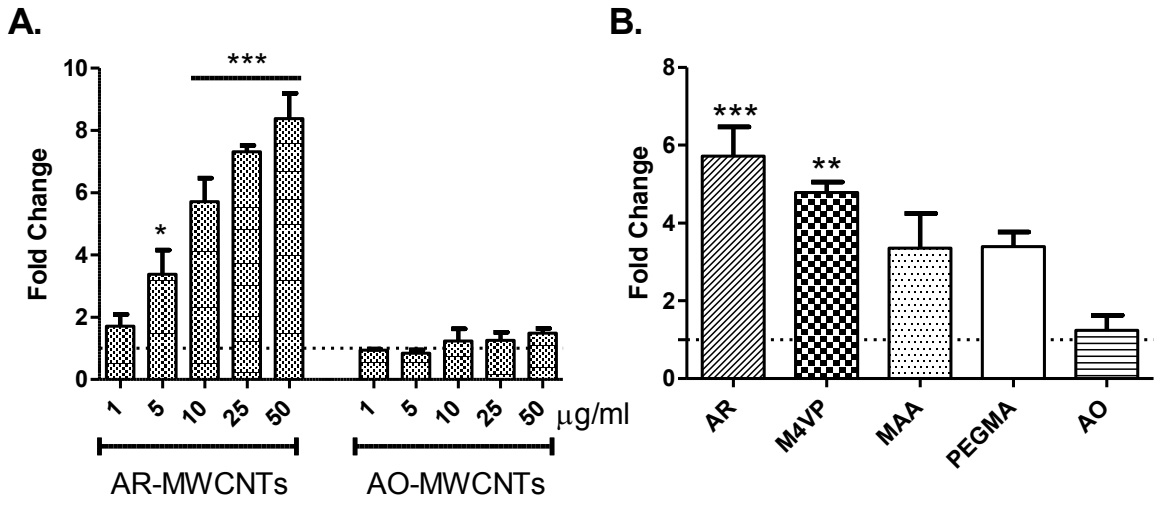


Figure 5.2.4 Endothelial barrier permeability determined by the EB-albumin permeability assay. HPMVECs were cultured on a permeable membrane and exposed to the A.) 1-50μg/ml AR or AO-MWNTs or B.) 10μg/ml AR, P(M4VP), P(MAA), P(PEGMA) or AO-MWNTs, HPMVEC monolayers were exposed to MWNTs for 24 hours. Following this exposure period, endothelial barrier permeability was determined by the EB-albumin permeability assay which involved the movement of Evan's Blue conjugated to albumin across the permeable membrane. Data is expressed as mean ± SEM, n=4. A.) One-way ANOVA followed by Dunnett's post-test; *p< 0.05, ***p< 0.001. B.) For statistical analysis values were transformed to their logarithms to make the distribution more Gaussian, a one-sample t-test was then performed with values compared to a non-treated control value of 0; **p< 0.01, ***p< 0.001

VE-cadherin/actin immunostaining

To investigate the molecular mechanisms behind barrier disruption, HPMVECSs were stained for f-actin and VE-cadherin (Figure 5.2.5 & Figure 5.2.6). In resting monolayers, f-actin was arranged cortically (red) and the adherens junction protein VE-cadherin (green) was strongly expressed at cell-cell junctions. Furthermore, in these cells there were very few visible gaps between cells. Following a 3 hour exposure to 10μg/ml AR and P(M4-VP)-MWNTs, large holes in the cell monolayer were apparent (indicated by an asterisk *) (Figure 5.2.5). Furthermore, smaller gaps between cells, with elongated VE-cadherin bridges, became apparent in AR, P(M4-VP), P(MAA) and P(PEGMA)-MWNT treated cells (indicated by arrow heads), and an increase in non-cortically arranged f-actin was observed. AO-MWNTs appeared to have no effect on the intensity of the VE-cadherin stain, the arrangement of f-actin or the formation of gaps at cell-cell junctions (Figure 5.2.5).

After 24 hours exposure, f-MWNTs caused further disruption to cell-cell junctions; larger, more widespread gaps appeared in the cell monolayers following exposure to AR or P(M4-VP)-MWNTs and there appeared to be a loss in the intensity of the VE-cadherin stain. In addition, further re-arrangement of f-actin was observed (Figure 5.2.6). As seen at 3 hour post-exposure, this effect was greatest in AR or P(M4-VP)-MWNT cells, AO-MWNTs exposure did not result in any apparent changes in f-actin or VE-cadherin. Small gaps between cells exposed to P(MAA) and P(PEGMA)-MWNTs were observed (indicated by arrow heads), however these holes were less numerous than in the AR or P(M4-VP)-MWNT cell monolayer (Figure 5.2.6).

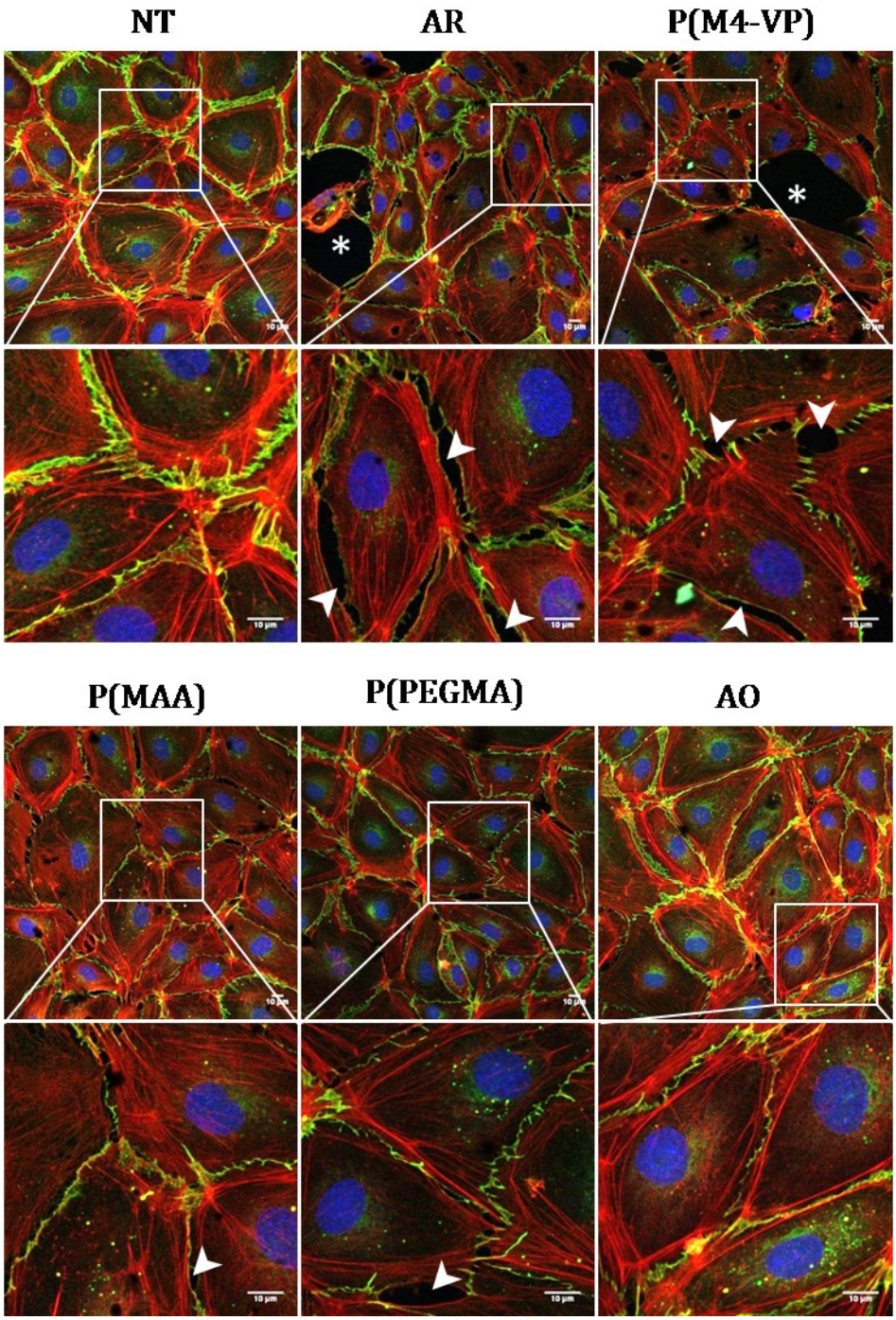


Figure 5.2.5 Immunostaining displaying the effect of a 3 hour f-MWNT exposure on HPMVEC junction integrity. The adherens junction protein VE-cadherin is depicted in green, f-actin in red and the cell nucleus in blue. Arrows indicate gaps forming between adjacent cells, stars indicate large holes in the cell monolayer, possibly formed by MWNT induced cell death. Area inside white box is shown at a higher resolution below, scale bars are 10μm.

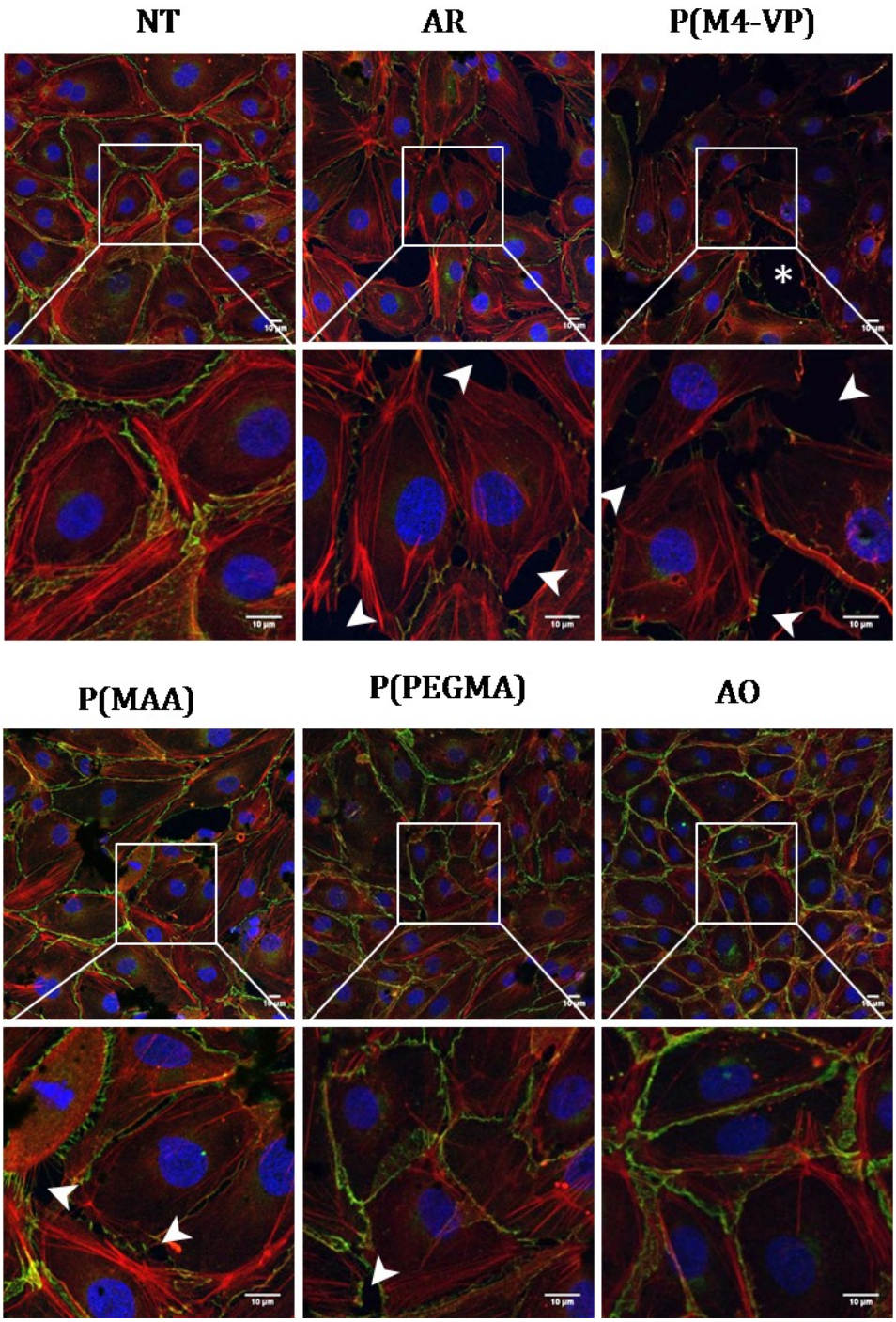


Figure 5.2.6 Immunostaining displaying the effect of a 24 hour f-MWNT exposure on HPMVEC junction integrity. The adherens junction protein VE-cadherin is depicted in green, f-actin in red and the cell nucleus in blue. Arrows indicate gaps forming between adjacent cells, stars indicate large holes in the cell monolayer, possibly formed by MWNT induced cell death. Area inside white box is shown at a higher resolution below, scale bars are 10µm.

VE-cadherin western blots

To further investigate the reduction in the intensity of the VE-cadherin stain following MWNT exposure, western blotting for VE-cadherin was performed. Exposure to 10μg/ml AR-MWNTs significantly reduced VE-cadherin protein expression as early as 1 hour (59%, $p<0.05$) and despite a slight, but non-significant, recovery around 6 hours, expression had almost completely diminished by 24 hours ($p<0.001$) (Figure 5.2.7). In contrast, HPMVECs treated with AO-MWNTs showed no significant loss of VE-cadherin protein (Figure 5.2.8).

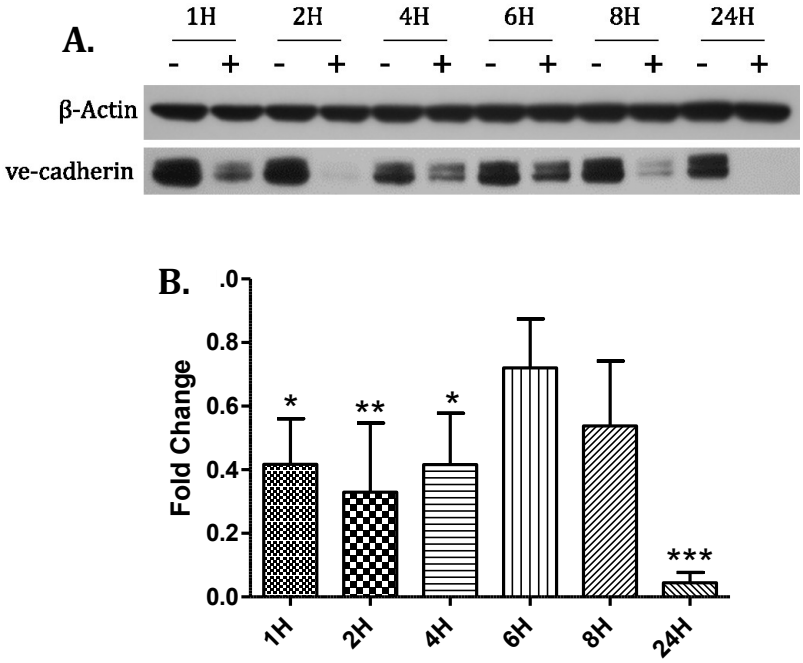


Figure 5.2.7 VE-cadherin protein expression following 10μg/ml AR-MWNT exposure determined by immunoblotting. HPMVECs were exposed to AR-MWNTs for 1, 2, 4, 6, 8 or 24 hours prior to protein collection. (A) Representative immunoblot, "-" indicates a non-treated control, "+" indicates exposure to the AR-MWNTs. (B) VE-cadherin expression relative to the non-treated control, values were normalised to a β-actin control. Data is expressed as mean ± SEM, n=3. One-sample t-test with values compared to a non-treated control value of 1; *p< 0.05, **p< 0.01, ***p< 0.001.

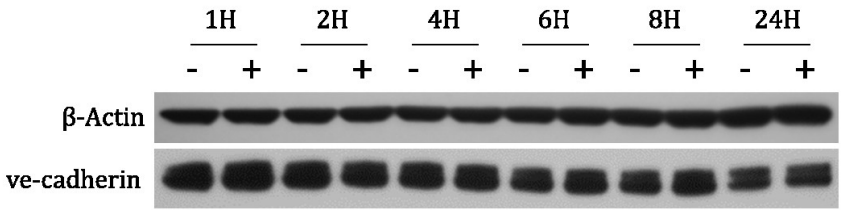


Figure 5.2.8 VE-cadherin protein expression following 10µg/ml AO-MWNT exposure determined by immunoblotting. HPMVECs were exposed to AO-MWNTs for 1, 2, 4, 6, 8 or 24 hours prior to protein collection. Representative immunoblot, "-" indicates a non-treated control, "+" indicates exposure to the AO-MWNTs.

5.3. Discussion

Following exposure to MWNT, the barrier permeability of TT1 and HPMVEC, but not AT2 monolayers increased. In both TT1 and HPMVEC *in vitro* systems, AO-MWNT had little effect on barrier permeability whereas AR-MWNTs and thermochemically functionalised MWNT exposure induced a pronounced increase in barrier permeability. Through the use of immunofluorescent microscopy it was clear that increased endothelial permeability was associated with the emergence of holes in the endothelial monolayer and the disruption of cell-cell interactions. This was accompanied by a loss of VE-cadherin protein.

The integrity of microvascular endothelial and alveolar epithelial barriers following f-MWNT exposure

MWNT exposure resulted in reduced barrier properties in both TT1 and HPMVEC monolayers. In the case of endothelial cells, this occurred despite the cells remaining confluent at 24 hours (Figure 3.2.8). This may be a result of VE-cadherin phosphorylation and partial internalisation of the junctional adhesive proteins, which can have profound effects on the transport of solutes (Dejana & Orsenigo, 2013). In the case of epithelial cells, the increase in barrier permeability was also independent of a reduction in cell viability, and is therefore likely due to breakdown in tight-junction complexes (Overgaard *et al*., 2012).

Exposure of AT2 cells to f-MWNTs resulted in no change in the cell index as indicated by the ECIS. This further confirms the resilience of this cell to MWNT exposure, indicating that there is a possibility this important progenitor cell may remain largely unaffected by direct interaction with this material following inhalation exposure. There was however a small change in the cell index of the type 1-like epithelial cell TT1 following exposure to f-MWNTs. The low cytotoxic response of these cells to MWNTs (Figure 3.2.6) indicates that this is likely to be due to disruption of the cell-cell junctions. Intercellular junctions in this cell line are however known to be weak, and it is thought that TT1 cells do not produce physiologically-relevant tight junctions (van den Bogaard *et al*., 2009). It was therefore decided not to investigate these findings further as they may not be transferrable to an *in vivo* situation.

In a similar response to that seen in TT1 cells following f-MWNT exposure, acid oxidised MWNTs had only a very small effect on HPMVEC cell index values. This indicates that AO-MWNTs are unlikely to induce increased barrier permeability at either the alveolar epithelial or microvascular endothelial interface, without signals from other resident cells. In contrast, non-acid oxidised MWNTs had a significant effect on epithelial and endothelial barrier permeability. P(M4-VP) functionalisation of MWNT resulted in the greatest increase in endothelial barrier permeability and reduced TT1 CI by 18%; exposure to this particle via the pulmonary or intravenous route could therefore have implications for the integrity of the blood-gas barrier. If however, long-term exposures found this response to be transient, the barrier disrupting properties of this particle could be exploited to deliver molecules across tightly regulated biological barriers. Using ECIS, P(PEGMA)-MWNTs induced the greatest increase in epithelial permeability however only the third greatest increase in endothelial permeability indicating that this particle may be more harmful if administered via the pulmonary rather than the intravenous route.

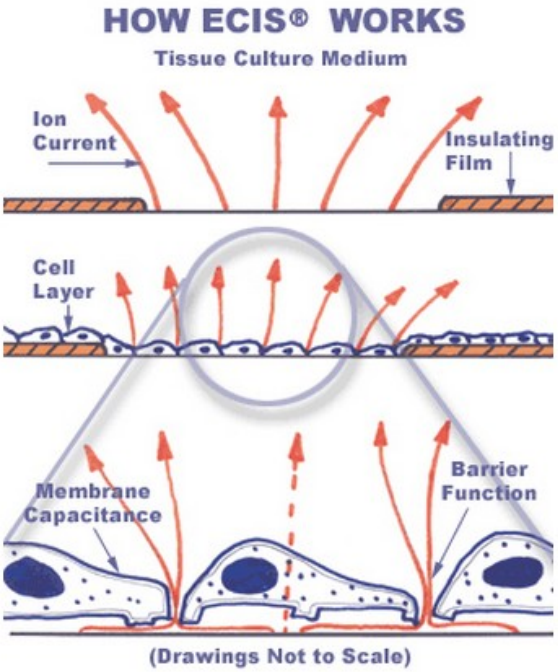


Figure 5.3.1 Diagram of the ECIS system. ECIS (Electric Cell-substrate Impedance Sensing) is a real-time, label-free, impedance-based method to study the activities of cells grown in tissue culture. These include morphological changes, cell locomotion, and other behaviours directed by the cell's cytoskeleton. ECIS can be used to monitor the barrier function or permeability of the cell monolayer. Figure adapted from Applied BioPhysics: http://www.biophysics.com/ecis-theory.php

Contrasting the Electrical Cell Impedance System with traditional permeability assays

Whereas the ECIS system provides information regarding the strength of intercellular junctions and hence the potential for molecule movement via the paracellular pathway other traditional permeability assays do not discriminate between the potential for para- and transcellular movement. The Evans Blue assay uses the movement of albumin conjugated to a coloured dye from one chamber of a transwell system to another. It is possible that movement of protein through this system could be due to energy-dependent transcellular movement rather than disruption of cell-cell interactions.

Using the EB-albumin assay it was determined that, as seen using the ECIS assay (results not shown), AR-MWNT exposure results in a dose dependent increase in HPMVEC barrier integrity. Similarly AO-MWNT exposure resulted in no change in barrier integrity as assayed using either the ECIS or EB-albumin permeability assays (Figure 5.2.4). Both the ECIS and EB-albumin systems indicated the same pattern of f-MWNT-induced disruption at the HPMVEC barrier with the pattern of toxicity P(M4-VP), AR, P(PEGMA) > P(MAA) > AO-MWNTs. As the ECIS result only

reflects changes in paracellular permeability, whereas the EB-albumin assay does not discriminate between transcellular and paracellular pathways, it can be presumed that the majority of permeability alterations are a result of changes in intercellular interactions. As the healthy endothelium maintains a highly selective barrier and alterations in the endothelial barrier permeability are associated with a number of severe diseases including pulmonary oedema and acute respiratory distress syndrome (ARDS) (Lum & Malik, 1994; Mehta *et al*., 2004; Mehta & Malik, 2006) it can be assumed that a loss of barrier function as a result of MWNT exposure measured by both assay systems can be seen as a marker of toxicity.

The EB-albumin assay and ECIS systems produced largely similar results, however ECIS allows us to view changes in barrier permeability and cell morphology continuously over time. Using the ECIS system we were able to observe that changes in barrier permeability between non-treated cells and f-MWNT treated cells occur soon after exposure, however these changes become more pronounced following longer exposure periods. Preliminary studies indicated that no change in barrier permeability could be observed using the EB-albumin assay at 4 hours (results not shown) indicating that the ECIS is a more sensitive system.

Endothelial adherens junctions disassembly following MWNT exposure

We hypothesised that the changes in HPMVEC paracellular permeability following exposure to f-MWNTs could be due to alterations in the adherens junctions protein complexes that HPMVEC have been shown to express *in vitro* (Luissint *et al*., 2012). Occasional large holes in the cell monolayer were observed following exposure to 10µg/ml AR or P(M4-VP) at 3 but not 24 hours which is possibly due to a loss in cell viability (see section 3.2). Our results demonstrated however, that disruption of intercellular junctions, and not a loss in cell viability was the likely primary cause of the increased barrier permeability.

With the exception of AO-MWNTs, exposure to MWNTs resulted in a rapid disruption of the endothelial adherens junction complex that coincided with increased barrier permeability

indicated by both the ECIS and the EB-albumin permeability assays. Intercellular VE-cadherin junctions were not only disrupted; immunostaining and immunoblotting indicated a decrease in the abundance of the VE-cadherin protein following exposure to AR-MWNT. Reactive oxygen species are known to mediate Rac-induced loss of adhesion junctions in endothelial cells (van Wetering *et al.*, 2002). Interestingly those particles that induced the greatest loss in VE-cadherin junctions also induced the greatest increase in ROS (see section 3.2) Acid oxidised MWNTs were the only particle to induce no increase in endothelial ROS and these were also the only particle to not disrupt VE-cadherin complexes. Although without further investigation into the effect of anti-oxidants on adherens junction integrity no causal relationship can be identified, it is highly likely that ROS play a part in the disruption of VE-cadherin complexes following MWNT exposure, and this warrants further investigation.

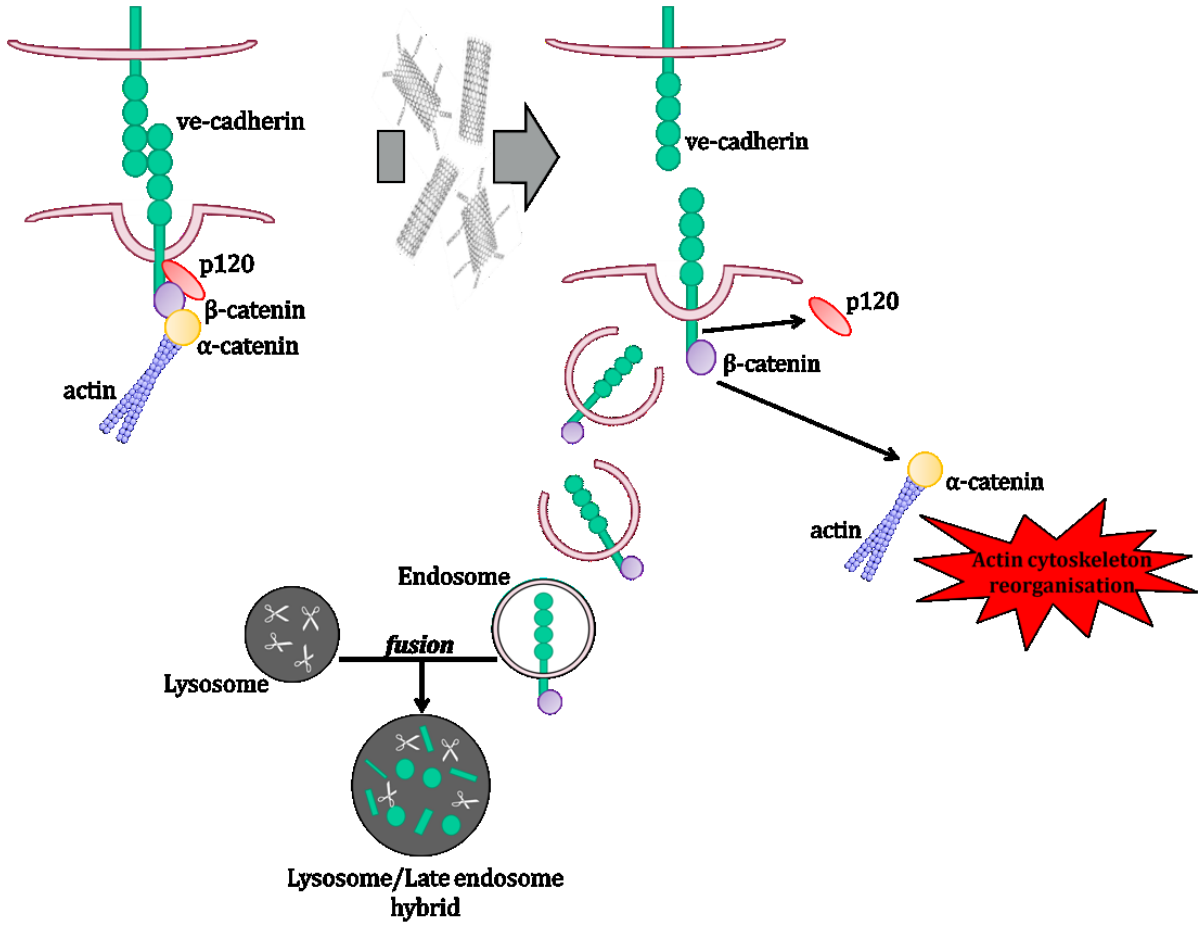


Figure 5.3.2 Diagram depicting the likely disassembly of adherens junction proteins, VE-cadherin lysis and actin cytoskeleton rearrangement following MWNT exposure.

It is possible that MWNT interference with the VE-cadherins complex could affect the rate of particle uptake. Activation of signalling cascades that result in VE-cadherin phosphorylation can lead to destabilisation of the VE-cadherin-catenin complex leading to VE-cadherin internalisation and actin skeleton remodelling. It is thought that if NPs are to interact with the VE-cadherin complex, concurrent internalisation of particle and protein may occur (Setyawati *et al*., 2013).

It is apparent through immunostaining, ECIS and the EB-albumin assay that the functionalisation of MWNTs with P(MAA) or P(PEGMA) groups abrogates the endothelial cell-cell junction disrupting properties of as-received MWNTs. Although AO-MWNT exposure may have the least effect on barrier function, these particles induced the greatest endothelial pro-inflammatory and pro-thrombotic response, indicating that these particles may induce other adverse effects *in vivo* (shown in Chapters 3 and 4). As P(MAA) functionalisation of the as-received MWNTs attenuated the barrier disrupting properties of these particles in both epi- and endothelial cells, this particle may be more suitable for biomedical applications, as P(MAA) functionalisation may reduce off-target effects. In TT1 cells, TEM showed that P(MAA)-MWNTs were often aligned parallel to, and not inserted into, the plasma membrane. It may be that this is a contributing factor to the reduced barrier disrupting properties of this particle. Similarly, in TT1 cells, P(M4-VP)-MWNTs were frequently observed inserted into the plasma membrane and P(M4-VP) functionalisation induced the greatest increase in barrier permeability. Studies wishing to exploit NP properties to administer molecules across tightly regulated barriers should therefore consider P(M4-VP) functionalisation.

5.4. Summary

Using ECIS, AR and thermochemically functionalised MWNT exposure was shown to induce changes in both TT1 and HPMVEC barrier permeability; furthermore the severity of the reaction was shown to be dependent on the functional group present at the MWNT surface. No change in AT2 barrier permeability was observed following exposure to f-MWNTs and AO-MWNT exposure induced no change in barrier permeability in any cell model. Disruption of VE-cadherin complexes at HPMVEC junctions and loss of the VE-cadherin protein was observed following exposure to AR, and thermochemically functionalised MWNTs. This effect was sustained at 24 hour post-exposure and suggests that VE-cadherin loss at the endothelial barrier may be responsible for the reduction in endothelial barrier integrity. Disruption of the alveolar-capillary barrier *in vivo* could have profound implication for human health and facilitate the translocation of NP across this biological barrier.

6. DEVELOPMENT OF A NOVEL 3D *IN VITRO* MODEL OF THE ALVEOLAR-CAPILLARY UNIT AND ITS RELEVANCE AS A NANOPARTICLE TOXICITY ASSAY

6.1. Introduction

An introduction to alveolar-capillary in vitro systems

A number of studies have recognised that there are disparities in the responses of pulmonary mono-culture *in vitro* systems and *in vivo* systems following exposures to nanoparticles. When assessing the pulmonary toxicity of diesel exhaust particulate using *in vitro* and *in vivo* systems, Seagrave and co-workers noted that the rank order of hazard potency from the *in vitro* assays in general did not correspond well to the ranking results from the *in vivo* comparisons of the same samples (Sayes *et al*., 2007; Seagrave *et al*., 2002; Seagrave, McDonald, & Mauderly, 2005). Furthermore Sayes and co-workers assessed the toxicity of a variety of particles ranging from 50-3000nm (carbonyl iron, crystalline silica, precipitated amorphous silica, and zinc oxide) using both *in vitro* and *in vivo* systems and discovered that, when considering the range of toxicity of the different particles, the comparisons of *in vivo* and *in vitro* measurements demonstrated little correlation (Sayes *et al*., 2007). In light of these findings, it has been suggested that "more sophisticated *in vitro* cell culture systems need further development and validation (relative to *in vivo* effects) to facilitate cost-effective screening systems to gauge the relative toxicity of inhaled particles" (Sayes *et al*., 2007). This has led to the generation of a number of *in vitro* systems attempting to replicate various aspects of pulmonary physiology.

Current co-culture models to study pulmonary nanoparticle toxicity

A wide range of *in vitro*, *ex vivo* and *in vivo* models are currently used to investigate the potential adverse effects of nano-sized particles in the lung. *in vitro* methods offer the advantage that cellular and subcellular processes and their underlying molecular pathways can be studied with

greater ease in a highly controlled system (Rothen-Rutishauser et al., 2008). In addition, the use of *in vitro* models is in line with the vision of the National Centre for the Replacement, Refinement and Reduction of Animals in Research (NC3Rs), which promotes the development of alternative methods to research involving the use of animals (Ministry of Health, 2008).

In vitro systems may be constructed using cells that are either freshly isolated from primary tissue (primary cells) or cells derived from an immortalised cell line. Cell lines are more homogenous than primary cells, and hence produce greater reproducibility, however they are arguably less representative of normal *in vivo* conditions. Continuous cell lines are poorly differentiated and lose many of the phenotypic *in vivo* characteristics of the cell type *in vivo* (Hartung *et al*., 2002). In contrast, each isolate of primary cells is unique, better reflecting the true inter-subject variation, and thus greater experimental variability in results is often observed. In addition, these cells are often difficult to culture and depend on the availability of tissue and the number of cells that can be harvested during each isolation (Hartung et al., 2002; Rothen-Rutishauser et al., 2008).

By studying cells in monocultures it is possible to gain an insight into the effects of direct particle interaction with a specific cell type, however *in vivo*, these cells are also affected by signals from neighbouring cells. There have been several attempts to mimic the cellular organisation of the peripheral lung using *in vitro* systems (summarised in Table 6.1.1), however the majority of these systems have focused on cell line models.

Component cells	Reference
A549 (human lung adenocarcinoma cell lines), EA.hy 926 (endothelial cells), THP-1 (differentiated macrophage-like cell line), HMC-1 (mast cells)	(Klein, Serchi, Hoffmann, Blömeke, & Gutleb, 2013)
A549 (alveolar type-2 cell line), Differentiated dendritic cells (DCs) Differentiated alveolar macrophages (AMs)	(Rothen-Rutishauser, Kiama, & Gehr, 2005)
Small airway epithelial cells (SEACs) Human Pulmonary Microvascular Cells (HMVECs)	(Snyder-Talkington *et al*., 2013)
Human Pulmonary Microvascular Cells (HPMECs) Human type-2 alveolar epithelial cells (AT2 cells) – allowed to differentiate to AT1-like cells	(Hermanns et al., 2009)
Human Pulmonary Microvascular Cells (HPMECs), A549/NC1 441 (human lung adenocarcinoma cell lines)	(Hermanns, Unger, Kehe, Peters, & Kirkpatrick, 2004)
A549 (human lung adenocarcinoma cell lines), THP-1 (differentiated macrophage-like cell line),	(Wottrich, Diabaté, & Krug, 2004)
Human type-2 alveolar epithelial cells (AT2 cells) – allowed to differentiate to AT1-like cells MDM (monocyte-derived macrophages) MDDC (monocyte-derived dendritic cells)	(Lehmann *et al*., 2011)
H441 (human lung adenocarcinoma cell line) ISO-HAS-1 (human microvascular endothelial cell line)	(Kasper *et al*., 2011)

Table 6.1.1 Published co-culture models representing the peripheral airways.

A primary model has previously been generated using AT2 cells and HPMVECs where the AT2 cells were cultured for 7-11 days until the cells exhibited an AT1-like morphology, however these cells contained both microvilli and caveolae, and contained remnants of lamellar bodies indicating that these cells may not have fully differentiated (Hermanns et al., 2009). In this system, the number of AT2 to TT1-like cells is difficult to regulate due to the longer culture period and progressive change from AT2 to AT1 like morphology. It has also been demonstrated that beyond 3 days in culture the electrical resistance of an AT2 monolayer decreases indicating that either the health of the monolayer or the intercellular junctions have been compromised (Figure 5.2.2). Alternatively, this drop in electrical resistance could be due to a change from AT2 to AT1-like morphology, with a subsequent change in intercellular junctions, however this is currently only speculative as there is no literature describing the electrical resistance of an AT2 monolayer during transition to an AT1-like morphology.

Several models of the alveolar-capillary barrier use endothelial cells which have been immortalised for use in cell culture. However, Unger and colleagues found that, "regardless of their origin, endothelial cell lines isolated from tumors, through fusion with other cells, or by introduction of specific "immortalisation" genes into primary cells exhibited not only changes in the normal growth control mechanisms allowing cells to replicate indefinitely *in vitro*, but almost always exhibited significantly reduced expression of specific endothelial characteristics compared with primary endothelial cells in culture" (Unger, Krump-Konvalinkova, Peters, & Kirkpatrick, 2002). Therefore, due to the loss of phenotype characteristics in cell lines and the paucity of data generated using primary cell models, it is our belief therefore that a three dimensional system comprising primary pulmonary microvascular endothelial cells and alveolar type 2 epithelial cells isolated from resected human tissue, alongside immortalised alveolar type 1-like epithelial cells, would provide a unique and effective model of the human air-blood interface.

Co-culture versus mono-culture findings

A number of studies have identified inconsistencies between monoculture and co-culture systems when investigating nanoparticle toxicology. As a result there has been a recent effort to determine which *in vitro* lung models are the most effective when studying the effects of nanoparticles.

A recent study by Clift *et al* (2014) compared the cytotoxic, inflammatory and oxidative effects of single and multi-walled carbon nanotubes in commonly used *in vitro* models. These models included human blood monocyte-derived macrophages (MDM), monocyte-derived dendritic cells (MDDC), 16HBE14o- epithelial cells, and a triple cell co- culture model incorporating all 3 previous mentioned cell types. The results demonstrated significant differences between the mono-culture and co-culture models; in MDM and MDDC monocultures, MWCNTs induced the greatest increase in TNFα release, whereas in the triple co-culture model, this was comparable to the effect of DEP and SWCNTs. In contrast, the trend in the decrease of the intracellular thiol GSH was greater in co-culture than mono-culture *in vitro* models; following exposure of crocidolite asbestos fibres, DEPs, SWCNTs, and MWCNTs the co-culture model showed a 10-fold, significant increase ($p<0.05$) in the intracellular reduced GSH content compared with each monoculture assessed, a result which supports previous findings (Gasser *et al*., 2012; Müller *et al*., 2010). Using the same triple cell co-culture model, it was noted that effects in triple cell co-cultures, including total antioxidant capacity, were in general attenuated compared to MDM alone. Furthermore, TNFα levels were higher than expected from the monoculture results (an effect also seen in the control samples), and IL-8 levels were lower, but these changes in cytokine/chemokine levels were not statistically significant. There is significant evidence therefore that, under certain conditions, there is a synergistic effect between cell types that modulates the oxidative and inflammatory response to nanoparticle exposure. In contrast to these findings, a number of other studies have however shown that co-cultures of pulmonary cells can have an increased inflammatory response to particle exposure than their monoculture

counterparts (Kasper *et al*., 2011; Tao & Kobzik, 2002; Wottrich *et al*., 2004). Thus, it is clear that the interaction between cells in co-culture models is complex and that there are a number of simultaneous events that result in differential toxicological outcomes.

Previous studies comparing the response of mono-cultures and co-cultures to nanoparticles have largely focused on epithelial-immune cell interactions, very few studies have investigated the response of an endothelial-epithelial co-culture system to particle insult. Kasper *et al* (2011) found that a co-culture using human lung adenocarcinoma and human microvascular endothelial cell lines was less sensitive in some aspects (viability, membrane integrity, TEER) following exposure to silica nanoparticles than the cells in monoculture, however the cells in monoculture showed release of IL-6 and IL-8 to the basolateral side at concentrations that were 10-100 fold less than the concentrations of the apically exposed co-culture. Other studies have shown that nanoparticles exposed to the epithelial side of a epithelial-endothelial co-culture are able to induce a response in the underlying endothelial cells, however these studies were not directly comparing mono-culture and co-culture results (Bengalli, Mantecca, Camatini, & Gualtieri, 2013; Snyder-Talkington *et al*., 2013).

Further investigation into co-culture systems representing the alveolar-capillary barrier is therefore needed to discern the effects of the cross-talk between these cells and the effect this may have on NP mediated toxicity.

Overview:

This chapter describes the implementation of a triple co-culture model, first describing the generation of an alveolar type-1 and alveolar type-2 co-culture and the response of this system to the study particles. A third cell type – the human pulmonary microvascular cell, is then incorporated into the cell culture system using a permeable membrane support and the release of inflammatory mediators and endothelial and epithelial specific mediators in response to f-MWNT exposure is analysed.

Hypothesis:

We hypothesised that primary AT2 cells, HPMVECs and immortalised TT1 cells would form a viable co-culture system that could be used as a model to study the interaction of nanoparticles at the blood-gas barrier. Furthermore we hypothesised that cells grown in co-culture would express a distinct toxicity profile to mono-cultured cells.

Our specific aims were to establish:

- Whether primary AT2 cells and immortalised TT1 cells could be cultured simultaneously using a single cell culture system
- Whether this AT2-TT1 co-culture expresses an inflammatory response when exposed to f-MWNTs and whether this response is distinct from that of the monoculture system
- If HPMVECs could be incorporated into the AT2/TT1 system to generate a triple cell culture model of the blood-gas barrier
- Whether the triple cell culture model could provide novel information regarding the toxicity of f-MWNTs at the blood gas barrier

6.2. Methods

Generation of a TT1 and AT2 cell co-culture model

AT2 cells were isolated from primary human lung tissue using the method described in section 2.2. Initial attempts to allow the AT2 cells to settle before the addition of TT1 cells were unsuccessful. TT1 cells were evident as large clusters of cells and were not evenly distributed across the cell culture surface. It was hypothesised that this could be due the secretion of surfactant by AT2 cells preventing TT1 cell adhesion. Thus, the cell suspension present after the 2 hour differential adherence stage was combined with a TT1 cell suspension at a ratio that would result in a 60:40 ratio of AT2 to TT1 cells in the final monolayer; the ratio was determined using the following calculus:

To achieve an approximate 60:40 ratio of AT2:TT1cells it was assumed that AT2 cells would not proliferate significantly in culture (Dobbs, 1990) and that TT1 cells had a doubling time of 16 hours.

The CI values provided by the iCELLigence system in section 5.2 were used to determine the doubling time of TT1 cells in culture. At t=3h the CI value was 0.30 (2dp) which increased to 6.72 (2dp) at t=46h. The CI value had therefore increased by a total of 6.42 (2dp) over 43 hours. Using this information, the following logarithmic equation was used to calculate the doubling time of TT1 cells.

$$2^x = 6.42$$

$$xlog2 = log6.42$$

$$x = log6.42/log2$$

$$x = 2.68 \text{ (2dp)}$$

$$43/2.68 = 16.04 \text{ (2dp)}$$

Using this equation it was therefore assumed that the doubling time of TT1 cells was approximately 16 hours.

If 100,000 AT2 cells are seeded per transwell insert, 67,000 TT1 cells are required at the time of exposure to achieve a 60:40 AT2:TT1 ratio. Assuming a doubling time of 16 hours and the total culture time before exposure of 48 hours, cells will undergo 3 cell divisions in the pre-exposure period. To determine the TT1 seeding density the following equation was used.

$$x = 67{,}000/2^3$$

$$x = 67{,}000/8$$

$$x = 8375$$

A seeding density of 100,000 AT2s and 8400 (2 sf) TT1s was therefore used to generate the AT2-TT1 co-culture model.

The AT2-TT1 cell suspension was transferred to a tissue culture plate or transwell filter (polyester, 1.12cm^2 growth surface area, 0.4µm pore size) (Appleton Woods, Brimingham, UK), that had been previously coated with1% PureCol collagen solution (Leimuiden, Netherlands; Type I collagen) and allowed to air dry. The cells were allowed to adhere overnight at 37°C, 5% CO_2 in DCCM-1 containing 10% newborn calf serum (NCS), 100 U/ml penicillin, 100 mg/ml streptomycin and 2 mM glutamine. The following day, adherent cells were washed with PBS to remove any non-adherent cells and the culture media was replaced with serum-free media. The AT2-TT1 co-culture was exposed to nanoparticles 24 hours after the addition of serum-free media using the method described in section 2.3.

Alkaline phosphatase staining was carried out in TT1 and AT2 mono and co-cultures using the method described in section 2.5. The viability of the co-culture system following f-MWNT exposure was determined using the MTS assay detailed in section 2.8 and the levels of the inflammatory mediator IL-6 and IL-8 were assayed by ELISA as described in section 2.12.

The addition of HPMVECs to form a triple cell co-culture model of the blood gas barrier

HPMVECs were isolated using the method described in section 2.2. The most effective method for culturing HPMVEC on the underside of a transwell membrane (polyester, 1.12cm^2 growth surface area, 0.4μm pore size) (Appleton Woods, Brimingham, UK), was to initially apply a concentrated cell suspension to the underside of the membrane, exploiting the surface tension of the media to ensure the cell suspension remained in place. 34,000 HPMVECs (30,000/cm^2) were suspended in 200μl EGM-2 MV, which was applied directly to the underside of the transwell membrane. HPMVECs were then allowed to attach for 2 hours at 37°C, 5% CO_2 in a humidified incubator. Following this incubation period, the bubble of media still remained on top of the inverted transwell insert. This was carefully removed and the transwell inserts were turned up the correct way and transferred to a 12 well plate containing 1.5ml EGM-2 MV in each well. Following 24 hours in culture at 37°C, 5% CO_2, the location of HPMVECs added to the underside of the transwell membrane was determined using confocal microscopy as described in section 2.7.

Once the HPMVECs had adhered to the underside of the transwell membrane, the AT2-TT1 cell suspension described above was applied to the collagen coated, apical side of the membrane, and cultured for 24 hours at 37°C, 5% CO_2. Figure 6.2.1 provides a simplistic overview of the conditions used to generate the triple cell culture model.

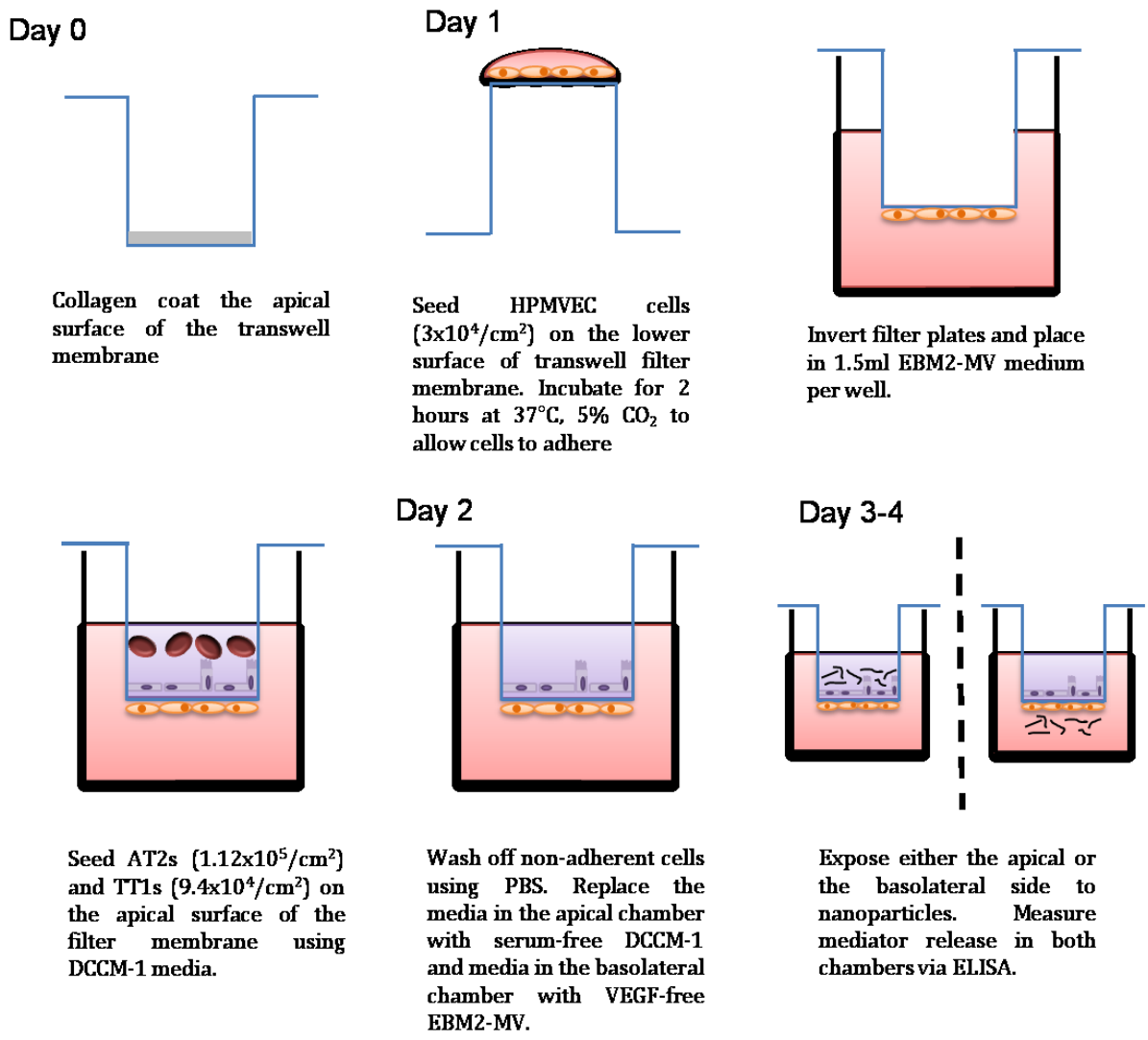


Figure 6.2.1 Set-up of the triple cell co-culture system. The apical surface of the transwell membrane is collagen coated and HPMVECs are seeded on the underside of the membrane. Following inversion, a mix of AT2 and TT1 cells are seeded on the apical surface of the membrane. Serum and VEGF are removed from the upper and lower chambers of the system respectively. The co-culture system is then used to study nanoparticle bio-reactivity.

At 24 hours the transwells were transferred to a fresh 12 well plate containing VEGF-free EGM-2 MV, and the apical side of the transwell was washed with pre-warmed PBS and the media was replaced with a serum-free alternative. The co-culture system was then cultured for a further 24 hours at which point model characterisation and MWNT exposure experiments were carried out.

To establish whether cells were present on both sides of the transwell filter membrane fluorescent confocal microscopy was employed as described in section 2.7. It was not possible

to discern this information using light microscopy as the presence of cells on one side of the membrane obscured the cells on the opposite side of the membrane from view. A non-cell specific wheat germ agglutinin (WGA) stain was used to visualise the cells. WGA is a lectin that binds to sialic acid and *N*-acetylglucosaminyl residues. The apical and basolateral sides of the transwell membrane were stained with WGA conjugated to the fluorescent probes Alexa Fluor 594 and Alexa Fluor 488 respectively as described in section 2.7.

The triple co-culture system was exposed to nanoparticles prepared using the method described in section 2.3. Functionalised MWNTs were added to either the apical or basolateral chamber of the co-culture system to mimic f-MWNT exposure via the inhalation or the injection route. Following exposure, mediators in the apical and basolateral chambers were measured via IL-6, IL-8, VEGF and E-selectin ELISAs as described in section 2.12.

6.3. Results

Co-culture model characterisation

To ascertain whether primary AT2 cells and immortalised TT1 cells could be co-cultured, alkaline phosphatase (AP) staining was carried out. AT2 cells produce alkaline phosphatase which hydrolyses napthol-AS-bisphophate in the presence of fast red violet LB salt to produce a red precipitate. TT1 cells do not however produce alkaline phosphatase and so the AP assay is a simple way of discerning AT2 and TT1 cells in co-culture

Figure 6.3.1 demonstrates the pink pigment generated by AT2 cells during the alkaline phosphatase assay (A) and the total absence of the pink pigment in a TT1 monolayer (C) using the same assay. When AT2 and TT1 cells were cultured using the method described above both alkaline phosphatase positive and negative cells were observed (B).

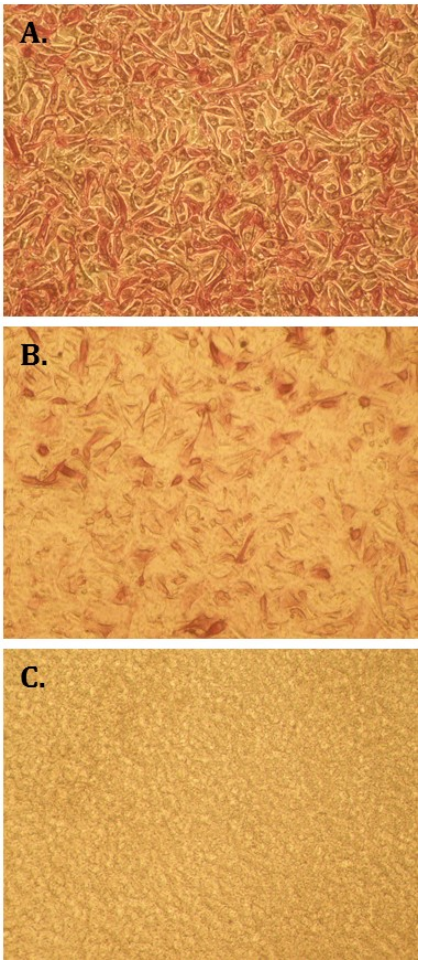


Figure 6.3.1 Alkaline phosphatase staining of TT1 and AT2 cells in mono and co-culture. Alkaline phosphatase (AP) staining of an (A.) AT2 monoculture, (B.) AT2-TT1 co-culture and (C.) TT1 monoculture. AT2 cells produce alkaline phosphatase which will hydrolyse napthol-AS-bisphophate in the presence of fast red violet LB salt to produce a red precipitate (A). TT1 cells do not produce alkaline phosphatase and therefore produce no red-precipitate (C). Both AP positive and negative cells are in evidence in the AT2-TT1 co-culture (B) indicating a mixed cell population.

HPMVECs applied directly to the underside of the transwell membrane (Figure 6.3.2-A) remained on top of the inverted transwell insert following a 2 hour incubation (B.). Following inversion HPMVECs adhered to the underside of the transwell membrane could be visualised using a light microscope (C.) and confocal microscopy confirmed that HPMVECs remained on the underside of the transwell filter following 24 hours in culture (D. + E.).

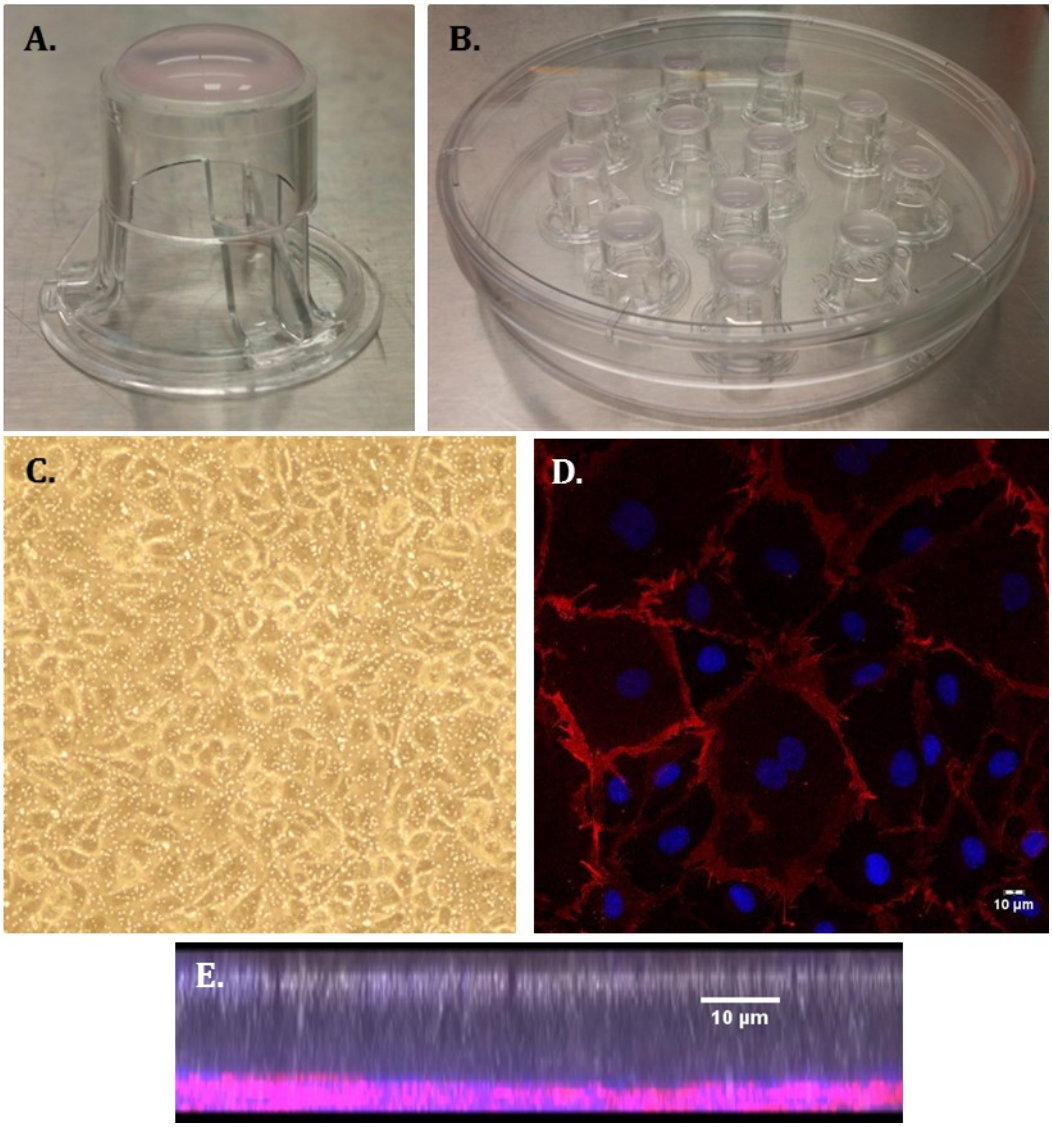


Figure 6.3.2 Culturing HPMVECs on the underside of a transwell filter membrane. (A.) Inverted transwell with 200µl EBM-MV2 media containing 34,000 HPMVECs. (B.) Inverted transwell filters following a 2 hour incubation at 37°C, 5% CO_2; the strong bonds between molecules in the solution ensure the solution remains on top of the porous filter. (C.) Light micrograph showing HPMVECs that have adhered to the underside of the transwell filter following the 2 hour incubation. (D.) Alexa Fluor 594-WGA labelled HPMVECs (E.) Z-stack image showing the location of the Alexa Fluor 594-WGA labelled HPMVECs on the lower side of the transwell filter following 24 hours in culture. Scale bars are 10µm.

Following the application of HPMVECs to the basolateral side of the membrane and TT1 and AT2 cells to the apical side of the membrane, it was observed that cells were present on both sides of the membrane by forming a z-stack of a cross-section of images. The cell population on either side of the membrane appear to be distinct with the contact inhibiting HPMVEC on the basolateral side and the mixed AT2-TT1 cells population on the apical side (Figure 6.3.3). Due to difficulties in identifying effective cell specific antibody markers that would be effective with the three different fluorescent secondary antibodies needed, an image depicting the exact position of all of the cells within the triple cell co-culture model was not obtained (Appendix VI).

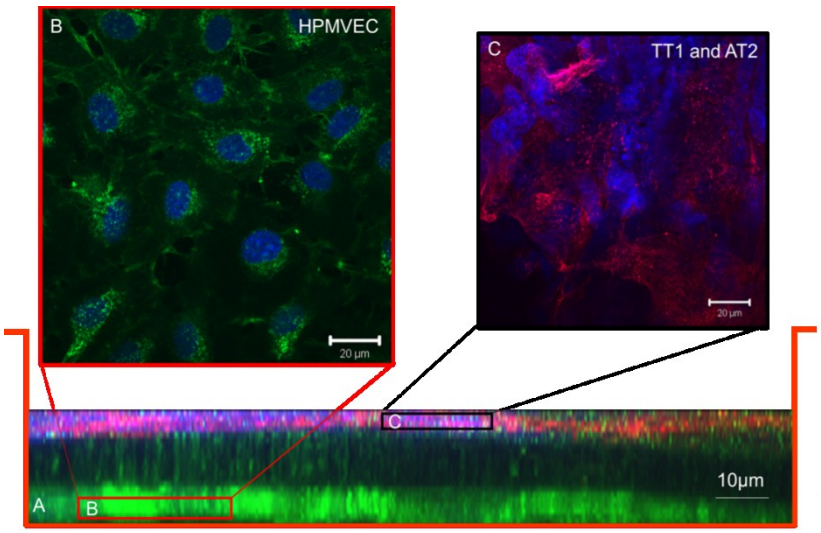


Figure 6.3.3 Micrograph depicting positioning of cells on both sides of a transwell filter membrane. (A.) Z-stack image showing the location of both the Alexa Fluor 488-WGA labelled endothelial cells and the Alexa Fluor 594-WGA labelled epithelial cells on the upper and lower sides of the transwell filter respectively. (B.) Alexa Fluor 488-WGA labelled endothelial cells. (C.) Alexa Fluor 594-WGA labelled epithelial cells. Scale bars are as denoted.

Viability

Functionalised MWNTs were not acutely cytotoxic to AT2-TT1 co-cultures cultured on collagen-coated tissue culture plates. P(M4-VP)-MWNTs resulted in a small (<8.5%) but significant ($p<0.05$) dose-dependent decrease in cell viability following a 24 hour exposure to concentrations greater than 10µg/ml. Low concentrations (1µg/ml) of AR and AO-MWNTs significantly increased the mitochondrial activity of the epithelial co-culture systems ($p<0.05$)

by 14.3% and 3.6% respectively (Figure 6.3.4). In both TT1 and AT2 monocultures, MWNTs did not induce a reduction in cell viability at 24 hours (Figure 3.2.6 & Figure 3.2.7).

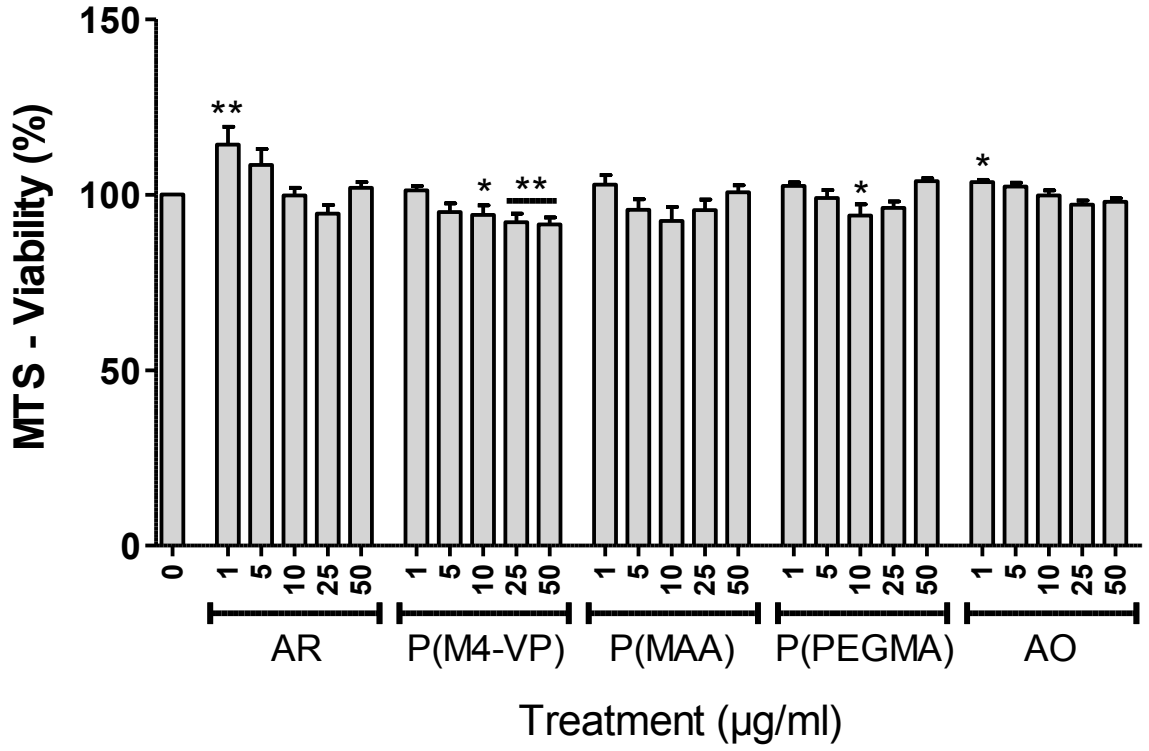


Figure 6.3.4 Viability of cells in a TT1-AT2 co-culture following exposure to f-MWNTs. Cells were exposed to 1-50µg/ml f-MWNTs for 24 hours and cell viability was measured via the MTS assay. Data is expressed as mean ± SEM, n=4. One-way ANOVA followed by Dunnett's post-test; *p< 0.05, **p< 0.01.

Release of inflammatory mediators in the TT1-AT2 co-culture

Baseline levels of the inflammatory mediators IL-6 and IL-8 were lower in the TT1-AT2 co-culture systems than the levels expressed by AT2 cells in monoculture and higher than the levels expressed by TT1 cells in monoculture, indicative of a mixed AT2 and TT1 cell population (Table 6.3.1).

	TT1 monoculture	AT2 monoculture	TT1-AT2 co-culture
Interleukin-6	29±4	259±86	153±60
Interleukin-8	5±2	1572±268	1184±191

Table 6.3.1 Summary of baseline inflammatory mediator release in TT1 and AT2 mono and co-culture systems. An intermediary baseline level of the inflammatory mediators IL-6 and IL-8 was present in the TT1-AT2 co-culture system. Data is expressed as mean ± SEM, n≥4.

Exposure of TT1-AT2 co-cultures to P(MAA) and P(PEGMA)-MWNTs did not induce any significant change in IL-6 or IL-8 levels. Conversely, IL-6 levels increased in a dose dependent manner following exposure to P(M4-VP)-MWNT however this was only significant at 50μg/ml ($p<0.05$) (Figure 6.3.5). In contrast, at 24 hours, no increase in IL-6 or IL-8 was observed in the epithelial mono-cultures following exposure to any MWNT (Figure 3.2.17 & Figure 3.2.18).

Interestingly, exposure to AR-MWNTs significantly decreased levels of IL-6 and IL-8 by 45% and 35% respectively ($p<0.05$) at the highest concentration, and AO-MWNT significantly inhibited IL-6 release by approximately 58%, at concentrations greater than 25μg/ml ($p<0.05$) (Figure 6.3.5). A reduction in the inflammatory mediators was also observed in the epithelial mono-cultures; IL-6 release was significantly reduced in TT1 mono-cultures exposed to MWNTs for 24 hours (Figure 3.2.17 & Figure 3.2.18).

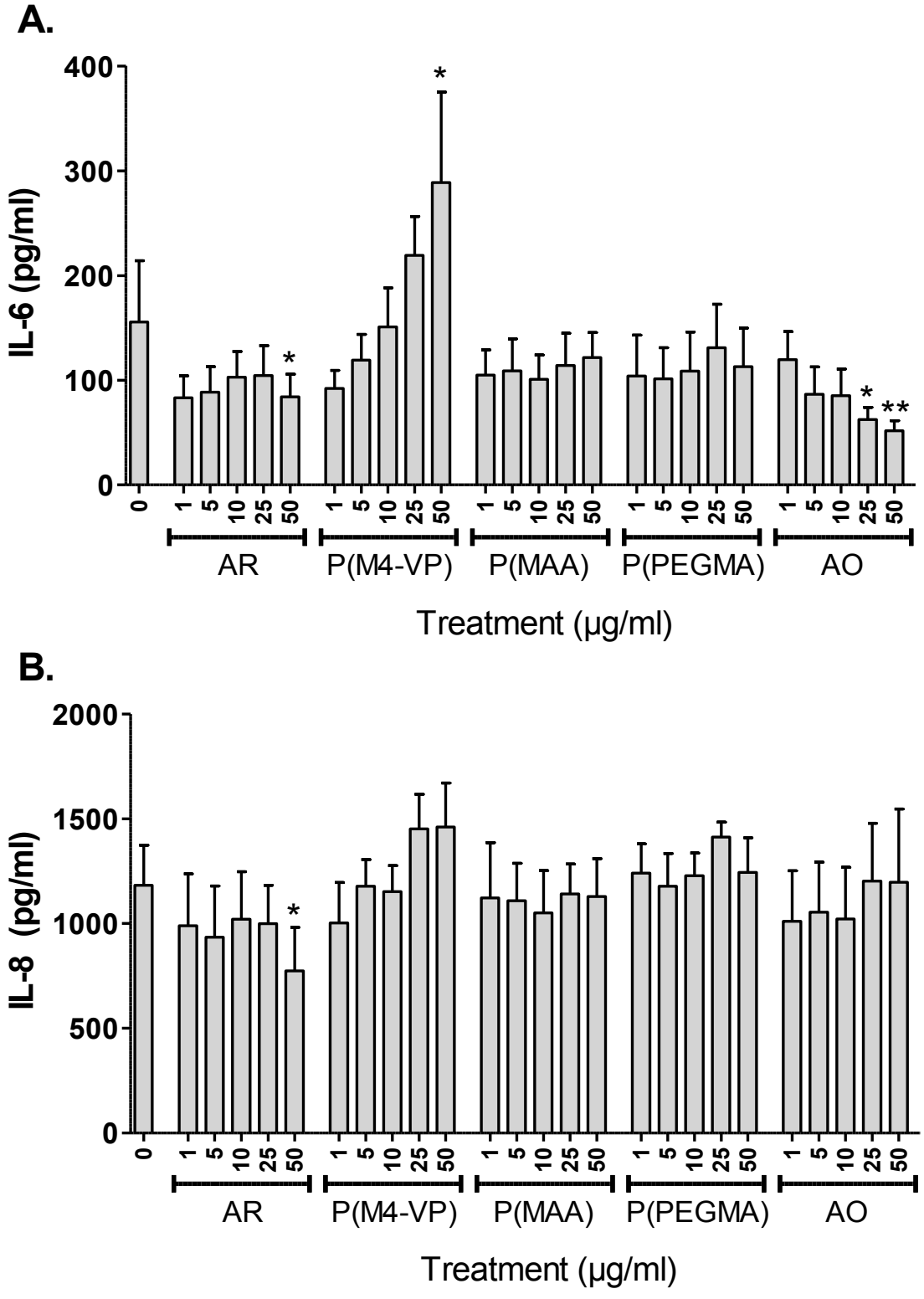


Figure 6.3.5 Release of inflammatory mediators from cells in a TT1-AT2 co-culture following exposure to f-MWNTs. Cells were exposed to 1-50µg/ml f-MWNTs for 24 hours and IL-6 and IL-8 levels in the cell culture supernatants were measured by ELISA. Data is expressed as mean ± SEM, n=4. One-way ANOVA followed by Dunnett's post-test; *p< 0.05, **p< 0.01.

Release of inflammatory and cell-specific mediators from the triple co-culture system

Only AO-MWNTs introduced to the basolateral chamber of the co-culture system induced an increase in levels of the inflammatory cytokine IL-6 (from 30 to 65pg/ml in the apical chamber and from 5 to 23pg/ml in the basolateral chamber), however this change was not significant (Figure 6.3.6). Similarly, in the monoculture systems 10μg/ml resulted in no significant increase in IL-6 release at 24 hours in any of the cell types, however a non-significant increase in IL-6 was observed in HPMVECs following exposure to 10μg/ml AO-MWNTs. This value increased from 3pg/ml to 200pg/ml, however there was a large SEM (±149pg/ml) and thus the increase was not significant (Figure 3.2.21).

10μg/ml AO-MWNTs induced a significant ($p<0.001$) increase in IL-8 levels in the bottom chamber of the co-culture system following both apical and basolateral exposure (88% and 150% respectively) (Figure 6.3.7). In contrast, exposure to 10μg/ml all study particles resulted in a significant increase in IL-8 in HPMVEC monocultures (Figure 3.2.21). An increase in IL-8 levels was also observed in the upper chamber of the co-culture system following apical and basolateral exposure to AO-MWNTs however this was not statistically significant. No increase in IL-8 was observed in the epithelial mono-cultures following exposure to any MWNT at 24 hours (Figure 3.2.17 & Figure 3.2.18). No statistically significant change in IL-6 or IL-8 was observed in any of the chambers of the co-culture system following exposure to AR, P(M4-VP), P(MAA) or P(PEGMA)-MWNTs (Figure 6.3.7).

No statistically significant change in E-selectin or VEGF was detected in the co-culture system following exposure to any of the study particles (Figure 6.3.8 & Figure 6.3.9). In contrast, all MWNTs induced an increase in soluble E-selectin in HPMVEC monocultures at 24 hours however this was only significant for P(MAA)-MWNTs, and values were very low with 10μg/ml AO-MWNT inducing the greatest level of soluble E-selectin at just 22pg/ml (Figure 4.2.4).

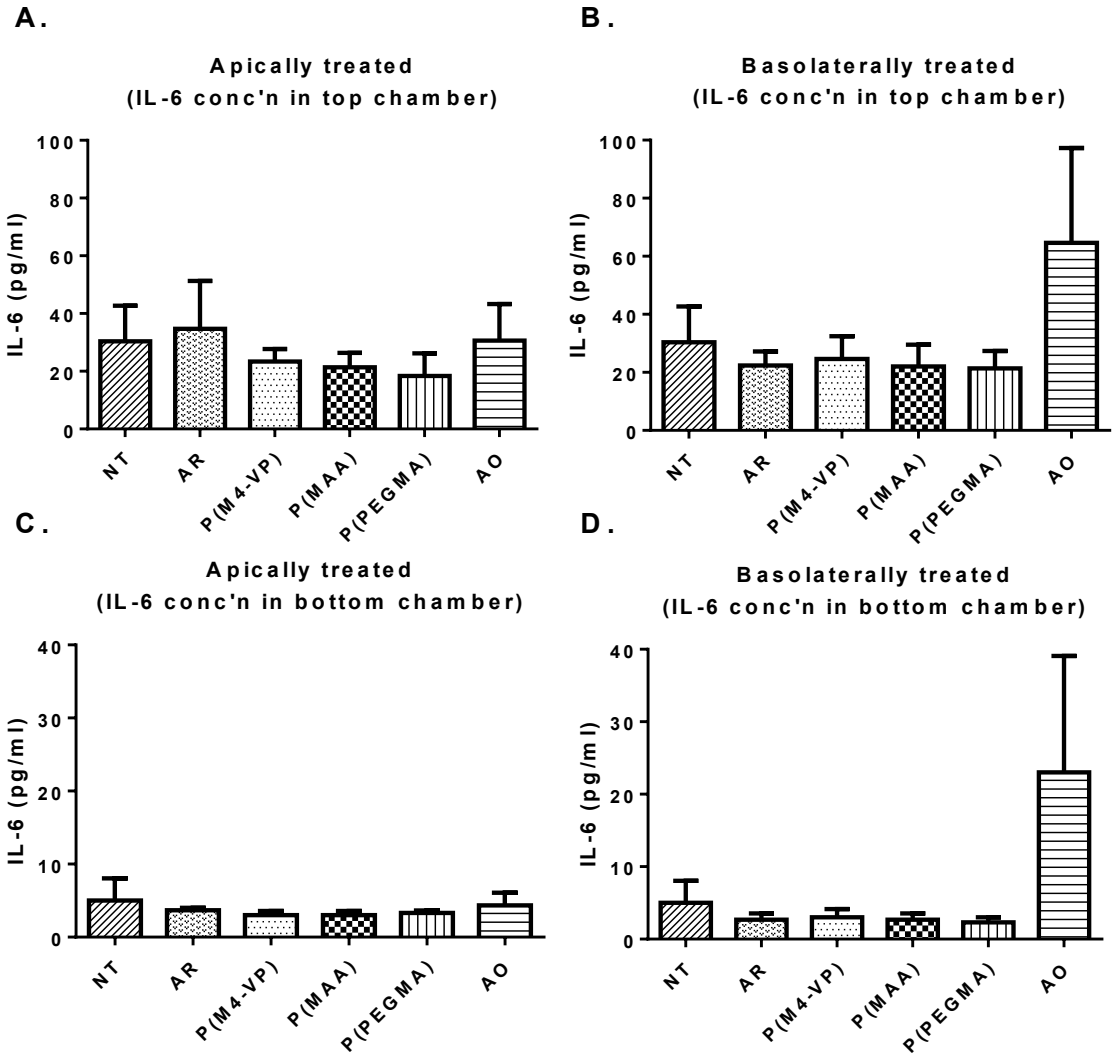


Figure 6.3.6 Release of the inflammatory mediators IL-6 from the co-culture model of the alveolar-capillary barrier following exposure to f-MWNTs for 24 hours. Cells were exposed either apically (A. & C.) or basolaterally (B. & D.) to 10µg/ml f-MWNTs for 24 hours and IL-6 was measured in both the upper and lower chambers. IL-6 levels in the cell culture supernatants were measured by ELISA. Data is expressed as mean ± SEM, n=3. One-way ANOVA followed by Dunnett's post-test.

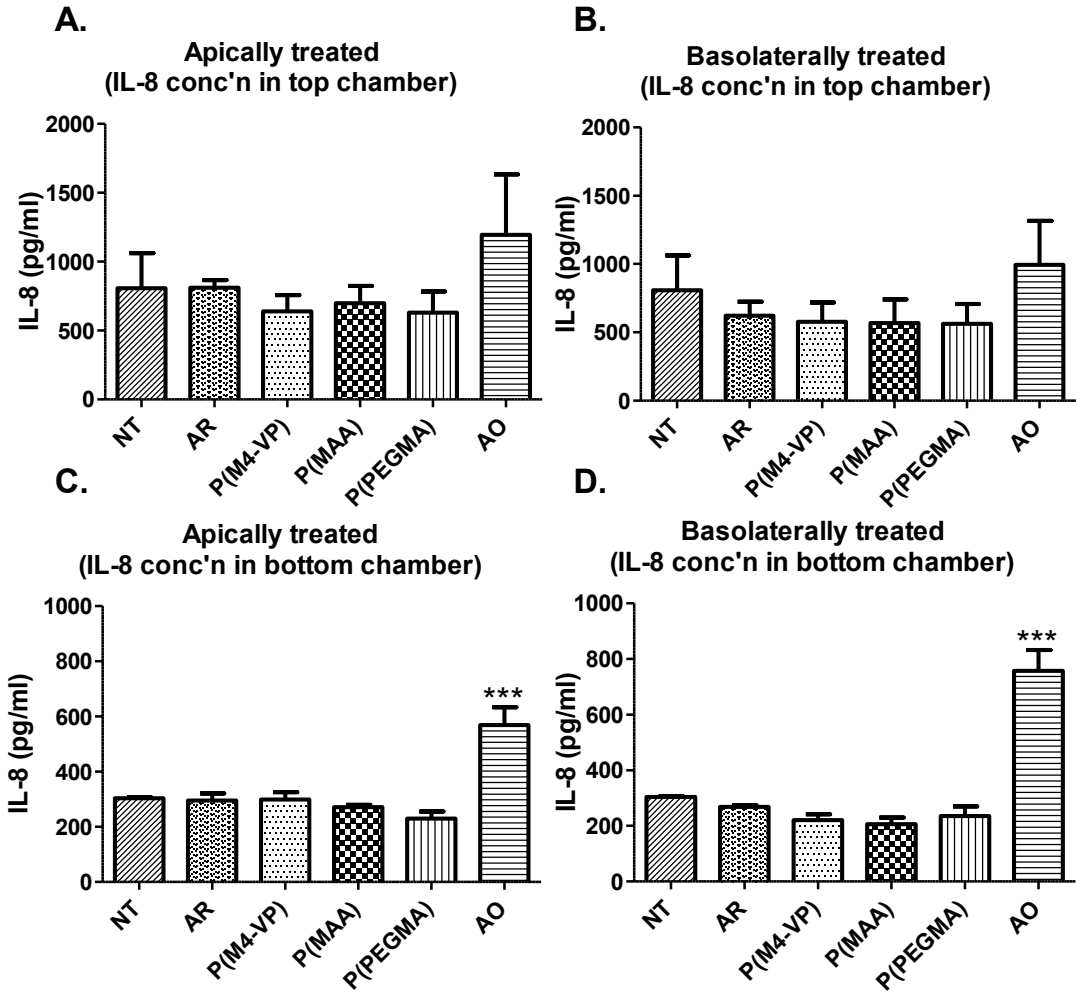


Figure 6.3.7 Release of the inflammatory mediators IL-8 from the co-culture model of the alveolar-capillary barrier following exposure to f-MWNTs for 24 hours. Cells were exposed either apically (A. & C.) or basolaterally (B. & D.) to 10µg/ml f-MWNTs for 24 hours and IL-8 was measured in both the upper and lower chambers. IL-8 levels in the cell culture supernatants were measured by ELISA. Data is expressed as mean ± SEM, n=3. One-way ANOVA followed by Dunnett's post-test; ***p< 0.001.

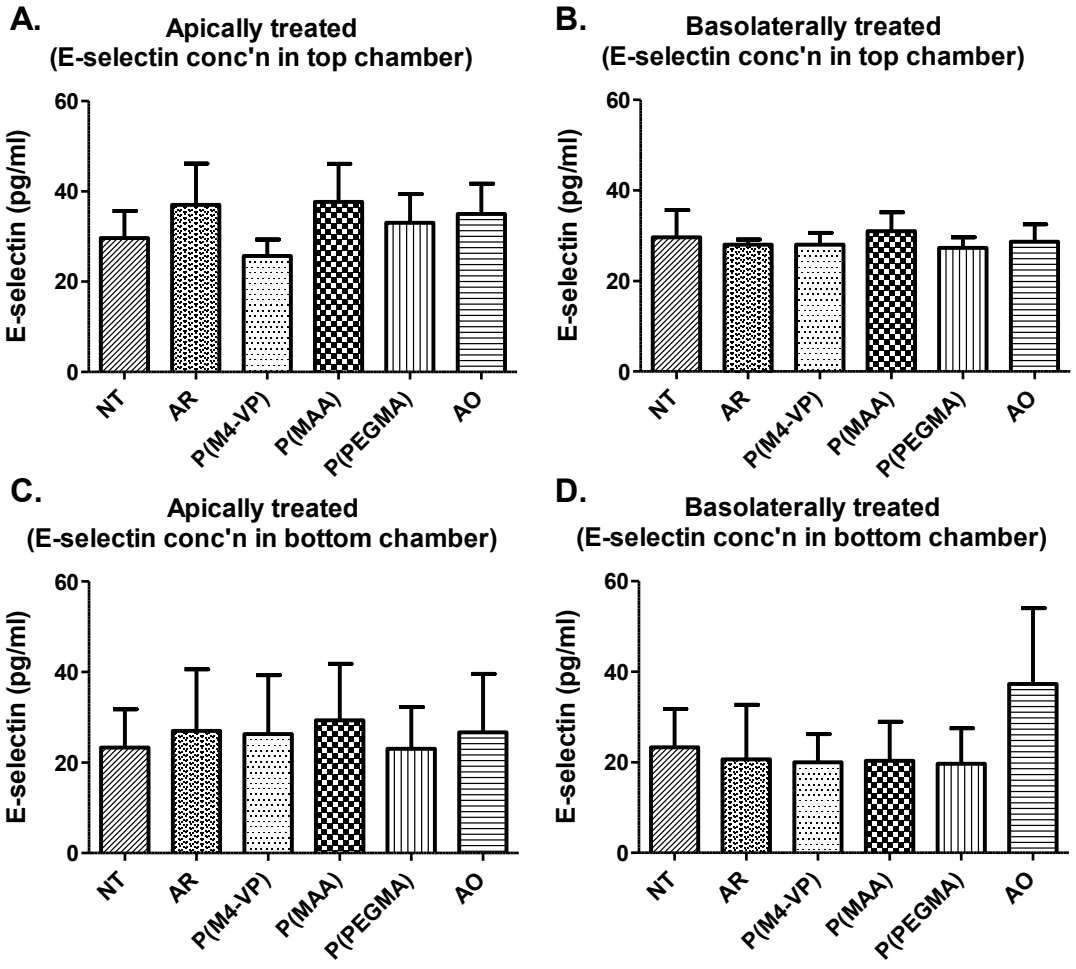


Figure 6.3.8 Release of the cell adhesion molecule E-selectin from the co-culture model of the alveolar-capillary barrier following exposure to f-MWNTs for 24 hours. Cells were exposed either apically (A. & C.) or basolaterally (B. & D.) to 10μg/ml f-MWNTs for 24 hours and E-selectin was measured in both the upper and lower chambers. E-selectin levels in the cell culture supernatants were measured by ELISA. Data is expressed as mean ± SEM, n=3. One-way ANOVA followed by Dunnett's post-test.

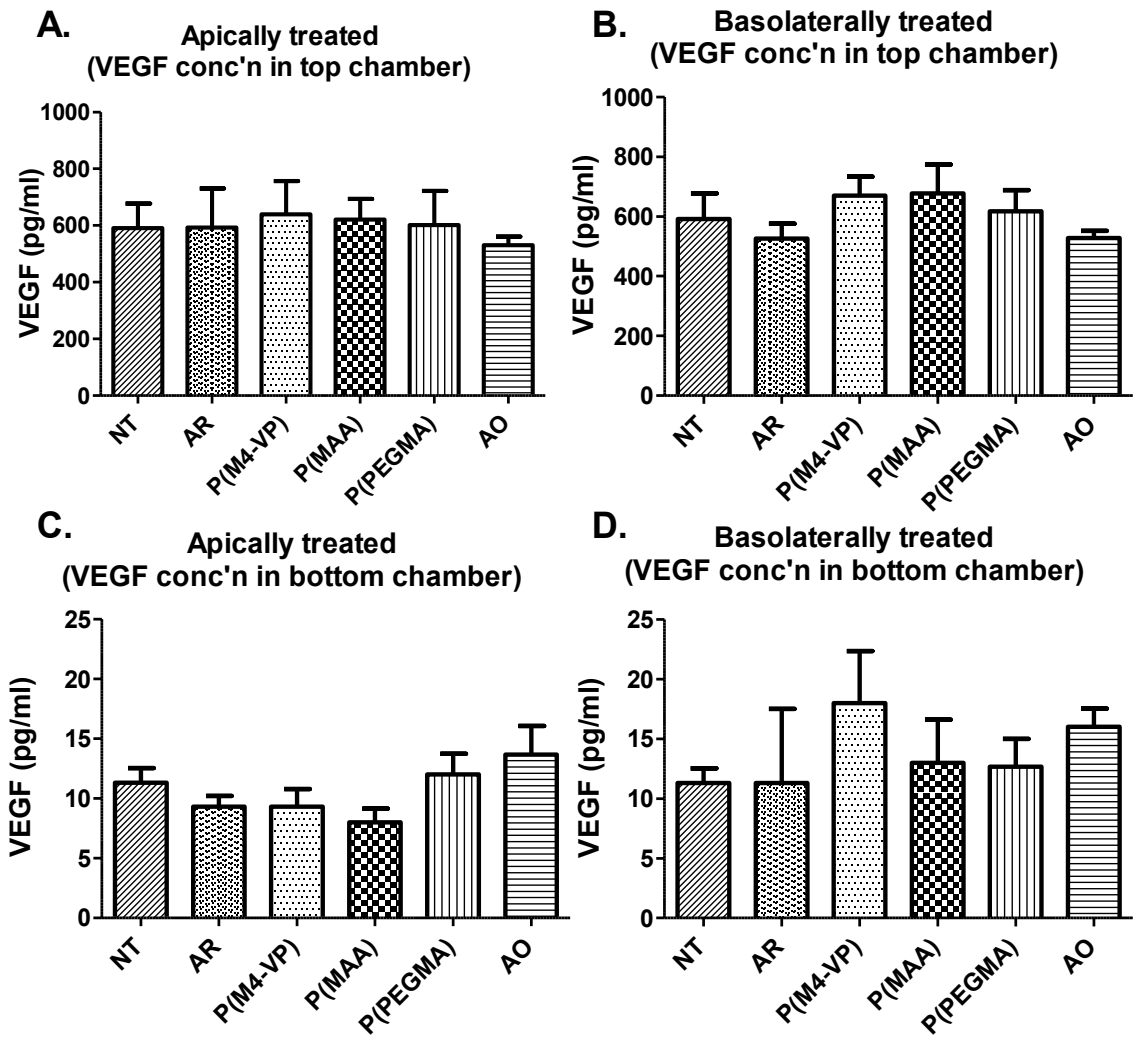


Figure 6.3.9. Release of the growth factor VEGF from the co-culture model of the alveolar-capillary barrier following exposure to f-MWNTs for 24 hours. Cells were exposed either apically (A. & C.) or basolaterally (B. & D.) to 10μg/ml f-MWNTs for 24 hours and VEGF was measured in both the upper and lower chambers. VEGF levels in the cell culture supernatants were measured by ELISA. Data is expressed as mean ± SEM, n=3. One-way ANOVA followed by Dunnett's post-test.

6.4. Discussion

Establishment of a triple co-culture system

In this chapter it has been demonstrated that it is possible to culture primary AT2 cells and immortalised TT1 cells simultaneously in a single system. Both alkaline phosphatase positive and negative cells were in evidence in the co-culture system indicating that both epithelial cell phenotypes are present in the co-culture system. Future work involving the co-culture system should investigate the relationship between these cells; TEER and immunostaining should be employed to discern whether functional inter-cellular junctions have formed between the two cell populations.

HPMVECs were successfully cultured on the underside of the transwell membrane, ensuring that the epithelial and endothelial cells were grown in closer association than if the HPMVECs had simply been cultured on the lower surface of the tissue culture plate as is seen in the co-culture system designed by Snyder-Talkington *et al* (2013). Immunofluorescent confocal microscopy confirmed that cells were present on both sides of the membrane and indicated that the cell populations on either side of the membrane were distinct. Development of the model should include cell specific marker to determine the locality of each cell and furthermore cell-cell junction staining should be employed to determine whether functional intercellular junctions have formed between TT1 and AT2 cells.

Although both AT2 cells and HPMVECs were derived from apparently healthy portions of lung tissue following surgical resection, it was not possible to include AT2 cells and HPMVECs from a single donor in a single co-culture experiment. This is due to the limited culture period of AT2 cells and the time needed to purify HPMVEC cultures. Alveolar epithelial cells and HPMVECs both express major histocompatibility complex (MHC) classes I and II (Cunningham et al, 1997) however in the absence of allogeneic T lymphocytes would not stimulate an adaptive immune

response. In certain situations, particularly where co-cultures incorporate immune cells, it might be important to include cells from the same donor in co-culture to improve correlation to the *in vivo* situation. This was recently demonstrated by Reed *et al* who used donor matched immune cells and stem cell-derived endothelial cells in co-culture to detect cytokine storm induction by biologics (Reed *et al*., 2015).

The epithelial TT1-AT2 co-culture vs. monoculture toxicity response

In monoculture there was no significant decrease in cell viability in TT1 or AT2 cells at 24 hours. When these cells were grown in co-culture a small, but significant decrease in cell viability was observed only after exposure to P(M4-VP)-MWNTs. An increase in LDH release was observed in TT1 cell monocultures at 72 hours following exposure to this particle. This particle can therefore be considered to have mildly cytotoxic effects in alveolar epithelial cells both in mono and co-culture. This experiment is unable to discern whether the decrease in cell viability observed in the co-culture system is isolated to the TT1 or AT2 cell population. This should be determined using markers specific for viable and non-viable cells such as calcein AM and ethidium homodimer-1 respectively. Simultaneous immunofluorescent staining for cell specific markers would elucidate whether the non-viable cell population is restricted to a specific cell phenotype.

From the monoculture results, it is likely that the reduction in cell viability may be primarily due to a reduction in TT1 cell viability; there was no increase in AT2 cell LDH release or reduction in mitochondrial activity following a chronic 72 hour exposure to 50µg/ml f-MWNTs. Conversely a small toxic effect was seen in TT1 cells following a prolonged exposure period.

That a small cytotoxic effect is observed at 24 hours in co-culture may indicate that there is a slightly greater cytotoxic potential of P(M4-VP)-MWNTs when TT1 and AT2 cells are not exposed in isolation. This indicates that the toxic potential of this particle may be underestimated using a monoculture system alone.

P(M4-VP)-MWNTs also induced a pro-inflammatory response in the TT1-AT2 co-culture system at 24 hours. Similarly to the viability response, this was not evident in the AT2 monoculture and was not evident in the TT1 monoculture until the extended culture period of 72 hours. This provides further evidence that the toxic potential of this particle at the alveolar epithelium may be underestimated using a type-1 or type-2 epithelial cell monoculture system.

A number of studies have observed that nanoparticles readily form a corona of proteins in a biological system (Lundqvist *et al*., 2008; Lynch, Salvati, & Dawson, 2009; Walczyk, Bombelli, Monopoli, Lynch, & Dawson, 2010). Furthermore it has been observed that the toxicity of these particles may be affected by the presence of this corona (Gasser *et al*., 2012; Lesniak *et al*., 2010, 2012; Monopoli *et al*., 2011). AT2 cells are secretory cells which produce a number of molecules including surfactant proteins A-D, phospholipids and anti-proteases (Fehrenbach, 2001). Recent evidence has shown that the presence of these proteins can greatly affect the bioreactivity of nanoparticles in *in vitro* systems (Gasser *et al*., 2012) and therefore it has been proposed that current research efforts should focus on discerning how the presence of these proteins affects the toxicity of particles in the lung (Schleh, Kreyling, & Lehr, 2013). It is plausible that the difference in the observed toxicity of the positively charged P(M4-VP)-MWNT particle in mono-culture and co-culture could be due to a change in the protein corona of the particle. TT1 cells in monoculture are in a surfactant-free environment and therefore would not be exposed to particles loaded with proteins such as surfactant or anti-proteases. Particles in the TT1-AT2 co-culture would however be exposed to these molecules which could potentially alter their bio-reactivity. Furthermore, if the functional groups on the surface of the particle inferred a different affinity for these biological molecules nanoparticle functionalisation could influence the character of the protein corona. This is not only an attribute which could be exploited, but also one which should be taken into account when considering the toxic potential of the particle.

Preliminary work demonstrated that indeed, functional groups on the surface of MWNTs greatly influenced the affinity between the particle and the molecule secretory leukocyte proteinase inhibitor (SLPI) (Appendix VII). The presence of AO-MWNTs greatly reduced the levels of SLPI detectable by ELISA. This occurred in a dose-dependent manner in a system containing both recombinant SLPI and a system containing endogenous SLPI. AO-MWNTs were shown not to interfere non-specifically with the ELISA. Similar findings were also reported by (Clift *et al*., 2014) who observed a significant adsorption ($p<0.05$) of the TNF-α protein to SWCNTs and MWCNTs at 0.04mg/ml.

Anti-proteases such as SLPI control the potential injurious effects of excess release of proteases secreted by inflammatory cells. In the lung, SLPI is produced by tracheal, bronchial, bronchiolar and type II alveolar cells, and is thought to play a role in anti-bacterial and anti-inflammatory processes (Sallenave, 2000). If SLPI bound to f-MWNTs was no longer available to cells this could have implications for the alveolar immune response. This is just one example of how the protein corona of a particle could influence particle toxicity.

The response of the epithelial-endothelial triple co-culture system to functionalised nanoparticles

Interestingly, in the triple cell co-culture system, only AO-MWNTs induced a significant inflammatory response, seen as an increase in IL-8 in the bottom chamber of the system following both apical and basolateral treatment. AO-MWNTs also induced the greatest increase in IL-8 in HPMVEC monocultures (10μg/ml AO-MWNTs increased IL-8 protein levels by 593%, Figure 3.2.21-D, Table 3.2.3), however this was attenuated in the co-culture system. The pro-inflammatory response observed in the HPMVEC monoculture following exposure to other MWNTs was completely absent in the triple co-culture system.

That P(M4-VP)-MWNTs did not induce a significant inflammatory response in the triple cell co-culture model was especially unexpected as this particle induced an inflammatory response in both the TT1-AT2 co-culture alone, and the HPMVECs cells in monoculture. This attenuation of

the toxic response has been observed in other co-culture systems, and is suggestive of intercellular communication between the component cells that modulates the response (Clift *et al*., 2014; Gasser *et al*., 2012; Müller *et al*., 2010).

AO-MWNTs administered to the apical chamber induced a significant increase in IL-8 in the lower chamber and a small but non-significant increase in IL-8 in the upper chamber of the system. Either AO-MWNTs are able to reach the endothelial cells through the epithelial cell layer and the permeable membrane, there is signalling occurring between the epithelial and endothelial cells that is triggering an inflammatory response, or alternatively, IL-8 is being actively transcytosed from the apical to the basolateral surface. This is especially interesting considering not only the increased thickness of the barrier seperating the epi- and endothelial cells in the *in vitro* model than is observed *in vivo,* but also that this effect is still apparent even in the presence of collagen which is likely to reduce the permeability of the permeable membrane support. It is reasonable to hypothesise that *in vivo* where epi- and endothelial cells and separated by a distance of just 100-200nm (Vaccaro & Brody, 1981), this effect may be even more pronounced.

AO-MWNT did not induce a pro-inflammatory response in the co-culture system containing TT1 and AT2 cells alone, and so the pro-inflammatory response can be attributed to the presence of the endothelial cells. This is an important finding as endothelial cells are frequently neglected when considering particle toxicity in the peripheral lung. Endothelial cells are closely associated with alveolar epithelial cells and the discovery that a particle that is relatively inert at the alveolar epithelium can induce a pro-inflammatory response both apically (representing the alveolar surface) and basolaterally (representing the vessel lumen) when applied to an epithelial-endothelial co-culture has significant implications. These findings indicate that endothelial reactivity could be at least partially responsible for the adverse cardiovascular effects observed following pulmonary CNT exposure, and furthermore that the endothelial response may exacerbate pulmonary toxicity. This has implication for both the inhalation and

intravenous exposure risk of CNTs and highlights the need to incorporate endothelial cells into toxicity models when considering the potential use or hazard of nanoparticles.

The increase in E-selectin observed in HPMVEC mono-cultures was absent in the co-culture model, even when the particles were applied to the lower chamber of the culture system containing the HPMVECs. This could be due to cellular cross-talk, where the epithelial cells are modulating the response or alternatively this could be due to the variation of the culture system. The HPMVEC monoculture exposures were carried out using cells cultured on tissue culture plates, as is common for toxicity experiments. In this experimental system however any particles that do not remain in suspension will deposit directly onto the cell monolayer. In the co-culture system, HPMVECs will not be exposed to any particle that drops out of suspension. Despite this, AO-MWNTs, an extremely water stable particle, did not induce any significant increase in E-selectin indicating this may be a contributing but not the causal factor. Particle deposition could be reduced using microfluidics to mimic blood flow or gentle agitation, however some degree of particle deposition is expected to occur in the *in vivo* situation.

Snyder-Talkington *et al* (2013) observed an increase in VEGF released by small airway epithelial cells, grown in co-culture with HPMVECs. No change in VEGF was evident in the current co-culture system which may be due to the differential responses of alveolar epithelial cells and small airway epithelial cells. Indeed, airway epithelial cells have been shown to increase VEGF production in response to TNFα, EGF and TGFβ at a greater rate than alveolar epithelial cells (Boussat *et al*., 2000). VEGF synthesized by the lung epithelial cells is however known to contribute to the endothelial repair and angiogenesis processes and following lung injury VEGF mRNA becomes very abundant in alveolar type II cells (Boussat *et al*., 2000; Maniscalco, Watkins, D'Angio, & Ryan, 1997). A lack of an increase in VEGF release may therefore be indicative of an absence of AT2 cell toxicity, however chronic exposures should be carried out to further investigate the role of this important molecule and the impact it may have on neighbouring endothelial cells.

6.5. Summary

A novel epithelial co-culture consisting of TT1 and AT2 cells was successfully generated which indicated that the interaction of these cells may exacerbate the cytotoxic and inflammatory response to MWNTs. P(M4-VP)-MWNT induced a pro-inflammatory response in this co-culture that was absent in epithelial mono-cultures at 24 hours.

HPMVECs were incorporated into this model to generate a novel 3D triple co-culture model of the blood-gas barrier. In this system, only AO-MWNT induced a significant release in IL-8 release, whereas all particles initiate a pro-inflammatory response in HPMVEC mono-cultures. It is possible that endothelial-epithelial cross-talk modulates the response to these particles. AO-MWNTs administered to the epithelial side of the co-culture system initiated both apical and basolateral release of IL-8, whereas AO-MWNT exposed to epithelial monocultures induced no pro-inflammatory response. The pro-inflammatory response was therefore attributed to the presence of the endothelial cells, through either direct MWNT-endothelial interaction following translocation or signalling between the epithelial and endothelial cells triggering an inflammatory response. This has highlighted the need to incorporate endothelial cells into toxicity models when considering the potential use or hazard of nanoparticles.

7. SUMMARY DISCUSSION

Humans have developed regulatory mechanisms to cope with inhaled ambient particulate matter, however the number of airborne particles is increasing. This is because both naturally occurring nanoparticles (NPs) and plume sources such as industry and vehicular exhausts act as condensation nuclei and adsorb gas and particle components (Kulmala & Kerminen, 2008). Furthermore, humans have only very recently been exposed to engineered NPs with highly controlled physicochemical properties. It is feasible to assume that humans may therefore, not be as adept at defending against the harmful effects of these particles. Indeed, urban UFP inhalation has been associated with cardiopulmonary effects in humans and the engineered NPs, carbon nanotubes (CNTs) have resulted in adverse cardiopulmonary effects during *in vivo* rodent studies. The mechanisms of toxicity underlying the cardiovascular effects of NP inhalation are poorly understood. Furthermore NPs, including CNTs, are being developed for biomedical applications including biosensors, biological scaffolds and drug delivery molecules (Sinha & Yeow, 2005), providing a potential direct route of entry into the body. Unmodified CNTs are however, insoluble in water, and in most organic solvents; thereby functionalisation of their surface is necessary to increase bio-compatibility (Battigelli *et al*., 2013)

The aim of these studies was to elucidate the potential reactivity of CNTs at the blood-gas barrier, in order to determine whether CNT interaction with this barrier could potentially induce cardiopulmonary effects. Furthermore, the studies aimed to elucidate whether CNT surface functionalisation affects CNT-induced alveolar-capillary reactivity with a view to determining which particles may be most appropriate for biomedical applications. This work was unique in its use of immortalised human alveolar type 1-like epithelial cells (TT1), primary human alveolar type 2 epithelial cells (AT2) and primary human pulmonary microvascular cells (HPMVEC). The use of TT1 cells enabled a novel insight into the interaction of functionalised CNTs with the cell that covers ~93% of the alveolar surface. As AT2 cells act as an alveolar epithelial cell stem cell capable of both self-maintenance and terminal differentiation, produce

surfactant and play a role in host defence, CNT-induced AT2 reactivity would likely impact on pulmonary health. Finally HPMVECs are in close association with the honeycomb structure of the alveolus and CNT interaction with this cell type could impact on both cardiovascular and pulmonary health. The use of these cell types allowed strong conclusion to be made on the potential adverse consequences of CNT interaction with the alveolar-capillary barrier.

Our overarching hypothesis anticipated that CNT functionalisation would determine their bio-reactivity at the alveolar-capillary barrier. We chose to test this hypothesis by studying the effect of CNTs with improved water-solubility made possible by a conventional acid-oxidation method; this created highly soluble CNTs carrying negatively charged carboxyl groups and a large degree of structural defects. We compared this particle to a non-modified CNT control and CNTs with functional groups generated by a novel grafting-from thermochemical reaction; this improved water-stability through covalent functionalisation of the CNT surface without damaging the structural integrity of the CNT. Firstly, to understand the basic differential response of the different cell types to functionalised CNTs, we characterised their cytotoxic and inflammatory responses. Furthermore we investigated whether CNT functionalisation affected their uptake by the study cell types.

Consequently, using exposures up to 72 hours in duration, it was determined that CNTs were not acutely toxic to alveolar epithelial cells, however following chronic exposure, CNTs were more reactive with TT1 cells than AT2 cells. This suggests that, alveolar epithelial cells, evolving in parallel with airborne particles, have some tolerance to nanoparticle exposure. CNTs induced no cytotoxicity or ROS formation in AT2 cells at 72 hours, however membrane damage and release of the inflammatory mediators IL-6 and IL-8 was observed in TT1 cells at 72 hours. This is an important finding considering the prolonged retention of NP in the peripheral lung due to the slow rate of NP clearance. This provides evidence that when assessing the potential toxic effect of CNTs it is important to consider not only acute toxicity but also the effect of prolonged epithelial exposure. It was those CNTs which had been

functionalised with the P(M4-VP) molecule that induced the greatest of these chronic TT1 responses. Transmission electron analysis revealed that internalisation of all particles was observed in TT1 cells, however the positively charged P(M4-VP)-MWNTs exhibited more frequent contact with the plasma membrane, whilst the negatively charged P(MAA)-MWNTs were frequently aligned parallel to the plasma membrane. These effects were presumed to be due to electrostatic attraction and repulsion of CNTs with the plasma membrane and may be at least partially responsible for the different toxicities of the particles. The finding that CNTs were more reactive with TT1 than AT2 cells is important as AT2 cells are able to proliferate and differentiate into AT1 cells. It is possible that damage as a result of AT1 toxicity could therefore be more transient than that as a result of AT2 toxicity due the fact that AT2 cells are required to proliferate in response to injury. AT1 cells do however cover the majority of the alveolar surface and provide a crucial barrier between the airspace and the alveolus and the underlying endothelium.

CNTs induced a far greater inflammatory response in endothelial cells than epithelial cells, suggesting that CNTs at this interface would be markedly more reactive. CNT exposure also induced early HPMVEC cytotoxicity, however increased cell proliferation ensured this loss in cell viability resolved by 24 hours. The HPMVEC uptake of P(M4-VP) and AO-MWNTs was greatest, and these particles also induced the greatest release of the pro-inflammatory mediators IL-6 and IL-8. ROS formation was observed following MWNT exposure in endothelial but not epithelial cells, however crucially, ROS formation did not directly correlate with inflammatory potential. AO-MWNT induced the greatest pro-inflammatory response, however induced no net increase in ROS. CNTs which had not been acid oxidised induced ROS formation but antioxidant treatment of cells did not entirely abrogate the inflammatory response, suggesting the inflammatory response is at least partially ROS-independent. Taken together, these finding indicated that CNTs interacting with the endothelium following inhalation or injection would initiate significant events including cell death, inflammation and ROS formation; characteristics all associated with cardiovascular and pulmonary disease pathology.

Following the substantial pro-inflammatory response observed following MWNT exposure, we went on to address our hypothesis that CNT functionalisation would be a critical determinant of other markers of endothelial activation associated with increased atheroma formation. We proposed that the surface functional groups would elicit variable expression of cell adhesion molecules and thrombotic mediators.

In agreement with our hypothesis, we showed that MWNT exposure increased CAM expression at the pre- and post-translational level. Furthermore, this translated into increased monocyte adhesion in co-culture, indicating that endothelial MWNT exposure *in vivo* would elicit increased recruitment of leukocyte to the endothelial wall. All particles increased CAM expression, however P(M4-VP) and AO-MWNTs induced the greatest increase and it was only these particles that induced a significant increase in monocyte adhesion in the co-culture model. P(M4-VP) and AO-MWNTs also induced the greatest increase in pro-thrombotic mediator release, and AO-MWNTs significantly down-regulated tissue plasminogen activator, a molecule involved in fibrin clot breakdown. We have therefore shown that all CNTs tested have the potential to be thrombogenic upon interaction with the endothelium, however the severity of this reaction is dependent on particle functionalisation, with P(M4-VP) and AO-MWNTs initiating the greatest response. In our studies, P(PEGMA) and P(MAA) functionalisation marginally abrogated the pro-thrombotic response observed following exposure to the as received CNTs. It may therefore be possible to moderate adverse cardiovascular exposure toxicity through selective functionalisation of CNTs, a promising result considering the sizeable investment into the development of MWNTs for use in medicine.

Expanding our investigations into CNT cellular reactivity, we further proposed that exposure to CNTs would disrupt intercellular junctions, resulting in increased barrier permeability. This is an important consideration when investigating the functionality of the alveolar-capillary barrier as there must be a highly specialised barrier separating air in the lung from fluid filled tissues for efficient gas exchange to occur. This work has demonstrated that CNTs can disrupt both TT1

epithelial and microvascular endothelial cell-cell junctions which results in increased barrier permeability. Increased alveolar-capillary barrier permeability can lead to increased fluid in the lungs affecting functionality. Furthermore, chronic low-level edema could result in lung injury and fibrosis. The MWNT induced reduction in cell-cell junctions observed in this study provides a potential mechanism underlying the oedema progression in mice following intratracheal instillation (Chen *et al*., 2015). Furthermore, increased paracellular transport at the alveolar-capillary barrier *in vivo* could facilitate particle transport from the alveolar sac to systemic organs. CNT translocation to systemic organs following pulmonary exposure has been observed in a number of studies (Chen *et al*., 2015; Mercer *et al*., 2013; Reddy *et al*., 2010), however the mechanism of transport has not yet been elucidated. Our findings that MWNTs disrupt cell-cell junctions at the alveolar-capillary barrier, in conjunction with *in vivo* findings that prolonged CNT are persistent in the alveolar space up to 30 days post-exposure (Chen *et al*., 2015) indicate that CNTs reach the alveolus where they are persistent and disrupt the alveolar-capillary barrier allowing CNTs direct access to the vasculature. Movement of particles via macrophage phagocytosis and subsequent movement up the mucocilary escalator is thought to be limited. This is due to the difficulty macrophages encounter both in recognising nano-sized particles and engulfing particles with a high-aspect ratio and also the ability of CNTs to pierce the macrophage membrane and induce toxicity (Cheng *et al*., 2009; Hirano, Kanno, & Furuyama, 2008). It is therefore crucial to discover the fraction of CNTs that cross the thin barrier separating the epi- and endothelium and whether this fraction is significant enough to elicit direct effects on the pulmonary microvasculature.

MWNT surface functionalisation altered the severity of cell-cell junction breakdown, however those particles that had the least effect on barrier permeability were not consistently less reactive. Acid oxidised (AO)-MWNTs induced negligible change in epithelial and endothelial barrier permeability however these particles induced the greatest pro-inflammatory and pro-thrombotic response. P(PEGMA) and P(MAA)-MWNTs induced the smallest pro-inflammatory response however, unlike AO-MWNTs still increased barrier permeability. This highlights the

need for multiple end-points to be assessed when investigating the hazard potential of novel materials; it is clear that cytotoxicity or inflammatory markers alone are insufficient as markers of CNT toxicity.

We hypothesised that increased HPMVEC barrier permeability would be characterised by alteration in the expression and function of the VE-cadherin adherens junction complex and actin filament rearrangement. Indeed, following exposure to all MWNTs except AO-MWNTs actin rearrangement to a non-cortical arrangement was observed indicative of cell contractility, and elongated VE-cadherin bridges and gaps between cells became evident. Furthermore, loss of the VE-cadherin protein was evident early after exposure to AR-MWNTs indicating a more than transient response. This was supported by the ECIS data which showed a persistent increase in barrier permeability up to 72 hours. It was those particles that resulted in the greatest increase in HPMVEC permeability (AR and P(M4-VP)-MWNTs) that also induced the greatest VE-cadherin junction interruption, indicating that this molecule is likely highly involved in the permeability response.

We designed a novel epithelial co-culture consisting of TT1 and AT2 cells to assess the importance of inter-epithelial interaction in MWNT mediated toxicity. The AT2-TT1 co-culture provides a more realistic model of the alveolar epithelium, especially as surfactant proteins and other AT2 cell products are absent in the TT1 monoculture system. P(M4-VP)-MWNT induced a pro-inflammatory response in this epithelial co-culture system, a response which was absent in the TT1 and AT2 monocultures. This may be in part due to the affinity of this particle to bind to proteins produced by AT2 cells, which may alter the particles bioreactivity. It is therefore important to consider the effects of the protein corona in CNT mediated toxicity, especially when assessing those particles which have a high affinity to endogenous proteins.

Finally, we built upon this epithelial model utilising a permeable membrane to co-culture TT1 and AT2 epithelial cells with microvascular cells to generate a novel 3D triple co-culture model of the blood-gas barrier. This is a novel system that has not been previously described and it

provides distinct advantages over other *in vitro* models of this barrier. Notably the incorporation of the TT1 epithelial cell provides a type-1 epithelial cell model without lengthy culture of primary AT2 cells until they partially differentiate into a type 1-like phenotype. We hypothesised that cellular crosstalk within this model would affect the toxicity of functionalised MWNTs at the blood gas barrier, and assessed this theory by monitoring the release of inflammatory and cell-specific mediator following MWNT exposure to the basolateral side of the co-culture (simulating intravenous exposure) and MWNT exposure to the apical side of the co-culture (simulating pulmonary exposure).

Acid oxidised CNTs administered to both the epithelial and endothelial side of the triple cell co-culture model induced a significant release of the inflammatory mediator IL-8 in the lower chamber, representative of inflammatory mediator release into the circulation. If this model accurately represents the *in vivo* situation, this particle could have the potential to induce adverse cardiovascular effects following inhalation or injection as inflammation can act as a prothrombotic trigger. Interestingly, the pro-inflammatory response observed in endothelial mono-cultures following exposure to non acid oxidised MWNTs was absent in the co-culture system, indicating that epithelial-endothelial cross-talk may be mediating this response. Treatment with CNTs at a concentration of 10μg/ml which had not been acid oxidised resulted in no increase in epithelial inflammatory mediator release in either mono- or co-cultures at 24 hours. These results clearly showed that there were discrepancies between the mono- and co-culture responses to f-MWNTs. Although our monoculture studies have provided useful information regarding the reactivity of the cell type in isolation, our co-culture studies provided an insight into how distinct cell types may communicate to alter this response.

Whilst it is has been demonstrated that the characteristics of the particular functional group present on the CNT surface can have a dramatic effect on the particle's toxicity, it is unclear which property is responsible for the altered toxicity profile. It was hypothesised that the varying charge of the particle may be responsible, especially considering that particles with

differing charges interacted with the plasma membrane in a differential manner. Furthermore, of the thermochemically grafted particles, the positively charged P(M4-VP)-MWNT elicited a greater response than the non-ionic (P(PEGMA)-MWNTs) and negatively charged (P(MAA)-MWNTs) counterparts in endothelial cells, indicating that the presence of positively charged functional groups may increase CNT toxicity at this interface. In contrast to the negative P(MAA)-MWNTs, AO-MWNTs, which contain an abundance of -COOH functional groups, induced a far greater degree of inflammation and were differentially uptaken in endothelial cells, indicating that other factors including the structural integrity of the CNT surface and the stability of the particle in solution are likely to also play a role in particle toxicity. Further analysis of the properties which define particle toxicity will enable the development of safer nanotechnologies including nanomedicines.

There is clear evidence that CNTs in medicine have the potential to deliver substantial benefits to the patient. There is already evidence that drug molecules conjugated to CNTs have fewer off-target effects than their non-conjugated counterparts which has been attributed to the increased circulation time, increased cellular uptake and selective targeting of the drug when bound to the CNT molecule (Wong *et al*., 2013). Due to the capacity for CNTs to be retained over long-periods of time and to elicit potential off-target effects in the cardiovascular system the benefit of CNT therapy should however be considered. It may be that CNTs as drug delivery molecules would only be viable when the side effects of the conjugated drug alone are severe. For example, the side effects of chemotherapeutic drugs are famously severe, and many patients in the latter stages of their disease are unable to tolerate chemotherapy due to the substantial off-target effects of the drug. If however, CNTs could be used to target the therapy to the tumour, reducing the severe systemic effects of the drug this could be of huge patient benefit (Zhuang Liu, Chen, *et al*., 2008). It is clear from this research however that the CNT vector should be chosen carefully to reduce unnecessary off-target cardiopulmonary effects of the molecule.

8. FUTURE WORK

This study has provided critical information about the nature and degree of functionalised CNT interaction with the alveolar-capillary barrier; however, in addressing our study hypothesis, a number of further questions were raised. We believe addressing these questions should take precedence in future studies relating to the present work.

Although the current study investigated barrier permeability in monoculture systems following MWNT exposure, it did not investigate cell-cell interactions in the co-culture model. Future studies using the model should focus on whether functional intercellular junctions are able to form between TT1 and AT2 cell junctions. Furthermore, whether MWNTs disrupt these junctions in the co-culture model should be investigated. This could be performed by using immunostaining to visualise epithelial and endothelial tight and adherens junction proteins. In addition, there are also a range of permeable supports that can be used with ECIS technology and so the permeability of the triple cell culture could be assessed using electrical resistance. This is an important aspect to study as cellular crosstalk may exacerbate or abrogate the barrier disrupting properties of the particles observed in mono-culture.

Furthermore, increased barrier permeability provides the potential for increased NP translocation across this barrier. Whether barrier integrity affects NP translocation should be investigated using transmission electron microscopy of the triple co-culture model to determine whether particle translocation across this barrier has occurred and whether this is a suitable model in which to study particle translocation. The permeable membrane is much thicker at ~10μm than the basement membrane separating epithelial and endothelial cells *in vivo*, however this is currently the best *in vitro* representation of the alveolar-capillary barrier. It is crucial to discover the fraction of CNTs that cross the thin barrier separating the epi- and endothelium and whether this fraction is significant enough to elicit direct effects on the pulmonary microvasculature.

Although we have observed that functionalised MWNT react with the cells of the blood gas barrier and that the nature of this reaction is largely dependent on surface functionalisation, many of the mechanisms underlying this toxicity are yet to be discovered. Particle uptake was observed in both epithelial and endothelial cells and functionalisation affected particle uptake, however it is not known whether the cellular responses are a result of active endocytosis of particles or particle interaction with the cell surface. This could be investigated by using endocytosis inhibitors such as RNA interference technology targeting caveolin or clathrin formation. Furthermore the signalling mechanisms underlying particle toxicity should be investigated as the activation of defined signalling pathways may be associated with specific disease pathologies. For example, reactive oxygen species (ROS) are known to mediate Rac-induced loss of adhesion junctions in endothelial cells (van Wetering *et al*., 2002). Whether the ROS formation observed in HPMVEC monocultures following MWNT exposure is responsible for the loss of VE-cadherin could therefore be studied using anti-oxidants and Rac pathway inhibitors. This would indicate whether particles which generate ROS are likely to increase endothelial barrier permeability, a characteristic which is associated with a number of disease pathologies including edema and acute respiratory distress syndrome.

In the present work, results of the mono-culture and co-culture experiments were not always in agreement. This indicates that a significant degree of cellular crosstalk occurs between epithelial and endothelial cells at the blood-gas barrier. In addition, the recognised ability for endogenous proteins to interact with the CNT surface could have a significant influence on the toxicity of the study particle. *In vivo* studies are therefore needed to correlate the *in vitro* findings with animal exposure models. *In vitro* findings should however influence the range of CNTs that are considered for medicinal use. The use of the commonly used acid-oxidised CNTs in medicine should be seriously reconsidered due to the ability of these particles to initiate a prevailing pro-inflammatory and pro-thromobotic response in vascular cells *in vitro*. These particles did not however induce cytotoxicity in this system or an increase in the vascular barrier integrity. Conversely, CNTs modified with P(PEGMA) or P(MAA) adducts may be viable

for medicinal use however it should be investigated how severe the barrier disrupting properties of these particles are *in vivo* and whether these effects could be tolerated. Crucially, for CNTs being developed as drug vectors, it is important to understand whether those particles which exhibited the least toxic potential still retain this status following secondary conjugation to a drug compound.

9. REFERENCES

Abarrategi, A., Gutiérrez, M. C., Moreno-Vicente, C., Hortigüela, M. J., Ramos, V., López-Lacomba, J. L., … del Monte, F. (2008). Multiwall carbon nanotube scaffolds for tissue engineering purposes. *Biomaterials*, *29*(1), 94–102. doi:10.1016/j.biomaterials.2007.09.021

Aiso, S., Yamazaki, K., Umeda, Y., Asakura, M., Kasai, T., Takaya, M., … Fukushima, S. (2010). Pulmonary toxicity of intratracheally instilled multiwall carbon nanotubes in male Fischer 344 rats. *Industrial Health*, *48*(6), 783–795. doi:10.2486/indhealth.MS1129

Aitken, R. J., Hankin, S. M., Tran, C. L., Donaldson, K., Stone, V., Cumpson, P., … Cash, S. C. (2007). *REFNANO: Reference materials for engineered nanoparticle toxicology and metrology.*

Ali-Boucetta, H., Al-Jamal, K. T., McCarthy, D., Prato, M., Bianco, A., & Kostarelos, K. (2008). Multiwalled carbon nanotube-doxorubicin supramolecular complexes for cancer therapeutics. *Chemical Communications (Cambridge, England)*, (4), 459–461. doi:10.1039/b712350g

Ali-Boucetta, H., Al-Jamal, K. T., Müller, K. H., Li, S., Porter, A. E., Eddaoudi, A., … Kostarelos, K. (2011). Cellular uptake and cytotoxic impact of chemically functionalized and polymer-coated carbon nanotubes. *Small*, *7*(22), 3230–8. doi:10.1002/smll.201101004

Ali-Boucetta, H., & Kostarelos, K. (2013a). Carbon nanotubes in medicine & biology - therapy and diagnostics. *Advanced Drug Delivery Reviews*, *65*(15), 1897–8. doi:10.1016/j.addr.2013.11.002

Ali-Boucetta, H., & Kostarelos, K. (2013b). Pharmacology of carbon nanotubes: toxicokinetics, excretion and tissue accumulation. *Advanced Drug Delivery Reviews*, *65*(15), 2111–9. doi:10.1016/j.addr.2013.10.004

Al-Jamal, K. T., Nerl, H., Müller, K. H., Ali-Boucetta, H., Li, S., Haynes, P. D., … Porter, A. E. (2011). Cellular uptake mechanisms of functionalised multi-walled carbon nanotubes by 3D electron tomography imaging. *Nanoscale*, *3*(6), 2627–35. doi:10.1039/c1nr10080g

Al-Jamal, K. T., Nunes, A., Methven, L., Ali-Boucetta, H., Li, S., Toma, F. M., … Kostarelos, K. (2012). Degree of chemical functionalization of carbon nanotubes determines tissue distribution and excretion profile. *Angewandte Chemie - International Edition*, *51*, 6389–6393. doi:10.1002/anie.201201991

Allingham, M. J., van Buul, J. D., & Burridge, K. (2007). ICAM-1-Mediated, Src- and Pyk2-Dependent Vascular Endothelial Cadherin Tyrosine Phosphorylation Is Required for Leukocyte Transendothelial Migration. *The Journal of Immunology*, *179*(6), 4053–4064. doi:10.4049/jimmunol.179.6.4053

Alon, R., & Feigelson, S. (2002). From rolling to arrest on blood vessels: leukocyte tap dancing on endothelial integrin ligands and chemokines at sub-second contacts. *Seminars in Immunology*, *14*(2), 93–104. doi:10.1006/smim.2001.0346

Al-Qadi, S., Grenha, A., Carrion-Recio, D., Seijo, B., & Remunan-Lopez, C. (2011). Microencapsulated chitosan nanoparticles for pulmonary protein delivery: In vivo evaluation of insulin-loaded formulations. *Journal of Controlled Release*, *157*(3), 383–90. doi:10.1016/j.jconrel.2011.08.008

Apopa, P. L., Qian, Y., Shao, R., Guo, N. L., Schwegler-Berry, D., Pacurari, M., … Flynn, D. C. (2009). Iron oxide nanoparticles induce human microvascular endothelial cell permeability through reactive oxygen species production and microtubule remodeling. *Particle and Fibre Toxicology*, *6*, 1. doi:10.1186/1743-8977-6-1

Atashbar, M. Z., Bejcek, B., Singamaneni, S., & Santucci, S. (2004). Carbon nanotube based biosensors. *Proceedings of IEEE Sensors, 2004.*, 1048–1051. doi:10.1109/ICSENS.2004.1426354

Azad, N., Iyer, A. K. V, Wang, L., Liu, Y., Lu, Y., & Rojanasakul, Y. (2013). Reactive oxygen species-mediated p38 MAPK regulates carbon nanotube-induced fibrogenic and angiogenic responses. *Nanotoxicology*, *7*(2), 157–68. doi:10.3109/17435390.2011.647929

Bailey, M. R. (1994). The New ICRP Model for the Respiratory Tract. *Radiat Prot Dosimetry*.

Balashazy, I., Hofmann, W., & Heistracher, T. (2003). Local particle deposition patterns may play a key role in the development of lung cancer. *Journal of Applied Physiology*, *94*(5), 1719–1725. doi:10.1152/japplphysiol.00527.2002

Balasubramanian, K., & Burghard, M. (2006). Biosensors based on carbon nanotubes. *Analytical and Bioanalytical Chemistry*, *385*(3), 452–468. doi:10.1007/s00216-006-0314-8

Baron, L., Gombault, a, Fanny, M., Villeret, B., Savigny, F., Guillou, N., … Couillin, I. (2015). The NLRP3 inflammasome is activated by nanoparticles through ATP, ADP and adenosine. *Cell Death and Disease*, *6*(2), e1629. doi:10.1038/cddis.2014.576

Battigelli, A., Ménard-Moyon, C., Da Ros, T., Prato, M., & Bianco, A. (2013). Endowing carbon nanotubes with biological and biomedical properties by chemical modifications. *Advanced Drug Delivery Reviews*, *65*(15), 1899–920. doi:10.1016/j.addr.2013.07.006

Becher, R., Bucht, A., Øvrevik, J., Hongslo, J. K., Dahlman, H. J., Samuelsen, J. T., & Schwarze, P. E. (2007). Involvement of NADPH oxidase and iNOS in rodent pulmonary cytokine responses to urban air and mineral particles. *Inhalation Toxicology*, *19*(8), 645–655. doi:10.1080/08958370701353528

Becker, B. F., Heindl, B., Kupatt, C., & Zahler, S. (2000). Endothelial function and hemostasis. *Zeitschrift Für Kardiologie*, *89*(3), 160–7. Retrieved from http://www.ncbi.nlm.nih.gov/pubmed/10798271

Bengalli, R., Mantecca, P., Camatini, M., & Gualtieri, M. (2013). Effect of nanoparticles and environmental particles on a cocultures model of the air-blood barrier. *BioMed Research International*, *2013*, 801214. doi:10.1155/2013/801214

Benincasa, M., Pacor, S., Wu, W., Prato, M., Bianco, A., & Gennaro, R. (2011). Antifungal activity of amphotericin B conjugated to carbon nanotubes. *ACS Nano*, *5*(1), 199–208. doi:10.1021/nn1023522

Bermudez, E., Mangum, J. B., Wong, B. a., Asgharian, B., Hext, P. M., Warheit, D. B., & Everitt, J. I. (2004). Pulmonary responses of mice, rats, and hamsters to subchronic inhalation of ultrafine titanium dioxide particles. *Toxicological Sciences*, *77*(2), 347–357. doi:10.1093/toxsci/kfh019

Bhattacharya, K., Andón, F. T., El-Sayed, R., & Fadeel, B. (2013). Mechanisms of carbon nanotube-induced toxicity: focus on pulmonary inflammation. *Advanced Drug Delivery Reviews*, *65*(15), 2087–97. doi:10.1016/j.addr.2013.05.012

Bhattacharya, K., Davoren, M., Boertz, J., Schins, R. P., Hoffmann, E., & Dopp, E. (2009). Titanium dioxide nanoparticles induce oxidative stress and DNA-adduct formation but not DNA-breakage in human lung cells. *Particle and Fibre Toxicology*, *6*, 17. doi:10.1186/1743-8977-6-17

Bianco, A., Kostarelos, K., Partidos, C. D., & Prato, M. (2005). Biomedical applications of functionalised carbon nanotubes. *Chemical Communications (Cambridge, England)*, (5), 571–577. doi:10.1039/b410943k

Biddlestone-Thorpe, L., Marchi, N., Guo, K., Ghosh, C., Janigro, D., Valerie, K., & Yang, H. (2012). Nanomaterial-mediated CNS delivery of diagnostic and therapeutic agents. *Advanced Drug Delivery Reviews*, *64*(7), 605–613. Retrieved from http://www.sciencedirect.com/science/article/pii/S0169409X11002948

Blankenberg, S., Rupprecht, H. J., Bickel, C., Peetz, D., Hafner, G., Tiret, L., & Meyer, J. (2001). Circulating cell adhesion molecules and death in patients with coronary artery disease. *Circulation*, *104*(12), 1336–1342. doi:10.1161/hc3701.095949

Bourdon, J. a, Halappanavar, S., Saber, A. T., Jacobsen, N. R., Williams, A., Wallin, H., … Yauk, C. L. (2012). Hepatic and pulmonary toxicogenomic profiles in mice intratracheally instilled with carbon black nanoparticles reveal pulmonary inflammation, acute phase response, and alterations in lipid homeostasis. *Toxicological Sciences : An Official Journal of the Society of Toxicology*, *127*(2), 474–84. doi:10.1093/toxsci/kfs119

Boussat, S., Eddahibi, S., Coste, a, Fataccioli, V., Gouge, M., Housset, B., … Maitre, B. (2000). Expression and regulation of vascular endothelial growth factor in human pulmonary epithelial cells. *American Journal of Physiology. Lung Cellular and Molecular Physiology*, *279*, L371–L378.

Boyoglu, C., He, Q., Willing, G., Boyoglu-Barnum, S., Dennis, V. a., Pillai, S., & Singh, S. R. (2013). Microscopic Studies of Various Sizes of Gold Nanoparticles and Their Cellular Localizations. *ISRN Nanotechnology*, *2013*, 1–13. doi:10.1155/2013/123838

Branchaud, R. M., MacDonald, J. L., & Kane, A. B. (1989). Induction of angiogenesis by intraperitoneal injection of asbestos fibers. *The FASEB Journal*, *3*, 1747–1752.

Breznan, D., Das, D., MacKinnon-Roy, C., Simard, B., Kumarathasan, P., & Vincent, R. (2015). Non-specific interaction of carbon nanotubes with the resazurin assay reagent: impact on in vitro assessment of nanoparticle cytotoxicity. *Toxicology in Vitro*, *29*(1), 142–7.

Budinger, G. R. S., Mutlu, G. M., Urich, D., Soberanes, S., Buccellato, L. J., Hawkins, K., … Chandel, N. S. (2011). Epithelial cell death is an important contributor to oxidant-mediated acute lung injury. *American Journal of Respiratory and Critical Care Medicine*, *183*(8), 1043–54. doi:10.1164/rccm.201002-0181OC

Cao, Y., Jacobsen, N. R., Danielsen, P. H., Lenz, A. G., Stoeger, T., Loft, S., … Møller, P. (2014). Vascular effects of multi-walled carbon nanotubes in dyslipidemic ApoE-/- mice and cultured endothelial cells. *Toxicological Sciences*, *138*(1), 104–116.

Cesari, M., Pahor, M., & Incalzi, R. A. (2010). Plasminogen activator inhibitor-1 (PAI-1): a key factor linking fibrinolysis and age-related subclinical and clinical conditions. *Cardiovascular Therapeutics*, *28*(5), e72–91. doi:10.1111/j.1755-5922.2010.00171.x

Chen, R., Zhang, L., Ge, C., Tseng, M. T., Bai, R., Qu, Y., … Chen, C. (2015). Subchronic Toxicity and Cardiovascular Responses in Spontaneously Hypertensive Rats after Exposure to Multiwalled Carbon Nanotubes by Intratracheal Instillation. *Chemical Research in Toxicology*, *28*(3), 440–450. doi:10.1021/tx5004003

Chen, S., Hu, S., Smith, E. F., Ruenraroengsak, P., Thorley, A. J., Menzel, R., … Shaffer, M. S. P. (2014). Aqueous cationic, anionic and non-ionic multi-walled carbon nanotubes, functionalised with minimal framework damage, for biomedical application. *Biomaterials*, *35*(17), 4729–4738. doi:10.1016/j.biomaterials.2014.02.002

Chen, S., Xiong, C., Liu, H., Wan, Q., Hou, J., He, Q., … Nie, Z. (2015). Mass spectrometry imaging reveals the sub-organ distribution of carbon nanomaterials. *Nature Nanotechnology*, *10*(2), 176–182. doi:10.1038/nnano.2014.282

Cheng, C., Müller, K. H., Koziol, K. K. K., Skepper, J. N., Midgley, P. a., Welland, M. E., & Porter, A. E. (2009). Toxicity and imaging of multi-walled carbon nanotubes in human macrophage cells. *Biomaterials*, *30*(25), 4152–4160. doi:10.1016/j.biomaterials.2009.04.019

Cheng, J., Fernando, K. a S., Veca, L. M., Sun, Y.-P., Lamond, A. I., Lam, Y. W., & Cheng, S. H. (2008). Reversible accumulation of PEGylated single-walled carbon nanotubes in the mammalian nucleus. *ACS Nano*, *2*(10), 2085–94. doi:10.1021/nn800461u

Choi, H. S., Ashitate, Y., Lee, J. H., Kim, S. H., Matsui, A., Insin, N., … Tsuda, A. (2010). Rapid translocation of nanoparticles from the lung airspaces to the body. *Nat Biotech*, *28*(12), 1300–1303. Retrieved from http://dx.doi.org/10.1038/nbt.1696

Clift, M. J. D., Endes, C., Vanhecke, D., Wick, P., Gehr, P., Schins, R. P. F., … Rothen-Rutishauser, B. (2014). A Comparative Study of Different In Vitro Lung Cell Culture

Systems to Assess the Most Beneficial Tool for Screening the Potential Adverse Effects of Carbon Nanotubes. *Toxicological Sciences*, *137*(1), 55–64. doi:10.1093/toxsci/kft216

Collins, R. G., Velji, R., Guevara, N. V., Hicks, M. J., Chan, L., & Beaudet, a. L. (2000). P-Selectin or Intercellular Adhesion Molecule (Icam)-1 Deficiency Substantially Protects against Atherosclerosis in Apolipoprotein E-Deficient Mice. *Journal of Experimental Medicine*, *191*(1), 189–194. doi:10.1084/jem.191.1.189

Conner, S. D., & Schmid, S. L. (2003). Regulated portals of entry into the cell. *Nature*, *422*(March), 37–44.

Crapo, J. D., Barry, B. E., Gehr, P., Bachofen, M., & Weibel, E. R. (1982). Cell number and cell characteristics of the normal human lung. *American Review of Respiratory Disease*, *126*(2), 332–7. Retrieved from http://www.ncbi.nlm.nih.gov/pubmed/7103258

Cronstein, B. N., & Weissmann, G. (1993). The adhesion molecules of inflammation. *Arthritis & Rheumatism*, *36*(2), 147–157. doi:10.1002/art.1780360204

Cunningham, a C., Zhang, J. G., Moy, J. V, Ali, S., & Kirby, J. a. (1997). A comparison of the antigen-presenting capabilities of class II MHC-expressing human lung epithelial and endothelial cells. *Immunology*, *91*(3), 458–463.

Czarny, B., Georgin, D., Berthon, F., Plastow, G., Pinault, M., Patriarche, G., … Dive, V. (2014). Carbon Nanotube Translocation to Distant Organs after Pulmonary Exposure : Insights from in Situ 14C- Radiolabeling and Tissue Radioimaging. *ACS Nano*, *8*(6), 5715–5724.

Dahl, J. A., Maddux, B. L. S., & Hutchison, J. E. (2007). Toward Greener Nanosynthesis. *Chemical Reviews*, *107*(6), 2228–2269. Retrieved from http://dx.doi.org/10.1021/cr050943k

Daigle, C. C., Chalupa, D. C., Gibb, F. R., Morrow, P. E., Oberdörster, G., Utell, M. J., & Frampton, M. W. (2003). Ultrafine particle deposition in humans during rest and exercise. *Inhalation Toxicology*, *15*, 539–552. doi:10.1080/08958370390205065

Dailey, L. A., Jekel, N., Fink, L., Gessler, T., Schmehl, T., Wittmar, M., … Seeger, W. (2006). Investigation of the proinflammatory potential of biodegradable nanoparticle drug delivery systems in the lung. *Toxicology and Applied Pharmacology*, *215*(1), 100–108.

Davda, J., & Labhasetwar, V. (2002). Characterization of nanoparticle uptake by endothelial cells. *International Journal of Pharmaceutics*, *233*(1-2), 51–59.

Davoren, M., Herzog, E., Casey, A., Cottineau, B., Chambers, G., Byrne, H. J., & Lyng, F. M. (2007). In vitro toxicity evaluation of single walled carbon nanotubes on human A549 lung cells. *Toxicology in Vitro*, *21*(3), 438–448. doi:10.1016/j.tiv.2006.10.007

De Volder, M. F. L., Tawfick, S. H., Baughman, R. H., & Hart, a J. (2013). Carbon nanotubes: present and future commercial applications. *Science (New York, N.Y.)*, *339*(6119), 535–9. doi:10.1126/science.1222453

Dejana, E., & Orsenigo, F. (2013). Endothelial adherens junctions at a glance. *Journal of Cell Science*, *126*(Pt 12), 2545–9. doi:10.1242/jcs.124529

Delfino, R. J., Sioutas, C., & Malik, S. (2005). Potential role of ultrafine particles in associations between airborne particle mass and cardiovascular health. *Environmental Health Perspectives*, *113*(8), 934–946. doi:10.1289/ehp.7938

Deng, X., Jia, G., Wang, H., Sun, H., Wang, X., Yang, S., … Liu, Y. (2007). Translocation and fate of multi-walled carbon nanotubes in vivo. *Carbon*, *45*(7), 1419–1424. doi:10.1016/j.carbon.2007.03.035

Dickinson, B. C., & Chang, C. J. (2011). Chemistry and biology of reactive oxygen species in signaling or stress responses. *Nature Chemical Biology*, *7*(8), 504–11. doi:10.1038/nchembio.607

Dimmeler, S., & Zeiher, a. M. (2000). Endothelial Cell Apoptosis in Angiogenesis and Vessel Regression. *Circulation Research*, *87*(6), 434–439. doi:10.1161/01.RES.87.6.434

Dobbs, L. G. (1990). Isolation and culture of alveolar type II cells. *The American Journal of Physiology*, *258*(4 Pt 1), L134–L147.

Dockery, D. W., Pope, C. A., Xu, X., Spengler, J. D., Ware, J. H., Fay, M. E., … Speizer, F. E. (1993). An assoication between air pollution and mortality in six U.S. cities. *The New England Journal of Medicine*, *329*(24), 1753–9.

Donaldson, K., Aitken, R., Tran, L., Stone, V., Duffin, R., Forrest, G., & Alexander, A. (2006). Carbon Nanotubes: A Review of Their Properties in Relation to Pulmonary Toxicology and Workplace Safety. *Toxicological Sciences*, *92*(1), 5–22. Retrieved from http://toxsci.oxfordjournals.org/content/92/1/5.abstract

Donaldson, K., Murphy, F. a, Duffin, R., & Poland, C. a. (2010). Asbestos, carbon nanotubes and the pleural mesothelium: a review of the hypothesis regarding the role of long fibre retention in the parietal pleura, inflammation and mesothelioma. *Particle and Fibre Toxicology*, *7*(5), 1–17. doi:10.1186/1743-8977-7-5

Donaldson, K., Poland, C. a, Murphy, F. a, MacFarlane, M., Chernova, T., & Schinwald, A. (2013). Pulmonary toxicity of carbon nanotubes and asbestos - similarities and differences. *Advanced Drug Delivery Reviews*, *65*(15), 2078–86. doi:10.1016/j.addr.2013.07.014

Donaldson, K., Stone, V., Seaton, A., & MacNee, W. (2001). Ambient particle inhalation and the cardiovascular system: potential mechanisms. *Environmental Health Perspectives*, *109 Suppl*(August), 523–7. Retrieved from http://www.pubmedcentral.nih.gov/articlerender.fcgi?artid=1240575&tool=pmcentrez&rendertype=abstract

Dowling, A., Clift, R., Grobert, N., Hutton, D., Oliver, R., O'Neill, O., … Whatmore, R. (2004). *Nanoscience and nanotechnologies: opportunities and uncertainties*.

Edwards, S. L., Werkmeister, J. a, & Ramshaw, J. a M. (2009). Carbon nanotubes in scaffolds for tissue engineering. *Expert Review of Medical Devices*, *6*(5), 499–505. doi:10.1586/erd.09.29

Endemann, D. H., & Schiffrin, E. L. (2004). Endothelial dysfunction. *Journal of the American Society of Nephrology : JASN*, *15*(8), 1983–92. doi:10.1097/01.ASN.0000132474.50966.DA

Erdely, A., Hulderman, T., Salmen, R., Liston, A., Zeidler-Erdely, P. C., Schwegler-Berry, D., … Simeonova, P. P. (2009). Cross-talk between lung and systemic circulation during carbon nanotube respiratory exposure. Potential biomarkers. *Nano Letters*, *9*(1), 36–43. doi:10.1021/nl801828z

Feazell, R. P., Nakayama-Ratchford, N., Dai, H., & Lippard, S. J. (2007). Soluble single-walled carbon nanotubes as longboat delivery systems for platinum (IV) anticancer drug design. *Journal of the American Chemical Society*, *129*(27), 8438–8439. doi:10.1021/ja073231f

Fehrenbach, H. (2001). Alveolar epithelial type II cell: defender of the alveolus revisited. *Respiratory Research*, *2*(1), 33–46. Retrieved from http://www.pubmedcentral.nih.gov/articlerender.fcgi?artid=59567&tool=pmcentrez&rendertype=abstract

Fenoglio, I., Greco, G., Tomatis, M., Muller, J., Raymundo-Pinero, E., Béguin, F., … Fubini, B. (2008). Structural Defects Play a Major Role in the Acute Lung Toxicity of Multiwall Carbon Nanotubes : Physicochemical Aspects. *Chemical Research in Toxicology*, *21*, 1690–1697.

Fenoglio, I., Tomatis, M., Lison, D., Muller, J., Fonseca, A., Nagy, J. B., & Fubini, B. (2006). Reactivity of carbon nanotubes: Free radical generation or scavenging activity? *Free Radical Biology and Medicine*, *40*(7), 1227–1233. Retrieved from http://www.sciencedirect.com/science/article/pii/S0891584905007082

Fernandez, I. E., & Eickelberg, O. (2012). New cellular and molecular mechanisms of lung injury and fibrosis in idiopathic pulmonary fibrosis. *Lancet*, *380*(9842), 680–8. doi:10.1016/S0140-6736(12)61144-1

Foldvari, M., & Bagonluri, M. (2008). Carbon nanotubes as functional excipients for nanomedicines: II. Drug delivery and biocompatibility issues. *Nanomedicine : Nanotechnology, Biology, and Medicine*, *4*(3), 183–200. doi:10.1016/j.nano.2008.04.003

Förster, C. (2008). Tight junctions and the modulation of barrier function in disease. *Histochemistry and Cell Biology*, *130*, 55–70. doi:10.1007/s00418-008-0424-9

Foster, K. A., Oster, C. G., Mayer, M. M., Avery, M. L., Audus, K. L., & Al, F. E. T. (1998). Characterization of the A549 Cell Line as a Type II Pulmonary Epithelial Cell Model for Drug Metabolism. *Experimental Cell Research*, *243*, 359–366.

Fu, P. P., Xia, Q., Hwang, H.-M., Ray, P. C., & Yu, H. (2014). Mechanisms of nanotoxicity: generation of reactive oxygen species. *Journal of Food and Drug Analysis*, *22*(1), 64–75. doi:10.1016/j.jfda.2014.01.005

Galkina, E., & Ley, K. (2007). Vascular adhesion molecules in atherosclerosis. *Arteriosclerosis, Thrombosis, and Vascular Biology*, *27*(11), 2292–301. doi:10.1161/ATVBAHA.107.149179

Garmann, W., & Stanfield, C. (2004). *Principles of Human Physiology* (2nd ed.). New York: Benjamin Cummings.

Gasser, M., Wick, P., Clift, M. J., Blank, F., Diener, L., Yan, B., … Rothen-Rutishauser, B. (2012). Pulmonary surfactant coating of multi-walled carbon nanotubes (MWCNTs) influences their oxidative and pro-inflammatory potential in vitro. *Particle and Fibre Toxicology*, *9*(1), 17. doi:10.1186/1743-8977-9-17

Ge, C., Li, Y., Yin, J.-J., Liu, Y., Wang, L., Zhao, Y., & Chen, C. (2012). The contributions of metal impurities and tube structure to the toxicity of carbon nanotube materials. *NPG Asia Materials*, *4*(12), e32. doi:10.1038/am.2012.60

Ge, C., Meng, L., Xu, L., Bai, R., Du, J., Zhang, L., … Chen, C. (2012). Acute pulmonary and moderate cardiovascular responses of spontaneously hypertensive rats after exposure to single-wall carbon nanotubes. *Nanotoxicology*, *6*(5), 526–42. doi:10.3109/17435390.2011.587905

Gonzalez, L., Lison, D., & Kirsch-Volders, M. (2008). Genotoxicity of engineered nanomaterials: A critical review. *Nanotoxicology*, *2*(4), 252–273. doi:10.1080/17435390802464986

Granger, D. N., & Senchenkova, E. (2010). Leukocyte-Endothelial Cell Adhesion. In *Inflammation and the Microcirculation*. San Rafael (CA): Morgan & Claypool Life Sciences.

Greater London Authority. (2002). *50 years on: The strugle for air quality in London since the great smog of December 1952*. *Mayor of London*. doi:ISBN 1 85261 428 5

Gwinn, M. R., & Vallyathan, V. (2006). Nanoparticles: Health Effects - Pros and Cons. *Environ Health Perspect*, *114*(12), 1818–1825. Retrieved from http://dx.doi.org/10.1289/ehp.8871

Hajra, L., Evans, a I., Chen, M., Hyduk, S. J., Collins, T., & Cybulsky, M. I. (2000). The NF-kappa B signal transduction pathway in aortic endothelial cells is primed for activation in regions predisposed to atherosclerotic lesion formation. *Proceedings of the National Academy of Sciences of the United States of America*, *97*(16), 9052–7. Retrieved from http://www.pubmedcentral.nih.gov/articlerender.fcgi?artid=16820&tool=pmcentrez&rendertype=abstract

Hamilton, R. F., Buford, M., Xiang, C., Wu, N., & Holian, A. (2012). NLRP3 inflammasome activation in murine alveolar macrophages and related lung pathology is associated with

MWCNT nickel contamination. *Inhalation Toxicology*, *24*(14), 995–1008. doi:10.3109/08958378.2012.745633

Harder, V., Gilmour, P., Lentner, B., Karg, E., Takenaka, S., Ziesenis, A., … Schulz, H. (2005). Cardiovascular responses in unrestrained WKY rats to inhaled ultrafine carbon particles. *Inhalation Toxicology*, *17*(1), 29–42. doi:10.1080/08958370590885681

Hartung, T., Balls, M., Bardouille, C., Blanck, O., Coecke, S., Gstraunthaler, G., & Lewis, D. (2002). Good Cell Culture Practice. ECVAM Good Cell Culture Practice Task Force Report 1. *Alternatives to Laboratory Animals : ATLA*, *30*(4), 407–414.

Heistracher, T., & Hofmann, W. (1997). Flow and deposition patterns in successive airway bifurcations. *Annals of Occupational Hygiene*, *41*(1992), 537–542. doi:10.1093/annhyg/41.inhaled_particles_VIII.537

Hermanns, M. I., Fuchs, S., Bock, M., Wenzel, K., Mayer, E., Kehe, K., … Kirkpatrick, C. (2009). Primary human coculture model of alveolo-capillary unit to study mechanisms of injury to peripheral lung. *Cell and Tissue Research*, *336*(1), 91–105.

Hermanns, M. I., Unger, R. E., Kehe, K., Peters, K., & Kirkpatrick, C. J. (2004). Lung epithelial cell lines in coculture with human pulmonary microvascular endothelial cells: development of an alveolo-capillary barrier in vitro. *Laboratory Investigation; a Journal of Technical Methods and Pathology*, *84*(6), 736–752. Retrieved from http://dx.doi.org/10.1038/labinvest.3700081

Hewett, P. W., & Murray, J. C. (1993). Human Lung Microvessel Endothelial Cells: Isolation, Culture, and Characterization. *Microvascular Research*, *46*(1), 89–102. Retrieved from http://www.sciencedirect.com/science/article/pii/S002628628371037X

Hirano, S., Kanno, S., & Furuyama, A. (2008). Multi-walled carbon nanotubes injure the plasma membrane of macrophages. *Toxicology and Applied Pharmacology*, *232*(2), 244–251. doi:10.1016/j.taap.2008.06.016

Ho, C.-C., Chang, H., Tsai, H.-T., Tsai, M.-H., Yang, C.-S., Ling, Y.-C., & Lin, P. (2011). Quantum dot 705, a cadmium-based nanoparticle, induces persistent inflammation and granuloma formation in the mouse lung. *Nanotoxicology*, (July), 1–11. doi:10.3109/17435390.2011.635814

Hoet, P., Brüske-Hohlfeld, I., & Salata, O. V. (2004). Nanoparticles–known and unknown health risks. *Journal of Nanobiotechnology*, *2*(1), 12.

Hofmann, W., Balásházy, I., & Heistracher, T. (2001). The Relationship between Secondary Flows and Particle Deposition Patterns in Airway Bifurcations. *Aerosol Science and Technology*, *35*(6), 958–968. doi:10.1080/027868201753306723

Hogg, N., Patzak, I., & Willenbrock, F. (2011). The insider's guide to leukocyte integrin signalling and function. *Nat Rev Immunol*, *11*(6), 416–426. Retrieved from http://dx.doi.org/10.1038/nri2986

Hubbard, R., Venn, a, Lewis, S., & Britton, J. (2000). Lung cancer and cryptogenic fibrosing alveolitis. A population-based cohort study. *American Journal of Respiratory and Critical Care Medicine*, *161*(1), 5–8. doi:10.1164/ajrccm.161.1.9906062

Hunt, B. J., & Jurd, K. M. (1998). Endothelial Cell Activation. *BMJ*, *316*, 1328–13329.

Ibald-Mulli, A., Wichmann, H.-E., Kreyling, W., & Peters, A. (2002). Epidemiological evidence on health effects of ultrafine particles. *Journal of Aerosol Medicine : The Official Journal of the International Society for Aerosols in Medicine*, *15*(2), 189–201. doi:10.1089/089426802320282310

ICRP. (1994). *Human Respiratory Tract Model for Radiological Protection. ICRP Publication 66*. Oxford :Pergamon.

Iijima, S. (1991). Helical microtubules of graphitic carbon. *Nature*, *354*, 56–58.

Ingle, T., Dervishi, E., Biris, A. R., Mustafa, T., Buchanan, R. a, & Biris, A. S. (2012). Raman spectroscopy analysis and mapping the biodistribution of inhaled carbon nanotubes in the lungs and blood of mice. *Journal of Applied Toxicology : JAT*, (February). doi:10.1002/jat.2796

Jachak, A., Lai, S. K., Hida, K., Suk, J. S., Markovic, N., Biswal, S., … Hanes, J. (2011). Transport of metal oxide nanoparticles and single-walled carbon nanotubes in human mucus. *Nanotoxicology*, 1–9. Retrieved from http://dx.doi.org/10.3109/17435390.2011.598244

Jain, S., Thakare, V. S., Das, M., Godugu, C., Jain, A. K., Mathur, R., … Mishra, A. K. (2011). Toxicity of multiwalled carbon nanotubes with end defects critically depends on their functionalization density. *Chemical Research in Toxicology*, *24*(11), 2028–2039. doi:10.1021/tx2003728

Jaques, P. a, & Kim, C. S. (2000). Measurement of total lung deposition of inhaled ultrafine particles in healthy men and women. *Inhalation Toxicology*, *12*, 715–731. doi:10.1080/08958370050085156

Jefferson, A., Wijesurendra, R. S., McAteer, M. a, Digby, J. E., Douglas, G., Bannister, T., … Choudhury, R. P. (2011). Molecular imaging with optical coherence tomography using ligand-conjugated microparticles that detect activated endothelial cells: rational design through target quantification. *Atherosclerosis*, *219*(2), 579–87. doi:10.1016/j.atherosclerosis.2011.07.127

Ji, Z., Zhang, D., Li, L., Shen, X., Deng, X., Dong, L., … Liu, Y. (2009). The hepatotoxicity of multi-walled carbon nanotubes in mice. *Nanotechnology*, *20*(44), 445101. doi:10.1088/0957-4484/20/44/445101

Jin, H., Heller, D. a, & Strano, M. S. (2008). Single-particle tracking of endocytosis and exocytosis of single-walled carbon nanotubes in NIH-3T3 cells. *Nano Letters*, *8*(6), 1577–85. doi:10.1021/nl072969s

Johnson-Tidey, R. R., McGregor, J. L., Taylor, P. R., & Poston, R. N. (1994). Increase in the adhesion molecule P-selectin in endothelium overlying atherosclerotic plaques. Coexpression with intercellular adhesion molecule-1. *The American Journal of Pathology*, *144*(5), 952–61. Retrieved from http://www.pubmedcentral.nih.gov/articlerender.fcgi?artid=1887356&tool=pmcentrez&rendertype=abstract

Kasahara, Y., Tuder, R. M., Cool, C. D., Lynch, D. a, Flores, S. C., & Voelkel, N. F. (2001). Endothelial cell death and decreased expression of vascular endothelial growth factor and vascular endothelial growth factor receptor 2 in emphysema. *American Journal of Respiratory and Critical Care Medicine*, *163*(3 Pt 1), 737–44. doi:10.1164/ajrccm.163.3.2002117

Kasper, J., Hermanns, M. I., Bantz, C., Maskos, M., Stauber, R., Pohl, C., … Kirkpatrick, J. C. (2011). Inflammatory and cytotoxic responses of an alveolar-capillary coculture model to silica nanoparticles: Comparison with conventional monocultures. *Particle and Fibre Toxicology*, *8*(6), 1–16.

Katwa, P., Wang, X., Urankar, R. N., Podila, R., Hilderbrand, S. C., Fick, R. B., … Brown, J. M. (2012). A carbon nanotube toxicity paradigm driven by mast cells and the IL-$_{33}$/ST$_2$ axis. *Small (Weinheim an Der Bergstrasse, Germany)*, *8*(18), 2904–12. doi:10.1002/smll.201200873

Kemp, S. J., Thorley, A. J., Gorelik, J., Seckl, M. J., O'Hare, M. J., Arcaro, A., … Tetley, T. D. (2008). Immortalization of Human Alveolar Epithelial Cells to Investigate Nanoparticle Uptake. *American Journal of Respiratory Cell and Molecular Biology*, *39*(5), 591–597.

Kiechl, S., Paré, G., Barbalic, M., Qi, L., Dupuis, J., Dehghan, A., … Ye, S. (2011). Association of variation at the ABO Locus with circulating levels of soluble intercellular adhesion molecule-1, Soluble P-selectin, and Soluble E-selectin: A meta-analysis. *Circulation: Cardiovascular Genetics*, *4*(6), 681–686. doi:10.1161/CIRCGENETICS.111.960682

Kim, K.-J., & Malik, A. B. (2003). Protein transport across the lung epithelial barrier. *American Journal of Physiology - Lung Cellular and Molecular Physiology*, *284*, L247–L259.

Kim, N. S., & Kim, S.-J. (1991). Isolation and Cultivation of Microvascular Endothelial Cells from Rat Lungs: Effects of Gleatin Substraum and Serum. *Yonsei Medical Journal*, *32*(4), 303–314.

Kim, Y. H., Fazlollahi, F., Kennedy, I. M., Yacobi, N. R., Hamm-Alvarez, S. F., Borok, Z., … Crandall, E. D. (2010). Alveolar epithelial cell injury due to zinc oxide nanoparticle exposure. *American Journal of Respiratory and Critical Care Medicine*, *182*(11), 1398–1409. doi:10.1164/rccm.201002-0185OC

Kimata, Y. I., Kimata, Y. I., Shimizu, Y., Abe, H., Farcasanu, I. C., Takeuchi, M., … Kohno, K. (2003). Genetic Evidence for a Role of BiP / Kar2 That Regulates Ire1 in Response to

Accumulation of Unfolded Proteins. *Molecular Biology of the Cell*, *14*(September), 2559–2569. doi:10.1091/mbc.E02

Kjaergaard, A. G., Dige, A., Krog, J., Tønnesen, E., & Wogensen, L. (2013). Soluble adhesion molecules correlate with surface expression in an in vitro model of endothelial activation. *Basic & Clinical Pharmacology & Toxicology*, *113*(4), 273–9. doi:10.1111/bcpt.12091

Klein, S. G., Serchi, T., Hoffmann, L., Blömeke, B., & Gutleb, A. C. (2013). An improved 3D tetraculture system mimicking the cellular organisation at the alveolar barrier to study the potential toxic effects of particles on the lung An improved 3D tetraculture system mimicking the cellular organisation at the alveolar barrier to. *Particle and Fibre Toxicology*, *10*(31), 1–17. doi:10.1186/1743-8977-10-31

Knaapen, A. M., Borm, P. J. a, Albrecht, C., & Schins, R. P. F. (2004). Inhaled particles and lung cancer. Part A: Mechanisms. *International Journal of Cancer. Journal International Du Cancer*, *109*(6), 799–809. doi:10.1002/ijc.11708

Knuckles, T. L., Lund, A. K., Lucas, S. N., & Campen, M. J. (2008). Diesel exhaust exposure enhances venoconstriction via uncoupling of eNOS. *Toxicology and Applied Pharmacology*, *230*(3), 346–351. doi:10.1016/j.taap.2008.03.010

Kostarelos, K. (2008). The long and short of carbon nanotube toxicity., *26*(7), 774–776. Retrieved from http://discovery.ucl.ac.uk/1350963/

Kostarelos, K., Lacerda, L., Pastorin, G., Wu, W., Wieckowski, S., Luangsivilay, J., … Bianco, A. (2007). Cellular uptake of functionalized carbon nanotubes is independent of functional group and cell type. *Nature Nanotechnology*, *2*(2), 108–13. doi:10.1038/nnano.2006.209

Kreyling, W. G., Hirn, S., & Schleh, C. (2010). Nanoparticles in the lung. *Nat Biotech*, *28*(12), 1275–1276. Retrieved from http://dx.doi.org/10.1038/nbt.1735

Kreyling, W. G., Semmler-behnke, M., Takenaka, S., & Oller, W. M. (2013). Differences in the Biokinetics of Inhaled Nano- versus Micrometer-Sized Particles. *Accounts of Chemical Research*, *46*(3), 714–722.

Kulmala, M., & Kerminen, V. M. (2008). On the formation and growth of atmospheric nanoparticles. *Atmospheric Research*, *90*(2-4), 132–150. doi:10.1016/j.atmosres.2008.01.005

Lacerda, L., Ali-Boucetta, H., Herrero, M. A., Pastorin, G., Bianco, A., Prato, M., & Kostarelos, K. (2008). Tissue histology and physiology following intravenous administration of different types of functionalized multiwalled carbon nanotubes. *Nanomedicine*, *3*(2), 149–161. doi:10.2217/17435889.3.2.149

Lacerda, L., Soundararajan, a., Singh, R., Pastorin, G., Al-Jamal, K. T., Turton, J., … Kostarelos, K. (2008). Dynamic Imaging of Functionalized Multi-Walled Carbon Nanotube Systemic Circulation and Urinary Excretion. *Advanced Materials*, *20*(2), 225–230. doi:10.1002/adma.200702334

Lam, C.-W., James, J. T., McCluskey, R., & Hunter, R. L. (2004). Pulmonary toxicity of single-wall carbon nanotubes in mice 7 and 90 days after intratracheal instillation. *Toxicological Sciences : An Official Journal of the Society of Toxicology*, *77*(1), 126–34. doi:10.1093/toxsci/kfg243

Lam, G. Y., Huang, J., & Brumell, J. H. (2010). The many roles of NOX2 NADPH oxidase-derived ROS in immunity. *Seminars in Immunopathology*, 1–16. doi:10.1007/s00281-010-0221-0

Lanone, S., Andujar, P., Kermanizadeh, A., & Boczkowski, J. (2013). Determinants of carbon nanotube toxicity. *Advanced Drug Delivery Reviews*, *65*(15), 2063–9. doi:10.1016/j.addr.2013.07.019

Lau, K., & Hui, D. (2002). The revolutionary creation of new advanced materials - carbon nanotube composites. *Composites: Part B*, *33*, 263–277.

Lawther, P. J., Ellison, J. M., & Waller, B. E. (1968). Some medical apsects of aerosol research. *Proceedings of the Royal Society A.*, *307*, 223–234.

Legramante, J. M., Valentini, F., Magrini, a, Palleschi, G., Sacco, S., Iavicoli, I., … Pietroiusti, a. (2009). Cardiac autonomic regulation after lung exposure to carbon nanotubes. *Human & Experimental Toxicology*, *28*(6-7), 369–75. doi:10.1177/0960327109105150

Lehmann, A. D., Daum, N., Bur, M., Lehr, C. M., Gehr, P., & Rothen-Rutishauser, B. M. (2011). An in vitro triple cell co-culture model with primary cells mimicking the human alveolar epithelial barrier. *European Journal of Pharmaceutics and Biopharmaceutics*, *77*(3), 398–406. doi:10.1016/j.ejpb.2010.10.014

Lesniak, A., Campbell, A., Monopoli, M. P., Lynch, I., Salvati, A., & Dawson, K. a. (2010). Serum heat inactivation affects protein corona composition and nanoparticle uptake. *Biomaterials*, *31*(36), 9511–9518. doi:10.1016/j.biomaterials.2010.09.049

Lesniak, A., Fenaroli, F., Monopoli, M. P., Åberg, C., Dawson, K. a, & Salvati, A. (2012). Effects of the presence or absence of a protein corona on silica nanoparticle uptake and impact on cells. *ACS Nano*, *6*(7), 5845–57. doi:10.1021/nn300223w

Ley, K., & Huo, Y. (2001). VCAM-1 is critical in atherosclerosis. *The Journal of Clinical Investigation*, *107*(10), 1209–10. doi:10.1172/JCI13005

Ley, K., Laudanna, C., Cybulsky, M. I., & Nourshargh, S. (2007). Getting to the site of inflammation: the leukocyte adhesion cascade updated. *Nature Reviews. Immunology*, *7*(9), 678–89. doi:10.1038/nri2156

Li, C., Mollahan, P., Baguneid, M. S., McMahon, R. F., Kumar, P., Walker, M. G., … Kumar, S. (2006). A comparative study of neovascularisation in atherosclerotic plaques using CD31, CD105 and TGF beta 1. *Pathobiology : Journal of Immunopathology, Molecular and Cellular Biology*, *73*(4), 192–7. doi:10.1159/000096020

Li, J. J., Muralikrishnan, S., Ng, C.-T., Yung, L.-Y. L., & Bay, B.-H. (2010). Nanoparticle-induced pulmonary toxicity. *Experimental Biology and Medicine (Maywood, N.J.)*, *235*(9), 1025–33. doi:10.1258/ebm.2010.010021

Li, J., Zhang, Y.-P., & Kirsner, R. S. (2003). Angiogenesis in wound repair: angiogenic growth factors and the extracellular matrix. *Microscopy Research and Technique*, *60*(1), 107–114. doi:10.1002/jemt.10249

Li, Z., Hulderman, T., Salmen, R., Chapman, R., Leonard, S. S., Young, S.-H., … Simeonova, P. P. (2007). Cardiovascular effects of pulmonary exposure to single-wall carbon nanotubes. *Environmental Health Perspectives*, *115*(3), 377–82. doi:10.1289/ehp.9688

Libby, P., & Simon, D. I. (2001). Inflammation and Thrombosis: The Clot Thickens. *Circulation*, *103*, 1718–1721.

Lindberg, H. K., Falck, G. C. M., Suhonen, S., Vippola, M., Vanhala, E., Catalán, J., … Norppa, H. (2009). Genotoxicity of nanomaterials: DNA damage and micronuclei induced by carbon nanotubes and graphite nanofibres in human bronchial epithelial cells in vitro. *Toxicology Letters*, *186*(3), 166–173. doi:10.1016/j.toxlet.2008.11.019

Lippi, G., Franchini, M., & Targher, G. (2011). Arterial thrombus formation in cardiovascular disease. *Nature Reviews. Cardiology*, *8*(9), 502–512. doi:10.1038/nrcardio.2011.91

Lippmann, M. (1990). Effects of fiber characteristics on lung deposition, retention, and disease. *Environmental Health Perspectives*, *88*, 311–317. doi:10.1289/ehp.9088311

Liu, X., Tao, H., Yang, K., Zhang, S., Lee, S. T., & Liu, Z. (2011). Optimization of surface chemistry on single-walled carbon nanotubes for in vivo photothermal ablation of tumors. *Biomaterials*, *32*(1), 144–151. doi:10.1016/j.biomaterials.2010.08.096

Liu, Y., Zhao, Y., Sun, B., & Chen, C. (2013). Understanding the toxicity of carbon nanotubes. *Accounts of Chemical Research*, *46*(3), 702–713. doi:10.1021/ar300028m

Liu, Z., Cai, W., He, L., Nakayama, N., Chen, K., Sun, X., … Dai, H. (2007). In vivo biodistribution and highly efficient tumour targeting of carbon nanotubes in mice. *Nature Nanotechnology*, *2*(1), 47–52. doi:10.1038/nnano.2006.170

Liu, Z., Chen, K., Davis, C., Sherlock, S., Cao, Q., Chen, X., & Dai, H. (2008). Drug delivery with carbon nanotubes for in vivo cancer treatment. *Cancer Research*, *68*(16), 6652–60. doi:10.1158/0008-5472.CAN-08-1468

Liu, Z., Davis, C., Cai, W., He, L., Chen, X., & Dai, H. (2008). Circulation and long-term fate of functionalized, biocompatible single-walled carbon nanotubes in mice probed by Raman spectroscopy. *Proceedings of the National Academy of Sciences of the United States of America*, *105*(5), 1410–1415. doi:10.1073/pnas.0707654105

Liu, Z., Miner, J. J., Yago, T., Yao, L., Lupu, F., Xia, L., & McEver, R. P. (2010). Differential regulation of human and murine P-selectin expression and function in vivo. *The Journal of Experimental Medicine*, *207*(13), 2975–87. doi:10.1084/jem.20101545

Liu, Z., Tabakman, S., Welsher, K., & Dai, H. (2009). Carbon Nanotubes in Biology and Medicine: In vitro and in vivo Detection, Imaging and Drug Delivery. *Nano Research*, *2*(2), 85–120. doi:10.1007/s12274-009-9009-8

Lloyd-Jones, D., Adams, R. J., Brown, T. M., Carnethon, M., Dai, S., De Simone, G., … Wylie-Rosett, J. (2010). Heart disease and stroke statistics--2010 update: a report from the American Heart Association. *Circulation*, *121*(7), e46–e215. doi:10.1161/CIRCULATIONAHA.109.192667

Lockman, P. R., Koziara, J. M., Mumper, R. J., & Allen, D. D. (2004). Nanoparticle surface charges alter blood-brain barrier integrity and permeability. *Journal of Drug Targeting*, *12*(December), 635–641. doi:10.1080/10611860400015936

Luissint, A.-C., Federici, C., Guillonneau, F., Chrétien, F., Camoin, L., Glacial, F., … Couraud, P.-O. (2012). Guanine nucleotide-binding protein Gαi2: a new partner of claudin-5 that regulates tight junction integrity in human brain endothelial cells. *Journal of Cerebral Blood Flow and Metabolism : Official Journal of the International Society of Cerebral Blood Flow and Metabolism*, *32*(5), 860–73. doi:10.1038/jcbfm.2011.202

Lum, H., & Malik, A. B. (1994). Regulation of vascular endothelial barrier function. *The American Journal of Physiology*, *267*(3 Pt 1), L223–41. Retrieved from http://www.ncbi.nlm.nih.gov/pubmed/7943249

Lum, H., & Roebuck, K. a. (2001). Oxidant stress and endothelial cell dysfunction. *American Journal of Physiology. Cell Physiology*, *280*(4), C719–C741.

Lundqvist, M., Stigler, J., Elia, G., Lynch, I., Cedervall, T., & Dawson, K. a. (2008). Nanoparticle size and surface properties determine the protein corona with possible implications for biological impacts. *Proceedings of the National Academy of Sciences of the United States of America*, *105*(38), 14265–14270. doi:10.1073/pnas.0805135105

Luscinskas, F. W., Ma, S., Nusrat, A., Parkos, C. a, & Shaw, S. K. (2002). Leukocyte transendothelial migration: a junctional affair. *Seminars in Immunology*, *14*(2), 105–13. doi:10.1006/smim.2001.0347

Lynch, I., Salvati, A., & Dawson, K. a. (2009). Protein-nanoparticle interactions: What does the cell see? *Nature Nanotechnology*, *4*(9), 546–547. doi:10.1038/nnano.2009.248

Maeda, H. (2001). The enhanced permeability and retention (EPR) effect in tumor vasculature: The key role of tumor-selective macromolecular drug targeting. *Advances in Enzyme Regulation*, *41*(00), 189–207. doi:10.1016/S0065-2571(00)00013-3

Magee, J. C., Stone, A. E., Oldham, K. T., & Guice, K. S. (1994). Isolation, culture, and characterization of rat lung microvascular endothelial cells. *American Journal of Physiology - Lung Cellular and Molecular Physiology*, *267*(4), L433–L441. Retrieved from http://ajplung.physiology.org/content/267/4/L433.abstract

Ma-Hock, L., Treumann, S., Strauss, V., Brill, S., Luizi, F., Mertler, M., … Landsiedel, R. (2009). Inhalation toxicity of multiwall carbon nanotubes in rats exposed for 3 months. *Toxicological Sciences : An Official Journal of the Society of Toxicology*, *112*(2), 468–81. doi:10.1093/toxsci/kfp146

Maniatis, N. a, Kotanidou, A., Catravas, J. D., & Orfanos, S. E. (2008). Endothelial pathomechanisms in acute lung injury. *Vascular Pharmacology*, *49*(4-6), 119–33. doi:10.1016/j.vph.2008.06.009

Maniscalco, W. M., Watkins, R. H., D'Angio, C. T., & Ryan, R. M. (1997). Hyperoxic injury decreases alveolar epithelial cell expression of vascular endothelial growth factor (VEGF) in neonatal rabbit lung. *American Journal of Respiratory Cell and Molecular Biology*, *16*(10), 557–567. doi:10.1165/ajrcmb.16.5.9160838

Manke, A., Luanpitpong, S., Dong, C., Wang, L., He, X., Battelli, L., … Rojanasakul, Y. (2014). Effect of fiber length on carbon nanotube-induced fibrogenesis. *International Journal of Molecular Sciences*, *15*(5), 7444–61. doi:10.3390/ijms15057444

Manke, A., Wang, L., & Rojanasakul, Y. (2012). Pulmonary Toxicity and Fibrogenic Response of Carbon Nanotubes. *Toxicology Mechanisms and Methods*. doi:10.3109/15376516.2012.753967

Manke, A., Wang, L., & Rojanasakul, Y. (2013). Mechanisms of nanoparticle-induced oxidative stress and toxicity. *BioMed Research International*, *2013*, 942916. doi:10.1155/2013/942916

Mann, K. G. (2002). The Dynamics of Thrombin Formation. *Arteriosclerosis, Thrombosis, and Vascular Biology*, *23*(1), 17–25. doi:10.1161/01.ATV.0000046238.23903.FC

Maynard, A. D., & Kuempel, E. D. (2005). Airborne nanostructured particles and occupational health. *Journal of Nanoparticle Research*, *7*, 587–614. doi:10.1007/s11051-005-6770-9

McDevitt, M. R., Chattopadhyay, D., Kappel, B. J., Jaggi, J. S., Schiffman, S. R., Antczak, C., … Scheinberg, D. a. (2007). Tumor targeting with antibody-functionalized, radiolabeled carbon nanotubes. *Journal of Nuclear Medicine : Official Publication, Society of Nuclear Medicine*, *48*(7), 1180–1189. doi:10.2967/jnumed.106.039131

Mehta, D., Bhattacharya, J., Matthay, M. a, & Malik, A. B. (2004). Integrated control of lung fluid balance. *American Journal of Physiology - Lung Cellular and Molecular Physiology*, *287*(6), L1081–L1090. doi:10.1152/ajplung.00268.2004

Mehta, D., & Malik, A. B. (2006). Signaling mechanisms regulating endothelial permeability. *Physiological Reviews*, *86*(1), 279–367. doi:10.1152/physrev.00012.2005

Meigs, J. B., Hu, F. B., Rifai, N., & Manson, J. E. (2004). Biomarkers of endothelial dysfunction and risk of type 2 diabetes mellitus. *JAMA : The Journal of the American Medical Association*, *291*(16), 1978–1986. doi:10.1001/jama.291.16.1978

Meng, H., Xia, T., George, S., & Nel, A. E. (2009). A Predictive Toxicological Paradigm for the Safety Assessment of Nanomaterials. *ACS Nano*, *3*(7), 1620–1627.

Menzel, R., Tran, M. Q., Menner, A., Kay, C. W. M., Bismarck, A., & Shaffer, M. S. P. (2010). A versatile, solvent-free methodology for the functionalisation of carbon nanotubes. *Chemical Science*, *1*(5), 603. doi:10.1039/c0sc00287a

Mercer, R. R., Scabilloni, J. F., Hubbs, A. F., Wang, L., Battelli, L. a, McKinney, W., … Porter, D. W. (2013). Extrapulmonary transport of MWCNT following inhalation exposure. *Particle and Fibre Toxicology*, *10*(1), 38. doi:10.1186/1743-8977-10-38

Mestas, J., & Ley, K. (2008). Monocyte-endothelial cell interactions in the development of atherosclerosis. *Trends in Cardiovascular Medicine*, *18*(6), 228–32. doi:10.1016/j.tcm.2008.11.004

Ministry of Health. (2008). *Our Vision*. Retrieved from http://213.42.151.126/en/Page_1040.aspx

Mitchell, L. A., Gao, J., Wal, R. Vander, Gigliotti, A., Burchiel, S. W., & McDonald, J. D. (2007). Pulmonary and systemic immune response to inhaled multiwalled carbon nanotubes. *Toxicological Sciences : An Official Journal of the Society of Toxicology*, *100*(1), 203–14. doi:10.1093/toxsci/kfm196

Mitchell, L. A., Lauer, F. T., Burchiel, S. W., & Mcdonald, J. D. (2009). Mechanisms for how inhaled multiwalled carbon nanotubes suppress systemic immune function in mice. *Nature Nanotechnology*, *4*, 451–456. doi:10.1038/NNANO.2009.151

Møller, P., Christophersen, D. V., Jensen, D. M., Kermanizadeh, A., Roursgaard, M., Jacobsen, N. R., … Loft, S. (2014). Role of oxidative stress in carbon nanotube-generated health effects. *Archives of Toxicology*, *88*(11), 1939–1964. doi:10.1007/s00204-014-1356-x

Monopoli, M. P., Walczyk, D., Campbell, A., Elia, G., Lynch, I., Bombelli, F. B., & Dawson, K. a. (2011). Physical-chemical aspects of protein corona: relevance to in vitro and in vivo biological impacts of nanoparticles. *Journal of the American Chemical Society*, *133*(8), 2525–34. doi:10.1021/ja107583h

Moon, H. K., Lee, S. H., & Choi, H. C. (2009). In vivo near-infrared mediated tumor destruction by photothermal effect of carbon nanotubes. *ACS Nano*, *3*(11), 3707–3713. doi:10.1021/nn900904h

Morimoto, Y., Ogami, A., Todoroki, M., Yamamoto, M., Murakami, M., Hirohashi, M., … Tanaka, I. (2010). Expression of inflammation-related cytokines following intratracheal instillation of nickel oxide nanoparticles. *Nanotoxicology*, *4*(2), 161–176. doi:10.3109/17435390903518479

Muller, J., Huaux, F., Moreau, N., Misson, P., Heilier, J.-F., Delos, M., … Lison, D. (2005). Respiratory toxicity of multi-wall carbon nanotubes. *Toxicology and Applied Pharmacology*, *207*(3), 221–31. doi:10.1016/j.taap.2005.01.008

Müller, L., Riediker, M., Wick, P., Mohr, M., Gehr, P., & Rothen-Rutishauser, B. (2010). Oxidative stress and inflammation response after nanoparticle exposure: differences between human lung cell monocultures and an advanced three-dimensional model of the human epithelial airways. *Journal of the Royal Society, Interface / the Royal Society*, *7 Suppl 1*(Suppl 1), S27–S40. doi:10.1098/rsif.2009.0161.focus

Muller, W. A. (2009). Mechanisms of transendothelial migration of leukocytes. *Circulation Research*, *105*(3), 223–230. doi:10.1161/CIRCRESAHA.109.200717

Muller, W. A. (2011). Mechanisms of leukocyte transendothelial migration. *Annual Review of Pathology*, *6*, 323–44. doi:10.1146/annurev-pathol-011110-130224

Nageh, M. F., Sandberg, E. T., Marotti, K. R., Lin, A. H., Melchior, E. P., Bullard, D. C., & Beaudet, A. L. (1997). Deficiency of Inflammatory Cell Adhesion Molecules Protects Against Atherosclerosis in Mice. *Arteriosclerosis, Thrombosis, and Vascular Biology*, *17*(8), 1517–1520. doi:10.1161/01.ATV.17.8.1517

Nan, B., Lin, P., Lumsden, A. B., Yao, Q., & Chen, C. (2005). Effects of TNF-alpha and curcumin on the expression of thrombomodulin and endothelial protein C receptor in human endothelial cells. *Thrombosis Research*, *115*(5), 417–426. doi:10.1016/j.thromres.2004.10.010

Naota, M., Shimada, A., Morita, T., Inoue, K., & Takano, H. (2009). Translocation Pathway of the Intratracheally Instilled C60 Fullerene from the Lung into the Blood Circulation in the Mouse: Possible Association of Diffusion and Caveolae-mediated Pinocytosis. *Toxicologic Pathology*, *37*(4), 456–462.

Napoli, C., Lerman, L. O., de Nigris, F., Gossl, M., Balestrieri, M. L., & Lerman, A. (2006). Rethinking primary prevention of atherosclerosis-related diseases. *Circulation*, *114*(23), 2517–27. doi:10.1161/CIRCULATIONAHA.105.570358

Nel, A., Xia, T., Mädler, L., & Li, N. (2006). Toxic potential of materials at the nanolevel. *Science (New York, N.Y.)*, *311*(5761), 622–7. doi:10.1126/science.1114397

Nemmar, A., Hoet, P. H. M., Vandervoort, P., Dinsdale, D., Nemery, B., & Hoylaerts, M. F. (2007). Enhanced peripheral thrombogenicity after lung inflammation is mediated by platelet-leukocyte activation: role of P-selectin. *Journal of Thrombosis and Haemostasis : JTH*, *5*(6), 1217–26. doi:10.1111/j.1538-7836.2007.02557.x

Nemmar, A., Hoylaerts, M. F., Hoet, P. H. M., & Nemery, B. (2004). Possible mechanisms of the cardiovascular effects of inhaled particles: systemic translocation and prothrombotic effects. *Toxicology Letters*, *149*(1-3), 243–53. doi:10.1016/j.toxlet.2003.12.061

Niessen, C. M. (2007). Tight junctions/adherens junctions: basic structure and function. *The Journal of Investigative Dermatology*, *127*(11), 2525–32. doi:10.1038/sj.jid.5700865

Nusrat, A., Turner, J. R., & Madara, J. L. (2000). IV. Regulation of tight junctions by extracellular stimuli: nutrients, cytokines, and immune cells. *American Journal of Physiology - Gastrointestinal and Liver Physiology*, *279*(5), G851–G857. Retrieved from http://ajpgi.physiology.org/content/279/5/G851.abstract

Nyga, A., Hart, A., & Tetley, T. D. (2015). Importance of the HIF pathway in cobalt nanoparticle-induced cytotoxicity and inflammation in human macrophages. *Nanotoxicology*, *00*(00), 1–13. doi:10.3109/17435390.2014.991430

Nymark, P., Jensen, K. A., Suhonen, S., Kembouche, Y., Vippola, M., Kleinjans, J., … Briedé, J. J. (2014). Free radical scavenging and formation by multi-walled carbon nanotubes in cell free conditions and in human bronchial epithelial cells. *Particle and Fibre Toxicology*, *11*, 4. doi:10.1186/1743-8977-11-4

O'Brien, K. D., Allen, M. D., Mcdonald, T., Chait, A., Harlan, J. M., Fishbein, D., … Alpers, C. E. (1993). Vascular Cell Adhesion Molecule-1 Is Expressed in Human Coronary Atherosclerotic Plaques: Implications for the Mode of Progression of Advanced Coronary Atherosclerosis. *The Journal of Clinical Investigation*, *92*(2), 945–951.

Oberdörster, G. (2000). Determinants of the pathogenicity of man-made vitreous fibers (MMVF). *International Archives of Occupational and Environmental Health*, *73 Suppl*, S60–S68. doi:10.1007/PL00014628

Oberdörster, G. (2002). Toxicokinetics and effects of fibrous and non-fibrous particles. *Inhalation Toxicology*, *14*, 29–56.

Oberdörster, G., Oberdörster, E., & Oberdörster, J. (2005). Nanotoxicology: An Emerging Discipline Evolving from Studies of Ultrafine Particles. *Environmental Health Perspectives*, *113*(7), 823–839. doi:10.1289/ehp.7339

Overgaard, C. E., Mitchell, L. a, & Koval, M. (2012). Roles for claudins in alveolar epithelial barrier function. *Annals of the New York Academy of Sciences*, *1257*, 167–74. doi:10.1111/j.1749-6632.2012.06545.x

Pacurari, M., Qian, Y., Fu, W., Schwegler-Berry, D., Ding, M., Castranova, V., & Guo, N. L. (2012). Cell permeability, migration, and reactive oxygen species induced by multiwalled carbon nanotubes in human microvascular endothelial cells. *Journal of Toxicology and Environmental Health. Part A*, *75*(2), 112–28. doi:10.1080/15287394.2011.615110

Pantarotto, D., Briand, J.-P., Prato, M., & Bianco, A. (2004). Translocation of bioactive peptides across cell membranes by carbon nanotubes. *Chemical Communications (Cambridge, England)*, (1), 16–7. doi:10.1039/b311254c

Pantarotto, D., Partidos, C. D., Hoebeke, J., Brown, F., Kramer, E., Briand, J., … Bianco, A. (2003). Immunization with Peptide-Functionalized Carbon Nanotubes Enhances Virus-Specific Neutralizing Antibody Responses. *Chem. Biol.*, *10*, 961–966. doi:10.1016/j

Papritz, M., Pohl, C., Wübbeke, C., Moisch, M., Hofmann, H., Hermanns, M. I., … Kehe, K. (2010). Side-specific effects by cadmium exposure: Apical and basolateral treatment in a coculture model of the blood–air barrier. *Toxicology and Applied Pharmacology*, *245*(3), 361–369.

Park, E. J., & Park, K. (2009). Oxidative stress and pro-inflammatory responses induced by silica nanoparticles in vivo and in vitro. *Toxicology Letters*, *184*(1), 18–25. doi:10.1016/j.toxlet.2008.10.012

Park, K. H., Chhowalla, M., Iqbal, Z., & Sesti, F. (2003). Single-walled Carbon Nanotubes Are a New Class of Ion Channel Blockers. *Journal of Biological Chemistry*, *278*(50), 50212–50216. doi:10.1074/jbc.M310216200

Pastorin, G., Wu, W., Wieckowski, S., Briand, J.-P., Kostarelos, K., Prato, M., & Bianco, A. (2006). Double functionalization of carbon nanotubes for multimodal drug delivery. *Chemical Communications (Cambridge, England)*, *1*(11), 1182–1184. doi:10.1039/b516309a

Peters, A., Wichmann, H. E., Tuch, T., Heinrich, J., & Heyder, J. (1997). Respiratory effects are associated with the number of ultrafine particles. *American Journal of Respiratory and Critical Care Medicine*, *155*(4), 1376–83. doi:10.1164/ajrccm.155.4.9105082

Plumlee, G. S., Morman, S. a., & Ziegler, T. L. (2006). The Toxicological Geochemistry of Earth Materials: An Overview of Processes and the Interdisciplinary Methods Used to Understand Them. *Reviews in Mineralogy and Geochemistry*, *64*, 5–57. doi:10.2138/rmg.2006.64.2

Podesta, J. E., Al-Jamal, K. T., Herrero, M. a., Tian, B., Ali-Boucetta, H., Hegde, V., … Kostarelos, K. (2009). Antitumor activity and prolonged survival by carbon-nanotube-mediated therapeutic sirna silencing in a human lung xenograft model. *Small*, *5*(10), 1176–1185. doi:10.1002/smll.200801572

Pogodin, S., & Baulin, V. A. (2010). Can a Carbon Nanotube Pierce through a Phospholipid Bilayer?, *4*(9), 5293–5300.

Porter, A. E., Gass, M., Muller, K., Skepper, J. N., Midgley, P. a, & Welland, M. (2007). Direct imaging of single-walled carbon nanotubes in cells. *Nature Nanotechnology*, *2*(11), 713–7. doi:10.1038/nnano.2007.347

Porter, D. W., Hubbs, A. F., Chen, B. T., McKinney, W., Mercer, R. R., Wolfarth, M. G., … Vincent, C. (2013). Acute pulmonary dose-responses to inhaled multi-walled carbon nanotubes. *Nanotoxicology*, *7*(7), 1179–94. doi:10.3109/17435390.2012.719649

Porter, D. W., Hubbs, A. F., Mercer, R. R., Wu, N., Wolfarth, M. G., Sriram, K., … Castranova, V. (2010). Mouse pulmonary dose- and time course-responses induced by exposure to multi-walled carbon nanotubes. *Toxicology*, *269*(2-3), 136–47. doi:10.1016/j.tox.2009.10.017

Potocnik, J. (2011). Commission Recommendation of 18 October 2011 on the definition of nanomaterial. *Official Journal of the European Union*.

Potter, M. D., Barbero, S., & Cheresh, D. a. (2005). Tyrosine phosphorylation of VE-cadherin prevents binding of p120- and β-catenin and maintains the cellular mesenchymal state. *Journal of Biological Chemistry*, *280*(36), 31906–31912. doi:10.1074/jbc.M505568200

Prasain, N., & Stevens, T. (2009). The actin cytoskeleton in endothelial cell phenotypes. *Microvascular Research*, *77*(1), 53–63. doi:10.1016/j.mvr.2008.09.012

Pulskamp, K., Diabaté, S., & Krug, H. F. (2007). Carbon nanotubes show no sign of acute toxicity but induce intracellular reactive oxygen species in dependence on contaminants. *Toxicology Letters*, *168*(1), 58–74. doi:10.1016/j.toxlet.2006.11.001

Qiang, S., Wu, M. H., & Yuan, S. Y. (2009). Endothelial contractile cytoskeleton and microvascular permeability. *Cell Health Cytoskelet.*, *2009*(1), 43–50.

Radomski, A., Jurasz, P., Alonso-Escolano, D., Drews, M., Morandi, M., Malinski, T., & Radomski, M. W. (2005). Nanoparticle-induced platelet aggregation and vascular thrombosis. *British Journal of Pharmacology*, *146*(6), 882–93. doi:10.1038/sj.bjp.0706386

Raffa, V., Ciofani, G., Vittorio, O., Riggio, C., & Cuschieri, A. (2010). Physicochemical properties affecting cellular uptake of carbon nanotubes. *Nanomedicine*, *5*(1), 89–97.

Rao, R. M., Yang, L., Garcia-Cardena, G., & Luscinskas, F. W. (2007). Endothelial-dependent mechanisms of leukocyte recruitment to the vascular wall. *Circulation Research*, *101*(3), 234–47. doi:10.1161/CIRCRESAHA.107.151860b

Reddy, a R. N., Krishna, D. R., Reddy, Y. N., & Himabindu, V. (2010). Translocation and extra pulmonary toxicities of multi wall carbon nanotubes in rats. *Toxicology Mechanisms and Methods*, *20*(5), 267–72. doi:10.3109/15376516.2010.484077

Reed, D. M., Paschalaki, K. E., Starke, R. D., Mohamed, N. a., Sharp, G., Fox, B., … Mitchell, J. a. (2015). An autologous endothelial cell:peripheral blood mononuclear cell assay that detects cytokine storm responses to biologics. *The FASEB Journal*. doi:10.1096/fj.14-268144

Rejman, J., Oberle, V., Zuhorn, I. S., & Hoekstra, D. (2004). Size-dependent internalization of particles via the pathways of clathrin- and caveolae-mediated endocytosis. *Biochemical Journal*, *377*(1), 159–169.

Ridker, P. M., Buring, J. E., & Rifai, N. (2001). Soluble P-selectin and the Risk of Future Cardiovascular Events. *Circulation*, *103*, 491–495. doi:10.1161/01.CIR.0000104566.10178.AF

Roche Diagnostics Ltd. (2011). Cytotoxicity Detection Kit (LDH). Version 08. West Sussex, UK.

Rogueda, P. G., & Traini, D. (2007). The nanoscale in pulmonary delivery. Part 1: deposition, fate, toxicology and effects. *Expert Opinion on Drug Delivery*, *4*(6), 595–606. doi:10.1517/17425247.4.6.595

Rothen-Rutishauser, B., Kiama, S. G., & Gehr, P. (2005). A three-dimensional cellular model of the human respiratory tract to study the interaction with particles. *American Journal of Respiratory Cell and Molecular Biology*, *32*(4), 281–289. doi:10.1165/rcmb.2004-0187OC

Rothen-Rutishauser, B., Mueller, L., Blank, F., Brandenberger, C., Muehlfeld, C., & Gehr, P. (2008). A newly developed in vitro model of the human epithelial airway barrier to study the toxic potential of nanoparticles. *ALTEX : Alternativen Zu Tierexperimenten*, *25*, 191–196. doi:10.1517/17425255.4.8.1075

Rotoli, B. M., Bussolati, O., Barilli, a, Zanello, P. P., Bianchi, M. G., Magrini, a, … Bergamaschi, E. (2009). Airway barrier dysfunction induced by exposure to carbon nanotubes in vitro: which role for fiber length? *Human & Experimental Toxicology*, *28*(6-7), 361–368. doi:10.1177/0960327109105159

Rotoli, B. M., Bussolati, O., Bianchi, M. G., Barilli, A., Balasubramanian, C., Bellucci, S., & Bergamaschi, E. (2008). Non-functionalized multi-walled carbon nanotubes alter the paracellular permeability of human airway epithelial cells. *Toxicology Letters*, *178*(2), 95–102. doi:10.1016/j.toxlet.2008.02.007

Sabatier, F. (2002). Interaction of endothelial microparticles with monocytic cells in vitro induces tissue factor-dependent procoagulant activity. *Blood*, *99*(11), 3962–3970. doi:10.1182/blood.V99.11.3962

Saber, A. T., Jacobsen, N. R., Jackson, P., Poulsen, S. S., Kyjovska, Z. O., Halappanavar, S., … Vogel, U. (2014). Particle-induced pulmonary acute phase response may be the causal link between particle inhalation and cardiovascular disease. *Wiley Interdisciplinary Reviews. Nanomedicine and Nanobiotechnology*. doi:10.1002/wnan.1279

Sakhtianchi, R., Minchin, R. F., Lee, K. B., Alkilany, A. M., Serpooshan, V., & Mahmoudi, M. (2013). Exocytosis of nanoparticles from cells: Role in cellular retention and toxicity. *Advances in Colloid and Interface Science*, *201-202*, 18–29. doi:10.1016/j.cis.2013.10.013

Sallenave, J. (2000). The role of secretory leukocyte proteinase inhibitor and elafin (elastase-specific inhibitor/skin-derived antileukoprotease) as alarm antiproteinases in inflammatory lung disease. *Respiratory Research*, *1*, 87–92.

Saptarshi, S. R., Duschl, A., & Lopata, A. L. (2013). Interaction of nanoparticles with proteins: relation to bio-reactivity of the nanoparticle. *Journal of Nanobiotechnology*, *11*(1), 26. doi:10.1186/1477-3155-11-26

Sato, Y., Yokoyama, A., Shibata, K., Akimoto, Y., Ogino, S., Nodasaka, Y., … Tohji, K. (2005). Influence of length on cytotoxicity of multi-walled carbon nanotubes against human acute monocytic leukemia cell line THP-1 in vitro and subcutaneous tissue of rats in vivo. *Molecular bioSystems*, *1*(2), 176–182. doi:10.1039/b502429c

Sayes, C. M., Reed, K. L., & Warheit, D. B. (2007). Assessing toxicity of fine and nanoparticles: comparing in vitro measurements to in vivo pulmonary toxicity profiles. *Toxicological Sciences : An Official Journal of the Society of Toxicology*, *97*(1), 163–80. doi:10.1093/toxsci/kfm018

Scheinberg, D. a, McDevitt, M. R., Dao, T., Mulvey, J. J., Feinberg, E., & Alidori, S. (2013). Carbon nanotubes as vaccine scaffolds. *Advanced Drug Delivery Reviews*, *65*(15), 2016–22. doi:10.1016/j.addr.2013.07.013

Schindelin, J., Arganda-Carreras, I., Frise, E., Kaynig, V., Longair, M., Pietzsch, T., … Cardona, A. (2012). Fiji: an open-source platform for biological-image analysis. *Nature Methods*, *9*(7), 676–82. doi:10.1038/nmeth.2019

Schleh, C., Kreyling, W. G., & Lehr, C.-M. (2013). Pulmonary surfactant is indispensable in order to simulate the in vivo situation. *Particle and Fibre Toxicology*, *10*(1), 6. doi:10.1186/1743-8977-10-6

Schmid, O., Möller, W., Semmler-Behnke, M., Ferron, G. a, Karg, E., Lipka, J., … Stoeger, T. (2009). Dosimetry and toxicology of inhaled ultrafine particles. *Biomarkers : Biochemical Indicators of Exposure, Response, and Susceptibility to Chemicals*, *14 Suppl 1*(2), 67–73. doi:10.1080/13547500902965617

Schwartz, J., & Morris, R. (1995). Air pollution and hospital admissions for cardiovascular disease in Detroit, Michigan. *American Journal of Epidemiology*, *142*(1), 23–35. doi:10.1097/00001648-199707000-00004

Seagrave, J., McDonald, J. D., Gigliotti, A. P., Nikula, K. J., Seilkop, S. K., Gurevich, M., & Mauderly, J. L. (2002). Mutagenicity and in Vivo Toxicity of Combined Particulate and Semivolatile Organic Fractions of Gasoline and Diesel Engine Emissions. *Toxicological Sciences* , *70* (2), 212–226. doi:10.1093/toxsci/70.2.212

Seagrave, J., McDonald, J. D., & Mauderly, J. L. (2005). In vitro versus in vivo exposure to combustion emissions. *Experimental and Toxicologic Pathology*, *57*(SUPPL. 1), 233–238. doi:10.1016/j.etp.2005.05.011

Seaton, A., Soutar, A., Crawford, V., Elton, R., McNerlan, S., Cherrie, J., … Stout, R. (1999). Particulate air pollution and the blood. *Thorax*, *54*(11), 1027–1032. doi:10.1136/thx.54.11.1027

Seaton, A., Tran, L., Aitken, R., & Donaldson, K. (2010). Nanoparticles, human health hazard and regulation. *Journal of the Royal Society, Interface / the Royal Society*, *7 Suppl 1*, S119–S129. doi:10.1098/rsif.2009.0252.focus

Segal, B. H., Grimm, M. J., Khan, a. N. H., Han, W., & Blackwell, T. S. (2012). Regulation of innate immunity by NADPH oxidase. *Free Radical Biology and Medicine*, *53*(1), 72–80. doi:10.1016/j.freeradbiomed.2012.04.022

Semmler, M., Seitz, J., Erbe, F., Mayer, P., Heyder, J., Oberdörster, G., & Kreyling, W. G. (2004). Long-term clearance kinetics of inhaled ultrafine insoluble iridium particles from the rat lung, including transient translocation into secondary organs. *Inhalation Toxicology*, *16*(6-7), 453–459. doi:10.1080/08958370490439650

Setyawati, M. I., Tay, C. Y., Chia, S. L., Goh, S. L., Fang, W., Neo, M. J., … Leong, D. T. (2013). Titanium dioxide nanomaterials cause endothelial cell leakiness by disrupting

the homophilic interaction of VE-cadherin. *Nature Communications*, *4*, 1673. doi:10.1038/ncomms2655

Shannahan, J. H., Kodavanti, U. P., & Brown, J. M. (2012). Manufactured and airborne nanoparticle cardiopulmonary interactions: a review of mechanisms and the possible contribution of mast cells. *Inhalation Toxicology*, *24*(5), 320–339. Retrieved from http://dx.doi.org/10.3109/08958378.2012.668229

Shantsila, E., & Lip, G. Y. H. (2009). The endothelium and thrombotic risk in heart failure. *Thrombosis and Haemostasis*, *102*(2), 185–7. doi:10.1160/TH09-06-0344

Shi, X., von dem Bussche, A., Hurt, R. H., Kane, A. B., & Gao, H. (2011). Cell entry of one-dimensional nanomaterials occurs by tip recognition and rotation. *Nature Nanotechnology*, *6*(11), 714–719. doi:10.1038/nnano.2011.151

Shvedova, A. A., Kisin, E., Murray, A. R., Johnson, V. J., Gorelik, O., Arepalli, S., … Kagan, V. E. (2008). Inhalation vs. aspiration of single-walled carbon nanotubes in C57BL/6 mice: inflammation, fibrosis, oxidative stress, and mutagenesis. *American Journal of Physiology. Lung Cellular and Molecular Physiology*, *295*(4), L552–65. doi:10.1152/ajplung.90287.2008

Shvedova, A. A., Kisin, E. R., Mercer, R., Murray, A. R., Johnson, V. J., Potapovich, A. I., … Baron, P. (2005). Unusual inflammatory and fibrogenic pulmonary responses to single-walled carbon nanotubes in mice. *American Journal of Physiology. Lung Cellular and Molecular Physiology*, *289*(5), L698–708. doi:10.1152/ajplung.00084.2005

Shvedova, A. A., Yanamala, N., Kisin, E. R., Tkach, a V, Murray, a R., Hubbs, A., … Castranova, V. (2014). Long-term effects of carbon containing engineered nanomaterials and asbestos in the lung: one year postexposure comparisons. *Am J Physiol Lung Cell Mol Physiol*, *306*(2), L170–82. doi:10.1152/ajplung.00167.2013

Silva, R. M., Anderson, D. S., Franzi, L. M., Peake, J. L., Edwards, P. C., Van Winkle, L. S., & Pinkerton, K. E. (2015). Pulmonary Effects of Silver Nanoparticle Size, Coating, and Dose over Time upon Intratracheal Instillation. *Toxicological Sciences*, *144*(1), 151–162. doi:10.1093/toxsci/kfu265

Simeonova, P. P., & Erdely, A. (2009). Engineered nanoparticle respiratory exposure and potential risks for cardiovascular toxicity: predictive tests and biomarkers. *Inhalation Toxicology*, *21 Suppl 1*(April), 68–73. doi:10.1080/08958370902942566

Sinha, N., & Yeow, J. T. W. (2005). Carbon nanotubes for biomedical applications. *IEEE Transactions on Nanobioscience*, *4*(2), 180–195. doi:10.1109/TNB.2005.850478

Smyth, E., Solomon, A., Vydyanath, A., Luther, P. K., Pitchford, S., Tetley, T. D., & Emerson, M. (2014). Induction and enhancement of platelet aggregation in vitro and in vivo by model polystyrene nanoparticles. *Nanotoxicology*, *5390*(3), 1–9. doi:10.3109/17435390.2014.933902

Snyder-Talkington, B. N., Schwegler-Berry, D., Castranova, V., Qian, Y., & Guo, N. L. (2013). Multi-walled carbon nanotubes induce human microvascular endothelial cellular

effects in an alveolar-capillary co-culture with small airway epithelial cells. *Particle and Fibre Toxicology*, *10*(1), 35. doi:10.1186/1743-8977-10-35

Song, Y., Li, X., & Du, X. (2009). Exposure to nanoparticles is related to pleural effusion, pulmonary fibrosis and granuloma. *European Respiratory Journal*, *34*(3), 559–567. doi:10.1183/09031936.00178308

Springer, T. A. (1990). Adhesion receptors of the immune system. *Nature*, *346*(6283), 425–434. Retrieved from http://dx.doi.org/10.1038/346425a0

Srivastava, R. K., Pant, A. B., Kashyap, M. P., Kumar, V., Lohani, M., Jonas, L., & Rahman, Q. (2011). Multi-walled carbon nanotubes induce oxidative stress and apoptosis in human lung cancer cell line-A549. *Nanotoxicology*, *5*(2), 195–207. doi:10.3109/17435390.2010.503944

Steffel, J., Lüscher, T. F., & Tanner, F. C. (2006). Tissue factor in cardiovascular diseases: molecular mechanisms and clinical implications. *Circulation*, *113*(5), 722–31. doi:10.1161/CIRCULATIONAHA.105.567297

Stevens, T. (2011). Functional and Molecular Heterogeneity of Pulmonary Endothelial Cells. *Proceedings of the American Thoracic Society*, *8*(6), 453–457. Retrieved from http://pats.atsjournals.org/content/8/6/453.abstract

Stone, V., Johnston, H., & Clift, M. J. D. (2007). Air pollution, ultrafine and nanoparticle toxicology: cellular and molecular interactions. *IEEE Transactions on Nanobioscience*, *6*(4), 331–40. Retrieved from http://www.ncbi.nlm.nih.gov/pubmed/18217626

Sun, J., Wang, S., Zhao, D., Hun, F. H., Weng, L., & Liu, H. (2011). Cytotoxicity, permeability, and inflammation of metal oxide nanoparticles in human cardiac microvascular endothelial cells: cytotoxicity, permeability, and inflammation of metal oxide nanoparticles. *Cell Biology and Toxicology*, *27*(5), 333–42. doi:10.1007/s10565-011-9191-9

Swain, R. J., Kemp, S. J., Goldstraw, P., Tetley, T. D., & Stevens, M. M. (2010). Assessment of cell line models of primary human cells by Raman spectral phenotyping. *Biophysical Journal*, *98*(8), 1703–11. doi:10.1016/j.bpj.2009.12.4289

Sweeney, S., Berhanu, D., Misra, S. K., Thorley, A. J., Valsami-Jones, E., & Tetley, T. D. (2014). Multi-walled carbon nanotube length as a critical determinant of bioreactivity with primary human pulmonary alveolar cells. *Carbon*, 1–12. doi:10.1016/j.carbon.2014.06.033

Tanaka, K. a, Key, N. S., & Levy, J. H. (2009). Blood coagulation: hemostasis and thrombin regulation. *Anesthesia and Analgesia*, *108*(5), 1433–46. doi:10.1213/ane.0b013e31819bcc9c

Tao, F., & Kobzik, L. (2002). Lung Macrophage – Epithelial Cell Interactions Amplify Particle-Mediated Cytokine Release. *American Journal of Respiratory Cell and Molecular Biology*, *26*(4), 499–505.

Thorley, A. J., Grandolfo, D., Lim, E., Goldstraw, P., Young, A., & Tetley, T. D. (2011). Innate Immune Responses to Bacterial Ligands in the Peripheral Human Lung - Role of Alveolar Epithelial TLR Expression and Signalling. *PLoS ONE*, *6*(7), e21827. Retrieved from http://dx.doi.org/10.1371/journal.pone.0021827

Thorley, A. J., Ruenraroengsak, P., Potter, T. E., & Tetley, T. D. (2014). Critical Determinants of Uptake and Translocation of Nanoparticles by the Human Pulmonary Alveolar Epithelium. *ACS Nano*, (11), 11778–11789.

Thorley, A. J., & Tetley, T. D. (2013). New perspectives in nanomedicine. *Pharmacology and Therapeutics*, *140*(2), 176–185. doi:10.1016/j.pharmthera.2013.06.008

Turowski, P., Martinelli, R., Crawford, R., Wateridge, D., Papageorgiou, A.-P., Lampugnani, M. G., … Greenwood, J. (2008). Phosphorylation of vascular endothelial cadherin controls lymphocyte emigration. *Journal of Cell Science*, *121*(Pt 1), 29–37. doi:10.1242/jcs.022681

Unger, R. E., Krump-Konvalinkova, V., Peters, K., & Kirkpatrick, C. J. (2002). In vitro expression of the endothelial phenotype: comparative study of primary isolated cells and cell lines, including the novel cell line HPMEC-ST1.6R. *Microvascular Research*, *64*(3), 384–397. doi:10.1006/mvre.2002.2434

Ursini, C. L., Cavallo, D., Fresegna, A. M., Ciervo, A., Maiello, R., Buresti, G., … Iavicoli, S. (2014). Differences in Cytotoxic, Genotoxic, and Inflammatory Response of Bronchial and Alveolar Human Lung Epithelial Cells to Pristine and COOH-Functionalized Multiwalled Carbon Nanotubes. *BioMed Research International*, *2014*, 359506. doi:10.1155/2014/359506

Vaccaro, C. a, & Brody, J. S. (1981). Structural Features of Alveolar Wal l Basement Membrane in the Adult Rat Lung. *Journal of Cell Biology*, *91*(11), 427–437. doi:10.1083/jcb.91.2.427

Van den Bogaard, E. H. J., Dailey, L. A., Thorley, A. J., Tetley, T. D., & Forbes, B. (2009). Inflammatory Response and Barrier Properties of a New Alveolar Type 1-Like Cell Line (TT1). *Pharmaceutical Research*, *26*(5), 1172–1180. doi:10.1007/s11095-009-9838-x

Van der Wal, a C., Das, P. K., Tigges, a J., & Becker, a E. (1992). Adhesion molecules on the endothelium and mononuclear cells in human atherosclerotic lesions. *The American Journal of Pathology*, *141*(6), 1427–33. Retrieved from http://www.pubmedcentral.nih.gov/articlerender.fcgi?artid=1886778&tool=pmcentrez&rendertype=abstract

Van Eeden, S., Leipsic, J., Paul Man, S. F., & Sin, D. D. (2012). The relationship between lung inflammation and cardiovascular disease. *American Journal of Respiratory and Critical Care Medicine*, *186*(1), 11–6. doi:10.1164/rccm.201203-0455PP

Van Hinsbergh, V. W. M. (2012). Endothelium--role in regulation of coagulation and inflammation. *Seminars in Immunopathology*, *34*(1), 93–106. doi:10.1007/s00281-011-0285-5

Van Wetering, S., van Buul, J. D., Quik, S., Mul, F. P. J., Anthony, E. C., ten Klooster, J.-P., … Hordijk, P. L. (2002). Reactive oxygen species mediate Rac-induced loss of cell-cell adhesion in primary human endothelial cells. *Journal of Cell Science*, *115*(Pt 9), 1837–46. Retrieved from http://www.ncbi.nlm.nih.gov/pubmed/11956315

Vincent, P. a, Xiao, K., Buckley, K. M., & Kowalczyk, A. P. (2004). VE-cadherin: adhesion at arm's length. *American Journal of Physiology. Cell Physiology*, *286*(5), C987–97. doi:10.1152/ajpcell.00522.2003

Walczyk, D., Bombelli, F. B., Monopoli, M. P., Lynch, I., & Dawson, K. a. (2010). What the cell "sees" in bionanoscience. *Journal of the American Chemical Society*, *132*(19), 5761–5768. doi:10.1021/ja910675v

Walker, V. G., Li, Z., Hulderman, T., Schwegler-Berry, D., Kashon, M. L., & Simeonova, P. P. (2009). Potential in vitro effects of carbon nanotubes on human aortic endothelial cells. *Toxicology and Applied Pharmacology*, *236*(3), 319–28. doi:10.1016/j.taap.2009.02.018

Wang, X., Katwa, P., Podila, R., Chen, P., Ke, P. C., Rao, A. M., … Brown, J. M. (2011). Multi-walled carbon nanotube instillation impairs pulmonary function in C57BL/6 mice. *Particle and Fibre Toxicology*, *8*, 24. doi:10.1186/1743-8977-8-24

Weichenthal, S. (2012). Selected physiological effects of ultrafine particles in acute cardiovascular morbidity. *Environmental Research*, *115*, 26–36. doi:10.1016/j.envres.2012.03.001

Wenzel, K., Ernst, M., Rohde, K., Baumann, G., & Speer, A. (1996). DNA polymorphisms in adhesion molecule genes - a new risk factor for early atherosclerosis. *Human Genetics*, *97*, 15–20.

Wichmann, H. E., & Peters, A. (2000). Epidemiological evidence of the effects of ultrafine particle exposure. *Philosophical Transactions of The Royal Society London A.*, *358*, 2751–2769.

Wick, P., Manser, P., Limbach, L. K., Dettlaff-Weglikowska, U., Krumeich, F., Roth, S., … Bruinink, A. (2007). The degree and kind of agglomeration affect carbon nanotube cytotoxicity. *Toxicology Letters*, *168*(2), 121–131. doi:10.1016/j.toxlet.2006.08.019

Witherden, I. R., & Tetley, T. D. (2001). Isolation and Culture of Human Alveolar Type II Pneumocytes. In D. F. Rogers & L. E. Donnelly (Eds.), (pp. 137–146). Totowa, NJ: Humana Press Inc.

Witherden, I. R., Vanden Bon, E. J., Goldstraw, P., Ratcliffe, C., Pastorino, U., & Tetley, T. D. (2004). Primary human alveolar type II epithelial cell chemokine release: effects of cigarette smoke and neutrophil elastase. *American Journal of Respiratory Cell and Molecular Biology*, *30*(4), 500–509. doi:10.1165/rcmb.4890

Wohlstadter, J. N., Wilbur, J. L., Sigal, G. B., Biebuyck, H. a., Billadeau, M. a., Dong, L., … Wohlstadter, S. J. (2003). Carbon nanotube-based biosensor. *Advanced Materials*, *15*(14), 1184–1187. doi:10.1002/adma.200304259

Wong, B. S., Yoong, S. L., Jagusiak, A., Panczyk, T., Ho, H. K., Ang, W. H., & Pastorin, G. (2013). Carbon nanotubes for delivery of small molecule drugs. *Advanced Drug Delivery Reviews*, *65*(15), 1964–2015. doi:10.1016/j.addr.2013.08.005

World Health Organisation (WHO). (2014). *World Health Statistics 2014*. Geneva. Retrieved from http://apps.who.int/iris/bitstream/10665/112738/1/9789240692671_eng.pdf?ua=1

Worle-Knirsch, J. M., Pulskamp, K., & Krug, H. F. (2006). Oops They Did It Again! Carbon Nanotubes Hoax Scientists in Viability Assays. *Nano Letters*, *6*(6), 1261–1268. Retrieved from http://pubs.acs.org/doi/abs/10.1021/nl060177c

Wottrich, R., Diabaté, S., & Krug, H. F. (2004). Biological effects of ultrafine model particles in human macrophages and epithelial cells in mono- and co-culture. *International Journal of Hygiene and Environmental Health*, *207*(4), 353–361. doi:10.1078/1438-4639-00300

Wu, W., Wieckowski, S., Pastorin, G., Benincasa, M., Klumpp, C., Briand, J. P., … Bianco, A. (2005). Targeted delivery of amphotericin B to cells by using functionalized carbon nanotubes. *Angewandte Chemie - International Edition*, *44*(39), 6358–6362. doi:10.1002/anie.200501613

Wynn, T. a. (2011). Integrating mechanisms of pulmonary fibrosis. *The Journal of Experimental Medicine*, *208*(7), 1339–1350. doi:10.1084/jem.20110551

Xiao, K., Garner, J., Buckley, K. M., Vincent, P. A., Chiasson, C. M., Dejana, E., … Kowalczyk, A. P. (2005). p120-Catenin Regulates Clathrin-dependent Endocytosis of VE-Cadherin. *Molecular Biology of the Cell*, *16*, 5141–5151. doi:10.1091/mbc.E05

Xu, J., Lupu, F., & Esmon, C. T. (2010). Inflammation , innate immunity and blood coagulation. *Hamostaseologie*, *30*(9), 5–9.

Xu, Y.-Y., Yang, J., Shen, T., Zhou, F., Xia, Y., Fu, J.-Y., … Zhu, X.-Q. (2012). Intravenous Administration of Multi-walled Carbon Nanotubes Affects the Formation of Atherosclerosis in Sprague-Dawley Rats. *Journal of Occupational Health*, *54*(5), 361–369. doi:10.1539/joh.12-0019-OA

Yacobi, N. R., Malmstadt, N., Fazlollahi, F., DeMaio, L., Marchelletta, R., Hamm-Alvarez, S. F., … Crandall, E. D. (2010). Mechanisms of Alveolar Epithelial Translocation of a Defined Population of Nanoparticles. *American Journal of Respiratory Cell and Molecular Biology*, *42*(5), 604–614. Retrieved from http://ajrcmb.atsjournals.org/cgi/content/abstract/42/5/604

Yacobi, N. R., Phuleria, H. C., Demaio, L., Liang, C. H., Peng, C. A., Sioutas, C., … Crandall, E. D. (2007). Nanoparticle effects on rat alveolar epithelial cell monolayer barrier properties. *Toxicology in Vitro*, *21*(8), 1373–1381. doi:10.1016/j.tiv.2007.04.003

Yamashita, K., Yoshioka, Y., Higashisaka, K., Morishita, Y., Yoshida, T., Fujimura, M., … Tsutsumi, Y. (2010). Carbon nanotubes elicit DNA damage and inflammatory response relative to their size and shape. *Inflammation*, *33*(4), 276–280. doi:10.1007/s10753-010-9182-7

Yang, H., Liu, C., Yang, D., Zhang, H., & Xi, Z. (2009). Comparative study of cytotoxicity, oxidative stress and genotoxicity induced by four typical nanomaterials: the role of particle size, shape and composition. *Journal of Applied Toxicology : JAT*, *29*(1), 69–78. doi:10.1002/jat.1385

Yang, S. -t., Guo, W., Lin, Y., Deng, X. -y., Wang, H. -f., Sun, H. -f., … Sun, Y.-P. (2007). Biodistribution of Pristine Single-Walled Carbon Nanotubes In Vivo. *Journal of Physical Chemistry C*, *111*(48), 17761–17764. doi:10.1021/jp070712c

Yang, W., Peters, J. I., & III, R. O. W. (2008). Inhaled nanoparticles—A current review. *International Journal of Pharmaceutics*, *356*(1-2), 239–247.

Ye, S., Wang, Y., Jiao, F., Zhang, H., Lin, C., Wu, Y., & Zhang, Q. (2011). The role of NADPH oxidase in multi-walled carbon nanotubes-induced oxidative stress and cytotoxicity in human macrophages. *Journal of Nanoscience and Nanotechnology*, *11*(5), 3773–3781. doi:10.1166/jnn.2011.3862

Yokohira, M., Kuno, T., Yamakawa, K., Hashimoto, N., Ninomiya, F., Suzuki, S., … Imaida, K. (2009). An Intratracheal Instillation Bioassay System for Detection of Lung Toxicity Due to Fine Particles in F344 Rats. *Journal of Toxicologic Pathology*, *22*(1), 1–10. doi:10.1293/tox.22.1

Yokohori, N., Aoshiba, K., & Nagai, A. (2004). Increased Levels of Cell Death and Proliferation in Alveolar Wall Cells in Patients With Pulmonary Emphysema *. *CHEST*, *125*(2), 626–632.

Yoshida, M., Takano, Y., Sasaoka, T., Izumi, T., & Kimura, A. (2003). E-selectin polymorphism associated with myocardial infarction causes enhanced leukocyte-endothelial interactions under flow conditions. *Arteriosclerosis, Thrombosis, and Vascular Biology*, *23*(5), 783–8. doi:10.1161/01.ATV.0000067427.40133.59

Zanello, L. P., Zhao, B., Hu, H., & Haddon, R. C. (2006). Bone cell proliferation on carbon nanotubes. *Nano Letters*, *6*(3), 562–7. doi:10.1021/nl051861e

Zhou, F., Wu, S., Wu, B., Chen, W. R., & Xing, D. (2011). Mitochondria-targeting single-walled carbon nanotubes for cancer photothermal therapy. *Small*, *7*(19), 2727–2735. doi:10.1002/smll.201100669

10. APPENDIX

Appendix I. Published works and copyright permissions. The following journal article detailing aspects of the work described in this thesis has been obtained with the relevant permissions from Elsevier, Licence Agreement number 3676170600813.

Biomaterials 35 (2014) 4729–4738

Contents lists available at ScienceDirect

Biomaterials

journal homepage: www.elsevier.com/locate/biomaterials

Aqueous cationic, anionic and non-ionic multi-walled carbon nanotubes, functionalised with minimal framework damage, for biomedical application

Shu Chen [a,1], Sheng Hu [b,1], Elizabeth F. Smith [c], Pakatip Ruenraroengsak [a], Andrew J. Thorley [c], Robert Menzel [b], Angela E. Goode [a], Mary P. Ryan [a], Teresa D. Tetley [c], Alexandra E. Porter [a], Milo S.P. Shaffer [b,*]

[a] Department of Materials and London Centre for Nanotechnology, Imperial College London, Exhibition Road, London SW7 2AZ, UK
[b] Department of Chemistry and London Centre for Nanotechnology, Imperial College London, Exhibition Road, London SW7 2AZ, UK
[c] National Heart and Lung Institute, Imperial College London, Dovehouse Street, London SW3 6LY, UK

ARTICLE INFO

Article history:
Received 6 January 2014
Accepted 4 February 2014
Available online 14 March 2014

Keywords:
Multiwalled carbon nanotubes
Thermal chemical functionalisation
Integrity structure
Surface charge
Cytotoxicity
Cell uptake

ABSTRACT

The use of a thermochemical grafting approach provides a versatile means to functionalise as-synthesised, bulk multi-walled carbon nanotubes (MWNTs) without altering their inherent structure. The associated retention of properties is desirable for a wide range of commercial applications, including for drug delivery and medical purposes; it is also pertinent to studies of intrinsic toxicology. A systematic series of water-compatible MWNTs, with diameter around 12 nm have been prepared, to provide structurally-equivalent samples predominantly stabilised by anionic, cationic, or non-ionic groups. The surface charge of MWNTs was controlled by varying the grafting reagents and subsequent post-functionalisation modifications. The degree of grafting was established by thermal analysis (TGA). High resolution transmission electron microscope (HRTEM) and Raman measurements confirmed that the structural framework of the MWNTs was unaffected by the thermochemical treatment, in contrast to a conventional acid-oxidised control which was severely damaged. The effectiveness of the surface modification was demonstrated by significantly improved solubility and stability in both water and cell culture medium, and further quantified by zeta-potential analysis. The grafted MWNTs exhibited relatively low bioreactivity on transformed human alveolar epithelial type 1-like cells (TT1) following 24 h exposure as demonstrated by 3-(4,5-dimethylthiazol-2-yl)-5-(3-carboxymethoxyphenyl)-2-(4-sulfophenyl)-2H-tetrazolium (MTS) and lactate dehydrogenase release (LDH) assays. The exposure of TT1 cells to MWNTs suppressed the release of the inflammatory mediators, interleukin 6 (IL-6) and interleukin 8 (IL-8). TEM cell uptake studies indicated efficient cellular entry of MWNTs into TT1 cells, via a range of mechanisms. Cationic MWNTs showed a more substantial interaction with TT1 cell membranes than anionic MWNTs, demonstrating a surface charge effect on cell uptake.

© 2014 Elsevier Ltd. All rights reserved.

1. Introduction

The biological interactions of carbon nanotubes (CNTs) are important for fundamental scientific studies [1,2], biomedical applications such as photothermal therapy [3,4], drug delivery [5,6] and bioimaging [7,8], and in order to understand their potential toxicities [5,9,10]. The poor solubility and lack of control over the physicochemical properties of CNTs have created significant obstacles to understanding their interactions with cells. Delivery of individualised CNTs either *in vitro* in cell medium or *in vivo* is rare, particularly for toxicology studies, in which agglomerated or even non-aqueous dispersions are commonly used. Surfactants, such as Triton X-100 [5,6,11] and sodium dodecyl sulphate (SDS) [7,8,12], can be used to stabilise aqueous dispersions but use is limited by surfactant toxicity which can cause confounding effects [9,10,13] and do not relate to many real life situations. In addition, surfactant dispersions are meta-stable, with a surface chemistry that evolves over time, and are generally unsuitable for *in vivo* use [14]. Where modified, water-stabilised CNTs have been used, the

* Corresponding author.
E-mail address: m.shaffer@imperial.ac.uk (M.S.P. Shaffer).
[1] These authors contributed equally to this work.

http://dx.doi.org/10.1016/j.biomaterials.2014.02.002
0142-9612/© 2014 Elsevier Ltd. All rights reserved.

chemistry or dispersion processes introduce damage or dimensional change [15,16], limiting controlled comparisons. Improved protocols are needed to produce water compatible CNTs with well-defined dimensions whilst minimising changes to their intrinsic properties. Furthermore, surface modification of MWNTs can provide a product with enhanced and desirable properties for medicinal and other purposes. In addition, reasonably large quantities are required for consistent sets of *in vivo* and *in vitro* experiments, as well as a wide range of other CNT applications [17,18] in which aqueous processing would be advantageous.

One of the most common approaches for preparing water dispersions of CNTs relies on oxidation using strong acids, particularly mixtures of HNO_3 and H_2SO_4 [19,20]. This covalent functionalisation method produces good aqueous dispersions [20], and provides a high degree of functionalisation with −COOH groups suitable for further modification [21,22]. However, CNT walls are inevitably etched, the length is significantly reduced [23,24], and the sample is contaminated with oxidation reaction debris, also known as carboxylated carbonaceous fragments (CCFs), which are difficult to completely remove [25–27], and may contribute to cytotoxic effects [28,29]. Although the cytotoxicity of the oxidation debris is not yet fully understood, it has been shown that these CCFs can significantly alter the physicochemical properties and biological interactions of the acid-oxidised CNTs [25,26,30,31]. Further, the oxidation reaction also introduces a wide range of different, oxygen-containing functional groups, obscuring the nature of the underlying CNTs and generating an ill-defined generally acidic surface. Derivitising these surface functional groups (or, in some cases, unremoved debris) to form other chemical functionalities does not counter the remaining fundamental drawbacks [32]. Other chemical methods have also been explored [33,34], but a versatile, scalable method for varying surface character independently of other characteristics is still needed. The recent development of a solvent-free thermochemical grafting approach offers advantages in the preparation of large quantities of clean, functionalised MWNTs with minimal framework damage [35]. The approach takes advantage of existing defective groups on the MWNT surface, remaining from the synthesis process, which decompose at high temperatures and generate free radicals, allowing covalent grafting of a range of monomers [35]. The intrinsic framework of the MWNTs is preserved and there is no production of debris or use of corrosive solutions. The approach is readily scalable as it is compatible with common chemical vapour deposition (CVD) capital infrastructure and can be operated to avoid time-consuming filtration steps. Here, this protocol was developed to produce water-compatible MWNTs with cationic, anionic or non-ionic character for biological studies. The vast majority of nanotubes produced commercially are multi-walled structures prepared by CVD; these materials are produced in significant quantities, by different companies, but with similar characteristics [36], and are most relevant to near term application and occupational hazards.

The effects of MWNTs on lung cells are particularly relevant to discovering possible nanotoxicological pathways, since inhalation is considered to be one of the greatest exposure risks [37,38]. Similar to other thin materials, regardless of length, MWNTs with diameters smaller than 1 μm are respirable and may be able to travel deeply into the lung alveolar region, where the thin gas–blood barrier (in some places <0.5 μm deep) is located to allow gas exchange [39,40]. Alveolar macrophages are the first line of defence against particulate material which deposit in the alveoli. Particles are taken up into macrophages through phagocytosis, and subsequently cleared out of the lung via the mucociliary escalator and lymphatic system. Particles that are not phagocytosed by macrophages will interact with the alveolar epithelium [40,41], which comprises a monolayer of alveolar type I (AT1) and alveolar type II (AT2) epithelial cells [42]. AT1 cells, which cover >95% of the alveolar surface area, are large squamous cells that facilitate gas exchange [43]. There is some concern that the interaction of high aspect ratio particles with alveolar epithelial cells could induce similar pathologies to those observed with high aspect ratio amphibole asbestos, including epithelial cell necrosis or apoptosis, release of pro-inflammatory cytokines, which could compromise the integrity of the epithelium, and increase the chance of particle translocation across the gas-blood barrier to the interstitium and systemic circulation [44].

This paper describes the generation and properties of a panel of surface functionalised MWNTs with anionic, cationic or non-ionic groups and high water solubility, relevant to a wide range of applications. Here, their bioreactivity with the human lung epithelium is studied *in vitro*. The effects on transformed human alveolar type 1-like epithelial cells (TT1) cell viability and mediator release have been assessed and the extent of uptake studied by TEM.

2. Materials and methods

2.1. Carbon nanotubes and chemicals

MWNTs (diameter 12.1 nm, s.d. 3.7 nm), synthesised by CVD, were obtained from Arkema SA (Lacq-Mourenx, France). Methyl methacrylate (MMA, >98.5%), 4-vinyl pyridine (4-VP, 95%), poly(ethylene glycol) methacrylate (PEGMA, average M_n = 530), 1-iodododecane (IDD, 98%), iodomethane (IMe, ≥ 99%), and lithium hydroxide (LiOH, 98%) were purchased from Sigma–Aldrich for MWNTs functionalisation. Before use, all chemicals were passed through a chromatographic column consisting of neutral and basic aluminium oxide powders (aluminium oxide 90 (0.063–0.200 mm), activity stage I for column chromatography, Merck Millipore, Germany) and further degassed by bubbling N_2 gas for 30 min, in order to remove radical inhibitors and oxygen.

2.2. Functionalisation of MWNTs

2.2.1. Thermochemical grafting

The thermal activation process was carried out in a custom-made 30 mm diameter quartz tube attached to a sample flask, and the whole setup was connected to a vacuum system. In a typical experiment, 100 mg MWNTs were heated to 1000 °C at a constant ramping rate of 10 °C/min under vacuum ($\sim 5 \times 10^{-4}$ mbar), in a three-zone tube furnace (PTF 12/38/500, Lenton Ltd, UK) and held at the activation temperature for 2 h. After the activation step, the quartz tube was slowly removed from the heating zone and allowed to cool to room temperature under vacuum. The MWNTs were then transferred to the connected round bottom flask by gravity. 8 mL of the reactant was then injected into the flask containing the thermally-activated MWNTs. The reaction mixture was stirred at room temperature overnight. The unreacted reactant was removed via filtration through a 0.45 μm pore size polytetrafluoroethylene (PTFE) membrane (Whatman, UK) under vacuum. The product was thoroughly washed with 3 × 90 mL of washing solvent, then dispersed in 90 mL of solvent and bath sonicated (USC300T, 45 kHz, 80W, VWR International, USA) for 15 min. The filtration–sonication cycle was repeated three times in order to remove any physically absorbed reactants. The functionalised MWNTs are named by the abbreviation of the grafted polymer: e.g. P(MMA)-MWNT. The other sample codes can be found in Table 1.

2.2.2. Synthesis of P(M4-VP)-MWNT

P(4-VP)-MWNTs (20 mg) were dispersed in 10 mL of methanol (99.8%, Sigma–Aldrich) by bath sonication for 5 min; IMe (3.12 mL, 50.0 mmol) was added dropwise, and the reaction mixture was heated to 60 °C overnight under N_2 atmosphere [45]. Afterwards, the mixture was cooled to room temperature and filtered through a 0.45 μm PTFE membrane. The MWNTs were washed with 3 × 30 mL of ethanol, then dispersed in 30 mL of ethanol and bath sonicated for 15 min. The filtration–sonication cycle was repeated three times in order to remove any physically absorbed reactants.

2.2.3. Synthesis of P(MAA)-MWNT

LiOH (40 mg) was dissolved in 20 mL 10:1 v/v THF/water cosolvent before adding 20 mg of P(MMA)-MWNT. The reaction mixture was bath sonicated for 5 min to obtain a good dispersion, and then stirred at room temperature overnight. Subsequently, 37% hydrochloric acid (HCl, AnalaR grade, BDH) was added drop-wise until the pH value of the solution reached pH 2 [46]. The mixture was stirred for another 12 h, then filtered on a 0.45 μm PTFE membrane, and washed with water (3 × 30 mL). The MWNT residue was dispersed in 30 mL of water by bath sonication for 15 min. The filtration–sonication cycle was repeated three times in order to remove any remaining salt and acid.

Table 1
Grafting ratios in weight loss, wt% (weight percentage of grafted oligomers in total grafted sample weight), grafting concentration (moles of monomer per gram of MWNTs) of MWNTs samples and estimated degree of polymerisation of monomers (monomer repeats), calculated based on TGA profiles (Fig. 1). Details of the grafting ratio calculations are described in the ESI-Figs. 1S–2S.

Sample code	Grafted compound (chemical name)	M_w	Grafting ratio (wt%)	Grafting concentration (μmol/g)	Monomer repeats
P(MMA)-MWNT	Methyl methacrylate	100.1	3.9	405	4.8
P(MAA)-MWNT	Methacrylic acid	86.1	3.4	409	4.9
P(4-VP)-MWNT	4-Vinylpyridine	105.1	4.1	407	4.8
P(M4-VP)-MWNT	N-methyl 4-vinylpyridine iodide	247.1	8.7	386	4.6
P(PEGMA)-MWNT	Poly (ethylene glycol) methacrylate	528.9	18.3	423	5.0
IDD-MWNT	1-Iodododecane	169.3	1.4	84	1

2.2.4. Acid oxidation functionalisation

In a typical reaction, 300 mg of Arkema MWNTs and 30 mL of concentrated sulphuric acid (A.R. grade, 98%, Sigma–Aldrich) mixed with nitric acid (puriss. p.a. plus, 65%, Fluka) with a volume ratio of 3:1 were heated to reflux at 120 °C. After 30 min, the reaction solution was cooled and then diluted with 500 mL of icy water [27]. In order to remove the carbonaceous debris generated, a base wash process was carried out [26]. The acid oxidised MWNTs (AO-MWNT) were first washed with distilled water through a sintered glass filter, using a 0.45 μm PTFE membrane, until the filtrate was colourless and the pH reached that of the distilled water (~5.5). Subsequently, the AO-MWNT were washed with approximately 500 mL of 0.01 mol/L sodium hydroxide (NaOH, AnalaR grade, BDH, UK), until the initially dark brown filtrate ran clear. The solution was then once again washed with distilled water until the filtrate reached neutral pH. Finally, the MWNTs were washed with approximately 500 mL of 0.01 mol/L HCl (AnalaR grade, BDH, UK) and then washed to neutral pH once again.

2.3. Characterisation of MWNTs

2.3.1. Electron microscopy

MWNTs were dispersed in HPLC water by bath sonication for 5 min, dropped on holey carbon copper TEM grids, and pre-dried for TEM imaging. Bright-field TEM (BF-TEM) imaging was carried out on an C_s-aberration-corrected FEI Titan 80/300 with an accelerating voltage of 80 kV, which is below the critical threshold energy predicted for severe knock-on damage in MWNTs [47]. A beam damage study confirmed that no visible damage to the MWNTs occurred during direct exposure to the beam with an electron dose of ~11000 electrons/nm^2/s for 60 min, in high resolution (HR)-TEM mode.

2.3.2. Thermogravimetric analysis (TGA)

TGA analyses were carried out using a Perkin Elmer Pyris 1, by heating 1.8 ± 0.2 mg MWNT samples to 100 °C, under a N_2 atmosphere (60 mL/min), and holding isothermally for 30 min to remove residual water and/or solvent; the temperature was then increased from 110 °C to 850 °C at a constant ramping rate of 10 °C/min under flowing N_2 (60 mL/min).

2.3.3. Zeta-potential measurement

Zeta-potential analyses were performed on a Brookhaven ZetaPALS. MWNT samples were dispersed in HPLC water with a concentration of 50 μg/mL by bath sonication for 15 min. The pH was adjusted using 0.1 or 0.01 M HCl/NaOH, measured by a digital pH meter (VWR sympHony™ meter, VWR International, USA).

2.3.4. Raman spectroscopy

Raman spectra (1000–1800 cm^{-1}) were collected on a LabRam Infinity Raman spectrometer, using a 532 nm laser (scan time 90 s, averagely 3 scan cycles). The average of D/G ratio was determined from the ratio of integrated areas under the Raman bands at around 1350 cm^{-1} (D-band) and 1580 cm^{-1} (G-band) respectively [48]. Average values and standard deviations were obtained from five independent measurements.

2.3.5. UV–vis spectroscopy

The water compatibility of MWNTs was characterised by UV-vis spectroscopy (Lambda 950, Perkin Elmer). For water solubility tests, as-received and functionalised MWNTs were bath sonicated (45 kHz, 80W, VWR International, USA) in HPLC water for 15 min with different initial powder loading concentrations of 100 μg/mL, 500 μg/mL, 1 mg/mL and 2 mg/mL. MWNT aggregates were settled by centrifugation for 15 min at 10, 000 g. For cell medium compatibility tests, as-received and functionalised MWNTs were bath sonicated (45 kHz, 80W, VWR International) in serum-free DCCM-1 tissue culture medium (Biological Industries Israel Beit-Haemek Ltd, Israel) for 15 min with 2 mg/mL initial powder loading concentrations. The supernatant was carefully decanted and the concentration of grafted MWNTs determined by UV absorbance and application of the Beer–Lambert law, $A = \varepsilon \times c \times d$, where A is the measured UV absorbance, ε is the extinction coefficient (35.10 mL·mg^{-1}·cm^{-1} for Arkema MWNTs at 800 nm [49]) and d is the light path length (1 cm cuvette length, in this study).

2.4. Endotoxin assay

Although, the thermal activation process guaranteed the sterility of the activated MWNTs [50], after synthesis the MWNTs were handled in a laminar flow cabinet to maintain sterility. An endotoxin assay was performed using LAL Chromogenic Endotoxin Quantitation Kit (Thermo Scientific, UK). All the glassware used for the CNT functionalisation, washing steps and LAL assay were used after oven sterilisation at 120 °C for at least 2 h.

2.5. Cell viability assay

2.5.1. Cell culture

Human TT1 cells are an immortal epithelial type I-like cell line derived from primary human AT2 cells [51]. TT1 cells were seeded at a density of 8000 cells per well in 96 well plates. The TT1 cells were cultured in DCCM-1 medium supplemented with 10% newborn calf serum (NCS), 100 U/ml penicillin, 100 μg/ml streptomycin and 2 mM glutamine. Once the cells reached confluence they were serum starved for 24 h prior to MWNT exposure.

2.5.2. MWNT exposures

Immediately prior to cell exposures, MWNTs were suspended in serum-free DCCM-1 at a concentration of 1 mg/mL, vortexed for 1 min and then sonicated in a water bath (42 kHz, 135 W, VWR International, USA) for 10 min. This stock solution was diluted in DCCM-1 to the required doses (0–50 μg/mL) and sonicated briefly prior to cell exposure. The cells were exposed to MWNTs with required doses (0–50 μg/mL) for 24 h. All exposures were performed in triplicate.

2.5.3. MTS assay

MTS is a tetrazolium compound that can be reduced by dehydrogenase enzymes within living cells demonstrating metabolic activity and cell viability. Such reduction in the presence of an electron coupling reagent, phenazineethosulfate (MPS), results in the production of formazan which is soluble in tissue culture medium; the absorbance of this formazan product was measured at a wavelength of 492 nm using spectrophotometer Following exposure to the MWNTs, cells were washed with PBS and incubated with medium containing MTS reagent (CellTiter 96® AQueous One Solution Assay, Promega, USA) according to the manufacturer's protocol.

2.5.4. LDH assay

LDH is a soluble cytosolic enzyme, the release of which is associated with the damage of cell plasma membrane and cell necrosis. The LDH assay was performed on the cell supernatants collected following the exposure, according to the manufacturer's instructions (Roche Applied Science, Indianapolis, USA). To control for residual particles, MWNT agglomerates were removed by centrifugation at 3000 rpm and the absorbance of the medium was determined at 492 nm prior to the LDH assay. The background absorbance of the conditioned medium was subtracted from the final absorbance value obtained upon analysis.

2.6. IL6/IL8 detection assay

Interleukin 8 (IL8) and interleukin 6 (IL6) are chemokines that can be produced by epithelial cells and are often cited as inflammatory mediators. Cell supernatants were collected from experiments performed in an identical manner to those described above and the concentration the inflammatory mediators IL-6 and IL-8 was determined using a sandwich ELISA according to the manufacturer's protocol (R&D Systems, Ltd, UK).

2.7. TEM cell uptake study

Functionalised MWNTs were first sonicated in a water bath (45 kHz, 80W, VWR International, USA) in HPLC water for 15 min with initial powder loading concentration of 1 mg/mL. MWNT aggregates were pelleted out by centrifugation for 15 min at 10,000 g, and the supernatants, containing dispersed MWNTs were used for cell

exposure studies. TT1 cells were seeded on 24 well plates to reach 100% confluence, as described above, and cells were then serum starved for 24 h before exposure to MWNT suspensions at a concentration of 5 μg/mL. After 24 h exposure, the cells were rinsed with HEPES buffer and were then fixed with 2.5% glutaraldehyde for 1 h. The samples were post-fixed in 1% osmium tetroxide for 30 min. Each sample was then dehydrated in a graded ethanol series of 50%, 70%, 90% and 100% (volume ratio of ethanol to DI-H_2O) ethanol for 15 min (3×) each, all at room temperature. After dehydration, samples were progressively infiltrated with 25% and 50% araldite resin/ethanol solution (Agar Scientific, UK) and each well was incubated for 15 min (2×), at room temperature, followed by infiltration in 100% resin. The specimens were then embedded into resin. The embedded cell monolayers were cut using an ultramicrotome with a 35° diamond knife to a thickness of 50–100 nm. The obtained sections were observed in a JEOL 2000 transmission electron microscope operated at an accelerating voltage of 80 kV. Multiple cells (>100 per sample) from three cell exposures were surveyed by TEM.

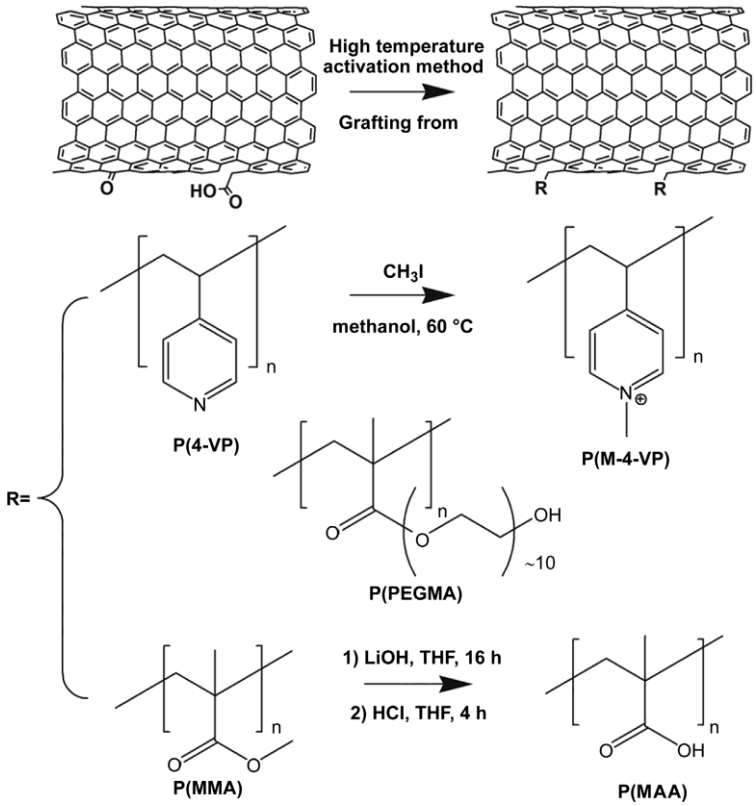
3. Results and discussion

The functionalised MWNTs (*f*-MWNTs) were prepared using an adaptation of the solvent-free thermochemical 'grafting from' protocols reported previously [35], taking advantage of pre-existing surface oxides on as-received MWNTs rather than an explicit oxidation step. The concentration of oxygen on the surface of typical ~10 nm (diameter) CVD MWNTs, as synthesised, is approximately one oxygen per 100–250 surface carbons [36]; some fraction of these groups will be suitable for generating radicals upon activation.

To prepare negatively-charged MWNTs (P(MAA)-MWNT), hydrophobic methyl methacrylate grafted MWNTs were hydrolysed in alkaline solution in order to generate carboxylic acid groups. 4-vinyl pyridine (4-VP) is a weak base [52], therefore, P(4-VP)-MWNT can provide a positive surface charge when protonated; in order to obtain more stable charges on the surface of MWNTs, a quaternisation reaction was carried out, through methylation of the pyridyl groups, to introduce positive charge onto the surface of the MWNTs. Non-ionic stabilisation was provided by grafting a side chain polyethylene glycol methacrylate (PEGMA) monomer (Scheme 1).

3.1. TGA analysis

The grafting ratio and degrees of polymerisation were characterised based on TGA analysis. As shown in Fig. 1 and SI-Fig. 1S, the TGA profile of grafted MWNTs displayed weight losses in the range 200–800 °C, in contrast to as-received (AR) and non-grafted thermal treated control (TTC) MWNTs, which can be attributed to the decomposition of the grafted organic oligomers. This step indicates the successful oligomer/polymer grafting. The grafting ratio was calculated based on the difference between the weight loss of the functionalised MWNTs and a thermally treated control (TTC) MWNTs, in order to exclude any effect of minor volatile/adsorbed impurities within the as-received (AR) MWNTs. The TTC sample was obtained using same activation protocol as functionalisation,



Scheme 1. Reaction scheme for the thermochemical 'grafting from' MWNTs with various functional reactants. Refer to Table 1 for further details about the organic reactants used.

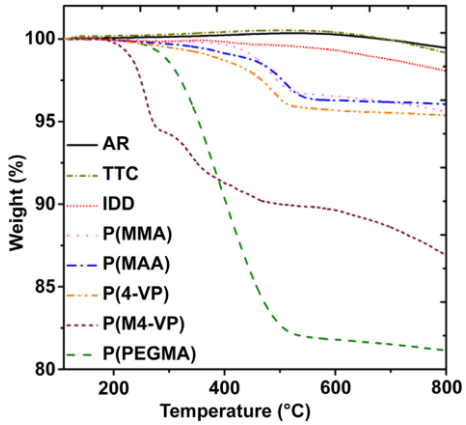


Fig. 1. TGA weight loss profiles of as received (AR) MWNTs, thermal treated control (TTC) MWNTs and various functionalised MWNTs (*f*-MWNT), heated in N_2 atmosphere at 10 °C/min ramping rate from 100 °C to 800 °C.

but exposing activated MWNTs to air rather than a monomer, at ambient temperatures. This process allows the surface to be re-oxidised at the original oxide defect sites, providing a simple baseline for the grafted products [49]. As a further control, to determine the number of active sites, the MWNTs were grafted with the non-polymerisable reagent 1-iodododecane (IDD). The grafting density and degree of polymerisation were then calculated (Table 1), assuming that IDD reacts stoichiometrically with all active radical sites, and the polymerisation processes is initiated at a radical site but can terminate anywhere on the MWNT surface.

The grafting ratio of the P(MMA)-MWNT (3.9 wt%) decreased slightly after the hydrolysis treatment (3.4 wt%), due to the loss of methyl groups. The grafting ratio of 4-VP-grafted MWNTs was 4.1 wt%, and the degree of polymerisation was very similar to that of P(MMA)-MWNT. TGA of the quaternised product retained the features of the P(4-VP)-MWNTs, associated with the combustion of the grafted oligomer, with an additional loss at around 200 °C, attributed to the methyl group and the associated iodide counterion. In order to account for the possible interaction of IMe with remaining surface oxides not involved in the grafting reaction, a methylated control sample (IMe-TTC) was prepared. Results (SI-Fig. 2S) indicated a small degree of secondary methylation (3.8 wt %), with the loss of quaternised IMe (5.3 wt%) at about 270 °C and remaining P(4-VP) framework (3.4 wt%), in the ranges expected.

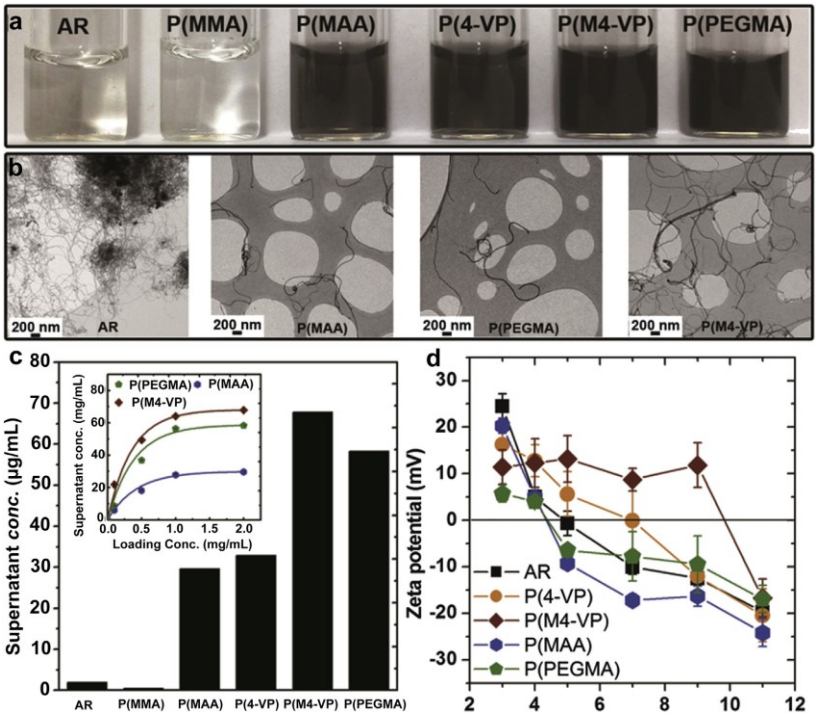


Fig. 2. (a) The water stability of MWNT samples is illustrated by photos showing the supernatants obtained by 15 min of bath sonication of MWNT-water mixtures with a starting concentration of 100 μg/mL followed by centrifugation (10,000 *g*, 15 min); (b) low resolution BF-TEM images showing the isolated nature of grafted MWNTs as compared to AR-MWNT; (c) the supernatant concentrations of various grafted MWNTs were quantitatively determined by UV absorbance with a loading concentration of 2 mg/mL; inset are the supernatant concentrations of various grafted MWNTs in HPLC water with various initial loading concentrations, quantified by UV absorbance and (d) MWNT zeta-potential curves as a function of pH.

Table 2
Maximum supernatant concentration (with loading concentration 2 mg/mL), zeta-potential in pH 7 HPLC water, isoelectric point (IEP) and D/G ratio of AR and grafted MWNTs. (The Raman spectra are presented in ESI Fig. 3S.)

Sample code	Maximum supernatant concentration in water (μg/mL)	Zeta-potential (mV) in pH 7 HPLC water	IEP	D/G ratio
AR-MWNT	6.0	−10.0 ± 1.6	4.9	1.09 ± 0.03
AR-MWNT	1.9	−10.0 ± 1.6	5.0	1.09 ± 0.03
P(MMA)-MWNT	0.5	N/A	N/A	1.07 ± 0.08
P(MAA)-MWNT	29.6	−17.2 ± 1.3	4.3	1.03 ± 0.07
P(4-VP)-MWNT	32.9	−0.1 ± 6.4	7.0	1.05 ± 0.02
P(M4-VP)-MWNT	67.8	8.7 ± 2.4	9.8	1.04 ± 0.03
P(PEGMA)-MWNT	58.3	−7.8 ± 5.3	4.6	1.13 ± 0.09

The higher grafting ratio of PEGylated MWNT, 18.3 wt%, is attributed to the high molecular weight of side chain of PEGMA monomer, and the degree of polymerisation is very similar to other monomers (Table 1).

3.2. MWNT water compatibility study

The functionalised MWNTs showed significantly enhanced water compatibility compared to AR-MWNT, as indicated by the dark colour of the supernatant solutions (Fig. 2a) after centrifugation (10,000 *g*, 15 min). The improvement after grafting is also illustrated by the individualised MWNTs visible by TEM, as compared to the AR-MWNT which remain aggregated after similar processing in water (Fig. 2b). The suspended concentration in HPLC water provides a quantitative measure of water compatibility, but it is important to understand the effect of increasing the amount of dry material supplied (Fig. 2c). Initially, the suspended concentration increases rapidly (P(M4-VP) > P(PEGMA) > P(MAA), indicating a minimum yield of dispersed, individualised species of around 17, 15 and 7% respectively. Subsequently, the MWNTs supernatant concentrations saturate, indicating the water solubility of the modified MWNT species. Taking the plateau values obtained at 2 mg/mL, the PEGMA-MWNT showed a much improved water compatibility compared to the pristine MWNTs, with a supernatant concentration of ~60 μg/mL attributed to the high grafting ratio and the steric stabilisation effects of the relatively bulky and hydrophilic PEG side chains. The P(4-VP)-MWNT offered a more modest improvement; in this case, the stabilisation is likely to depend on the electrostatic contribution of the protonated pyridyl groups. However, since the pyridyl group is a weak base [52], there is only limited protonation, and hence low stability, near pH 7. In order to increase the stability, the pyridyl groups were methylated to create a positive charge and a stronger columbic repulsion. The success of this strategy is illustrated by the 4-fold increase in P(M4-VP)-MWNT solubility to ~70 μg/mL. P(MMA)-MWNT showed very low water stability, similar to the parent AR-MWNT, as PMMA itself is not water-soluble. After the introduction of carboxyl acid groups through hydrolysis of grafted P(MMA), the stability of MWNTs was significantly increased to 30 μg/mL for P(MAA)-MWNT, again indicating the success of the intended reaction. For the P(MAA)-MWNT, P(M4-VP)-MWNT and P(PEGMA)-MWNT samples, less than 20% of MWNTs precipitated out after 2 weeks, as determined by UV–vis analysis, providing good stability for *in vitro* experiments.

3.3. Zeta potential analysis

The zeta potential analysis further confirmed successful grafting of the MWNTs with anionic, non-ionic and cationic oligomers (Fig. 2d). The AR-MWNT and thermal treated controls are weakly acidic, with an iso-electric point (IEP) of 5.0 and 4.3, as expected given the surface oxides, including carboxylic acid groups, present on the surface of such MWNTs [53]. The MAA modification increases the concentration of carboxylic acid groups, with a similar

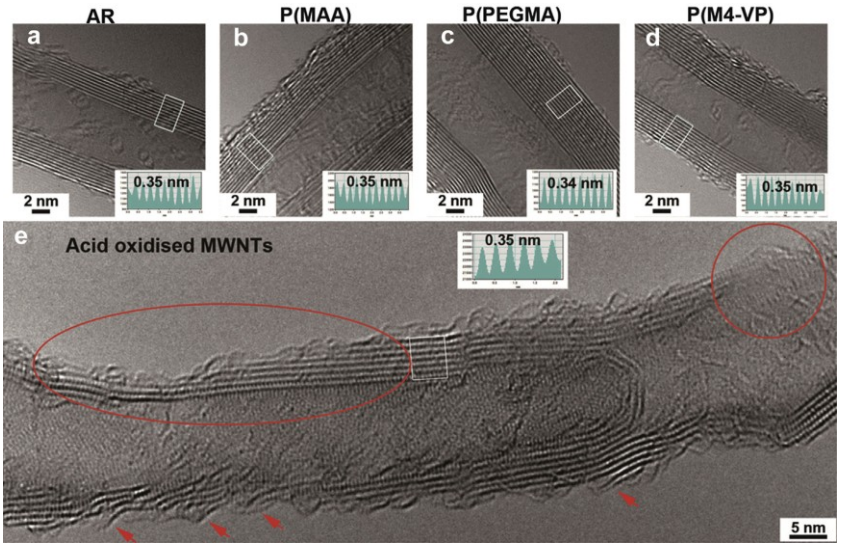


Fig. 3. HRTEM images and inserted intensity profiles taken from boxed areas to show the morphology and crystallinity of an (a) AR-MWNT, (b) P(PMAA)-MWNT, (c) P(PEGMA)-MWNT, (d) P(M4-VP)-MWNT and (e) acid oxidised MWNT. The characteristic features of the delamination, etching and pitting to the MWNT framework caused by acid oxidation process are marked.

pKa, such that the IEP (4.3) is approximately unchanged, but the plateau zeta potential is greater in magnitude. The grafted PEGMA is non-ionic so does not shift the IEP of the baseline groups; however, some of the oxygen species were consumed by the grafting process, leading to a lower plateau potential. Nevertheless, it is worth re-emphasising that the water compatibility is driven by the non-ionic PEG chains. The 4-VP functionalised systems introduce positively-charged groups, shifting the IEP to higher pH. By introducing a positive charge through quaternisation, the IEP of P(M4-VP)-MWNT was successfully increased to about pH 9.8.

3.4. HRTEM and Raman spectroscopy analysis

The thermochemically-grafted MWNTs were undamaged by the process, as anticipated. The two main Raman peaks for MWNTs, at around 1580 cm^{-1} (G) and 1350 cm^{-1} (D), are associated with graphitic quality and defects, respectively. The integrated peak area ratio (D/G) gives a semi-quantitative indication of the purity/defect density. The D/G ratios of the products (Table 2, SI-Fig. 3S) were unchanged, within error, relative to the as-received starting material value of 1.09 ± 0.03. Furthermore, HRTEM (Fig. 3a–d) showed no discernible change in the structure of the tubes, including no change in surface crystallinity, nanotube dimensions, or graphitic interlayer spacing (0.35 ± 0.01 nm). The grafted organic oligomers cannot be directly imaged due to their conformational freedom and high beam sensitivity. In total contrast to the thermochemical process, the liquid phase acid oxidation significantly damaged the framework of the MWNTs. Even after base washing to remove debris [26], the D/G ratio increased by 46% (SI-Fig. 3S). By HRTEM (Fig. 3e), obvious MWNTs framework damage, such as peeling and thinning of MWNTs walls (marked by arrows and oval) and generation of holes (circled area), was observed. This framework damage will inevitably effect the intrinsic properties of MWNTs, likely altering their toxicity and fate *in vivo*. Acid oxidised MWNTs are, therefore, not good models for studying the biological interactions of the majority of commercially-produced materials.

3.5. Cytotoxicity study

Before assessing the cytotoxicity of *f*-MWNTs, the endotoxin content of the samples was assessed. The results (SI-Fig. 4S) showed that the panel of *f*-MWNTs were negative for endotoxin by normal standards, demonstrating that the thermochemical functionalisation treatment and post-functionalisation reactions do not introduce any significant level of endotoxin; in fact, the high temperature treatment provides useful sterilisation.

The cytotoxicity of MWNTs on TT1 cells was assessed using MTS (Fig. 4a) and LDH (Fig. 4b) assays. None of the MWNTs showed any

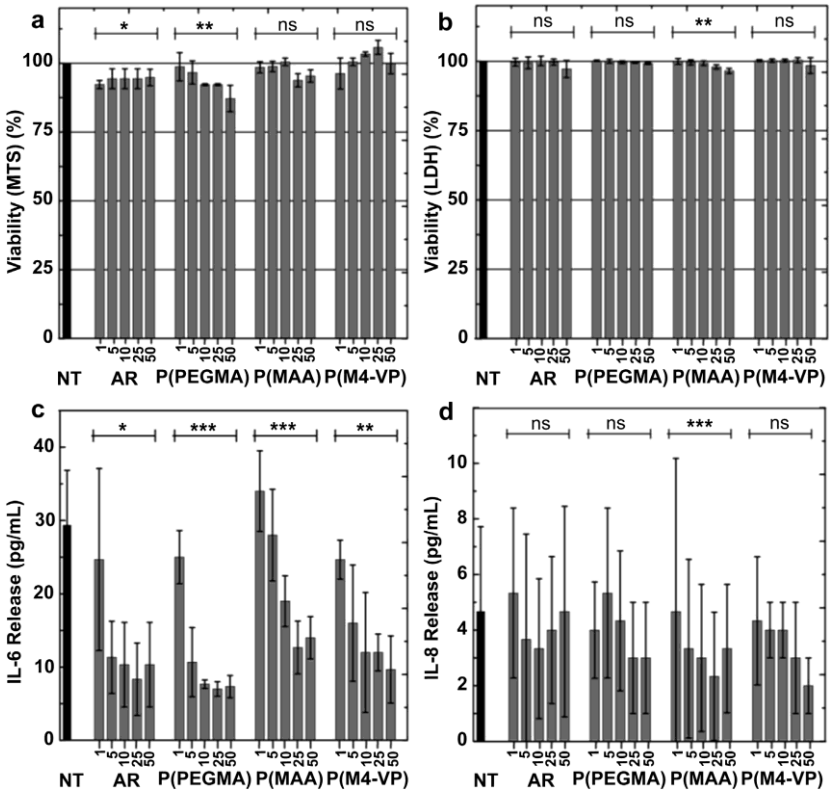


Fig. 4. Cytotoxicity (MTS assay (a), LDH assay (b)) and release of IL-6 (c) and IL-8 (d) induced by MWNTs on TT1 cells, following a 24 h exposure at increasing concentrations up to 50 μg/mL. Error bars are mean ± SD ($n = 3$). *, $p < 0.05$; **, $p < 0.01$; ***, $p < 0.001$.

significant TT1 cell cytotoxicity after 24 h exposure to concentrations up to 50 μg/mL (Fig. 4a). Only a slight toxic effect of AR MWNTs was observed (less than 10% cell death, $n = 3$ replicates). The low cell viability damage suggested by the MTS assay was confirmed by LDH assays (Fig. 4b), showing no detectable cell death.

However, exposure of TT1 cells to MWNTs suppressed IL-6 (Fig. 4c and d) and IL-8 release in a dose-dependent fashion. All of the MWNTs, even the lowest dose of 1 μg/ml, caused some inhibition; the effect became highly significant at higher doses, with values falling to a third of that of control. Cationic P(M4-VP) may be slightly less inhibitory than the rest of the panel, but the difference was not significant. A similar inflammatory mediator suppression effect was reported following exposure of A549 adenocarcinoma cells and a single subject sample of primary NHBE human airway lung epithelial cells to single wall carbon nanotubes (SWNTs), which led to the suppression of IL-6, IL-8 and MCP-1, which was further suppressed by addition of dipalmitoylphosphatidylcholine (DPPC) [54]. In contrast, exposure of the BEAS 2B human airway cell line to a highly purified vapour-grown multiwalled carbon fibre, HTT2800 [55], or commercial MWNT synthesised by catalytic chemical vapour deposition (CCVD) [56], caused increased IL-6 and IL-8 release. As different cell lines, as well as carbon nanomaterials of different dimensions and surface functionalisation were studied, it is difficult to make a comparison with these contrasting literature results. Importantly in the current study, the AR-MWNTs have been surface modified to enhance dispersibility and modify bioreactivity and tested using highly relevant, well characterised, human lung alveolar epithelial cells (rather than airway epithelium and cancer cells). One key question, however, is to what extent these cells interact with the test panel of MWNTs.

3.6. TEM cell uptake study

Consequently, a TEM study was carried out to investigate alveolar epithelial cell interactions with cationic, anionic and non-ionic MWNTs. The stable water dispersions of individual *f*-MWNTs (see Fig. 2a) provide an excellent route for cell exposure. In contrast, on exposing TT1 cells directly to uncentrifuged suspensions of AR-MWNT containing agglomerates due to its limited water dispensability, the majority of AR-MWNTs were localised in TT1 cells as large clusters inside cellular vesicles, indicating internalisation via endocytic pathways (SI-Fig. 5S). Uptake of *f*-MWNTs by TT1 cells proceeded by a variety of mechanisms (Fig. 5). The non-ionic P(PEGMA)-MWNTs were observed inside vesicular structures (Fig. 5a), possibly utilising energetic endocytosis pathways [57]. A collection of P(PEGMA)-MWNTs were also identified in the process of being taken up by macropinocytosis, as featured by the presence of large protrusions of the plasma membrane (>1 μm) around the MWNTs [58] (Fig. 5a). Other types of endocytic uptake were observed (see Fig. 5b, marked by arrows) involving relatively smaller sized vesicles, compared to those involved in macropinocytosis. Individual P(PEGMA)-MWNTs were also present inside the cytoplasm (Fig. 5a, circled and Fig. 5c). These individual MWNTs

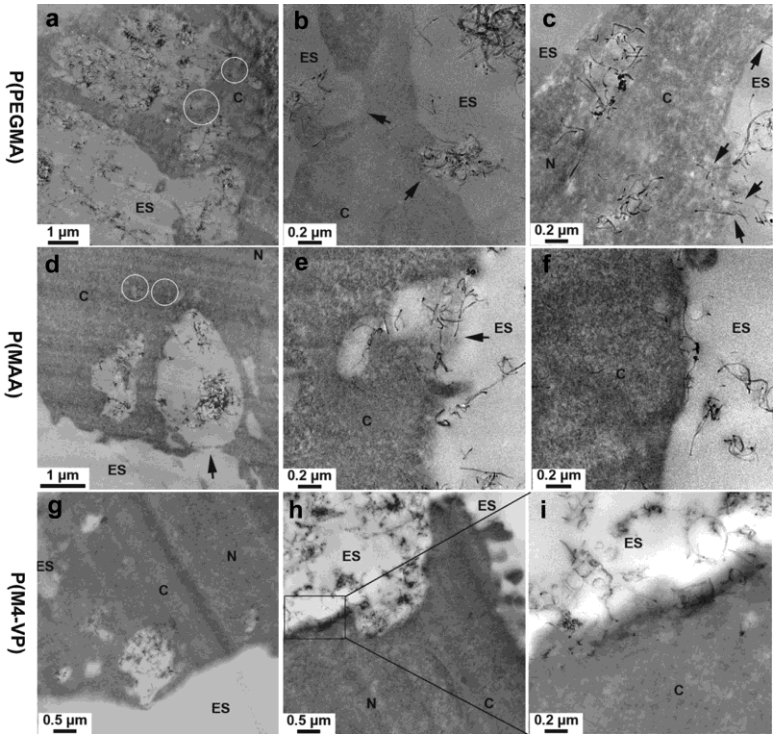


Fig. 5. TEM images showing the cellular distribution and interaction of (a–c) P(PEGMA)-MWNTs, (d–f) P(PMAA)-MWNTs and (g–i) P(M4-VP)-MWNTs with TT1 epithelial cells after 24 h exposure. Individual MWNTs are indicated by circles. (i) is a higher resolution TEM image of boxed area in (h). ES = extracellular space; C = cytoplasm; N = nucleus.

might have entered the cell cytoplasm by directly penetrating cell membranes [59,60], as indicated by arrows in Fig. 5c. There was also a surface charge effect on the interaction of these functionalised MWNTs with epithelial cells. Thus, a large population of anionic, negatively charged P(MAA)-MWNTs were observed localised inside vesicular structures (Fig. 5d–e), while a sub-population of individual P(MAA)-MWNTs were also detected within the cytoplasm (Fig. 5d, circled). Macropinocytosis (Fig. 5d, arrow) and other endocytic mechanisms were also observed for this type of MWNTs (Fig. 5e, arrow). Furthermore, P(MAA)-MWNTs, were frequently aligned parallel to, and did not insert into, the plasma membrane, possibly due to the electrostatic repulsion of negatively charge MWNTs with the negatively charged plasma membrane (Fig. 5f, SI-Fig. 6S). The cationic, positively charged M(4-VP)-grafted MWNTs also distributed to both the cytoplasm and endocytic vesicular structures (Fig. 5g–i). However, P(M4-VP)-MWNT exhibited more frequent contact with the plasma membrane than the other MWNTs. The M(4-VP)-MWNTs inserted into the plasma membrane with both high and low contact angles, presumably due to electrostatic attraction [61–63].

3.7. *Wider context*

The versatile, scalable functionalisation method used in this paper can also be applied for other modifications of MWNTs, in order to change their surface charge or functional character. Non-cytotoxic MWNTs with defined surface charges have many perceived biological applications ranging from acting as intracellular transporters for various therapeutic and diagnostic agents to cell growth substrates or tissue scaffolds [64]. Furthermore, water dispersible MWNTs may be used to simplify processing in a range of applications from printing conductive inks, to assembling filters and electrodes. In many cases, avoiding MWNT damage, and the property degradation associated with acid oxidation, as well as improving the scalability of the chemistry, will be significantly advantageous. Controlled and stably grafted surface charge provides options to use electrostatically-driven techniques such as layer-by-layer (LBL) assembly and electrophoretic deposition (EPD) [65]. The versatile chemistry described allows model sets of surface-modified MWNTs to be prepared without changing dimensions or structure; for example, as shown here, the structural integrity of commercially-grown MWNTs can be retained whilst producing water-stable dispersions with different surface character. Understanding this type of industrial MWNTs is particularly important as annual production capacity is in the order of thousands of tons [66], vastly exceeding any other nanotube material. The methods presented in this study are also likely to be suitable for the functionalisation of other carbon-related materials such as carbon black and graphene, which may thus provide useful controls for exploring geometric effects.

4. Conclusions

In this study, a thermochemical approach was successfully applied for preparation of water-compatible MWNTs, stabilised by cationic, anionic, or non-ionic grafted species. In contrast to traditional acid oxidation protocols, the thermochemical method has a significant advantage of minimising the damage to the nanotube framework. The functionalised MWNTs showed significantly enhanced water compatibility; the concentration of individualised, grafted MWNTs in water ranged from ~30 to 70 μg/mL, high enough for most biological research purposes. None of the MWNTs showed significant cytotoxicity toward human alveolar epithelial cells (<10%). In addition, exposure of TT1 cells to MWNTs led to the suppression of IL-6 and IL-8, suggesting that they would not trigger an inflammatory response if deposited within the respiratory units. Nevertheless, TEM showed marked uptake of all types of MWNTs by TT1 cells. MWNTs were found residing in cellular vesicular structures and cytoplasm, with both endocytic uptake pathways and direct penetration of cell surface membrane implicated as important cellular entry mechanisms. Surface charge appears to be important, since cationic MWNTs showed greater direct interaction with cell membranes, involving more substantial direct penetration of the membranes than anionic MWNTs. These fundamental factors controlling nanomaterial–cell interactions must be understood, in order to build up a generally applicable model.

Acknowledgements

The authors would like to thank NIEHS (grant# U19ES019536) for the funding of this project. AP acknowledges an ERC starting grant (CNTBBB project number 257182) for supporting AEG and SC. TT acknowledges funding from Leverhulme for supporting PR, and MRC-PHE Centre for Environment and Health for supporting ES, which is funded by Public Health England and the UK Medical Research Council (grant ref: MRC G0801056). However, the views expressed in this paper are solely of the authors and do not necessarily reflect those of the funding agencies.

Appendix A. Supplementary data

Supplementary data related to this article can be found online at http://dx.doi.org/10.1016/j.biomaterials.2014.02.002.

References

[1] Gagner JE, Shrivastava S, Qian X, Dordick JS, Siegel RW. Engineering nanomaterials for biomedical applications requires understanding the nano-bio interface: a perspective. J Phys Chem Lett 2012;3:3149–58.
[2] Shannahan JH, Brown JM, Chen R, Ke PC, Lai XY, Mitra S, et al. Comparison of nanotube-protein corona composition in cell culture media. Small 2013;9:2171–81.
[3] Moon HK, Lee SH, Choi HC. *In vivo* near-infrared mediated tumor destruction by photothermal effect of carbon nanotubes. ACS Nano 2009;3:3707–13.
[4] Wang L, Shi JJ, Zhang HL, Li HX, Gao Y, Wang ZZ, et al. Synergistic anticancer effect of RNAi and photothermal therapy mediated by functionalized single-walled carbon nanotubes. Biomaterials 2013;34:262–74.
[5] Bhirde AA, Patel V, Gavard J, Zhang GF, Sousa AA, Masedunskas A, et al. Targeted killing of cancer cells *in vivo* and *in vitro* with EGF-directed carbon nanotube-based drug delivery. ACS Nano 2009;3:307–16.
[6] Chen ML, He YJ, Chen XW, Wang JH. Quantum dots conjugated with Fe_3O_4-filled carbon nanotubes for cancer-targeted imaging and magnetically guided drug delivery. Langmuir 2012;28:16469–76.
[7] de la Zerda A, Liu ZA, Bodapati S, Teed R, Vaithilingam S, Khuri-Yakub BT, et al. Ultrahigh sensitivity carbon nanotube agents for photoacoustic molecular imaging in living mice. Nano Lett 2010;10:2168–72.
[8] Delogu LG, Vidili G, Venturelli E, Menard-Moyon C, Zoroddu MA, Pilo G, et al. Functionalized multiwalled carbon nanotubes as ultrasound contrast agents. Proc Natl Acad Sci U S A 2012;109:16612–7.
[9] Zhang XY, Hu WB, Li J, Tao L, Wei Y. A comparative study of cellular uptake and cytotoxicity of multi-walled carbon nanotubes, graphene oxide, and nanodiamond. Toxicol Res-Uk 2012;1:62–8.
[10] Nel A, Xia T, Meng H, Wang X, Lin SJ, Ji ZX, et al. Nanomaterial toxicity testing in the 21st century: use of a predictive toxicological approach and high-throughput screening. Acc Chem Res 2013;46:607–21.
[11] Li JQ, Zhang Q, Li H, Chan-Park MB. Influence of triton X-100 on the characteristics of carbon nanotube field-effect transistors. Nanotechnology 2006;17:668–73.
[12] Duan WH, Wang Q, Collins F. Dispersion of carbon nanotubes with SDS surfactants: a study from a binding energy perspective. Chem Sci 2011;2:1407–13.
[13] Li MH. Effects of nonionic and ionic surfactants on survival, oxidative stress, and cholinesterase activity of planarian. Chemosphere 2008;70:1796–803.
[14] Ma G, Allen HC. New insights into lung surfactant monolayers using vibrational sum frequency generation spectroscopy. Photochem Photobiol 2006;82:1517–29.
[15] Huang YY, Terentjev EM. Dispersion of carbon nanotubes: mixing, sonication, stabilization, and composite properties. Polymers-Basel 2012;4:275–95.
[16] Bussy C, Pinault M, Cambedouzou J, Landry MJ, Jegou P, Mayne-L'hermite M, et al. Critical role of surface chemical modifications induced by length

shortening on multi-walled carbon nanotubes-induced toxicity. Part Fibre Toxicol 2012;9:46.
[17] Baati R, Ihiawakrim D, Mafouana RR, Ersen O, Dietlin C, Duportail G. Hexahistidine-Tagged single-walled carbon nanotubes (His6-tagSWNTs): a multifunctional hard template for hierarchical directed self-assembly and nanocomposite construction. Adv Funct Mater 2012;22:4009–15.
[18] Guo XF. Single-molecule electrical biosensors based on single-walled carbon nanotubes. Adv Mater 2013;25:3397–408.
[19] Shaffer MSP, Fan X, Windle AH. Dispersion and packing of carbon nanotubes. Carbon 1998;36:1603–12.
[20] Wang YB, Iqbal Z, Mitra S. Rapidly functionalized, water-dispersed carbon nanotubes at high concentration. J Am Chem Soc 2006;128:95–9.
[21] Gonzalez-Dominguez JM, Gonzalez M, Anson-Casaos A, Diez-Pascual AM, Gomez MA, Martinez MT. Effect of various aminated single-walled carbon nanotubes on the epoxy cross-linking reactions. J Phys Chem C 2011;115:7238–48.
[22] Li KD, Zhang C, Du ZJ, Li HQ, Zou W. Preparation of humidity-responsive antistatic carbon nanotube/PEI nanocomposites. Synt Met 2012;162:2010–5.
[23] Tchoul MN, Ford WT, Lolli G, Resasco DE, Arepalli S. Effect of mild nitric acid oxidation on dispersibility, size, and structure of single-walled carbon nanotubes. Chem Mater 2007;19:5765–72.
[24] Datsyuk V, Kalyva M, Papagelis K, Parthenios J, Tasis D, Siokou A, et al. Chemical oxidation of multiwalled carbon nanotubes. Carbon 2008;46:833–40.
[25] Verdejo R, Lamoriniere S, Cottam B, Bismarck A, Shaffer M. Removal of oxidation debris from multi-walled carbon nanotubes. Chem Commun; 2007:513–5.
[26] Fogden S, Verdejo R, Cottam B, Shaffer M. Purification of single walled carbon nanotubes: the problem with oxidation debris. Chem Phys Lett 2008;460:162–7.
[27] Cho J, Inam F, Reece MJ, Chlup Z, Dlouhy I, Shaffer MSP, et al. Carbon nanotubes: do they toughen brittle matrices? J Mater Sci 2011;46:4770–9.
[28] Wang RH, Mikoryak C, Li SY, Bushdiecker D, Musselman IH, Pantano P, et al. Cytotoxicity screening of single-walled carbon nanotubes: detection and removal of cytotoxic contaminants from carboxylated carbon nanotubes. Mol Pharm 2011;8:1351–61.
[29] Stefani D, Paula AJ, Vaz BG, Silva RA, Andrade NF, Justo GZ, et al. Structural and proactive safety aspects of oxidation debris from multiwalled carbon nanotubes. J Hazard Mater 2011;189:391–6.
[30] Heister E, Lamprecht C, Neves V, Tilmaciu C, Datas L, Flahaut E, et al. Higher dispersion efficacy of functionalized carbon nanotubes in chemical and biological environments. ACS Nano 2010;4:2615–26.
[31] Yamashita T, Yamashita K, Nabeshi H, Yoshikawa T, Yoshioka Y, Tsunoda S, et al. Carbon nanomaterials: efficacy and safety for nanomedicine. Materials 2012;5:350–63.
[32] Li R, Wang X, Ji Z, Sun B, Zhang H, Chang CH, et al. Surface charge and cellular processing of covalently functionalized multiwall carbon nanotubes determine pulmonary toxicity. ACS Nano 2013;7:2352–68.
[33] Tagmatarchis N, Prato M. Functionalization of carbon nanotubes via 1,3-dipolar cycloadditions. J Mater Chem 2004;14:437–9.
[34] Hodge SA, Fogden S, Howard CA, Skipper NT, Shaffer MSP. Electrochemical processing of discrete single-walled carbon nanotube anions. ACS Nano 2013;7:1769–78.
[35] Menzel R, Tran MQ, Menner A, Kay CWM, Bismarck A, Shaffer MSP. A versatile, solvent-free methodology for the functionalisation of carbon nanotubes. Chem Sci 2010;1:603–8.
[36] Tessonnier JP, Rosenthal D, Hansen TW, Hess C, Schuster ME, Blume R, et al. Analysis of the structure and chemical properties of some commercial carbon nanostructures. Carbon 2009;47:1779–98.
[37] Castranova V, Schulte PA, Zumwalde RD. Occupational nanosafety considerations for carbon nanotubes and carbon nanofibers. Acc Chem Res 2013;46:642–9.
[38] Morimoto Y, Horie M, Kobayashi N, Shinohara N, Shimada M. Inhalation toxicity assessment of carbon-based nanoparticles. Acc Chem Res 2013;46:770–81.
[39] Murphy FA, Schinwald A, Poland CA, Donaldson K. The mechanism of pleural inflammation by long carbon nanotubes: interaction of long fibres with macrophages stimulates them to amplify pro-inflammatory responses in mesothelial cells. Part Fibre Toxicol 2012;9:8.
[40] Murphy FA, Poland CA, Duffin R, Donaldson K. Length-dependent pleural inflammation and parietal pleural responses after deposition of carbon nanotubes in the pulmonary airspaces of mice. Nanotoxicology 2013;7:1157–67.
[41] Maynard RL, Donaldson K, Tetley TD. Type 1 pulmonary epithelial cells: a new compartment involved in the slow phase of particle clearance from alveoli. Nanotoxicology 2013;7:350–1.
[42] Crapo JD, Young SL, Fram EK, Pinkerton KE, Barry BE, Crapo RO. Morphometric characteristics of cells in the alveolar region of mammalian lungs. Am Rev Respir Dis 1983;128:S42–6.
[43] Isakson BE, Seedorf GJ, Lubman RL, Boitano S. Heterocellular cultures of pulmonary alveolar epithelial cells grown on laminin-5 supplemented matrix. In Vitro Cell Dev-Anim 2002;38:443–9.
[44] Shimada A, Kawamura N, Okajima M, Kaewamatawong T, Inoue H, Morita T. Translocation pathway of the intratracheally instilled ultrafine particles from the lung into the blood circulation in the mouse. Toxicol Pathol 2006;34:949–57.
[45] Alunni S, Laureti V, Ottavi L, Ruzziconi R. Catalysis of the beta-elimination of HF from isomeric 2-fluoroethylpyridines and 1-methyl-2-fluoroethylpyridinium salts. Proton-activating factors and methyl-activating factors as a mechanistic test to distinguish between concerted E2 and E1cb irreversible mechanisms. J Org Chem 2003;68:718–25.
[46] Runyon SP, Brieaddy LE, Mascarella SW, Thomas JB, Navarro HA, Howard JL, et al. Analogues of (3R)-7-Hydroxy-N-[(1S)-1-[[(3R,4R)-4-(3-hydroxyphenyl)-3,4-dimethyl-1-piperidinyl]methyl]-2-methylpropyl)-1,2,3,4-tetrahydro-3-isoquinolinecarboxamide (JDTic). Synthesis and in vitro and in vivo opioid receptor antagonist activity. J Med Chem 2010;53:5290–301.
[47] Li SP, Wu W, Campidelli S, Sarnatskaia V, Prato M, Tridon A, et al. Adsorption of carbon nanotubes on active carbon microparticles. Carbon 2008;46:1091–5.
[48] Delhaes P, Couzi M, Trinquecoste M, Dentzer J, Hamidou H, Vix-Guterl C. A comparison between Raman spectroscopy and surface characterizations of multiwall carbon nanotubes. Carbon 2006;44:3005–13.
[49] Tran MQ, Tridech C, Alfrey A, Bismarck A, Shaffer MSP. Thermal oxidative cutting of multi-walled carbon nanotubes. Carbon 2007;45:2341–50.
[50] Delogu LG, Stanford SM, Santelli E, Magrini A, Bergamaschi A, Motamedchaboki K, et al. Carbon nanotube-based nanocarriers: the importance of keeping it clean. J Nanosci Nanotechnol 2010;10:5293–301.
[51] Kemp SJ, Thorley AJ, Gorelik J, Seckl MJ, O'Hare MJ, Arcaro A, et al. Immortalization of human alveolar epithelial cells to investigate nanoparticle uptake. Am J Respir Cell Mol Biol 2008;39:591–7.
[52] Franck-Lacaze L, Sistat P, Huguet P. Determination of the pK(a) of poly (4-vinylpyridine)-based weak anion exchange membranes for the investigation of the side proton leakage. J Membr Sci 2009;326:650–8.
[53] Menendez JA, Phillips J, Xia B, Radovic LR. On the modification and characterization of chemical surface properties of activated carbon: in the search of carbons with stable basic properties. Langmuir 1996;12:4404–10.
[54] Herzog E, Byrne HJ, Casey A, Davoren M, Lenz AG, Maier KL, et al. SWCNT suppress inflammatory mediator responses in human lung epithelium *in vitro*. Toxicol Appl Pharmacol 2009;234:378–90.
[55] Tsukahara T, Haniu H. Cellular cytotoxic response induced by highly purified multi-wall carbon nanotube in human lung cells. Mol Cell Biochem 2011;352:57–63.
[56] Hirano S, Fujitani Y, Furuyama A, Kanno S. Uptake and cytotoxic effects of multi-walled carbon nanotubes in human bronchial epithelial cells. Toxicol Appl Pharm 2010;249:8–15.
[57] Mu QX, Broughton DL, Yan B. Endosomal leakage and nuclear translocation of multiwalled carbon nanotubes: developing a model for cell uptake. Nano Lett 2009;9:4370–5.
[58] Conner SD, Schmid SL. Regulated portals of entry into the cell. Nature 2003;422:37–44.
[59] Shi XH, von dem Bussche A, Hurt RH, Kane AB, Gao HJ. Cell entry of one-dimensional nanomaterials occurs by tip recognition and rotation. Nat Nanotechnol 2011;6:714–9.
[60] Al-Jamal KT, Nerl H, Muller KH, Ali-Boucetta H, Li SP, Haynes PD, et al. Cellular uptake mechanisms of functionalised multi-walled carbon nanotubes by 3D electron tomography imaging. Nanoscale 2011;3:2627–35.
[61] Pantarotto D, Briand JP, Prato M, Bianco A. Translocation of bioactive peptides across cell membranes by carbon nanotubes. Chem Commun; 2004:16–7.
[62] Hauck TS, Ghazani AA, Chan WCW. Assessing the effect of surface chemistry on gold nanorod uptake, toxicity, and gene expression in mammalian cells. Small 2008;4:153–9.
[63] Nan AJ, Bai X, Son SJ, Lee SB, Ghandehari H. Cellular uptake and cytotoxicity of silica nanotubes. Nano Lett 2008;8:2150–4.
[64] Heister E, Brunner EW, Dieckmann GR, Jurewicz I, Dalton AB. Are carbon nanotubes a natural solution? Applications in biology and medicine. ACS Appl Mater Interfaces 2013;5:1870–91.
[65] Boccaccini AR, Cho J, Roether JA, Thomas BJC, Minay EJ, Shaffer MSP. Electrophoretic deposition of carbon nanotubes. Carbon 2006;44:3149–60.
[66] De Volder MFL, Tawfick SH, Baughman RH, Hart AJ. Carbon nanotubes: present and future commercial applications. Science 2013;339:535–9.

Supplementary Information

Aqueous cationic, anionic and non-ionic multi-walled carbon nanotubes, functionalised with minimal framework damage, for biomedical applications

Shu Chen,[a‡] Sheng Hu,[b‡] Elizabeth F. Smith,[c] Pakatip Ruenraroengsak,[a] Andrew J. Thorley,[c] Robert Menzel,[b] Angela E. Goode,[a] Mary P. Ryan,[a] Teresa D. Tetley,[c] Alexandra E. Porter,[a] Milo S. P. Shaffer[b*†]

[a] *Department of Materials and London Centre for Nanotechnology, Imperial College London, Exhibition Road, London SW7 2AZ, UK*

[b] *Department of Chemistry and London Centre for Nanotechnology, Imperial College London, Exhibition Road, London SW7 2AZ, UK*

[c] *National Heart and Lung Institute, Imperial College London, Dovehouse Street, London SW3 6LY, UK*

‡ These authors contributed equally to this work

[*] *Corresponding author. Department of Chemistry and London Centre for Nanotechnology, Imperial College London, Exhibition Road, London SW7 2AZ, UK. E-mail addresses: m.shaffer@imperial.ac.uk (M. S. P. Shaffer)*

† Electronic supplementary information (ESI) available: Grafting ratio calculation, details of Raman spectroscopy of carbon nanotubes.

The determination of grafting ratios of MWNTs samples [1], using P(MMA)-MWNT as an example:

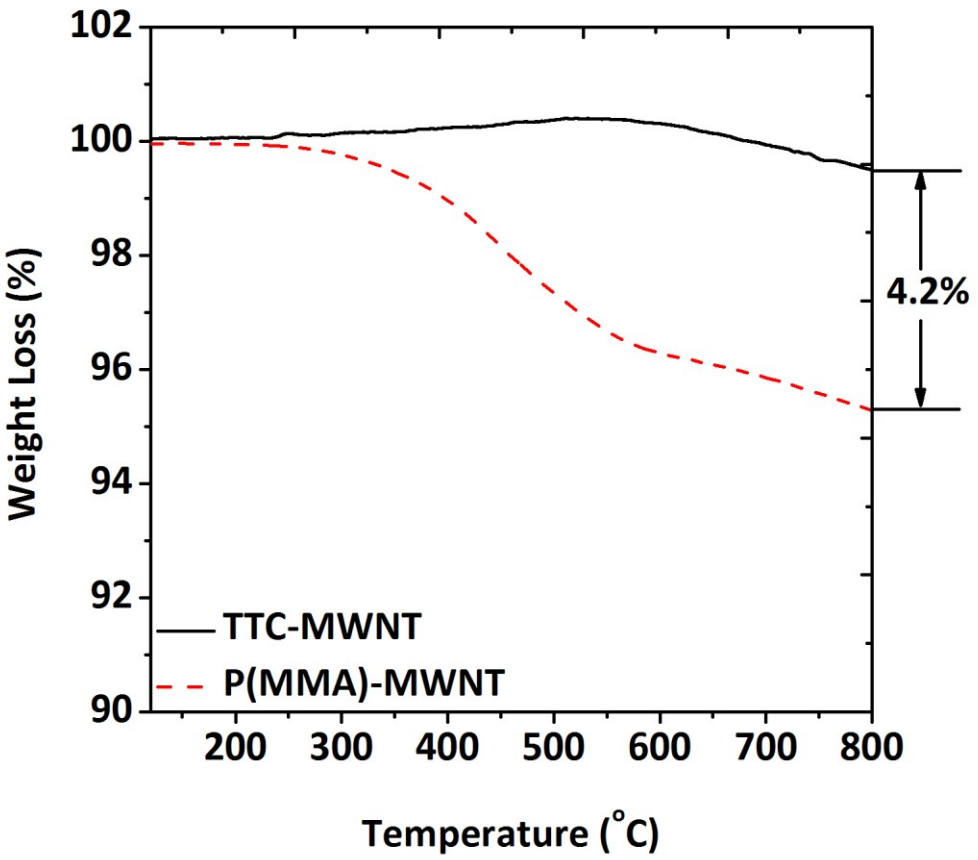


Figure 6.5.1S: TGA weight loss profiles of P(MMA)-MWNT and TTC-MWNT, illustrating the determination of the grafting ratio by the weight loss differences of two samples at 800 °C.

The grafting ratio, i.e.

$$\Delta\ (\text{wt}\ \%) = \frac{weight\ of\ grafted\ organics}{total\ weight\ of\ final\ product}\ (\%)$$

was determined from the TGA data as depicted in Figure 6.5.1S.

The determination of grafting ratio of P(M4-VP)-MWNT:

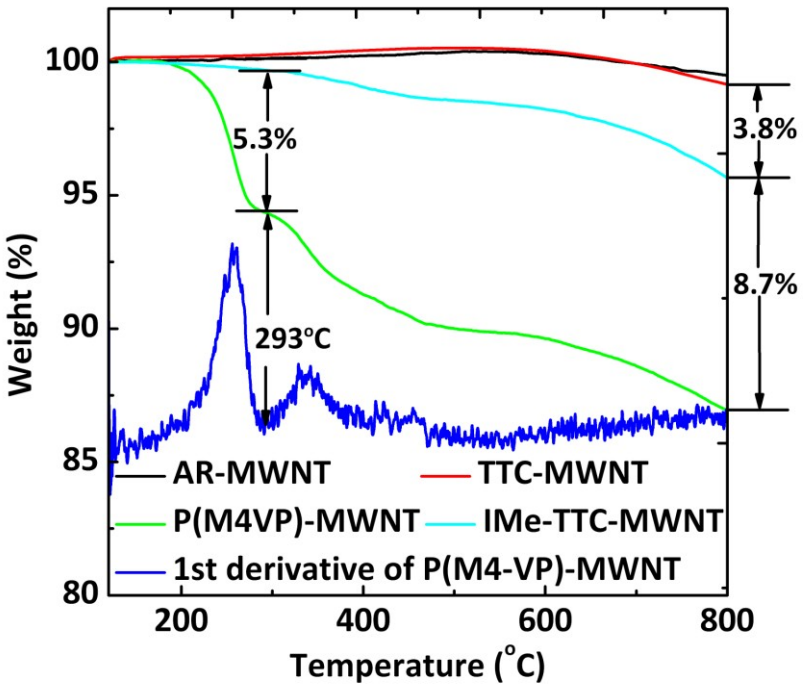


Figure 6.5.2S: TGA weight loss profiles of AR-MWNT, TTC-MWNT, P(M4-VP)-MWNT, and the control of methylated TTC MWNTs (IMe-TTC-MWNT), illustrating the determination of the grafting ratio, Δ in two stages. The T_{comb} was determined using the same method shown in Figure 1S.

Raman spectra of MWNT samples:

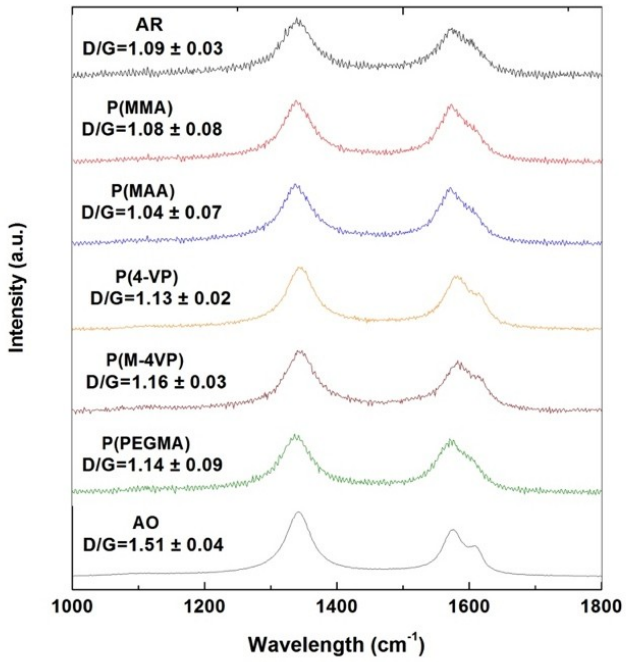


Figure 3S: Raman spectra of thermal grafted MWNTs, with D/G indicated as compared to AR-MWNT and AO-MWNT.

The two main peaks at around 1580 cm^{-1}, the graphite band (G-band), and 1350 cm^{-1}, the defect band (D-band), are the main features of Raman spectra of MWNTs. The G-band is associated with the in-plane vibrations within (intact) graphene layers of the CNTs walls, while the defect band (D-band) is attributed to disorder in the graphene structure, carbon vacancies, functional groups, graphene layer edges or amorphous carbon content [1]. Therefore, the relative integration peak area ratio of the D- and the G-band (D/G) gives an indication of the defect/purity density of a CNT material. The D/G ratios of various grafted MWNTs were identical, within error, to the as-received starting material value of 1.09 ± 0.03. In contrast, even

after base washing to remove debris, D/G ratio of acid oxidized MWNTs was increased by 46 % (3S.), indicating CNTs framework damage induced by acid treatment.

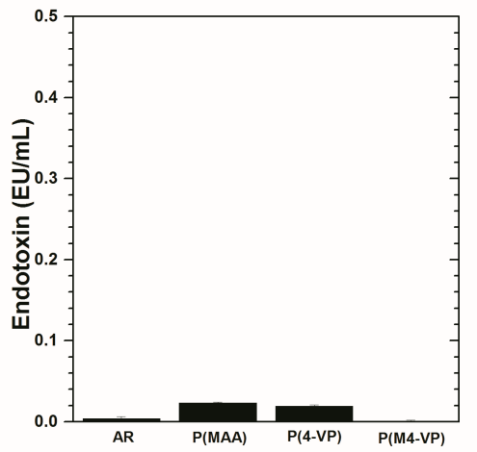


Figure 4S: Endotoxin level of AR-MWNTs and *f*-MWNTs samples. The United States Pharmacopeia (USP) standard, the Water for Injection, Sterile Water for Injection and Sterile Water for Irrigation have an allowable endotoxin limit of 0.25 Endotoxin Units (EU)/ml, EU=Unit of measurement for endotoxin activity) [2]. The low level of endotoxin reflects the thermochemical functionalisation treatment and post-functionalisation reactions did not introduce significant level of endotoxin.

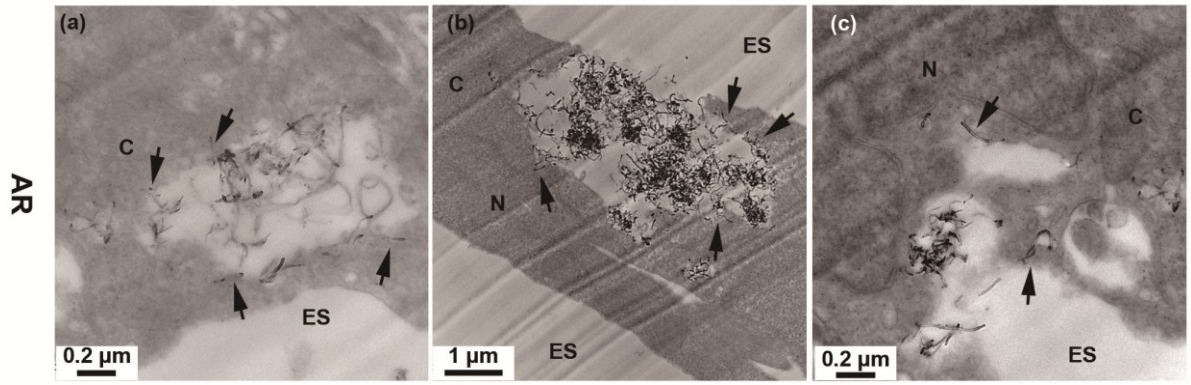


Figure 5S. TEM images (a-c) showing the cellular distribution and interaction of AR-MWNTs (a-c). ES= extracellular space; C=cytoplasm; N=nucleus.

The majority of AR-MWNTs were localized as large clusters inside cellular vesicles (Figure 5Sa and b). The clustered AR-MWNTs were probably internalised via endocytic pathways. Figure 5S b shows an evidence of macropinocytosis as featured by the presence of large size plasma membrane

protrusions (> 1 μm) around the large clusters of AR-MWNTs. Uptake of relatively smaller size AR-MWNTs clusters was also observed through other endocytic pathways, as suggested by the formation of smaller size of endocytic vesicles, as compared to macropinocytosis (Figure 5Sc) [3]. A small population of individual AR-CNTs were also found inside the cytoplasm and translocating from plasma membrane or vesicles into the cytoplasm (Figure 5Sa-c, as indicated by arrows).

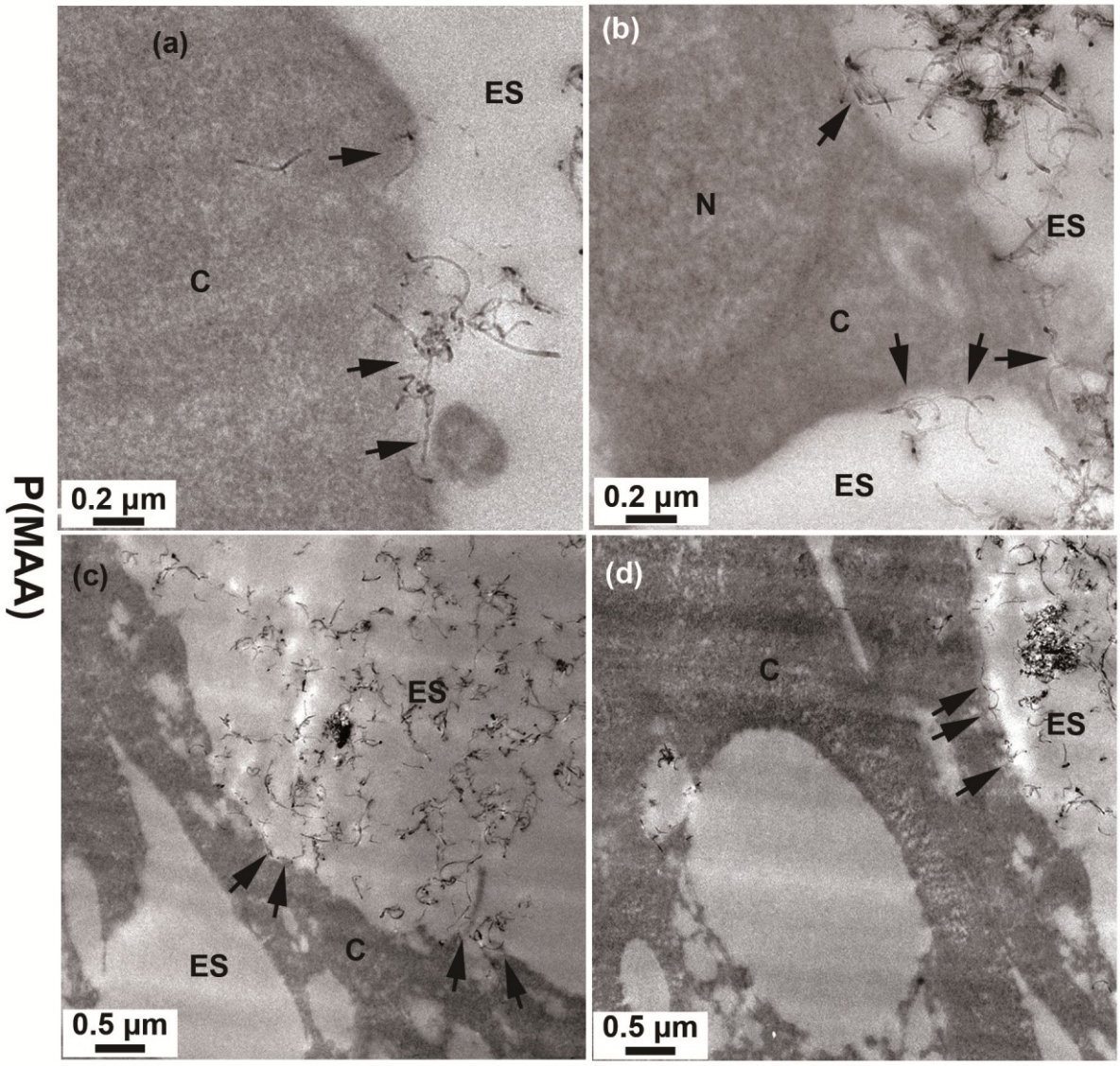


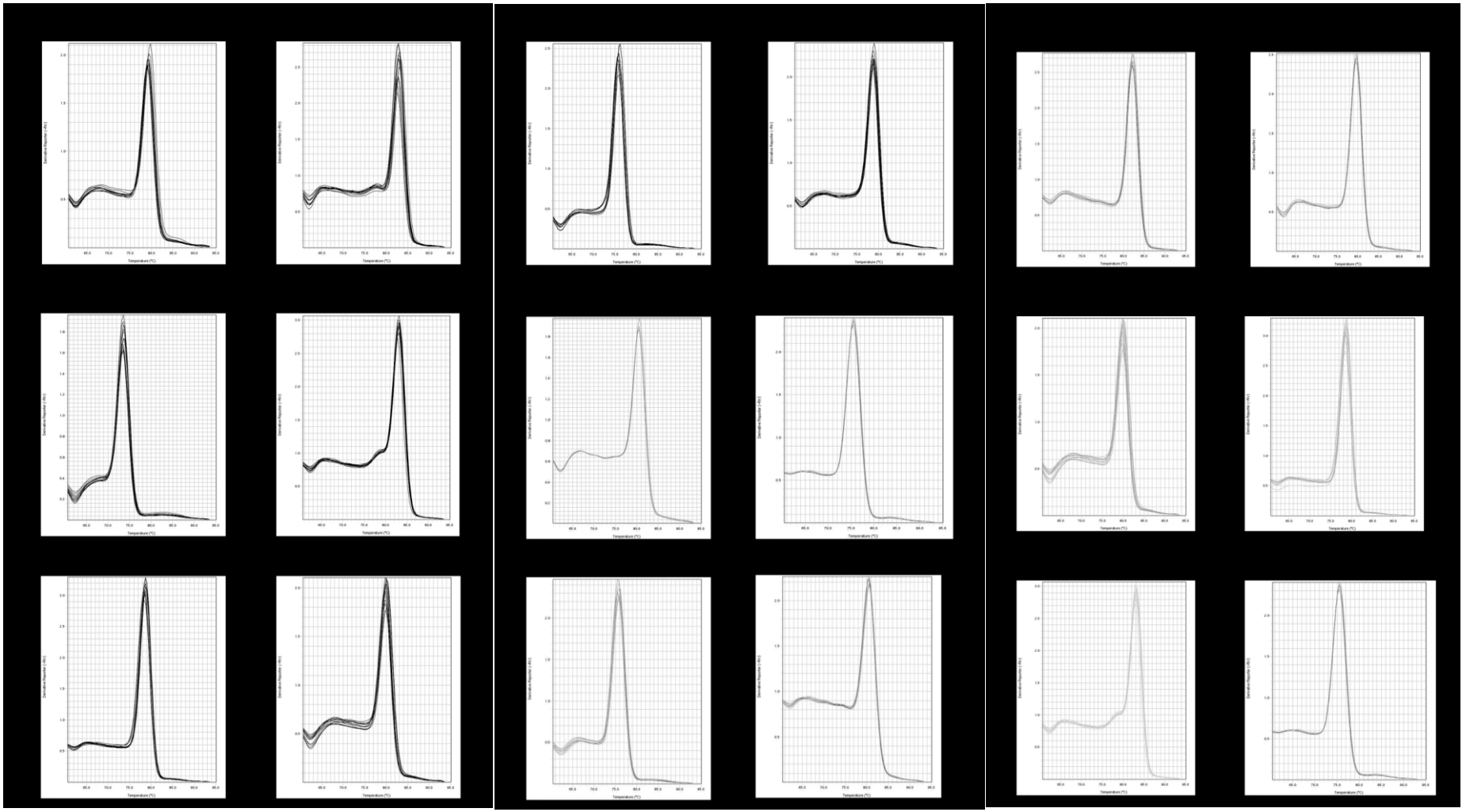
Figure 6S. TEM image showing negatively charged P(MAA)-MWNTs were frequently found aligned parallel to, and did not insert into, the plasma membrane, as marked by arrows.

Reference:

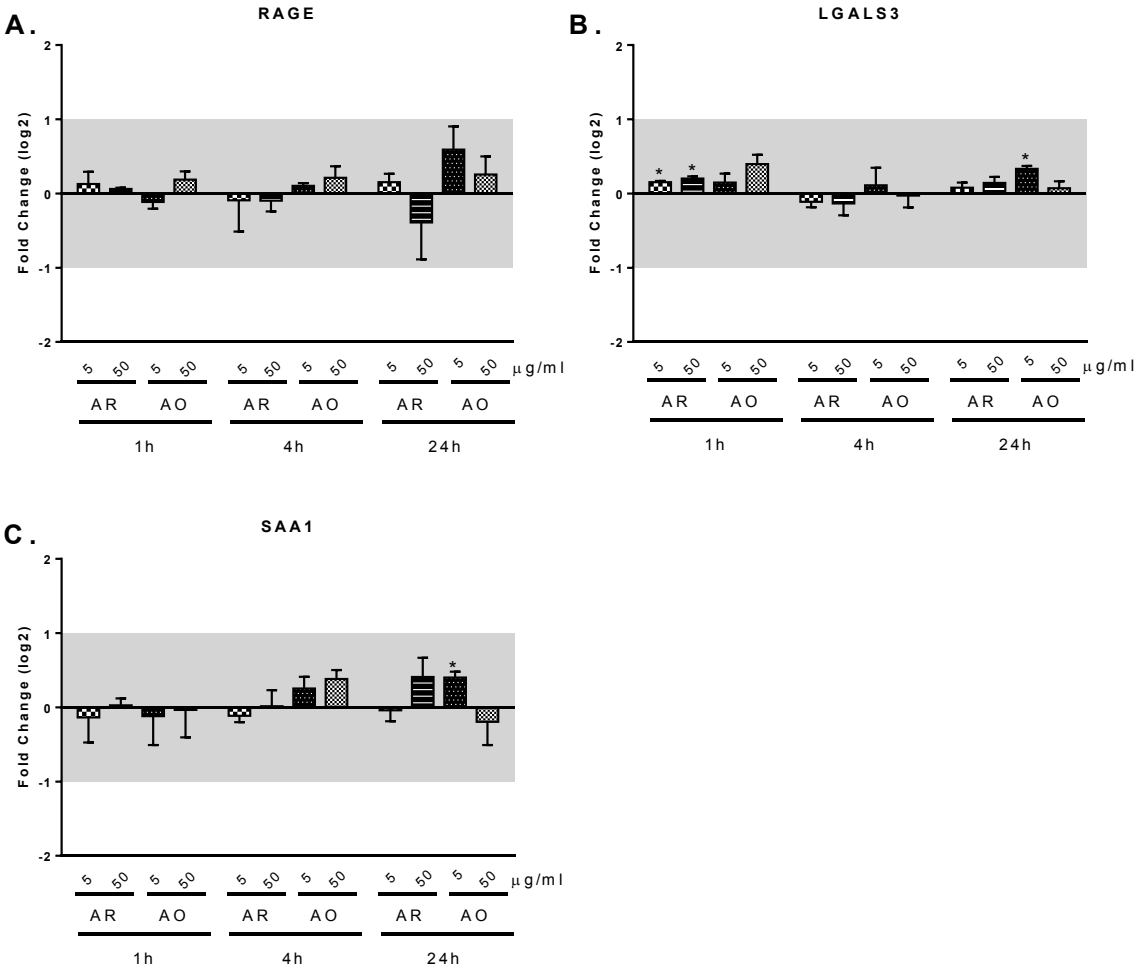
[1] Menzel R, Tran MQ, Menner A, Kay CWM, Bismarck A, Shaffer MSP. A versatile, solvent-free methodology for the functionalisation of carbon nanotubes. Chem Sci. 2010;1:603-8.

[2] Bacterial Endotoxins/Pyrogens. 3/20/85 ed: Dept. of Health, Education, and Welfare Public Health Service Food and Drug Administration.

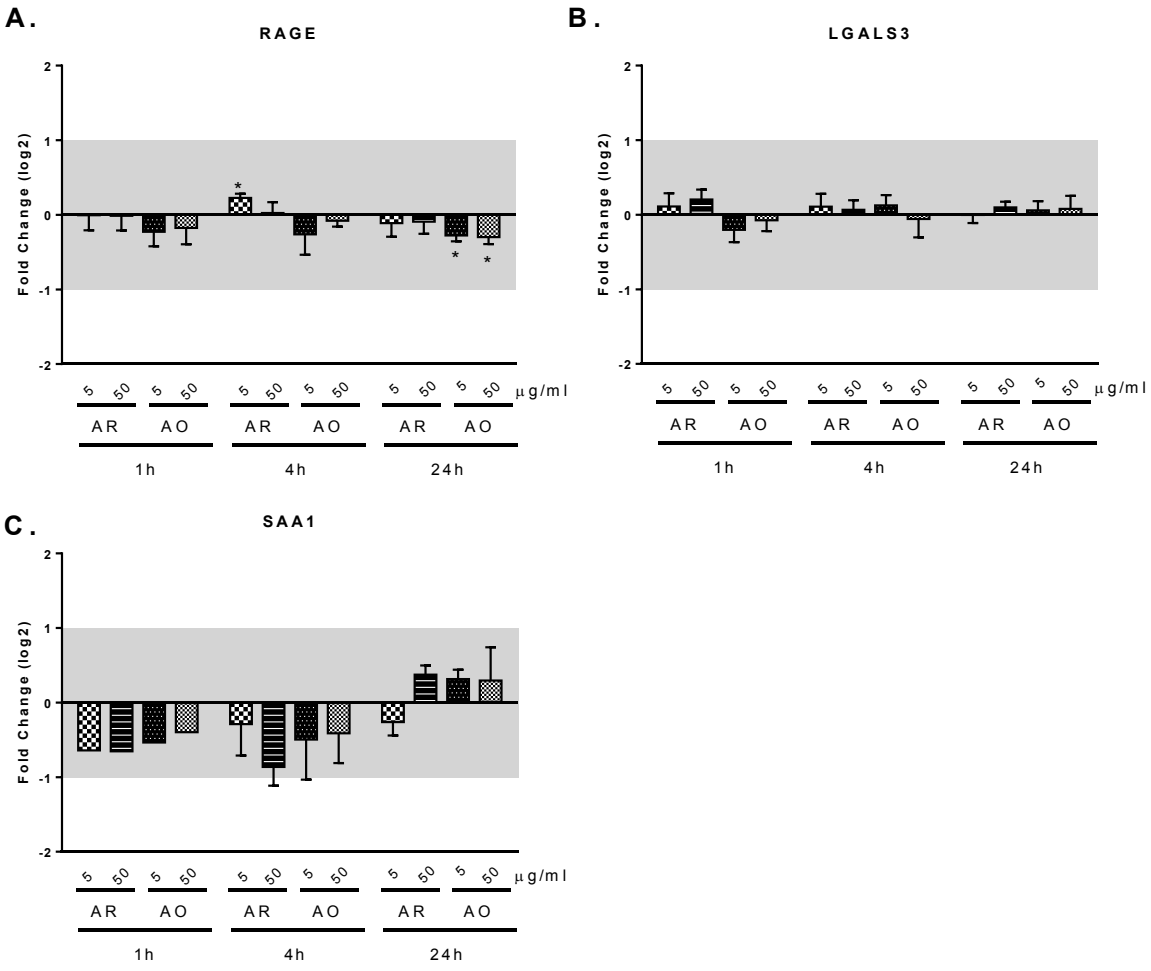
[3] Conner SD, Schmid SL. Regulated portals of entry into the cell. Nature. 2003;422:37-44.



Appendix II. Melt curve analysis. The single peak present following melt curve analysis indicates the overwhelming presence of a DNA molecule of a singles size. This in turn indicates that a single gene product has been generated during the polymerase chain reaction (PCR) however melt curve analysis is unable to distinguish between two distinct PCR products of a similar molecular weight. Melt curve analysis is commonly used alternative to gel electrophoresis to determine PCR efficiency.

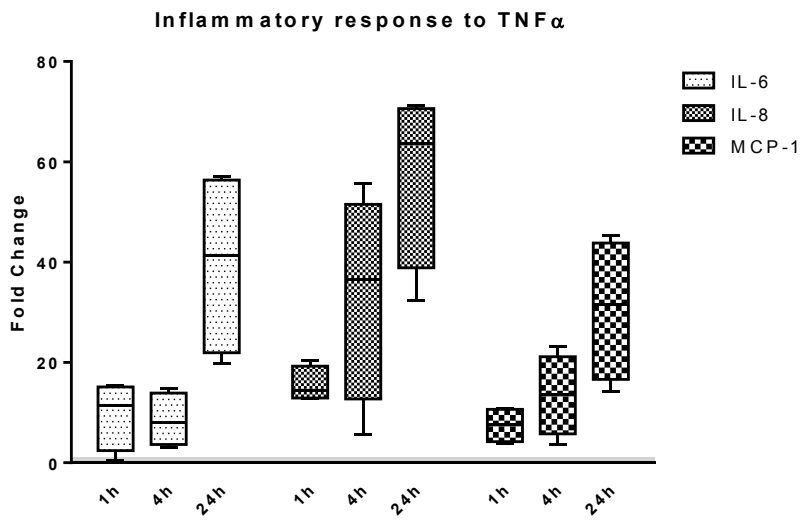


Appendix III. TT1 *RAGE, LGAL3* and SAA-*1* gene regulation in response to a 5 or 50µg/ml AR or AO MWNT exposure for 1, 4 or 24 hours. Values were normalised to a GAPDH loading control and compared to an untreated control using the ΔΔCt method. Data is expressed as mean ±SEM, n=4. For statistical analysis a one sample t-test was performed with values compared to a non-treated control value of 0, *p<0.05

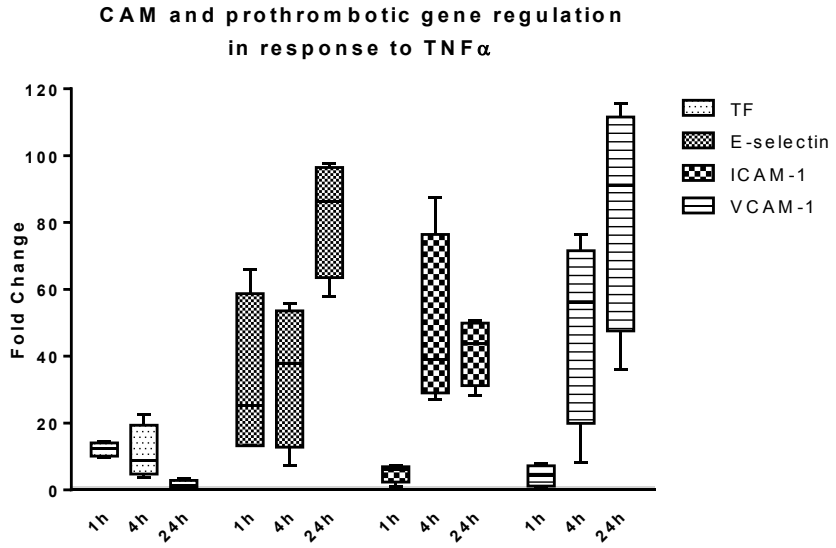


Appendix IV. AT2 *RAGE, LGAL3* and SAA-*1* gene regulation in response to a 5 or 50µg/ml AR or AO MWNT exposure for 1, 4 or 24 hours. Values were normalised to a GAPDH loading control and compared to an untreated control using the ΔΔCt method. Data is expressed as mean ±SEM, n=1-4. For statistical analysis a one sample t-test was performed with values compared to a non-treated control value of 0, *p<0.05

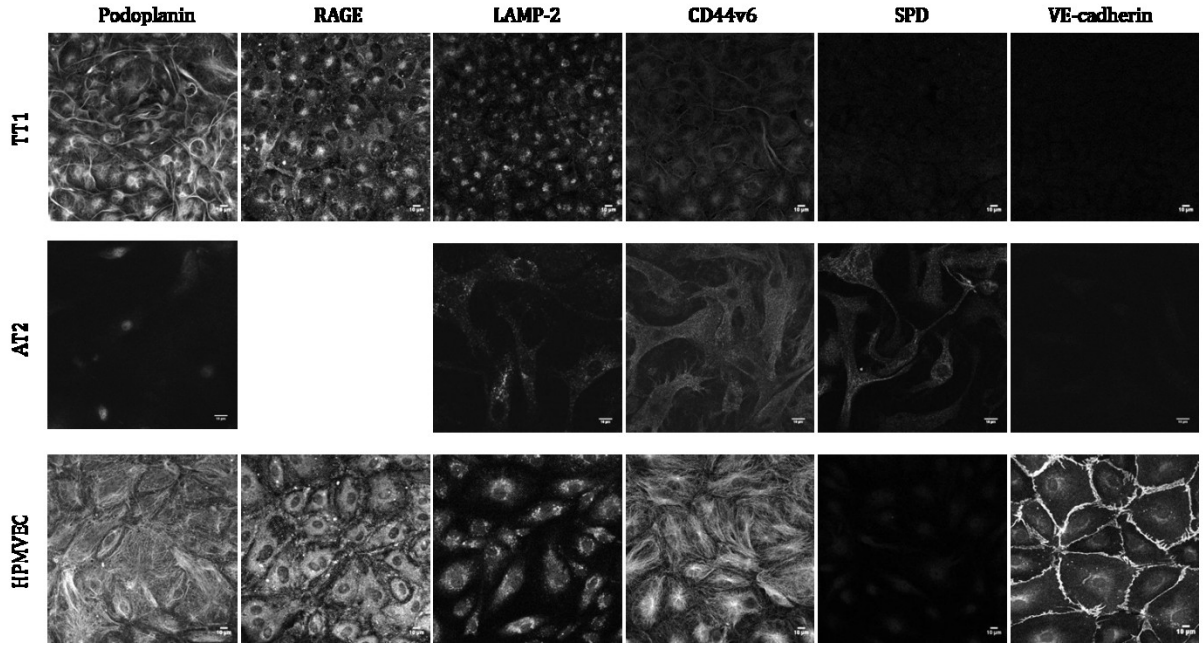
A.



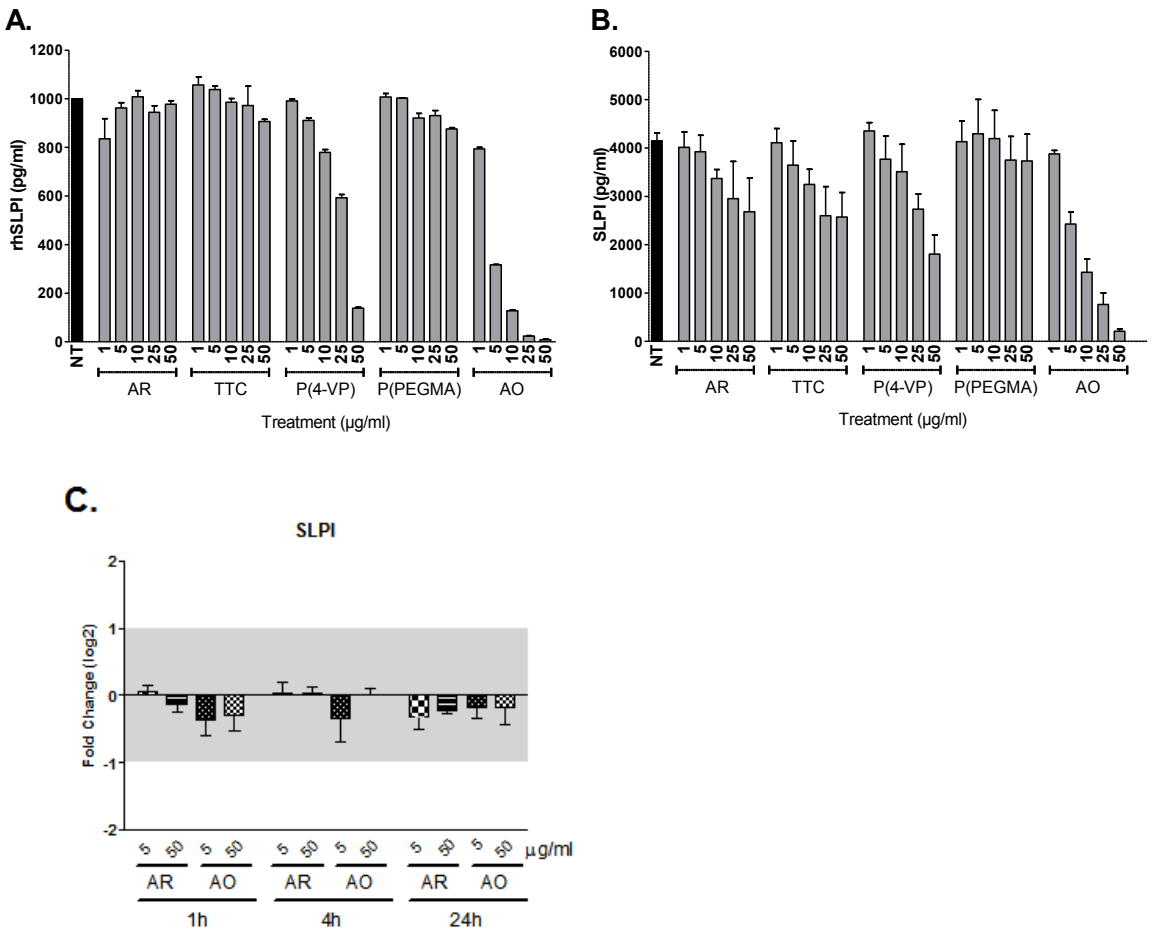
B.



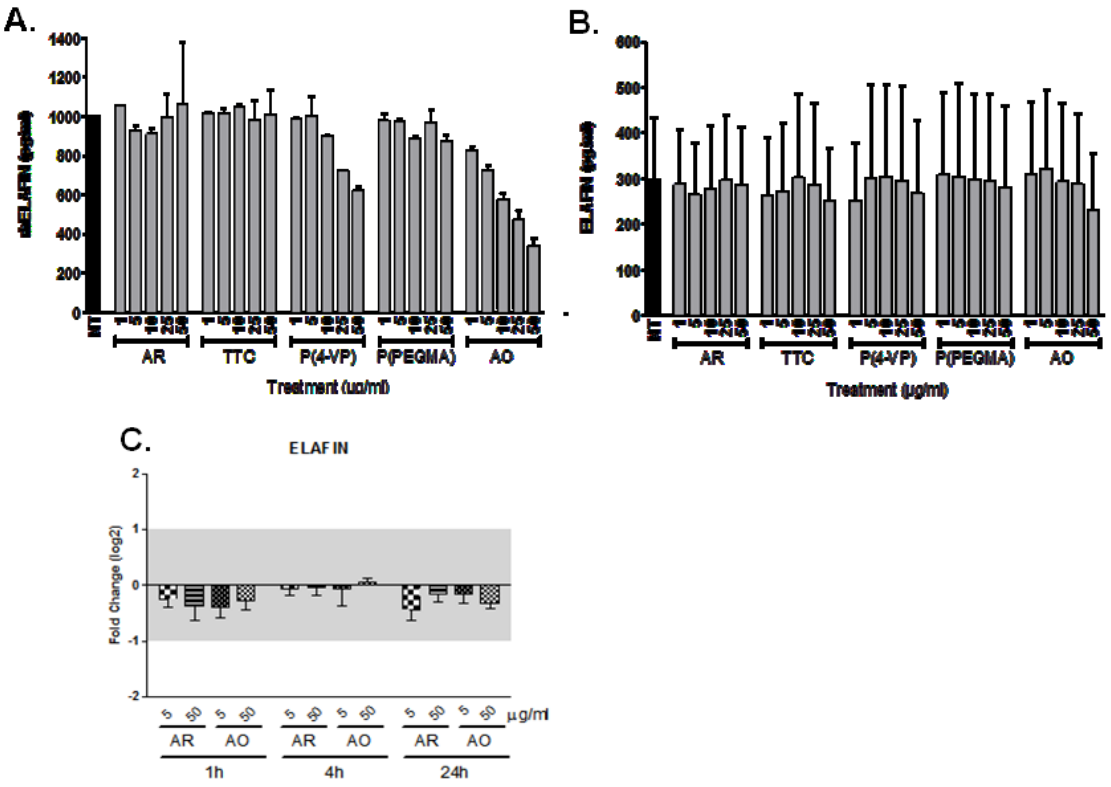
Appendix V. HPMVEC inflammatory, CAM and thombotic gene regulation followng exposure to TNFα. HPMVEC were exposed to 10ng/ml TNFα for 1, 4 or 24 hours. mRNA levels of the inflammatory genes IL-6, IL-8 and MCP-1 (A.), the thrombotic mediator tissue factor (TF) and the cell adhesion molecules (CAMs) E-selectin, ICAM-1 and VCAM-1 (B.) were assayed via RT-PCR. There was variability in the magnitude of gene up-regulation, suggestive of a degree of inter-donor variability in response to an inflammatory stimuli. Values were normalised to a GAPDH loading control and compared to an untreated control using the ΔΔCt method. Data is expressed as mean ±SEM, n=4.



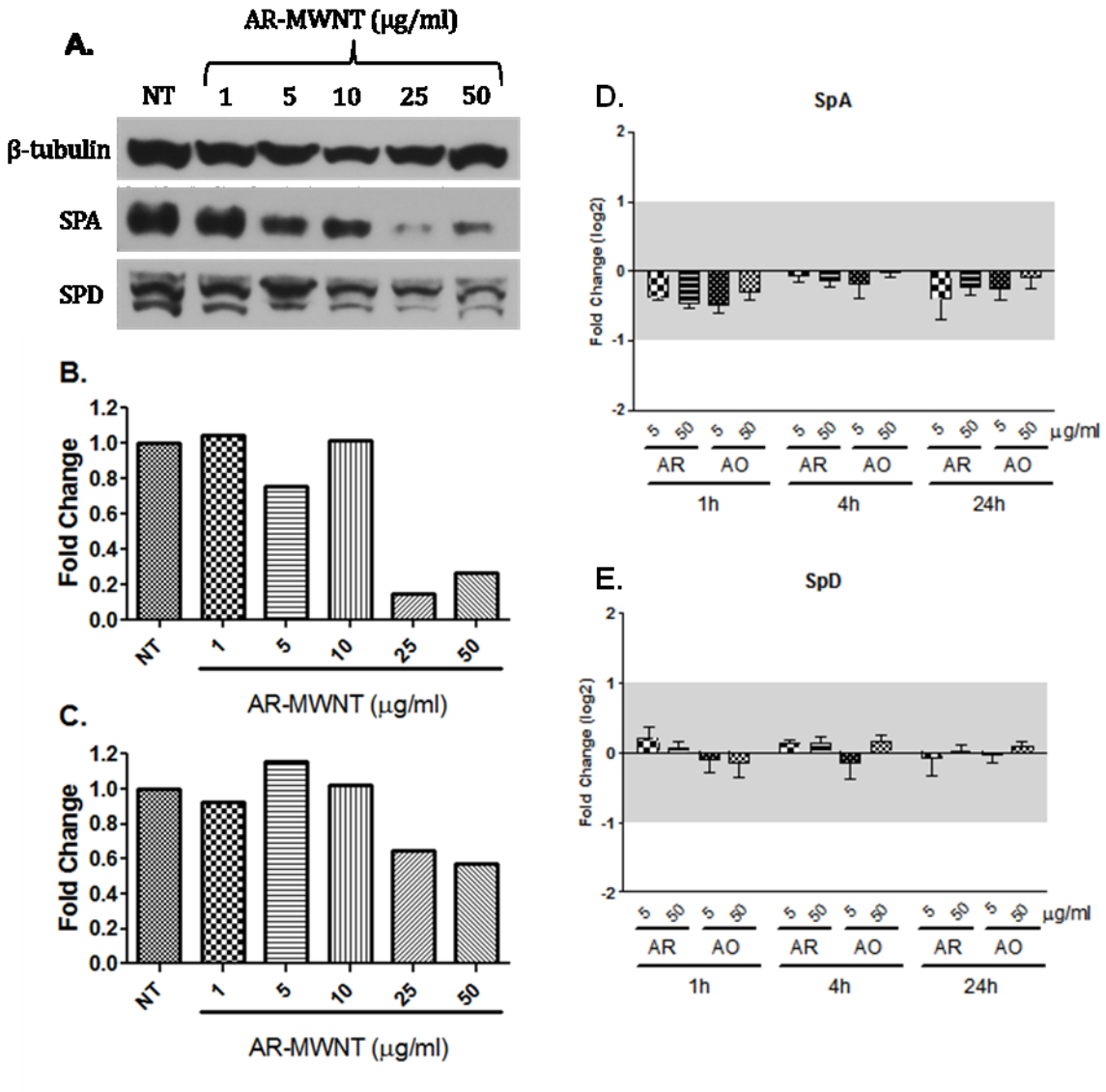
Appendix VI. Immunostaining optimisation for staining of co-culture system. TT1 markers podoplanin and RAGE , and the AT2 marker CD44v6 exhibited a large degree of non-specific staining.



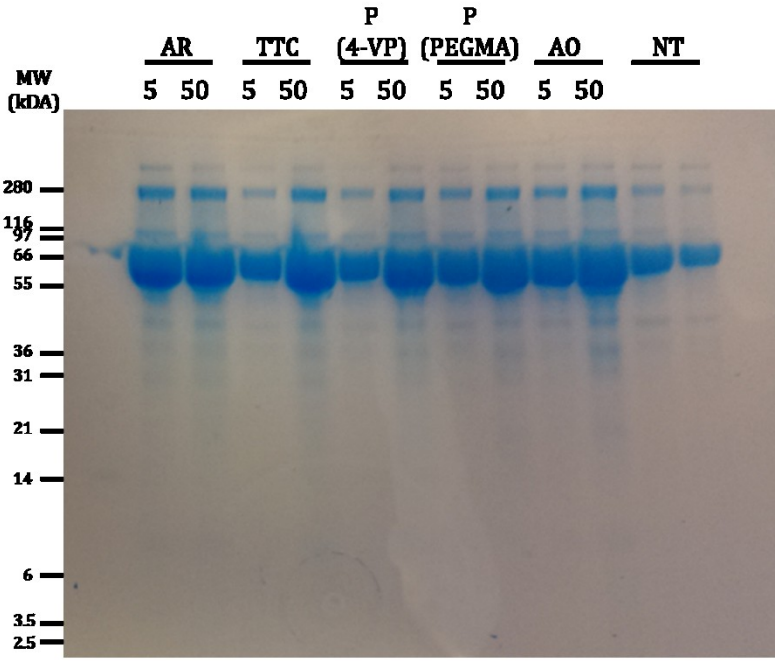
Appendix VII. SLPI adsorption to f-MWNTs and *SLPI* gene regulation in AT2 cells.
Adsorptive patterns observed in a medium containing either (A.) recombinant human secretory leukocyte protease inhibitors (rhSLPI) or (B.) endogenous secretory leukocyte protease inhibitors (SLPI) and f-MWNTS. (C.) No change in SLPI mRNA was observed following exposure to 5 or 50µg/ml of AR or AO-MWNTs at 1, 4 or 24 hours post exposure. Data is expressed as mean ±SEM, n=2. For statistical analysis a one-way sample t-test was performed with values compared to a non-treated control value of 0.



Appendix VIII. Elafin adsorption to f-MWNTs and *Elafin* gene regulation in AT2 cells. Adsorptive patterns observed in a medium containing either (A.) recombinant Elafin or (B.) endogenous Elafin and f-MWNTS. (C.) No change in SLPI mRNA was observed following exposure to 5 or 50µg/ml of AR or AO-MWNTs at 1, 4 or 24 hours post exposure. Data is expressed as mean ±SEM, n=2. For statistical analysis a one-way sample t-test was performed with values compared to a non-treated control value of 0.

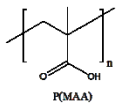
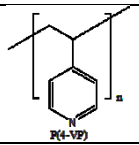
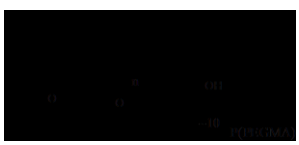


Appendix IX. Depletion of surfactant proteins A and D following MWNT exposure. (A.) Immunoblot depicting surfactant proteins A and D in cell lysates following a 24 hour AR-MWNT exposure (1-50µg/ml) and densitometry of the immunoblot in (A) depicting (B.) surfactant protein A and (C.) surfactant protein D protein expression. AT2 cell surfactant protein A (D.) and surfactant protein D (E.) gene expression following a 5 or 50µg/ml AR or AO MWNT exposure for 1, 4 or 24 hours. Values were normalised to a GAPDH loading control and compared to a untreated control using the ΔΔCt method. Data is expressed as mean ±SEM, n=3. For statistical analysis a one-way sample t-test was performed with values compared to a non-treated control value of 0.



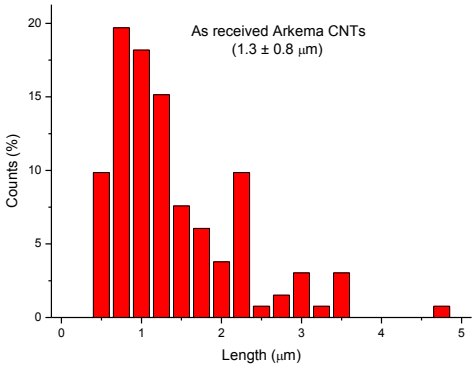
Appendix X. Total protein recovered from ultracentrifuged fraction of cell supernatant following MWNT exposure. Cell culture media was removed 24 hours following exposure to 5 and 50µg/ml f-MWNTs and centrifuged at 17,000 x g for 20 minutes. The resulting pellet was washed 3 times by resuspending the pellet in PBS and repeating the centrifugation step. Finally the CNT-protein aggregate was resuspended in PBS and the bound protein were denatured at 90°C for 10 minutes, before being resolved on a 4-12% NuPAGE Bis-Tris gel. Total protein was visualised using the EZBlue Coomassie Brilliant Blue stain (Sigma-Aldrich, Poole, UK).

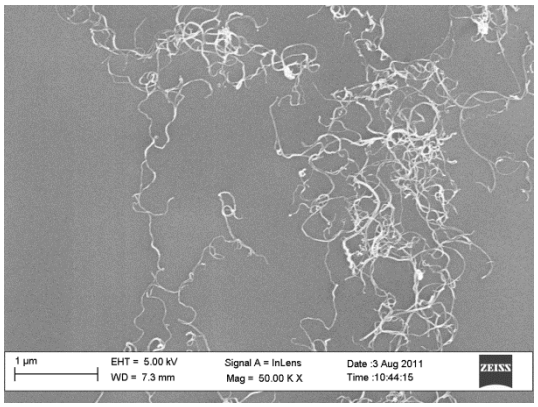
Appendix XI. CNT length as determined by SEM. Data produced by Dr Shu Chen (Imperial College London).

Sample	Length (µm)	Structure
AR (as-received Arkema MWNTs)	1.3±0.8	N/A
P(MAA) Poly (Methyl methacrylic acid)	0.51±0.30	
P(4-VP) Poly(4-Vinylpyridine)	0.62±0.32	
P(PEGMA) Poly (Poly (ethyleneglycol) methacrylate)	0.59±0.44	
AO (acid oxidised)	0.45±0.35	N/A

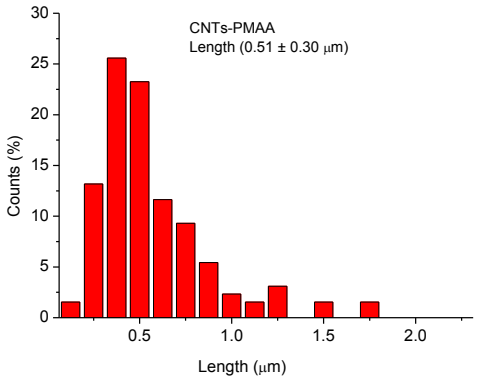
All the CNTs samples contain big aggregates and individual CNTs. The latter was characterized by SEM for length measurement.

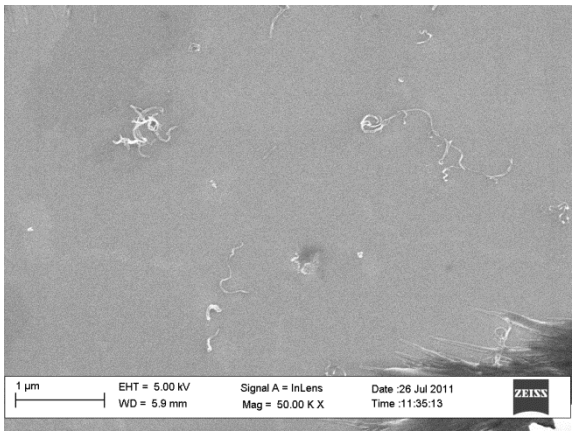
AR-MWNT



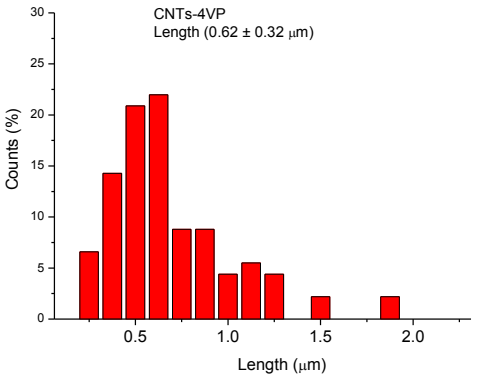


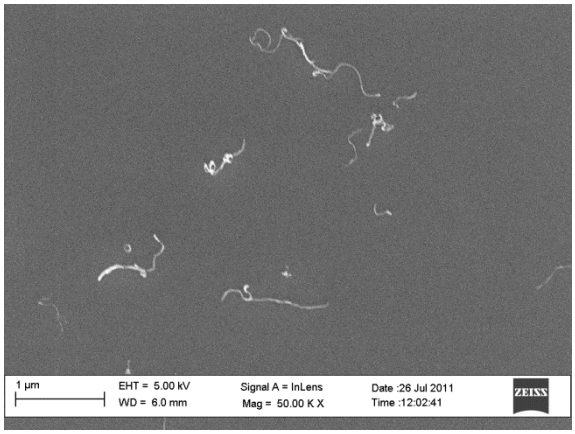
P(MAA)-MWNT



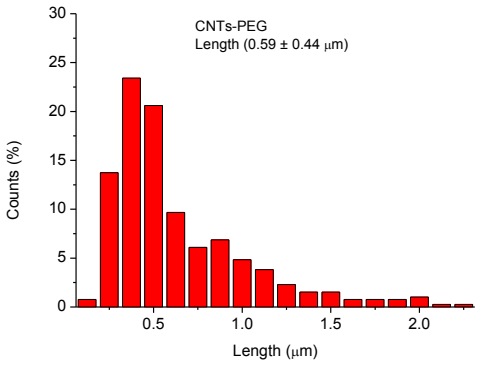


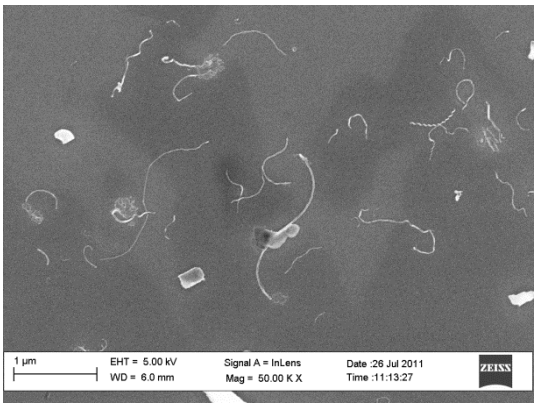
P(4-VP)-MWNT





P(PEGMA)-MWNT





AO-MWNTs

